Mathematical Model of the Cell Cycle Control and Asymmetry Development in *Caulobacter crescentus*

Chunrui Xu

Dissertation submitted to the Faculty of the
Virginia Polytechnic Institute and State University
in partial fulfillment of the requirements for the degree of

Doctor of Philosophy
in
Genetics, Bioinformatics and Computational Biology

Yang Cao, Chair
John J. Tyson, Co-chair
Zhaoming Yang
William T. Baumann

June 6, 2022
Blacksburg, Virginia

Keywords: Mathematical model, Stress response, Asymmetrical cell cycle, Protein regulatory networks

Mathematical Model of the Cell Cycle Control and Asymmetry Development in *Caulobacter crescentus*

Chunrui Xu

ABSTRACT

Caulobacter crescentus goes through a classic dimorphic cell division cycle to adapt to the stringent environment and reduce intraspecific competition. *Caulobacter* mother cell gives rise to two progenies with distinct morphology - a motile swarmer cell equipped with a flagellum and a sessile stalked cell equipped with a stalk. Because of the nature of dimorphic lifestyle, *Caulobacter* becomes a model bacterium to study the cell differentiation, signalling transduction, stress response, and asymmetry development of prokaryotes. The dimorphic cell cycle of *Caulobacter* is driven by the elaborate spatiotemporal organization of regulatory molecules through regulations of synthesis, degradation, phosphorelay, and localization. There is a wealth of experimental observations about gene/protein interactions and localizations accumulated in recent decades, while several mathematical models have been proposed to study the cell cycle progression in *Caulobacter*. However, the specific control mechanisms of stress response and spatial asymmetry establishment are yet clearly elucidated, while these mechanisms are of fundamental importance to understanding the bacterial survival strategy and developing the microbial industry.

Here we utilize mathematical modeling to study the regulatory network of cell cycle control in *C. crescentus*, focusing on the stress response and asymmetry development. First, we investigate the starvation response of *Caulobacter* through the connection of phosphotransferase systems (PTS) and guanine nucleotide-based second messenger system. We have developed a mathematical model to capture the temporal dynamics of vital regulatory second messengers, c-di-GMP (cdG) and guanosine pentaphosphate or tetraphosphate (pppGpp or ppGpp), under normal and stressful conditions. This research suggests that the RelA-SpoT homolog enzymes have the potential to effectively influence the cell cycle in response to nutrition changes by regulating cdG and (p)ppGpp levels. We further integrate the second messenger network into a temporal cell cycle model to investigate molecular mechanisms underlying responses of *Caulobacter* to nutrition starvation. Our model suggests that the cdG-relevant starvation signal is essential but not sufficient to robustly arrest the cell cycle of *Caulobacter*. We also demonstrate that there may be unknown pathway(s) reducing CtrA under starvation conditions, which results in delayed cytokinesis in starved stalked cells.

The cell cycle development of *Caulobacter* is determined by the periodical activation and deactivation of the master regulator CtrA. cdG is an essential component of the ClpXP pro-

tease complex, which is specifically responsible for the degradation of CtrA. We propose a mathematical model for the hierarchical assembly of ClpXP complexes, together with modeling DNA replication, transcription, and protein interactions, to characterize the *Caulobacter* cell cycle. Our model suggests that the ClpXP-based proteolysis system contributes to the timing and robustness of the cell cycle progression.

Furthermore, we construct a spatiotemporal model with Turing-pattern mechanism to study the morphogenesis and asymmetry establishment during the cell cycle of *Caulobacter*. We apply reaction-diffusion equations to capture the spatial dynamics of scaffolding proteins PodJ, PopZ, and SpmX, which organize two distinct poles of *Caulobacter*. The spatial regulations influence the activity and distribution of key cell cycle regulators, governing the dimorphic lifestyle of *Caulobacter*. Our model captures major spatiotemporal experimental observations of wild-type and mutant cells. It provides predictions of novel mutant strains and explains the spatial regulatory mechanisms of bacterial cell cycle progression.

Mathematical Model of the Cell Cycle Control and Asymmetry Development in *Caulobacter crescentus*

Chunrui Xu

GENERAL AUDIENCE ABSTRACT

Cell is the basic unit of life that undergoes a process called 'cell cycle' consisting of DNA replication and cell division to exhibit various functions, abilities, and behaviors. The cell cycle is well organized by complex regulations in time and space that determine when and where changes take place. The regulations behind cell cycle development play important roles for living organisms but are not fully understood. In this dissertation, we utilize mathematical models and focus on a model bacterium, *Caulobacter crescentus*, to capture characteristics of cell cycle and study the underlying regulations. *Caulobacter* is widely distributed in freshwater, including environments with poor nutrients. It divides asymmetrically, generating a pair of daughter cells with different appearances and replicative potentials. Therefore, *Caulobacter* population has the flexibility to save energy by halting DNA replication and to reduce the competition with siblings by settling into different places. We utilize the nature of the asymmetrical division of *Caulobacter* to quantitatively investigate the control mechanisms of cell cycle development, including how cells detect and respond to external cues and develop different organelles at specific times and locations.

Acknowledgments

Time flies. I still remember the moment when I kissed my family goodbye and boarded the flight to the U.S. for the first time in my life. It has been a fantastic five-year journey for me.

First and foremost, I would like to express my deepest gratitude to my advisor Dr. Yang Cao and co-advisor Dr. John J. Tyson, for guiding me like a lighthouse during my Ph.D. study. Every step I moved forward in the ocean of science benefited from their patient mentoring. I felt lucky and reassured with them being my advisors.

Dr. Cao is a great scientist and advisor. He provided idea, advice, support and encouragement when I needed it. He guided the direction of my research, encouraged me to face challenges, and reviewed and modified my work with enormous patience. I could not experience such a happy and fulfilling Ph.D. study life without him.

In my eyes, Dr. Tyson is a shining academic icon. He is an intelligent, gentle, and conscientious scientist, who keeps seeking the truth and perfection in science. Dr. Tyson's classes and talks were attractive, understandable, and helpful. He mentored me responsibly and patiently throughout my Ph.D. study and guided me to climb higher on the mountain of science.

I would like to express appreciation to my committee members, Dr. Zhaoming Yang and Dr. William T. Baumann for their valuable time and advice. They reviewed my work and plan responsibly, proposed constructive comments and suggestions, and encouraged me to dig deeper in research.

I would like to thank my previous lab mates, Dr. Bronson R. Weston and Dr. Minghan Chen. Bronson spent plenty of time and effort leading me into the world of *Caulobacter* modeling. His passion and vision in *Caulobacter* modeling motivated me to work hard and move forward. Minghan is my good friend and helpful colleague, who gave me a lot of supports and help.

I would like to thank my husband Shulin Xie and my cute cookie Gus for giving me endless love, support, consolation, and companionship during my Ph.D. study.

I would like to thank my parents, sister, and parents-in-law for supporting and respecting my

decisions emotionally and financially. Because of my family, I can always get over difficulties, failures, and depression; I can always be promising and optimistic.

I am very lucky to meet a lot of kind and outstanding people during these five years. Thanks to all wonderful people I met here.

Attributions

This work received support from the National Science Foundation (NSF) under awards MCB-1613741, and CCF-1909122. The funders had no role in study design, data analysis, publication, or manuscripts.

Chapter 2 and Chapter 3 in this dissertation consist of manuscripts that have been published. Chapter 4 is the extension of Chapter 2, which is part of the manuscript collaborated with Bronson R. Weston and expected to be submitted for publication in the future. Chapter 5 consists of the manuscript that will be submitted shortly.

Chapter 2: Chunrui Xu, Bronson R. Weston, John J. Tyson, Yang Cao. (2020). Cell cycle control and environmental response by second messengers in *Caulobacter crescentus*. BMC Bioinformatics. 21(Suppl 14): 408.

Chapter 3: Chunrui Xu, Henry Hollis, Michelle Dai, Xiangyu Yao, Layne T. Watson, Yang Cao, Minghan Chen. (2022). Modeling the temporal dynamics of master regulators and CtrA proteolysis in *Caulobacter crescentus* cell cycle. PLOS Computational Biology, 18(1): e1009847.

Chapter 4: Bronson R. Weston, Chunrui Xu, John J. Tyson, Yang Cao. Molecular mechanisms of cell cycle arrest in carbon and nitrogen starved *Caulobacter* populations. (To be submitted)

Chapter 5: Chunrui Xu, John J. Tyson, Yang Cao. Turing-pattern model of scaffolding proteins that establishes spatial asymmetry during the cell cycle of *Caulobacter crescentus*. (To be submitted)

The contributions of co-authors are as follows:

Dr. Yang Cao mentored the conceptualization and computational methods of models. He is the corresponding author of the publication and manuscript corresponding to Chapter 2, 4, and Chapter 5.

Dr. John J. Tyson aided in the biochemical conceptualization of the publication and manuscript corresponding to Chapter 2, Chapter 4, and Chapter 5.

Dr. Minghan Chen helped in the conceptualization and parameterization of the publication

corresponding to Chapter 3. She is the corresponding author of this publication.

Dr. Bronson R. Weston is the co-first author on the publication corresponding to Chapter 2 and the co-first author on the manuscript corresponding to Chapter 4.

For the publication corresponding to Chapter 3, Henry Hollis and Michelle Dai helped in plotting and writing; Xiangyu Yao helped in part of coding; Dr. Layne T. Watson provided insights into optimization methods.

Contents

List of Figures

List of Tables

Chapter 1

Introduction

1.1 Cell cycle regulation in bacteria

Bacteria is enormously diverse, with a wide range of cellular volumes and genome sizes [1]. All bacterial species must coordinate their cellular growth, division, shape, and volume with the inheritance of genetic expression based on environmental changes to survive in diverse ecosystems worldwide [1, 2]. On the other hand, events and activities of the bacterial cell cycle have to be precisely operated in time and space. The coordination and regulation of bacterial cell cycle are referred as 'complex', which cover not only the transcriptional control but non-transcriptional mechanisms such as phospho-signalling and subcellular localization [3].

A few master regulatory proteins constitute a core transcriptional regulatory network to control the bacterial cell cycle [3]. For instance, CtrA in *Caulobacter crescentus* directly controls the transcription of more than 90 genes [3]. It also coordinates with other regulators, including DnaA and GcrA, to control the initiation of chromosome replication [4].

Many bacterial species go through multiple states in response to environmental changes, such as asymmetrical cell divisions and morphogenesis [1]. *C. crescentus* cells always divide asymmetrically, producing distinct daughter cells to adapt to oligotrophic environments. *Bacillus subtilis* cells divide asymmetrically to produce a forespore under nutrient starvation conditions. The sporulation is determined by a master regulator Spo0A, which is parallel in many aspects to CtrA in *C. crescentus* [3, 5]. Both CtrA and Spo0A are response regulators of two-component transduction signaling pathways (TCS), which are activated (phosphorylated) by the phosphorelay kinases CckA-ChpT and Spo0F-Spo0B, respectively [5]. In addition to the control of DNA replication, phosphorylated CtrA modulates the flagella biogenesis and pili structure [3]. Phosphorylated Spo0A regulates the transcription of hundreds of genes and determines the location of septum [5]. The dynamics of TCS proteins play important roles in the precise timing and asymmetry development during the asymmetrical

cell cycle.

Moreover, the phosphotransfer pathways provide fast signaling to integrate internal status and external cues, enabling bacterial cells to rapidly respond to environmental changes. For example, the nitrogen-related phosphotransferase system (PTS^{Ntr}) receives nitrogen signals from environments and downstream mediates the activity of a bifunctional enzyme SpoT in *C. crescentus*. SpoT transfers the metabolic cues into the internal system by regulating levels of guanine-based second messengers (p)ppGpp and cyclic-di-GMP, which participate in multiple cell cycle progression activities, such as morphogenesis, cell cycle-dependent proteolysis, and cell growth [6].

The subcellular localization of key molecules is essential for bacterial cell morphogenesis. In *B. subtilis*, Spo0A-regulated transcriptions differ on the two sides of the septum, resulting in the asymmetry between the mother cell and forespore [5]. *C. crescentus* cells develop two poles with distinct spatial localization of proteins, such as the new polar scaffolding protein PodJ and the old polar scaffolding protein PopZ [7]. Although spatial observations and data have been accumulated in recent years, the underlying principles and mechanisms are poorly understood.

1.2 The asymmetrical cell cycle in *Caulobacter crescentus*

Caulobacter crescentus is a model organism for the study of cell cycle regulation and asymmetry establishment in prokaryotes. It is widely discovered in freshwater and some kinds of soils, even in oligotrophic environments [8, 9]. The successful survival in harsh environments benefits from its asymmetrical cell cycle. *Caulobacter* expresses different organelles in different phases and undergoes an asymmetrical cell division during the cell cycle, giving rise to two distinct daughter cells [10] (Fig. 1.1). One daughter, called 'swarmer cell', is equipped with a flagellum and several pili, which allow the cell to move and search for nutrients in environments. Swarmer cell is in the G1 phase, where DNA replication and cell reproduction are halted. The other daughter is called 'stalked cell', which expresses a holdfast and a stalk, clinging to a solid surface in environments. The stalked cell is ready to replicate DNA and to enter the next reproduction cycle. Given favorable environments, the swarmer cell will differentiate into a stalked morphological cell by rejecting its flagellum and synthesizing a stalk [11, 12]. Simultaneously, the *Caulobacter* cell initiates DNA replication and enters the S-phase during the differentiation stage.

The asymmetrical lifestyle makes *Caulobacter* easily synchronized and tracked in wet lab, which greatly helps molecular data collection [10]. The rapid synchronization of *Caulobacter* can be performed in a large-scale format by density centrifugation, which permits gene expression profiling, western blot assays, and fluorescence analysis [10, 13, 14, 15].

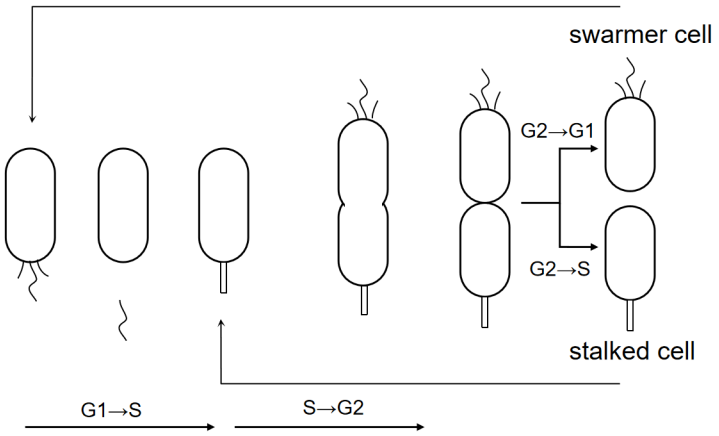

Figure 1.1: **The asymmetrical cell cycle of *C. crescentus*.**
The mother cell produces two distinct daughter cells. The stalked daughter cell is non-motile with a holdfast. The swarmer daughter cell is motile with pili and a flagellum. The swarmer cell transforms into a stalked cell before DNA replication commences, while the stalked cell enters the S-phase and initiates DNA replication immediately.

1.3 Mathematical models for the study of cell cycle regulation

With the revolution of biotechnology, a great amount of data for biological systems has remarkably been made available, from molecule to single-cell and to the population levels [16, 17]. Both temporal and spatial observations for the cell cycle development have been accumulated from multiple sources of data [14, 7, 13, 15]. To interpret these data, many conceptual models with simple diagrams that describe involved species and their relationships within cells have been proposed following experiments [7, 18]. However, conceptual models only superficially explain subsystems rather than a global system with multiple pieces integrated. It is still challenging to understand and integrate detailed mechanisms of the complex regulatory system of cell cycle.

Mathematical modeling has been successfully applied in many biological systems to integrate and provide hypotheses on known and/or unknown pathways and mechanisms to explain experimental observations [19, 20, 21]. It also has the potential to integrate data from different sources for different subsystems into a whole-cell model [22]. Additionally, mathematical models can be used to compare hypotheses and identify which hypothesis is more reasonable to explain certain experimental observations. Another application of mathematical models is to predict unrevealed behaviors and phenomena. Mathematical models can suggest further experimental directions, reduce the range of hypotheses to be verified, and save time and labor.

1.4 Summary of research

This work aims to integrate various levels and types of experimental observations to formulate a mathematical model that can explain the control mechanisms underlying precise cell development, asymmetry establishment, and stress responses during the cell cycle of *Caulobacter crescentus*.

In Chapter 2, we model a second messenger network to investigate the detection and response to environmental nutrition changes in *Caulobacter*. This work characterizes PTS^{Ntr} with empirical data and explains how PTS^{Ntr} enzymes detect external nitrogen and carbon signals - the environmental abundance of glutamine, phosphoenolpyruvate (PEP) and pyruvate (Pyr). Our model quantitatively describes the signal transmission within PTS^{Ntr} via phosphotransfer cascades and the connection to the downstream regulatory second messengers - guanosine derivative (p)ppGpp and c-di-GMP (cdG). As (p)ppGpp and cdG both play important roles in key cellular processes, such as cell growth and differentiation, this model provides a significant perspective to quantitatively explore the bacterial response to environments.

In Chapter 3, we propose a deterministic model described by a set of ordinary differential equations to characterize the underlying mechanisms of cell cycle regulation, which integrates replication, methylation, transcription, and hierarchical proteolysis of key cell cycle regulators in *Caulobacter*. ClpXP is a vital protease in *Caulobacter*, which hierarchically recruits helpers to constitute different protease complexes that degrade many proteins such as CtrA, TacA, PdeA, and so on. The second messenger cdG, investigated in Chapter 2, is a key member of the ClpXP protease complex, which is specifically responsible for the proteolysis of CtrA. We explicitly model the hierarchical recruitment by ClpXP and use this quantitative module to simulate the proteolysis of relevant proteins. Considering the good consistency between our simulations with experimental observations in the dynamics of mRNA and proteins of wild type as well as mutant strains, our model can be used to investigate the contribution of proteolysis and predict unknown behaviors of novel mutant cells. Additionally, the connection between Chapter 2 and Chapter 3 provides a perspective to understand the environmental response through the cdG-CtrA pathway.

Chapter 4 integrates the second messenger model of Chapter 2 into a large temporal frame of cell cycle regulation, which is originally proposed by a previous lab member, Dr. Weston [22]. The previous temporal model explained regulatory mechanisms of cell cycle in *Caulobacter* by modeling genetic regulations and multiple interactions of essential master regulators. Although our second messenger network (Chapter 2) easily transmits nutrition cues into the temporal regulatory network, it is not sufficient to capture all behaviors of starved populations observed in experiments. Thus, we thoroughly reviewed, modified, and improved the temporal model focusing on pathways related with environmental responses. Roughly and wrongly modelled pathways have been improved or corrected, such as the adjustment of ClpXP protease complexes. An important cdG-relevant pathway, ShkA-TacA-SpmX, has been integrated to reform the modeling of SpmX and CtrA. Other starvation signaling pathways, such as RpoD-targeted transcription and supplementary phosphatase CckN-regulated phospho-signaling, have been taken into the large frame to improve our simulation. Our new temporal model is able to reproduce and explain a series of observed changes under nutrition shifts.

In Chapter 5, we provide a spatiotemporal mathematical model to analyze the asymmetry establishment during the cell cycle in *Caulobacter*. We combine the Turing-pattern mechanism with interactions among three scaffolding proteins - PodJ, PopZ, and SpmX - to explain the initial organization of two distinct poles of *Caulobacter* cells. Building on the network of scaffolding proteins, we further integrate spatial regulations with phosphotransfer and temporal regulations to explore the non-uniform distributions of key regulators, such as DivK and CtrA. Our model captures phenotypes of both wild-type and mutant cells. Besides explanation for the spatial development of the asymmetrical cell cycle, this model also provides predictions of novel mutants, gives a good application of multiobjective parameterization, and helps to resolve controversial hypotheses.

Chapter 2

Cell cycle control and environmental response by second messengers in *Caulobacter crescentus*

Chunrui Xu[1*], Bronson R. Weston[1*], John J. Tyson[2], Yang Cao[3]

1 Genetics, Bioinformatics, and Computational Biology, Virginia Tech, Blacksburg, VA, USA
2 Department of Biological Science, Virginia Tech, Blacksburg, VA, USA
3 Department of Computer Science, Virginia Tech, Blacksburg, VA, USA
* Equal contributor

2.1 Abstract

Second messengers, c-di-GMP and (p)ppGpp, are vital regulatory molecules in bacteria, influencing cellular processes such as biofilm formation, transcription, virulence, quorum sensing, and proliferation. While c-di-GMP and (p)ppGpp are both synthesized from GTP molecules, they play antagonistic roles in regulating the cell cycle. In *C. crescentus*, c-di-GMP works as a major regulator of pole morphogenesis and cell development. It inhibits cell motility and promotes S-phase entry by inhibiting the activity of the master regulator, CtrA. On the contrary, the intracellular (p)ppGpp accumulates under starvation, which helps bacteria to survive under stressful conditions by regulating nucleotide levels and halting proliferation. (p)ppGpp responds to nitrogen levels through RelA-SpoT homolog enzymes, detecting glutamine concentration using a nitrogen phosphotransferase system (PTS^{Ntr}).

This work relates the guanine nucleotide-based second messenger regulatory network with the bacterial PTS^{Ntr} system and investigates how bacteria respond to nutrient availability.

We propose a mathematical model to capture the dynamics of c-di-GMP and (p)ppGpp in *C. crescentus* and investigate how the guanine nucleotide-based second messenger system responds to certain environmental changes communicated through the PTS^{Ntr} system. In this chapter, we demonstrate how the PTS^{Ntr} system influences (p)ppGpp, c-di-GMP, GMP and GTP concentrations. While this model does not consider all aspects of PTS^{Ntr} signaling, such as cross-talk with the carbon PTS system, here we present our first effort to develop a model of nutrient signaling in *C. crescentus*. Our simulations are consistent with experimental observations and suggest, among other predictions, that SpoT can effectively decrease cdG levels in response to nitrogen starvation just as well as it increases (p)ppGpp levels. Thus, the activity of SpoT (or its homologues in other bacterial species) can likely influence the cell cycle by influencing both cdG and (p)ppGpp.

2.2 Introduction

Caulobacter crescentus is an oligotrophic, Gram-negative α-proteobacterium, frequently found in freshwater environments. *C. crescentus* undergoes asymmetrical cell division, yielding two distinct progeny cells (Fig. 2.1): a non-motile 'stalked' cell (st) immediately re-enters the cell cycle and initiates DNA replication, while a motile 'swarmer' cell (sw) explores its environment before differentiating into a stalked cell and re-entering the cell cycle [4]. The stalked cell is equipped with a holdfast to attach to solid surfaces in its environment, whereas the swarmer cell develops a flagellum to move around in search of a suitable nutrient environment. The asymmetrical cell cycle affords *C. crescentus* a certain flexibility to cope with the vagaries of life in an oligotrophic, aquatic environment [23].

Since asymmetrical cell division plays an essential role in survival for *C. crescentus*, understanding how the asymmetry is regulated provides insights into the life cycle of many bacteria with similar characteristics. Many proteins, genes, and other molecules involved in the asymmetrical pattern have been reported [23, 24]. CtrA, a master regulator of the *C. crescentus* life cycle, regulates more than 100 genes involved in flagellum biogenesis, DNA replication, and cell division [25, 26]. As CtrA inhibits the initiation of DNA replication, active CtrA (the phosphorylated form) must be eliminated during the swarmer-to-stalked (G1-to-S) transition (Fig. 2.1). There are two pathways to inactivate CtrA: proteolysis by ClpXP [27] and dephosphorylation by CckA [28].

In *C. crescentus*, the spatio-temporally regulated proteolysis of CtrA requires protease ClpXP and additional factors called adaptors [27, 29]. The protease complex consists of CpdR, RcdA, PopA, and a second messenger c-di-GMP (cdG) (Fig. 2.2). ClpXP primed by unphosphorylated CpdR localizes at the old pole (Fig. 2.1) and recruits the adaptor RcdA which directly interacts with PopA. PopA must be bound with cdG to adapt CtrA to the

entire protease complex, which means cdG is indispensable for CtrA proteolysis. In addition to regulating CtrA proteolysis, cdG also participates in CtrA dephosporylation through CckA [28] (Fig. 2.2). CckA is a bifunctional enzyme, which can act as both a phosphatase and a kinase to regulate the phosphorylation state of CtrA and CpdR. When cdG binds with CckA, CckA activity favors the phosphatase state over the kinase state. When cdG level peaks during the G1-to-S transition, the dephosphorylation of CtrA and CpdR is rapidly stimulated, which allows DNA replication to initiate [30]. In this way, cdG stimulates the initiation of DNA replication by activating the dephosphorylation and degradation of CtrA (Fig. 2.2).

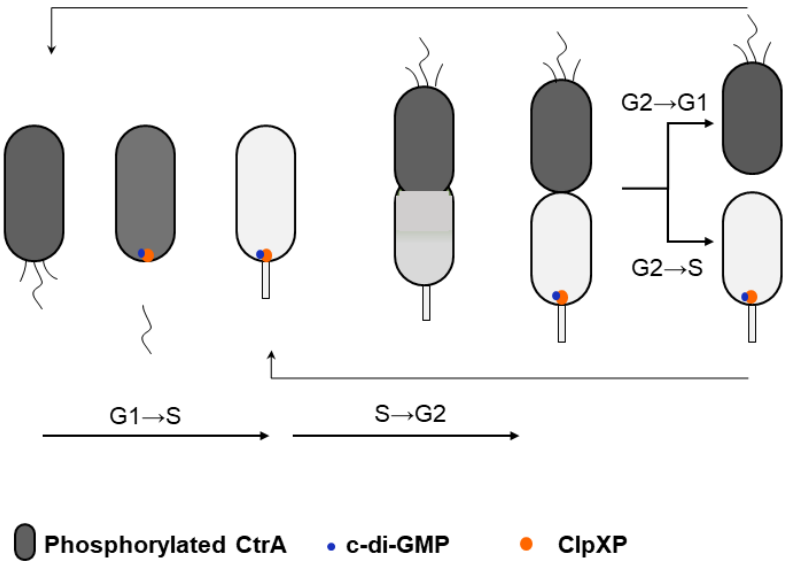

Figure 2.1: **The asymmetrical cell cycle and nonuniform distributions of molecules of *C. crescentus*.**
The nascent swarmer daughter cell is differentiated into the stalked morphology and then initiates DNA replication, while the nascent stalked cell is ready to reproduce. CtrA regulates cell cycle progression in time and space. CtrA is eliminated during the G1-to-S transition. The gray intensity indicates the concentrations of CtrA during cell cycle progression. ClpXP, a protease specific for CtrA, shows up at the flagellated pole of a cell to degrade CtrA. c-di-GMP cooperates with ClpXP for CtrA proteolysis.

While cdG stimulates the G1-to-S transition, alternative guanine-nucleotide based secondary messengers, guanosine tetraphosphate and guanosine pentaphosphate ((p)ppGpp), promote the mobility and cell cycle arrest in *C. crescentus*. While the exact mechanisms are unknown, it is understood that (p)ppGpp indirectly promotes the stabilization of CtrA and degradation of DnaA, as well as interacting with RNA polymerase to influence global gene expression [31]. Additionally, cdG and (p)ppGpp control several key processes to help bacteria adjust to environmental cues, such as depletion of nutrients [31, 32].

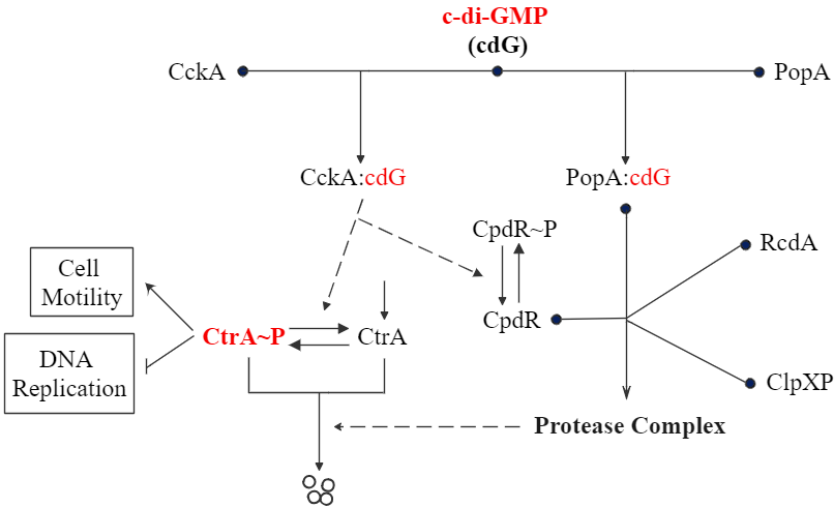

Figure 2.2: **c-di-GMP regulates DNA replication and cell motility through CtrA.** (Left-hand side) cdG directly stimulates the phosphatase activity of CckA, thereby dephosphorylating CtrA to allow the initiation of DNA replication. (Right-hand side) cdG is also required for CtrA proteolysis.

There is evidence that bacteria accumulate (p)ppGpp in response to carbon and/or nitrogen limitation [31] by regulating RelA-SpoT homolog (RSH) enzymes. Furthermore, bacteria respond to the availability of carbon through cdG-regulated signaling processes [32]. However, the specific mechanisms by which stressful conditions affect cell cycle progression through the second messenger system and other key proteins in *C. crescentus* is not clear.

In this work, we combine cdG, (p)ppGpp, and GTP into one mathematical model to investigate the dynamics of these second messengers and how they respond to environmental changes through the PTS^{Ntr}. Our model suggests that the concentration of cdG decreases dramatically following nitrogen deprivation in response to increased synthetase and decreased hydrolase activity of the bifunctional enzyme, SpoT. This observation suggests a novel mechanism by which *C. crescentus* may regulate its cell cycle in response to nitrogen availability. Our model also suggests that (p)ppGpp-associated stability of CtrA may be a result of reduced cdG activity due to the depletion of GTP. The dynamics of PTS^{Ntr} enzymes have not yet been measured experimentally, however our model predicts how they might behave under various levels of nitrogen availability. Intracellular glutamine, phosphoenolpyruvate (PEP), and pyruvate (Pyr) affect the phosphorylation state of PTS^{Ntr} enzymes in our model, which suggests that a stringent response to nutrient availability by guanine nucleotide-based second messengers may be enforced through both glutamine level and the concentrations of PEP and Pyr.

2.3 Methods

2.3.1 Diagram construction

Metabolism and characterization of c-di-GMP

The cellular concentration of cdG is regulated by its synthesis by diguanylate cyclases (DGCs) and its degradation by phosphodiesterases (PDEs) [33]. DGCs (like PleD and DgcB), whose activities reside in the highly conserved GGDEF domain, act as dimers to produce cdG from two GTP molecules [34]. cdG negatively regulates its own synthesis by allosterically binding with the I-site of DGCs to inhibit the synthetase activity [33].

PDEs (such as PdeA and PdeB) cleave cdG to linear diguanylate (pGpG) or to GMP, based on the conserved EAL domain or HD-GYP domain, respectively [34]. As pGpG is eventually converted into GMP (Fig. 2.3), we ignore pGpG in the model and consider two molecules of GMP as the product of cdG degradation. In addition, the activity of some PDEs in *C. crescentus* is activated by binding GTP [35]. The initial velocity of hydrolysis by PDEs reaches $V_{max}/2$ when the concentration of GTP is 4μM. Because GTP concentration in bacteria is much higher than 4μM [36, 37, 38], we assume PDEs are constantly saturated with GTP and do not include this interaction in our model.

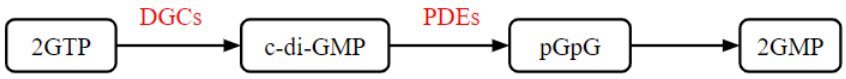

Figure 2.3: **Schematic diagram of cdG metabolism.**
DGCs catalyze the synthesis of cdG. PDEs cleave cdG into pGpG, which is subsequently cleaved to two molecules of GMP.

Metabolism and characterization of (p)ppGpp

(p)ppGpp accumulates in most bacteria under stressful conditions, such as nutrient starvation [31, 6]. In *C. crescentus*, (p)ppGpp delays the entry into S phase and the swarmer-to-stalked cell transition. This response gives *C. crescentus* an advantage in nutrient-deprived environments by maintaining its mobility to search for better environments and by delaying DNA replication to conserve energy [32]. *C. crescentus* utilizes the bifunctional enzyme SpoT, an RSH homologue, to catalyze the conversion between (GTP)GDP and (p)ppGpp [39, 6, 40] (Fig. 2.4, Fig. 2.5).

It has been reported that (p)ppGpp inhibits the synthesis of GMP and GDP through binding the corresponding synthetases, such as HPRT, GMK, and their homologues [41, 42]. The binding affinity of HPRT for pppGpp is $K_d = 3.38$ μM in *E. coli*, but only 0.24 μM in *C.*

crescentus [42]. We ignored this inhibition (Fig. 2.5) because the HPRT homologue should be saturated with basal levels of (p)ppGpp in bacteria (10-50 μM [32, 42]).

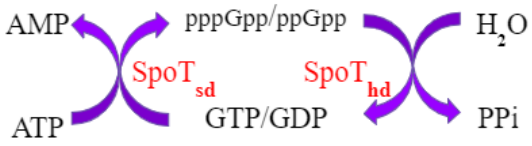

Figure 2.4: **Metabolism of (p)ppGpp.**
SpoT, a bifunctional enzyme in *C. crescentus*, catalyzes both the synthesis and hydrolysis of (p)ppGpp. $SpoT_{sd}$ and $SpoT_{hd}$ indicate the synthetase and hydrolase activity of SpoT, respectively.

Nitrogen phosphotransferase system

It has been well documented that (p)ppGpp responds to carbon and nitrogen deprivations [32, 39, 41]. While the specific mechanism underlying carbon starvation is not yet clear, the mechanism responsible for nitrogen starvation has been recently elucidated [31]. The accumulation of (p)ppGpp following nitrogen starvation is regulated by the nitrogen phosphotransferase system (PTS^{Ntr}) [31, 6].

The PTS^{Ntr} consists of three components (EI^{Ntr}, NPr, and $EIIA^{Ntr}$) which form a phosphorylation cascade (Fig. 2.5). The first protein EI^{Ntr} initiates the cascade through autophosphorylation using PEP as the phosphoryl donor. Then the phosphoryl group is transferred from EI^{Ntr} to NPr and then to $EIIA^{Ntr}$. This process is reversible, so three components exchange phosphate groups and reach a steady state. $EIIA^{Ntr}$ can transfer its phosphate group to other unknown molecules [43]. We assume that the rate of phosphoryl transfer from $EIIA^{Ntr}$ to these other molecules outside of the PTS^{Ntr} is far slower than the transfer rate among PTS^{Ntr} proteins and the exchange with PEP and pyruvate. Therefore, we do not consider to include a terminal phosphate sink in our model of the PTS^{Ntr}.

Glutamine binds to the conserved GAF domain of EI^{Ntr} (Fig. 2.6) to prevent its autophosphorylation. Because glutamine works as a powerful nitrogen signal, enzymes involved in the PTS^{Ntr} become highly phosphorylated under nitrogen starvation when the intracellular level of glutamine decreases rapidly [31]. The PTS^{Ntr} influences cdG dynamics by its effects on SpoT activity. Bacterial two-hybrid assays and mutant experiments [6] indicate that phosphorylated $EIIA^{Ntr}$ directly interacts with SpoT to inhibit its hydrolase activity, whereas phosphorylated NPr activates SpoT synthetase activity indirectly (Fig. 2.5). In this way, the PTS^{Ntr}, which senses nitrogen availability through glutamine, subsequently regulates SpoT activity and (p)ppGpp levels.

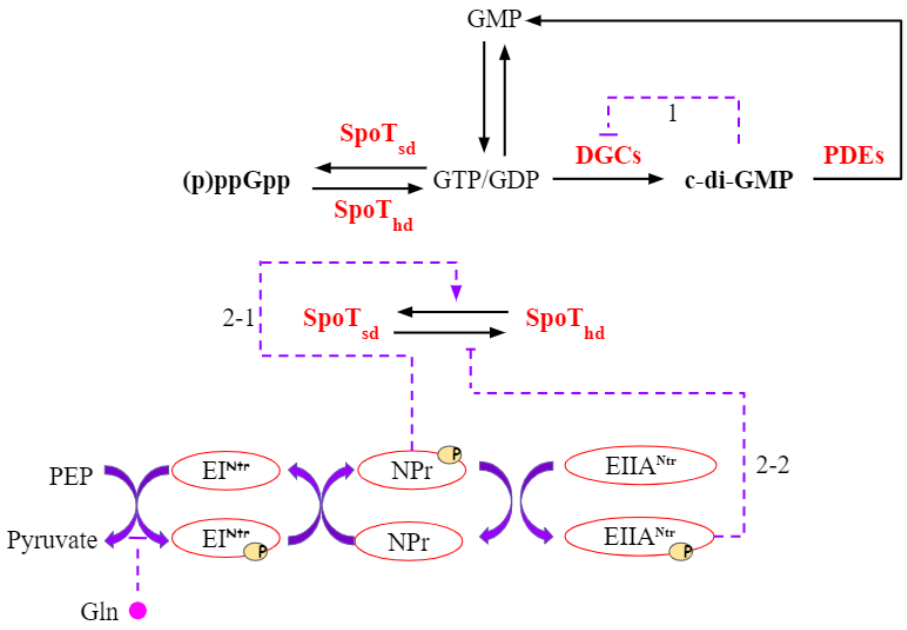

Figure 2.5: **Diagram of the second messenger regulatory network.** Glutamine (Gln) acts as the nitrogen signal, which regulates the phosphorylation state of PTS^{Ntr} enzymes. Solid black arrows represent conversion between molecular species. Solid purple lines indicate transfer of phosphoryl groups between species, where the phosphoryl transfer is reversible. Dashed lines represent allosteric influences on reaction rates (an arrow-head represents activation and a bar-head inhibition). Dashed line 1 indicates the product-inhibition based on cdG binding to the I-site of DGCs. Dashed line 2-1 indicates that phosphorylated NPr indirectly activates the synthase activity of SpoT, and dashed line 2-2 indicates that phosphorylated $EIIA^{Ntr}$ directly inhibits the hydrolase activity of SpoT.

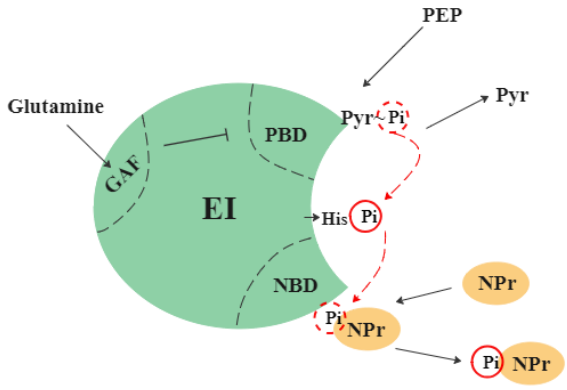

Figure 2.6: **Schematic diagram of EI$^{\mathrm{Ntr}}$ structure and phosphate transfer.** The C-terminus of EI$^{\mathrm{Ntr}}$ bears a PEP-binding domain (PBD) and the N-terminus is responsible for binding NPr (NBD). The red dashed arrows indicate the direction of phosphate transfer. The separate GAF domain senses nitrogen availability by binding glutamine, which inhibits phosphoryl group transferred from PEP to EI$^{\mathrm{Ntr}}$.

2.3.2 Mathematical model

Based on the diagram in Fig. 2.5, the reactions of our model are as follows.

The activity of DGCs is subject to the product inhibition through binding of cdG. As two cdG molecules bind allosterically to each DGC dimer, we assumed that cdG inhibition of DGC is a cooperative process. Thus we expressed the activity of [DGC] as a Hill function with a Hill exponent of 2 (Table 2.1, Equation (1)). Unlike DGCs, PDEs act as monomers, which convert cdG to pGpG or GMP [34]. pGpG is subsequently converted into GMP [31]. We assumed this reaction is very fast and ignored the intermediate pGpG.

$$2\,\mathrm{GTP} \xrightarrow{\mathrm{DGCs}} \text{c-di}-\mathrm{GMP} \xrightarrow{\mathrm{PDEs}} 2\,\mathrm{GMP}.$$

As GDP and GTP can be interconverted and their products, ppGpp and pppGpp, with similar behaviour [39, 44, 32], we lumped GDP and GTP into a single variable, 'GTP', and ppGpp and pppGpp are also condensed into one variable, (p)ppGpp. These 'variables' are interconverted by the synthetase and hydrolase activities of SpoT ($\mathrm{SpoT_{sd}}$ and $\mathrm{SpoT_{hd}}$, respectively). To take the direct and indirect effects of NPr∼P and EIIA$^{\mathrm{Ntr}}$ ∼P into consideration [45], we define a variable α (Table 2.1) as the synthetase:hydrolase ratio of SpoT.

$$(\mathrm{p})\mathrm{ppGpp} \underset{\mathrm{SpoT_{sd}}}{\overset{\mathrm{SpoT_{hd}}}{\rightleftharpoons}} \mathrm{GTP}.$$

The interconversion of GTP, GDP and GMP is described compactly in our mathematical

model by the reversible reaction

$$\mathrm{GTP} \underset{k_{\mathrm{s.GTP}}}{\overset{k_{\mathrm{d.GTP}}}{\rightleftharpoons}} \mathrm{GMP}.$$

PEP binds to the C-terminal domain of EI and donates a phosphoryl group to His-189 (Fig. 2.6). Then the phosphoryl group is transferred to the next two enzymes, NPr and $\mathrm{EIIA^{Ntr}}$, in sequence [46, 47]. Glutamine binds to an allosteric site of $\mathrm{EI^{Ntr}}$ (the GAF domain) [48] and inhibits phosphoryl transfer to His-189 [31, 49] (Fig. 2.6). The phosphorylation cascade is summarized by the following reactions:

$$\mathrm{EI} + \mathrm{PEP} \underset{\mathrm{k_{b_{-1}}}}{\overset{\mathrm{k_{b_1}}}{\rightleftharpoons}} \mathrm{EI^{PEP}},$$

$$\mathrm{EI^{PEP}} \underset{\mathrm{k_{-1}}}{\overset{\mathrm{k_1(inhibited\ by\ Gln)}}{\rightleftharpoons}} \mathrm{EI{\sim}P^{Pyr}},$$

$$\mathrm{EI{\sim}P^{Pyr}} \underset{\mathrm{k_{b_2}}}{\overset{\mathrm{k_{b_{-2}}}}{\rightleftharpoons}} \mathrm{EI{\sim}P} + \mathrm{Pyr},$$

$$\mathrm{EI{\sim}P_{tot}} + \mathrm{NPr} \underset{\mathrm{k_{-2}}}{\overset{\mathrm{k_2}}{\rightleftharpoons}} \mathrm{EI_{tot}} + \mathrm{NPr{\sim}P},$$

$$\mathrm{NPr{\sim}P} + \mathrm{EIIA} \underset{\mathrm{k_{-3}}}{\overset{\mathrm{k_3}}{\rightleftharpoons}} \mathrm{NPr} + \mathrm{EIIA{\sim}P}\,\cdot$$

where $\mathrm{EI{\sim}P_{tot}}$= $\mathrm{EI{\sim}P}$ + $\mathrm{EI{\sim}P^{Pyr}}$ and $\mathrm{EI_{tot}}$= EI + $\mathrm{EI^{PEP}}$. $\mathrm{EI^{PEP}}$ and $\mathrm{EI{\sim}P^{Pyr}}$ indicate EI bound with PEP and EI∼P bound with Pyr, respectively. $k_{\pm i}$ $(i = 1, 2, 3)$ are the rate constants of phosphorylation reactions, while $k_{b_{\pm j}}$ $(j = 1, 2)$ are the rate constants of binding reactions.

Here, we make several assumptions to describe $\mathrm{PTS^{Ntr}}$ reactions effectively:
(1) As PEP binding to EI is a rapid process [46, 50], we assumed that PEP and Pyr binding reactions are much faster than phosphorylation reactions (reaching quasi-steady state) [46]. Therefore, we converted the binding reactions into algebraic equations (Table 2.1, Equation (8, 9)).
(2) We assumed that EI∼P and $\mathrm{EI{\sim}P^{Pyr}}$ phosphorylate NPr at the same rate, but $\mathrm{EI^{Pyr}}$ is unstable and immediately dissociates into EI and Pyr. Similarly, we assumed that EI and $\mathrm{EI^{PEP}}$can be phosphorylated by NPr∼P, but $\mathrm{EI{\sim}P^{PEP}}$ is unstable and immediately dissociates into EI∼P and PEP.
(3) Since there is limited experimental data for the kinetic rate constants of the nitrogen PTS, we utilized experiments on the carbon PTS system to estimate these rate constants in our model. The kinetics of the carbon and nitrogen PTSs are likely very similar as they are homologues [51, 52].
(4) The total concentrations of $\mathrm{EI^{Ntr}}$, NPr and $\mathrm{EIIA^{Ntr}}$ are assumed to be constants [53]. We estimated the total concentrations to be: $[\mathrm{EI^{Ntr}}]_{\mathrm{T}} = 10\mu\mathrm{M}$, $[\mathrm{NPr}]_{\mathrm{T}} = 30\mu\mathrm{M}$, and $[\mathrm{EIIA^{Ntr}}]_{\mathrm{T}} = 30\mu\mathrm{M}$ [54, 55, 56].

The resulting mathematical model consists of seven ODEs and five algebraic equations (Table 2.1 and Appendix A.1). Parameters are defined in Table 2.2. Whenever possible, we estimated parameters from experimental data. Initial conditions in Table 2.3 were estimated from the intracellular concentrations in bacteria. The maximum concentration of cdG in *C. crescentus* is around 2.8μM [57]. The basal levels of (p)ppGpp and GTP in Gram-negative bacteria during normal conditions are around 50μM and 1000μM [36], respectively. The ratio of [(p)ppGpp] to [GTP] in *C. crescentus* varies from 0.15 to 1.9 under rich and limited nitrogen conditions [58, 59, 40]. We used these values to calibrate our model. The ODEs were solved in MATLAB with ode15s.

Table 2.1: Equations of the second messenger model.

(1) $$d[\mathrm{cdG}]/dt = k_{\mathrm{s.cdG}} \cdot [\mathrm{DGC}] \cdot \frac{K_1^2}{K_1^2+[\mathrm{cdG}]^2} \cdot \frac{[\mathrm{GTP}]^2}{[\mathrm{GTP}]^2+K_{\mathrm{m1}}^2} - k_{\mathrm{d.cdG}} \cdot [\mathrm{PDE}] \cdot \frac{[\mathrm{cdG}]}{[\mathrm{cdG}]+K_{\mathrm{m2}}}$$

(2) $$d[\mathrm{(p)ppGpp}]/dt = k_{\mathrm{s.(p)ppGpp}} \cdot \{\mathrm{SpoT_{sd}}\} \cdot \frac{[\mathrm{GTP}]}{[\mathrm{GTP}]+K_{\mathrm{m3}}} - k_{\mathrm{d.(p)ppGpp}} \cdot \{\mathrm{SpoT_{hd}}\} \cdot \frac{[\mathrm{(p)ppGpp}]}{[\mathrm{(p)ppGpp}]+K_{\mathrm{m4}}}$$

(3) $$d[\mathrm{GTP}]/dt = k_{\mathrm{s.GTP}} \cdot [\mathrm{GMP}] - k_{\mathrm{d.GTP}} \cdot [\mathrm{GTP}] - k_{\mathrm{s.(p)ppGpp}} \cdot \{\mathrm{SpoT_{sd}}\} \cdot \frac{[\mathrm{GTP}]}{[\mathrm{GTP}]+K_{\mathrm{m3}}}$$
$$+k_{\mathrm{d.(p)ppGpp}} \cdot \{\mathrm{SpoT_{hd}}\} \cdot \frac{[\mathrm{(p)ppGpp}]}{[\mathrm{(p)ppGpp}]+K_{\mathrm{m4}}} - 2 \cdot k_{\mathrm{s.cdG}} \cdot [\mathrm{DGC}] \cdot \frac{K_1^2}{K_1^2+[\mathrm{cdG}]^2} \cdot \frac{[\mathrm{GTP}]^2}{[\mathrm{GTP}]^2+K_{\mathrm{m1}}^2}$$

(4) $$d[\mathrm{GMP}]/dt = 2 \cdot k_{\mathrm{d.cdG}} \cdot [\mathrm{PDE}] \cdot \frac{[\mathrm{cdG}]}{[\mathrm{cdG}]+K_{\mathrm{m2}}} + k_{\mathrm{d.GTP}} \cdot [\mathrm{GTP}] - k_{\mathrm{s.GTP}} \cdot [\mathrm{GMP}]$$

(5) $$d[\mathrm{EI} \sim \mathrm{P}]_{\mathrm{tot}}/dt = k_1 \cdot \frac{K_4+\epsilon[\mathrm{Gln}]}{K_4+[\mathrm{Gln}]} \cdot [\mathrm{EI}^{\mathrm{PEP}}] - k_{-1} \cdot [\mathrm{EI} \sim \mathrm{P}^{\mathrm{Pyr}}]$$
$$-k_2 \cdot [\mathrm{EI} \sim \mathrm{P}]_{\mathrm{tot}}[\mathrm{NPr}] + k_{-2} \cdot [\mathrm{NPr} \sim \mathrm{P}][\mathrm{EI}]]_{\mathrm{tot}}$$

(6) $$d[\mathrm{NPr} \sim \mathrm{P}]/dt = k_2 \cdot [\mathrm{EI} \sim \mathrm{P}]]_{\mathrm{tot}}[\mathrm{NPr}] - k_{-2} \cdot [\mathrm{NPr} \sim \mathrm{P}][\mathrm{EI}]]_{\mathrm{tot}}$$
$$-(k_3 \cdot [\mathrm{NPr} \sim \mathrm{P}][\mathrm{EIIA}] - k_{-3} \cdot [\mathrm{NPr}][\mathrm{EIIA} \sim \mathrm{P}])$$

(7) $$d[\mathrm{EIIA} \sim \mathrm{P}]/dt = k_3 \cdot [\mathrm{NPr} \sim \ \mathrm{P}][\mathrm{EIIA}] - k_{-3} \cdot [\mathrm{NPr}][\mathrm{EIIA} \sim \mathrm{P}]$$

(8) $$[\mathrm{EI}][\mathrm{PEP}] = K_{\mathrm{d_1}} \cdot [\mathrm{EI}^{\mathrm{PEP}}]$$

(9) $$[\mathrm{EI} \sim \mathrm{P}][\mathrm{Pyr}] = K_{\mathrm{d_2}} \cdot [\mathrm{EI} \sim \mathrm{P}^{\mathrm{Pyr}}]$$

(10) $$[\mathrm{EI}]_{\mathrm{T}} = [\mathrm{EI}]+[\mathrm{EI}^{\mathrm{PEP}}]+[\mathrm{EI} \sim \mathrm{P}^{\mathrm{Pyr}}] + [\mathrm{EI} \sim \mathrm{P}]$$

(11) $$[\mathrm{NPr}]_{\mathrm{T}} = [\mathrm{NPr}] + [\mathrm{NPr} \sim \mathrm{P}]$$

(12) $$[\mathrm{EIIA}]_{\mathrm{T}} = [\mathrm{EIIA}] + [\mathrm{EIIA} \sim \mathrm{P}]$$

* $\mathrm{SpoT_{sd}} = \frac{\alpha}{1+\alpha}$, $\mathrm{SpoT_{hd}} = \frac{1}{1+\alpha}$,$\alpha = K_{\mathrm{SpoT}} \cdot \frac{\mathrm{NPr}\sim \mathrm{P}}{\mathrm{NPr}\sim \mathrm{P}+K_2} / \frac{K_3}{\mathrm{EIIA}\sim\mathrm{P}+K_3}$. $\{\mathrm{SpoT_{sd}}\}$ and $\{\mathrm{SpoT_{hd}}\}$ represent the fraction of total SpoT for synthetase and hydrolase, respectively.

Table 2.2: Parameters of the second messenger model.

parameter	description	source
$k_{\mathrm{s.cdG}} = 33.5/\mathrm{min}$	scaled synthesis rate of cdG	this study
$k_{\mathrm{d,cdG}} = 100/\mathrm{min}$	scaled degradation rate of cdG	this study
$K_1 = 0.5\mu\mathrm{M}$	dissociation constant for product inhibition	[60]
K_{m1}=1500μM	binding affinity of GTP	this study
$K_{\mathrm{m2}} = 0.06\mu\mathrm{M}$	binding affinity of cdG	[60]
[DgcB]=0.7μM	scaled DgcB level	[61]
[basal PDEs]=0.2μM	scaled basal PDE level	this study
$k_{\mathrm{s.(p)ppGpp}} = 170\mu\mathrm{M}/\mathrm{min}$	synthesis rate of (p)ppGpp	this study
$k_{\mathrm{d.(p)ppGpp}} = 160\mu\mathrm{M}/\mathrm{min}$	degradation rate of (p)ppGpp	this study
$K_2 = 75\mu\mathrm{M}$	binding affinity of NPr∼P	this study
$K_3 = 10\mu\mathrm{M}$	dissociation constant of EIIA∼P	this study
$K_{\mathrm{SpoT}} = 4$	constant of SpoT activity	this study
$K_{\mathrm{m3}} = 1000\mu\mathrm{M}$	binding affinity of GTP	this study
$K_{\mathrm{m4}} = 2000\mu\mathrm{M}$	binding affinity of (p)ppGpp	this study
$K_4 = 75.63\mu\mathrm{M}$ $\epsilon = 0.1$	parameters of glutamine inhibition	[62]
$k_{\mathrm{s.GTP}} = 1500/\mathrm{min}$	synthesis rate of GTP	this study
$k_{\mathrm{d.GTP}} = 100/\mathrm{min}$	degradation rate of GTP	this study
$[\mathrm{EI}]_{\mathrm{T}} = 10\mu\mathrm{M}$ $[\mathrm{NPr}]_{\mathrm{T}} = 30\mu\mathrm{M}$ $[\mathrm{EIIA}]_{\mathrm{T}} = 30\mu\mathrm{M}$	total enzymes levels	[54, 55, 56]
$k_1 = 52.4/\mathrm{min}$ $k_{-1} = 67.2/\mathrm{min}$	phosphotransfer constants	this study, [62, 47]
$k_{\pm 2} = 1.2 \times 10^4/(\mathrm{min} \cdot \mu\mathrm{M})$ $k_{\pm 3} = 3.7 \times 10^3/(\mathrm{min} \cdot \mu\mathrm{M})$		[53, 47]
$K_{\mathrm{d1}} = \frac{k_{b_{-1}}}{k_{b_1}} = 350\mu\mathrm{M}$ $K_{\mathrm{d2}} = \frac{k_{b_{-2}}}{k_{b_2}} = 670\mu\mathrm{M}$	dissociation constants	[47]

Table 2.3: Initial Conditions of the second messenger model.

Variables	Initial Conditions (μM)
c-di-GMP	0.3
GTP	1300
(p)ppGpp	100
GMP	20
EI∼P	10
NPr∼P	30
EIIA∼P	30

2.4 Simulations and results

2.4.1 Oscillations of DGCs and PDEs

Two well-known DGCs in *C.crescentus* are DgcB and PleD [61, 57]. DgcB level stays constant over the cell cycle, while the concentration and activity of PleD vary [61]. Hence, we model [DGC] as the sum of constant [DgcB] and variable [PleD]. Because experimental data on the fluctuation of active (phosphorylated) PleD over the course of the *C. crescentus* cell cycle is not available, we used the total PleD fluctuation as a substitute. Fig. 2.7A shows immunoblot measurements (red dots) of total PleD, extracted by ImageJ from Abel et al [61] and the corresponding curve fitted by MATLAB (R-square is 0.66). It appears that the second data point from Abel et al [61] is inaccurate because PleD activity should peak around t=20, since cdG needs to be produced at a high level at this time to deplete active CtrA and initiate the G1-to-S transition. Assuming that the second experimental point is an error, we re-fit the total PleD without this point (Fig. 2.7B, R-square is 0.84). In agreement with our expectations, the fitted curve in Fig. 2.7B increases during G1-to-S transition and peaks around 30 min. The corresponding accuracy of curve fitting improves as well. Additionally, we borrowed the active PleD simulation of a mathematical model proposed by Weston et al [22] (Fig. 2.7C, magenta curve) which captures the dynamics of phosphorylation of PleD. Weston's simulation of PleD∼P (Fig. 2.7C) shows a similar trend with the experimental data and re-fitted curve of total PleD (Fig. 2.7B,C), which serves to justify our methods for calibrating a curve for PleD activity. The different scaled levels between Weston's simulation and experimental points are due to different normalization methods.

While PdeA is the most active phosphodiesterase enzyme in *C. crescentus* [63], other PDEs, including PdeB, PdeC, and PdeD, have been identified in bacterial species *B. subtilis*, *E. coli* and *L. monocytogenes* [64]. Assuming there are other PDEs in *C. crescentus* as well, we represented total [PDE] in our model as the sum of [basal PDE] plus a variable [PdeA] estimated by the curve-fitting tool in MATLAB applied to quantitative PdeA measurements derived

from Western blots of Abel et al [65] using ImageJ. The PdeA points and the corresponding curve are shown in Fig. 2.7D with R-square being 0.77.

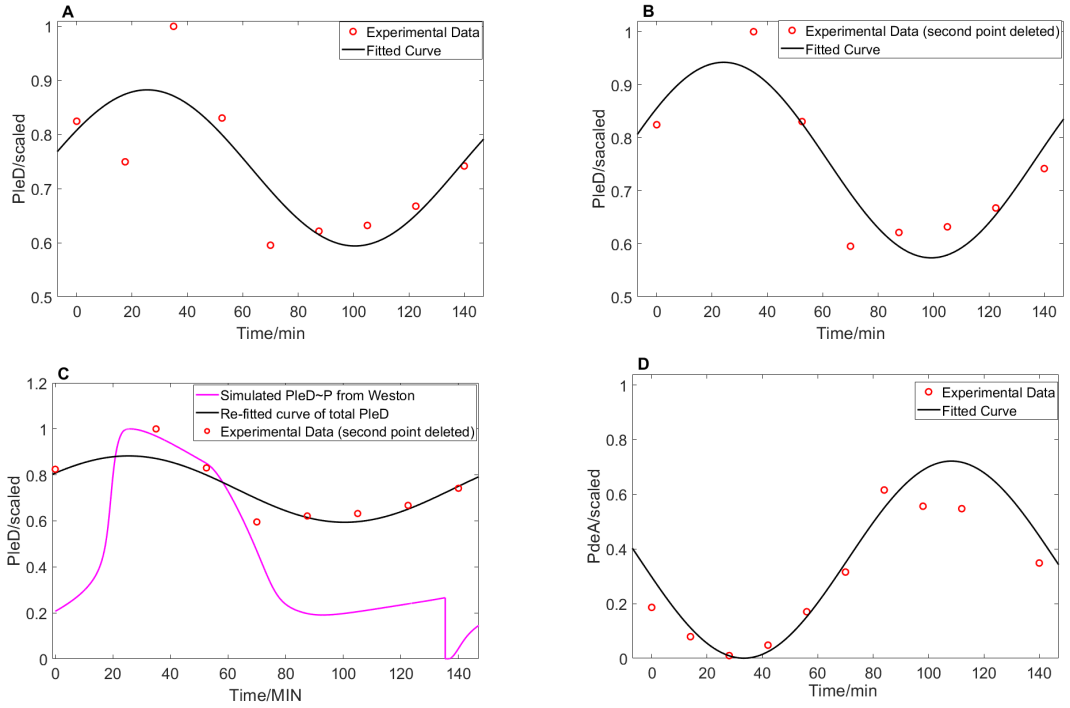

Figure 2.7: **Curve-fitting of PleD and PdeA data.**
(A). Original experimental data of total PleD [61] and a curve fitted to the data by MATLAB. Function is $0.1442\times\sin(\frac{\pi}{75}t+0.5037)+0.7384$. (B). Refitted PleD curve after deleting the second data point. New function is $0.1834\times\sin(\frac{\pi}{75}t+0.5587)+0.7579$. (C). Weston's simulation [22] of phosphorylated PleD and comparison with re-fitted curve and experimental data from B. (D). Experimental measurements of PdeA[66] and its fitted curve. Function is -0.3605$\times$ $\sin(\frac{\pi}{75}t+0.1767)+0.361$.

2.4.2 Oscillation of c-di-GMP over the cell cycle in *C. crescentus*

We used experimental data of cdG concentration (peak point) [57] and bacterial nucleotide concentrations to estimate parameters that are not available in publications. Experimentally, cdG peaks at the swarmer-to-stalked transition ($\approx 0.28\mu$M) and then decreases until reaching the lowest value ($<0.1\mu$M) in the swarmer cell after cell division. Our simulation of cdG over time fits experimental data well and shows a stable oscillation through the cell cycle under nutrient-rich conditions (Fig. 2.8), in agreement with experimental data [57].

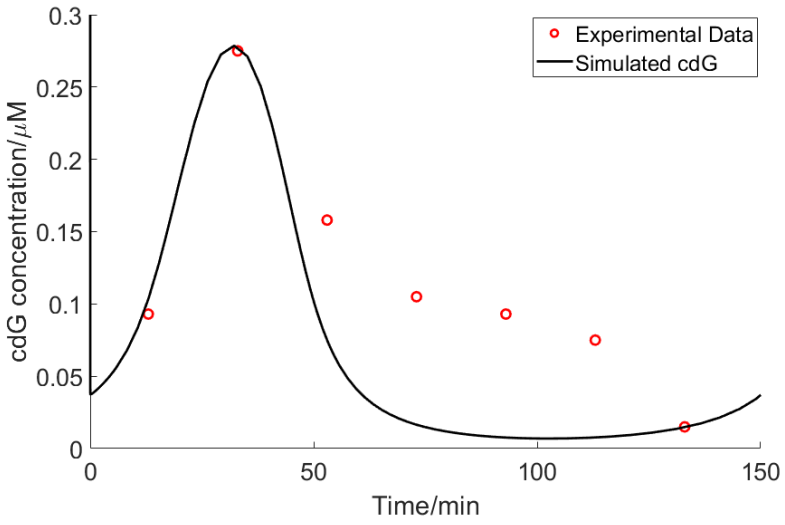

Figure 2.8: **c-di-GMP oscillates during the swarmer cell cycle.**
Red circles indicate experimental data of c-di-GMP in a single *C. crescentus* wild-type cell during one cell cycle [57]. Black line indicates the simulated c-di-GMP in a swarmer cell at Gln=10000μM, PEP=300μM, and Pyr=1500μM.

2.4.3 Comparison of simulated PTS$^{\mathrm{Ntr}}$ to carbon-PTS experimental data

PTS and PTS$^{\mathrm{Ntr}}$ have a lot in common. Enzymes of PTS$^{\mathrm{Ntr}}$ (EI$^{\mathrm{Ntr}}$, NPr, and EIIA$^{\mathrm{Ntr}}$) are homologues of carbon-PTS enzymes (EI, HPr, and EIIA/B/C) [51]. They have similar structures and play parallel roles in nutrient uptake. In addition, these PTSs communicate with each other by phosphate exchange [48, 67]. PEP acts as the phosphoryl donor for both carbon and nitrogen PTSs. There are two significant differences between these systems [48]: (1) Enzymes II in PTS (juxtamembrane EIIB and transmembrane EIIC) assist in the transmembrane transport of sugars [68] whereas PTS$^{\mathrm{Ntr}}$ does not aid in sugar transport [52]. (2) PTS$^{\mathrm{Ntr}}$ is regulated by glutamine levels as part of the nitrogen signaling pathway in prokaryotes, while PTS senses carbon sources in the environment through regulating transport and phosphorylation of carbohydrates like glucose [54, 68].

There is limited quantitative data for PTS$^{\mathrm{Ntr}}$ in publications. Based on the similarities between PTS$^{\mathrm{Ntr}}$ and PTS, we introduced some parameters obtained from PTS experiments to simulate PTS$^{\mathrm{Ntr}}$ [47, 53] (Tabel 2.2). In order to calibrate the PTS$^{\mathrm{Ntr}}$ model, we set [Gln] to 0 and compared simulations with carbon PTS experiments.

Kundig and Roseman [69, 46] measured how EI and HPr levels affect phosphorylation of PTS quantitatively (Table 2.4). We set our initial conditions to the experimental conditions of the paper, substituting [Npr] and [EI$^{\mathrm{Ntr}}$] for [Hpr] and [EI], respectively. As there is

no information about pyruvate concentrations in their experiments, we estimated the [Pyr] based on one set of experimental data in Table 2.4. The Table indicates that our PTS^{Ntr} simulations fit the experimental data well.

Table 2.4: Effect of EI and HPr (NPr) concentrations on phosphorylation of EI and HPr (NPr) in PTS system.

Condition		Experiment*[69]	Simulation
EI(μM)	HPr(NPr)(μM)	EI$\sim$P+HPr$\sim$P(μM)	EI$\sim$P+NPr$\sim$P(μM)
0.157	24.4	6	6.8
0.3125	24.4	6.5	6.9
0.729	24.4	7	7**
1.57	24.4	7.5	7.2
0.729	0	>0***	0.2
0.729	12.2	3	3.6
0.729	36.6	9.1	10.5

* PEP=160μM.

** This row has been used to estimate Pyr level; Pyr=48.5μM.

*** Too small to recognize the specific value from the original figure [69].

2.4.4 Simulations under different nutrients conditions

Goodwin et al [62] measured quantitatively how glutamine inhibits EI^{Ntr} activity. In Table 2.5, we show model simulations under a range of glutamine levels. Lee et al [70] showed that cellular glutamine in *E. coli* is very low under nitrogen-starvation and increases to more than 10000μM when environmental ammonium is increased. Therefore, in our simulations, we used [Gln]=1μM to represent limited nitrogen and [Gln]=10000μM to describe abundant nitrogen.

PEP, the phosphoryl donor of PTS^{Ntr}, is an important indicator of carbon availability [71]. However, Osanai et al [72] and Yuan et al [73] showed that PEP and Pyr levels are stable under nitrogen shifts. Hogema et al [74] measured intracellular PEP and Pyr in *E. coli* under different carbon conditions: cells were initially grown in minimal medium (ammonia with limited carbon) and had PEP and pyruvate concentrations of 2800μM and [Pyr]=900μM, respectively. After adding 10mM glucose to the medium (now ammonia with high carbon), PEP and pyruvate concentrations shifted to 300μM and 1500μM, respectively. In consideration of this experimental data, we set '[PEP]=300μM, [Pyr]=1500μM, [Gln]=10000μM' to represent 'ammonia with high carbon'; and '[PEP]=300μM, [Pyr]=1500μM, [Gln]=1μM' to represent 'nitrogen-starved' condition. As cells require carbon and nitrogen to synthesize glutamine, we regard limited glutamine (proposed as 1000-2000μM in Table 2.5) and

'[PEP]=2800μM and [Pyr]=900μM' as 'ammonia with limited carbon'.

Table 2.5: Simulations under different nutrient conditions.

	[Gln]	10000μM	2000μM	1000μM	100μM	10μM	1μM
	cdG range	**0.01-0.28** *	0.01-0.26	0.01-0.25	0-0.09	0-0.03	**0-0.02** **
	(p)ppGpp (μM)	**118**	150	187	582	895	**939**
	GTP (μM)	**1221**	1192	1156	787	493	**452**
[PEP]=300μM	$\frac{[(p)ppGpp]}{[GTP]}$	**0.10**	0.13	0.16	0.74	1.8	**2.1**
[Pyr]=1500μM	GMP (μM)	**81**	79	77	52	33	**30**
	EI $\sim$ P (μM)	**0.5**	0.6	0.8	2.0	3.2	**3.4**
	NPr $\sim$ P (μM)	**1.6**	1.9	2.4	6.1	9.5	**10.2**
	EIIA $\sim$ P (μM)	**1.6**	1.9	2.4	6.1	9.5	**10.2**
	cdG range	0.01-0.20	**0.01-0.17** ***	**0.01-0.13** ***	0-0.02	0-0.01	0-0.01
	(p)ppGpp (μM)	294	**371**	**458**	993	1160	1178
	GTP (μM)	1056	**984**	**902**	401	244	227
[PEP]=2800μM	$\frac{[(p)ppGpp]}{[GTP]}$	0.28	**0.38**	**0.51**	2.5	4.8	5.2
[Pyr]=900μM	GMP (μM)	70	**66**	**60**	27	16	15
	EI $\sim$ P (μM)	1.1	**1.4**	**1.6**	3.7	5.2	5.4
	NPr $\sim$ P (μM)	3.4	**4.2**	**4.9**	11.1	15.6	16.3
	EIIA $\sim$ P (μM)	3.4	**4.2**	**4.9**	11.1	15.6	16.3

* Proposed to be under condition of ammonia with high carbon.
** Proposed to be under condition of nitrogen starvation.
*** Proposed to be under condition of ammonia with limited carbon.

Table 2.5 summarizes the results of our simulations. cdG oscillations peak at 0.28μM under 'ammonia with high carbon', and peak at 0.02μM under nitrogen depletion. These results suggest that depletion of nitrogen should result in cell cycle arrest, which is consistent with experimental observations [75]. In general, as glutamine concentrations decrease, cdG, GTP and GMP levels decrease while (p)ppGpp levels increase.

When we simulate conditions of 'ammonia with limited carbon', we find that cdG oscillations decrease in amplitude; however, concentrations are presumably not so low to induce cell cycle arrest. Thus, our results are consistent with the fact that *C. crescentus* continues to grow under such conditions [74]. Interestingly, our results suggest that (p)ppGpp levels should increase when decreasing carbon availability. Our results suggest that shifts in PEP and pyruvate concentrations due to limiting carbon availability will make the cell more sensitive to shifts in nitrogen. Table 2.5 suggests, that shifts in the direction of increased [PEP] and decreased [Pyr] favor increased activity in SpoT synthetase. Based on steady state analysis of ODEs in our model, phosphorylation of PTS^{Ntr} proteins depends non-linearly on the [PEP]:[Pyr] ratio (Appendix A2). Increases in the ratio generally trend towards SpoT synthetase activity, while decreases trend toward hydrolase activity.

Our simulations show that the shift of c-di-GMP and (p)ppGpp levels in response to changes of nutrients is due to both a shift in internal glutamine concentration and an adjustment to the PEP and pyruvate levels (Table 2.5). Our model suggests that the PEP and Pyr levels regulating PTS^{Ntr} is one potential pathway of (p)ppGpp response to carbon availability. Enzymes within the PTS^{Ntr} system become highly phosphorylated under nitrogen starvation (Table 2.5), which is consistent with the existing qualitative analysis as well [31]. Additionally, our simulation fits the experimental observations (Table 2.6) well.

Table 2.6: Experimental information for concentrations and changes under starvation.

Variables	Nutrient-rich	Nutrient-starved	Species	Reference
(p)ppGpp	50μM	-	*E.coli*	[32]
	10-30μM	millimolar	*B.subtilis*	[42]
GTP	900μM	-	*E.coli*	[37]
	-	3-fold drop (arginine starved)	*B.subtilis*	[41]
	1000-3000μM	-	*B.subtilis*	[38]
	-	3-fold drop (glucose starved)	marine *Vibrio*	[76]
GDP	100μM	-	*E.coli*	[37]
	-	14-fold drop (arginine starved)	*B.subtilis*	[41]
GMP	24μM	-	*E.coli*	[77]
[pppGpp]:[GTP] ratio	≈0.1	≈0.3 (arginine starved)	*B.subtilis*	[58]
	0.08	-	*E.coli*	[78]
[ppGpp]:[GTP] ratio	≈0.25	≈1.2 (arginine starved)	*B.subtilis*	[58]
	0.16	-	*E.coli*	[78]
	≈0.1	≈1.5 (arginine starved) ≈2.5 (glucose starved)	*C.crescentus*	[40]

Response to environmental change

Given the oligotrophic environments *C. crescentus* populates, we postulate that *C. crescentus* would have to respond rapidly to sudden shifts in nutrients in order to increase its fitness in these environments. Fig. 2.9 shows how *C. crescentus* responds to environmental nitrogen-shifts in our simulation. The response time for starvation is within one cell replication cycle, which means *C. crescentus* can respond to nutrient deprivation quickly according to our model. Perhaps even more importantly, our model suggests that *C. crescentus* also recovers quite quickly to normal cell cycle oscillations when we reset glutamine to the starting value. A response within the time frame of one cell cycle would be a useful characteristic for *C. crescentus* to survive in oligotrophic environments.

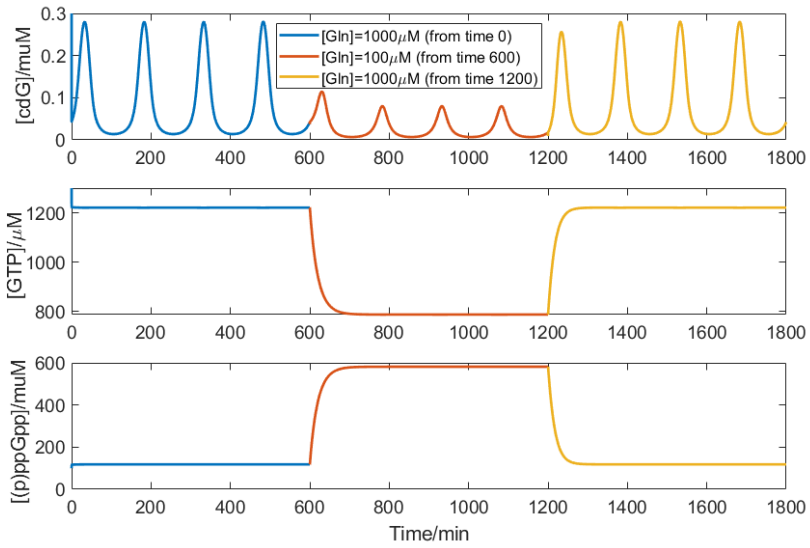

Figure 2.9: **Response to nitrogen-shifts in our simulation.**
Blue line indicates simulated levels of cdG, GTP, and (p)ppGpp when [Gln]=10000μM. Red line indicates simulated levels of these three molecules when glutamine changes to 100μM at simulation time 600. Yellow line indicates the simulation when the glutamine recovers to 10000μM. The end point of previous simulation is used to be the initial point of the following simulation at a different glutamine level.

2.5 Discussion

Progression through the cell cycle in *C. crescentus* requires precise coordination of metabolic and morphological events. The guanine nucleotide-based second messenger network, including cdG and (p)ppGpp, plays significant roles in regulating bacterial morphology and metabolism, such as controlling the activity of CtrA and adapting bacteria to environmental changes. In this study, we proposed a mathematical model to simulate the guanine nucleotide-based second messenger network, and investigated how this network responds to nutrient shifts through PTS^{Ntr}.

We calibrated our model using experimental data, and investigated two aspects influencing phosphorylation of PTS^{Ntr} in simulations: 1) glutamine levels, which affects autophosphorylation of EI^{Ntr} [48, 31]; and 2) PEP and Pyr levels, which influence the flux of phosphorus through the PTS^{Ntr} system (Table 2.5, Appendix A2).

Simulations of nitrogen deprivation suggest that as (p)ppGpp accumulates in *C. crescentus*, GTP and cdG concentrations decrease significantly as a result of increasing SpoT synthetase activity. While it is suggested that (p)ppGpp stabilizes CtrA in *C. crescentus* [79], the exact mechanism is unknown. As cdG is essential for CtrA proteolysis, the stability of CtrA may increase due to diminished cdG concentration as a result of SpoT synthetase activity, rather than downstream effects of (p)ppGpp signaling. Thus, we propose that *C. crescentus* may respond to nitrogen starvation by stimulating the PTS^{Ntr} system to induce SpoT synthetase activity, resulting in depletion of GTP and cdG levels to induce cell cycle arrest via stabilization of the chromosome replication inhibitor, CtrA.

Importantly, our results also suggest that changes to intracellular concentrations of PEP and pyruvate can have a significant impact on SpoT activity. We find that shifts in PEP and pyruvate concentrations in response to decreased sugar availability result in an increase in SpoT synthetase activity and an increase in sensitivity to shifts in glutamine concentration. Thus, two potential avenues to influence the PTS^{Ntr} and SpoT are through adjusting PEP and pyruvate levels as well as glutamine.

Chapter 3

Modeling the temporal dynamics of master regulators and CtrA proteolysis in *Caulobacter crescentus* cell cycle

Chunrui Xu[1], Henry Hollis[3], Michelle Dai[3], Xiangyu Yao[1], Layne T. Watson[2], Yang Cao[2], Minghan Chen[3]

1 Genetics, Bioinformatics, and Computational Biology, Virginia Tech, Blacksburg, Virginia, United States of America
2 Department of Computer Science, Virginia Tech, Blacksburg, Virginia, United States of America
3 Department of Computer Science, Wake Forest University, Winston-Salem, North Carolina, United States of America

3.1 Abstract

The cell cycle of *Caulobacter crescentus* involves the polar morphogenesis and an asymmetrical cell division driven by precise interactions and regulations of proteins, which makes *Caulobacter* an ideal model organism for investigating bacterial cell development and differentiation. The abundance of molecular data accumulated on *Caulobacter* motivates system biologists to analyze the complex regulatory network of cell cycle via quantitative modeling. In this paper, We propose a mathematical model to accurately characterize the underlying

mechanisms of cell cycle regulation based on the study of: **a)** chromosome replication, methylation and transcription; **b)** interactive pathways of five master regulatory proteins including DnaA, GcrA, CcrM, CtrA, and SciP, as well as novel consideration of their corresponding mRNAs; **c)** cell cycle-dependent proteolysis of CtrA through a hierarchical assembly of protease complex. The temporal dynamics of our simulation results can closely replicate an extensive set of experimental observations and capture the main phenotype of seven mutant strains of *Caulobacter crescentus*. Collectively, the proposed model can be used to predict phenotypes of other mutant cases, especially for nonviable strains which are hard to cultivate and observe. Moreover, the module of cyclic proteolysis is an efficient tool to study the metabolism of proteins with similar mechanisms.

3.2 Introduction

Caulobacter crescentus (*C. crescentus*) is a model organism for exploring cell development and cell cycle regulation in prokaryotes. *C. crescentus* undergoes an asymmetrical cell division producing two distinct progenies: a sessile stalked cell equipped with a stalk and a motile swarmer cell equipped with a flagellum (Fig 3.1). While the stalked cell immediately initiates chromosome replication and enters the next cell cycle, the swarmer cell searches for suitable environments and differentiates into a stalked cell (sw-to-st transition) before entering the cell cycle replication [80]. The dimorphic lifestyle makes *C. crescentus* feasible to survive in oligotrophic waters.

The timed asymmetrical cell progression of *C. crescentus* is highly regulated by a cell cycle-dependent regulatory network including four master regulators - DnaA, GcrA, CtrA, and CcrM [81, 82]. DnaA, GcrA, and CtrA are transcriptional factors that control over 200 cell cycle-regulated genes in *C. crescentus*. These proteins form a loop to control each other. DnaA activates *gcrA* expression, GcrA regulates the expression of *ctrA* and *dnaA*, and CtrA in turn influences the transcription of *dnaA* [20, 83, 84]. Furthermore, DnaA is a conserved DNA replication initiator, activating replication by binding directly with the chromosome origin (*Cori*) [85]. In addition, there are five binding sites for CtrA on *Cori*, where replication initiation is suppressed when being bound by the phosphorylated form of CtrA (CtrA$\sim$P) [20]. CcrM, a conserved methyltransferase, is turned on at the completion of DNA replication to fully methylate the motif GANTC, which is carried by promoters of *ctrA*, *dnaA*, and *ccrM* (see Fig 3.2) [79, 86]. The short window of CcrM allows the maintenance of hemimethylated chromosome during replication, ensuring the robustness of cell cycle development. Moreover, CcrM has been reported to influence the expressions of more than 10% genes [19, 79]. Among these CcrM-regulated genes, more than 100 genes are likely influenced by a GANTC motif-dependent pathways, while the mechanisms of the rest genes are not clear [79]. Here, we take the CcrM-dependent methylation of GANTC motif into the regulatory network. Additionally, SciP is an antagonist of CtrA which is instrumental in cell cycle regulations but receives little attention. SciP spatiotemporally

represses the transcription of CtrA-induced genes because most of these genes contain a SciP binding site upstream of a CtrA binding site in their promoters [81].

A wealth of experimental data for cell cycle-regulated genes and proteins in *C. crescentus* have been accumulated in last decade [87, 88]. System biologists have proposed different quantitative models to analyze underlying mechanisms and pathways of cell cycle regulation. For example, Li *et al.* [20, 89] quantitatively modeled the interactions between CtrA, DnaA, GcrA, and CcrM and studied the simulated behaviors of some mutants. Murray *et al.* [19] proposed a simplified model incorporating CtrA, CckA, and GcrA to capture the cell cycle features of *C. crescentus* and predict the behaviors of $\Delta gcrA$ cells. However, the proteolysis of CtrA is not explicitly modeled. Li *et al.* [20, 89] borrowed DivK while Murray *et al.* [19] used CckA to describe the proteolysis of CtrA; but both DivK and CckA are indirect factors influencing the proteolysis of CtrA through phosphorelay pathways [90]. There are a series of models working on the spatial regulatory networks in *C. crescentus*. Li et al. investigated the spatial regulations focusing on CtrA in a stochastic model [91], which preliminarily revealed roles of spatial phosphorylation on the asymmetrical cell cycle in *C. crescentus*. Further, Chen et al. [92] and Xu et al. [93] proposed spatial models for the scaffolding protein PopZ in *C. crescentus*, which complemented Li et al.'s model [91] about the initial localization factors. Although previous mathematical models revealed some mechanisms of *Caulobacter* cell development, the mRNA abundance and transcription process based on master regulators have yet been explicitly investigated. Additionally, there is no mathematical model describing the cyclic proteolysis of master regulator CtrA, which plays important roles for cell development especially for the sw-to-st transition [27].

In this paper, we focus on five core components–DnaA, GcrA, CtrA, CcrM, and SciP that control over 90% of cell cycle-regulated genes, and propose a mathematical model that considers the regulation of DNA replication, methylation, and transcription, as well as the gene-protein and protein-protein interactions. Since CtrA is essential in the cell cycle regulation and its proteolysis is distinctively and spatiotemporally regulated, we construct a hierarchical ClpXP complex network for the proteolysis reactions, which is then integrated into the entire model. The simulated dynamics of mRNA and proteins are consistent with experimental observations. The ClpXP complex model can be used as a quantitative analysis tool to simulate other cyclic proteolysis in *C. crescentus*, such as the proteolysis of ShkA and TacA [94, 95].

3.3 Materials and methods

3.3.1 Model description

The regulatory network of bacterial cell cycle includes a series of complex mechanisms, such as genetic regulations, degradations, phosphorylation, dephosphorylation, and so on. The

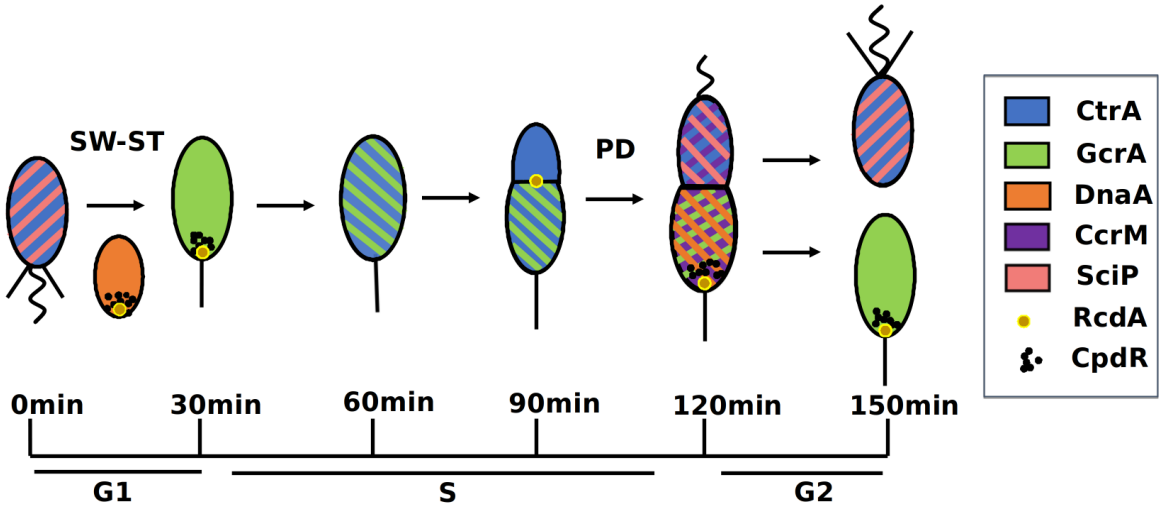

Figure 3.1: **The asymmetrical cell cycle of *C. crescentus* with spatial distribution of regulators.**
C. crescentus cell grows in G1, replicates DNA in S phase, and prepares for cell division in G2 phase. The predivisional (PD) cell divides asymmetrically into two different progenies: motile swarmer (SW) cell and non-motile stalked cell (ST). The dynamics of CtrA, GcrA, DnaA, CcrM, SciP, RcdA, and CpdR is indicated by color during each stage of the cell cycle.

details of the complex regulatory network will be described in the following.

Module 1: The core regulatory network of cell cycle. The master regulatory network of *C. crescentus*, as summarized in Fig 3.3, is composed of DnaA (*dnaA*), GcrA (*gcrA*), CtrA (*ctrA*), CcrM (*ccrM*), and SciP (*sciP*). Specifically, DnaA promotes the expression of *gcrA*, while GcrA inhibits DnaA and activates one of the promoters (P1) of CtrA [85]. Conversely, CtrA∼P suppresses the initiation of DNA replication [96], activates the transcription of *dnaA* [20], inhibits the activity of P1, and activates itself through another promoter (P2) [82]. The accumulation of CtrA promotes the expressions of *ccrM* and *sciP*, where CcrM controls the methylation state of P1 of *ctrA* [97]. SciP downregulates CtrA and CcrM [81]. The regulatory network of the five master proteins and mRNAs governs cell cycle-regulated genes, thereby driving the cell cycle progression [87].

In normal cell cycle progression, active CtrA (phosphorylated form, blue color in Fig 3.1) is cleared during the sw-to-st transition; CtrA concentrations are generally low in stalked cells when the Z-ring is closed [98]. The activity of CtrA is controlled by synthesis, degradation, and phosphorylation, the latter of which is driven by the CckA-dependent pathway [27, 99] (Fig 3.3). As CckA∼P is the only known phosphoryl donor of CtrA [90], we involve the CckA-dependent phosphotransfer into our model. CtrA proteolysis depends on a particular protease complex comprising the protease ClpXP and four additional adaptors–CpdR, RcdA, PopA, and c-di-GMP (cdG) [27]. While the protease ClpXP presents throughout the entire

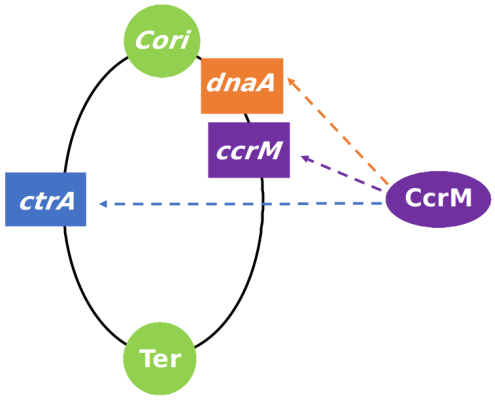

Figure 3.2: **Methylation site locations of different genes on *C. crescentus* chromosome.**
The elliptical curve represents the DNA fork in replication. *Cori* is the origin of DNA replication and *Ter* is the termination site. The CcrM methylation site is located upstream of the *dnaA*, *ccrM* and *ctrA* genes, represented as rectangles.

cell cycle, RcdA and CpdR co-localize at the stalked pole during sw-to-st transition and stay in the predivisional cell's stalked compartment (gold and black circles in Fig 3.1) [100]. The phosphorylation of CpdR is also regulated by CckA, thus CckA regulates the activity of CtrA through both phosphorylation and proteolysis. Additionally, CtrA controls the expression of RcdA and CpdR in *C. crescentus*.

Module 2: Cell cycle-dependent proteolysis of CtrA. The stability and activity of proteins strictly regulate cell cycle processes. Accordingly, proteolysis plays a significant role in cell development and response to internal/external stimuli [24, 27]. ClpXP, a highly conserved protease, is responsible for the proteolysis of a wide range of proteins including CtrA in *C. crescentus* [27]. Many substrates of ClpXP are cell cycle-regulated. Although ClpXP levels do not change significantly throughout the cell cycle, it requires additional cell cycle-dependent adaptors to cyclically degrade proteins [27]. Substrates of ClpXP-based proteolysis require different classes of protease complex assemblies [29]. A few substrates, such as PdeA, only require ClpXP primed by unphosphorylated CpdR; we name this type of substrates as the first class substrate. Similarly, the second class substrates require primed ClpXP additionally with RcdA assembled; and the third class substrates, such as CtrA, require binding between PopA and c-di-GMP connected with the second class protease complex (see Fig 3.4).

In this study, we use 'Complex 1', 'Complex 2', and 'Complex 3' to name the protease complexes that degrade the first, second, and third class substrates, respectively (see Fig 3.5). Unphosphorylated CpdR primes ClpXP to function as the first class protease complex (Complex 1) which degrades CpdR in turn [90]. (Table 3.1, Eq. 20). Primed ClpXP (Complex 1) recruits RcdA (Complex 2) to deliver the second class substrates to the protease ClpXP [29] (Table 3.1, Eq. 23). Additionally, the RcdA proteolysis has been shown to be catalyzed by

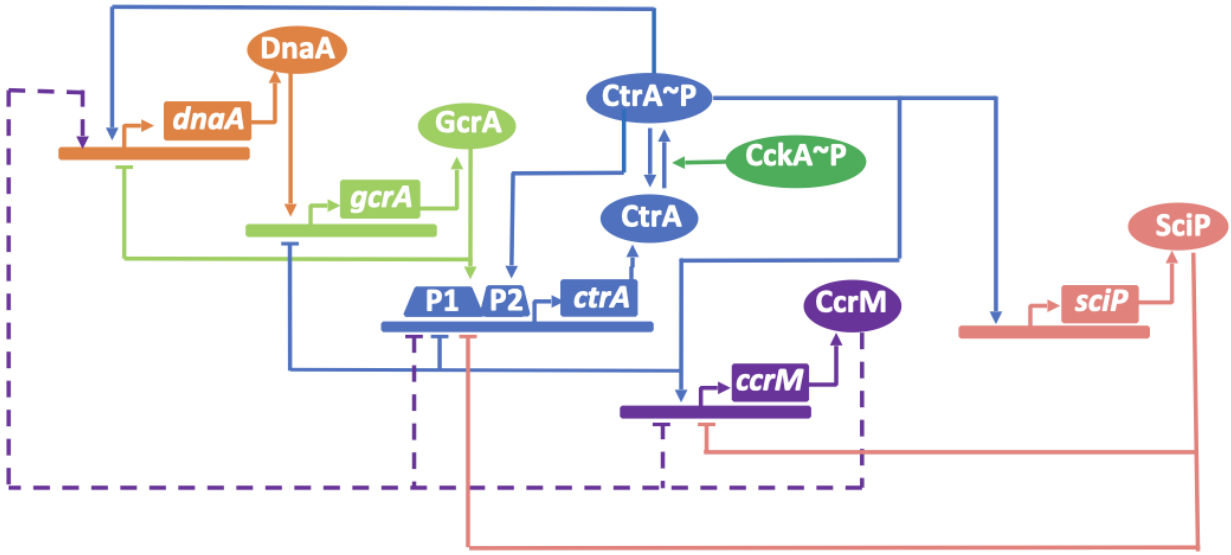

Figure 3.3: **The master regulatory network of *C. crescentus*.**
Solid lines represent activation/inhibition influences of master regulators (DnaA, GcrA, CcrM, CtrA, SciP) with arrow/bar, respectively. The dashed lines represent the methylation effects on *dnaA*, *ctrA*, *ccrM* genes from CcrM.

Complex 1 [95]. Besides CpdR and RcdA, the third class proteolysis requires PopA bound with cdG, where cdG-bound PopA directly interacts with RcdA and CtrA ensuring the specific degradation of CtrA [27]. The diguanylate cyclase PleD and phosphodiesterase PdeA are included in our system as the main synthetase and hydrolase of cdG, respectively, where the expression of *pleD* and *pdeA* is controlled by CtrA∼P [33]. PdeA is proteolyzed by Complex 1, shown in Fig 3.5. As PopA bears a GGDEF domain and two receiver domains akin to PleD, we assume PopA functions as a dimer; thus, PopA dimer binds with two cdG molecules in the same way as PleD does [101, 102] . Since cdG levels in *C. crescentus* are less than 0.3 μM [57], which is much lower than most protein levels, we use cdG to represent the PopA:2c-di-GMP binding species in this model (Fig 3.5). Moreover, the phosphorylation of CpdR is controlled by the kinase CckA, similarly with CtrA [90]. cdG binds to CckA to inhibit its kinase activity [28], which means cdG participates in the degradation and dephosphorylation of CtrA. CckA and cdG connect the master regulatory network and ClpXP-based proteolysis system through CtrA (Fig 3.5).

Only phosphorylated form of PleD is active to catalyze the synthesis of cdG [28]. As the phosphorylation of PleD is controlled by more than three enzymes, including PleC, DivJ, CckN, and at least one unknown kinase [103, 104], it is complicated to thoroughly involve phosphorylation pathway of PleD. We initially assumed that phosphorylated PleD has a similar trend over cell cycle with total PleD and used total PleD as the synthetase of cdG; but cdG simulation in predivisional cell was super high, inconsistent with experiments, although both PleD and PdeA fit data well. We hypothesize PleD∼P is relatively low in predivisional

cell due to the regulation of its main phosphatase PleC and kinase DivJ. To verify our hypothesis, we quantify western blots of DivJ and PleC over cell cycle using ImageJ [14, 105] (Fig 3.6). Experimental data indicates that DivJ almost does not change during the cell cycle and PleC is high in predivisional cell. Therefore, it is reasonable that PleD∼P decreases in predivisional cell because of high phosphatase activity of PleC. We fit PleC data points with trigonometric functions: $80.09 \times \sin(0.013t + 1.74) + 78.77 \times \sin(0.013t + 4.85)$ (Fig 3.6A). The function of PleC is then introduced into our model to represent the PleC level regulating the phosphorylation of PleD.

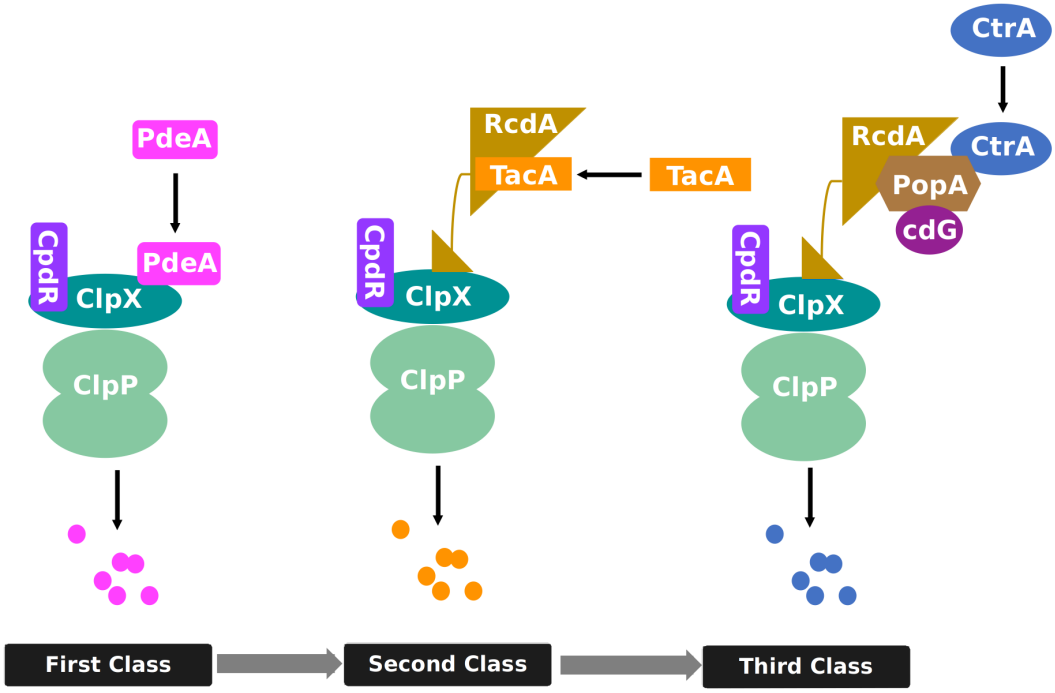

Figure 3.4: **Hierarchical proteolysis of the first (eg. PdeA), second (eg. TacA), and third (eg. CtrA) substrate.**
The degradation of different substrates is dependent on the degree of adaptor assembly. Priming of the protease ClpXP by unphosphorylated CpdR results in PdeA decay, which recruits additional adaptor RcdA to degrade TacA. RcdA tethers cdG-bound PopA with the primed ClpXP, which is responsible for the proteolysis of CtrA.

Module 3: Chromosome replication and methylation We build the module for DNA replication following the recognized principle in Li et al's work [20], which consists of initiation, elongation, and termination phases. During the sw-to-st transition, *C. crescentus* requires high levels of DnaA and low levels of CtrA to initiate DNA replication [89]. As DNA synthesis proceeds, the fully methylated chromosome becomes hemimethylated due to the semiconservative replication. Replication will not be initiated again until CcrM re-methylates *Cori* once more [89]. Additionally, the master regulator genes *ctrA*, *dnaA*, and *ccrM* have CcrM-targeted sequence GANTC in their promoters (see Fig 3.2). Therefore,

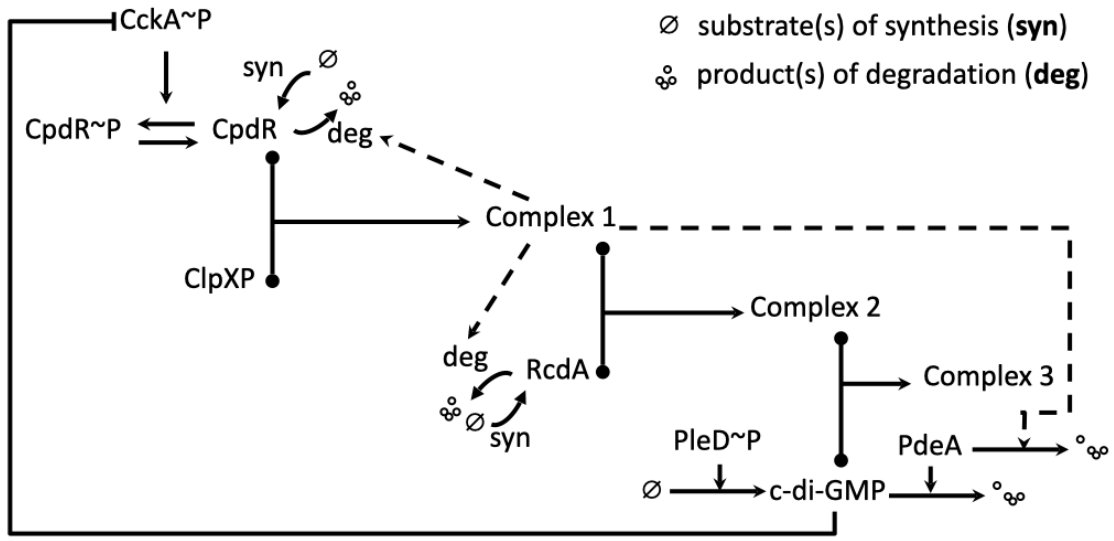

Figure 3.5: **Hierarchical diagram of protease complexes.**
Solid lines with arrow denote metabolisms; solid lines with filled circles denote binding processes; dashed lines with arrow denote activation effects. Complex 1 decays the first class of substrates; Complex 2 degrades the second class of substrates; Complex 3 degrades the third class of substrates.

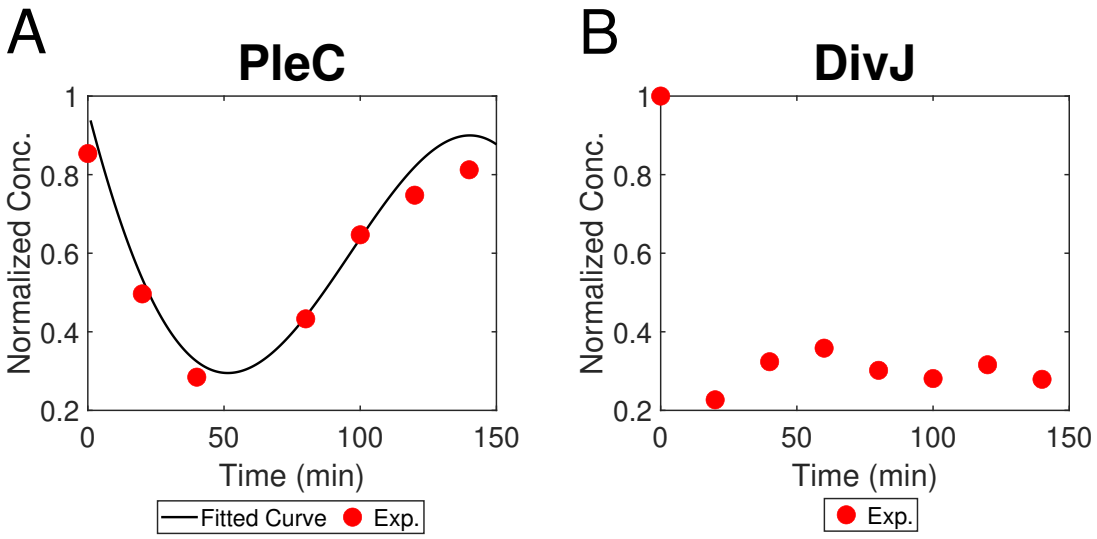

Figure 3.6: **Quantification of experimental data of PleC and DivJ.**
(A) Black curve is fitted from experimental data [14] by MATLAB. The fitting function is $80.09 \times \sin(0.013t + 1.74) + 78.77 \times \sin(0.013t + 4.85)$. (B) Experimental data of DivJ [105] indicates DivJ levels sharply drop during the sw-to-st transition and then almost do not change.

the methylation state of these genes are likely influenced by CcrM abundance and the progression of replication. Taken together, the initiation of DNA replication occurs when CtrA concentration is low, DnaA concentration is high, and *Cori* is fully methylated. Once initiated, DNA replication continues in a bidirectional manner along circular chromosomes and terminates in the late predivisional cell [106]. Finally, the newly replicated chromosomes are separated into two daughter cells with the Z-ring constriction.

We use variables *Ini* and *Elong* to model the initiation and elongation phase of DNA replication, respectively, where *Elong* was built by Li et al [20] (Table 3.1, Eqs. 1-2). *Ini* is activated by DnaA, repressed by CtrA, and affected by the methylation of *Cori*. When *Ini* increases to a threshold, $Ini = P_{\text{elong}}$, the elongation phase is triggered, where $P_{\text{elong}} = 0.05$ [89] (Table. 3.2). DNA replication is terminated when $Elong = 1$ and we reset $Elong = 0$ once replication is terminated (see Fig 3.8A). h, indicating the probability of hemimethylation [20], is introduced in this study to describe the methylation influences on transcript rate (see Table 3.1, Eqs. 7-12). During the simulation of DNA replication, h is switched from 0 to 1 when the replication fork passes the corresponding gene on chromosome (Table. 3.2). As the position of *dnaA* is very close to *Cori* (see Fig 3.2) and *dnaA* transcription rate reduces to half when it is hemimethylated [83], '$(2-h_{Cori})$' is used to represent the methylation effect of *dnaA* [20]. I is introduced for a time delay. The chromosomes are separated with Z-ring constriction; however, the Z-ring event is not modeled in this study. Experiments indicate the S-phase period of *Caulobacter* is approximately 90 min. Here, we introduce a variable *Zring* to control the timing of Z-ring constriction and cell division. The increase rate of *Zring* is set as a particular constant to control the time for *Zring* rising from 0 to 1; and we use the time event $Zring = 1$ (Table 3.2) to signal the separation of chromosomes, where the count of chromosomes (*Count*) goes from 2 to 1 [84]. Throughout the execution of our simulation, several events representing cellular phenomena, including time points of replication initiation and chromosome segregation, can be triggered given particular conditions (summarized in Table 3.2).

3.3.2 Model derivation

Some proteins are not uniformly distributed in *Caulobacter* cells (see Fig 3.1). As we focus on temporal dynamics of regulators and their contributions to cell development, we ignore the non-uniform distributions and assume the whole cell is well-mixed at this stage. We use the law of mass action to describe the general synthesis/degradation and binding/unbinding processes, while protein effects–activation and inhibition–are described by Hill functions. To be more specific,

$$x \xrightarrow{k_{\text{s,X}}} \text{X} \xrightarrow{k_{\text{d,X}}} \emptyset$$

is converted as

$$\frac{d[\text{X}]}{dt} = k_{\text{s,X}} \cdot x - k_{\text{d,X}} \cdot [\text{X}] \tag{3.1}$$

where X represents protein, x is the mRNA of X, $k_{\mathrm{s,X}}$ is the rate constant of synthesis, and $k_{\mathrm{d,X}}$ indicates the rate constant of degradation.

$\mathrm{A} + \mathrm{B} \underset{\mathrm{k^-(unbind)}}{\overset{\mathrm{k^+(bind)}}{\rightleftharpoons}} \mathrm{C}$ is converted as

$$\frac{d[\mathrm{C}]}{dt} = k^+ \cdot [\mathrm{A}] \cdot [\mathrm{B}] - k^- \cdot [\mathrm{C}] \tag{3.2}$$

A binds to B to produce C, where k^+ and k^- represent binding and unbinding rates, respectively. Activation and inhibition effects are described by Hill functions as follow:

$$H_{\mathrm{a}}(\mathrm{X}) = \frac{\mathrm{X}^n}{J_{a,x}^n + \mathrm{X}^n}, \quad H_{\mathrm{i}}(\mathrm{X}) = \frac{J_{\mathrm{i},x}^n}{J_{\mathrm{i},x}^n + \mathrm{X}^n}, \tag{3.3}$$

where $H_{\mathrm{a}}(\mathrm{X})$ indicates activation, and $H_{\mathrm{i}}(\mathrm{X})$ indicates inhibition. Variables n, J represent the corresponding Hill coefficient and the microscopic dissociation constant, respectively.

3.3.3 Model parameters

Experimental data. To compare our simulations with experimental observations from different publications, we first normalize experimental data to [0, 1] as follows:

$$z_i = \frac{x_i - \min(x_i)}{\max(x_i) - \min(x_i)}, \tag{3.4}$$

where x_i indicates the original data point; z_i is the scaled normalized value of experiments. Second, considering the relative abundance of different species in experiments [13], we set different targeted ranges for different species in the model. For example, the abundances of DnaA and CcrM are relatively low while those of CtrA and SciP are relatively high in experiments [13] and our simulations (Fig 3.10). For the figures in the Result section, the normalized experimental data are scaled to the range of our simulations to evaluate the temporal dynamics.

Parameter description. All 86 parameters used in this study are summarized in Table 3.3. Among them, seven parameters are obtained from previous experimental or modeling publications (see Table 3.3). The rest of the parameters are split into two groups: 1) 47 parameters (summarized in Table B.3) that characterize major functionality of mRNAs and proteins, such as synthesis and degradation, are chosen for optimization; 2) the remaining 32 parameters are set with fixed values, including most dissociation constants.

Multiobjective optimization. Let $\chi \in \mathbb{R}^p, p = 47$ be the vector of parameters to be estimated in the *caulobactor* cell cycle model. For this optimization problem, we focus on two aspects: the quantitative difference between experimental data and simulated results, and the cell cycle time, both for wild type cells. The reasoning behind the two objectives

is that the experimental data have inconsistent concentration levels between the beginning ($t = 0$ min) and ending ($t = 150$ min) states of the cell cycle, whereas our model must be consistent to ensure stable cell cycle regulation. This is also validated in our initial optimization test using a single objective function, where we observe minimizing the difference in species concentration results in high deviation in cell cycle time, and vice versa. Due to this conflict, we cannot use the common scalarization scheme to sum up the two objectives using weights, i.e., $F(\chi) = w_1 f_1(\chi) + w_2 f_2(\chi)$. Our parameter optimization is therefore defined as a multiobjective optimization problem (MOP). The two objective functions are:

$$f_1(\chi) = \frac{1}{nm} \sum_{i}^{n} \sum_{j}^{m} (x_{i,j} - y_{i,j})^2, \quad f_2(\chi) = |T_c - 150|, \tag{3.5}$$

where $x_{i,j}$ denotes the simulated concentration of species i at time j, $y_{i,j}$ denotes the experimental data of species i at time j, and T_c is the simulated cell cycle time. Here, we have the experimental data for $n = 15$ species (see Table B.2) and the number of data points m varies for different species. Note that we only use available observations of *C. crescentus* wild type (WT) cells for parameter fitting. The mutant cases of *C.* cell are used as our model validation. The optimization problem to be solved is

$$\min_{[L,U]} f_1(\chi), \quad \min_{[L,U]} f_2(\chi), \tag{3.6}$$

where $[L, U]$ is a search box in $\mathbb{R}^p$ for model parameters. See the lower and upper bounds of parameters in Table B.3.

We apply two MOP algorithms to our optimization problem for comparison: one is the widely used nondominated sorting genetic algorithm (NSGA-II) [107]; the other is the more recent VTMOP [108] based on VTdirect [109] and QNSTOP [110, 111] that uses response surface and trust region methodologies, and an adaptive weighting scheme. Initial values in Table B.1 are the levels of corresponding variables used as the beginning state of each simulated cell cycle. Fig 3.7 shows the combined Pareto front from both methods after multiple runs with different optimization settings. Observe that the Pareto front is a nonconvex curve, showing that the multiobjective optimization problem is very difficult. The best parameter estimates are found by VTMOP and listed in Table 3.3, with $f_1 = 1.57$ and $f_2 = 0.02$. The sensitivity of parameters is 18% for experimental data fitting (f_1) and 72% for cell cycle time (f_2) if we perturb the parameters of three Pareto points (marked as black circle in Fig 3.7) by 10%. Note that the sensitivity of the second objective is large when f_2 is very close to zero, thus points near zero are not included in the analysis. The root mean square error (goodness of fit) is RMS(f_1) ≈ 1.51, RMS(f_2) ≈ 0.84 for the three selected Pareto points.

3.4 Results

Integrating the hierarchical proteolysis (Fig 3.5) into the master regulatory network (Fig 3.3), we propose a model to capture the temporal dynamics of cell cycle regulators and glean

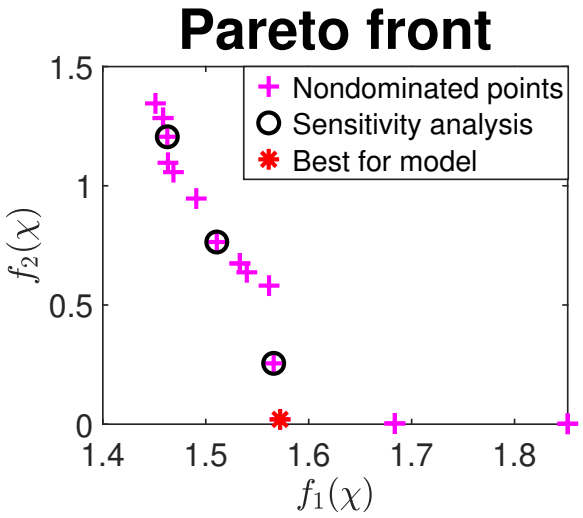

Figure 3.7: **Pareto front returned by NSGA-II and VTMOP.** $f_1(\chi)$ and $f_1(\chi)$ are the two objective function values. The red point is selected as the best parameter set for our model.

insights about bacterial protein proteolysis systems. Non-uniform distributions of molecules in space are ignored at this stage.

3.4.1 Our model accurately describes gene transcription patterns and temporal dynamics of key regulators during the replication cycle of *Caulobacter* wild type cells

Chromosome Replication and Methylation. We follow the DNA replication process as the rationale to formulate a set of ordinary differential equations (ODEs) modeling initiation, elongation, and termination of DNA replication as well as methylation states, as shown in Table 3.1 (Eqs. 1-6). The initiation of DNA replication requires a fully methylated state (both strands methylated, $h_* = 0$), while semiconservative replication creates two hemimethylated copies of genes. As such, the variables h_* in our model spike when the corresponding gene is being replicated (Fig 3.8). Later in the cell cycle, the hemimethylated copies ($h_* = 1$) are re-methylated by CcrM, returning to the fully methylated state. Therefore, h_* then plunge as the newly created, hemimethylated copies become fully methylated by CcrM. The CcrM-dependent methylation in the control system ensures DNA replication initiates once per cell cycle.

The proteolysis of CtrA is controlled by hierarchical protease complexes. In ad-

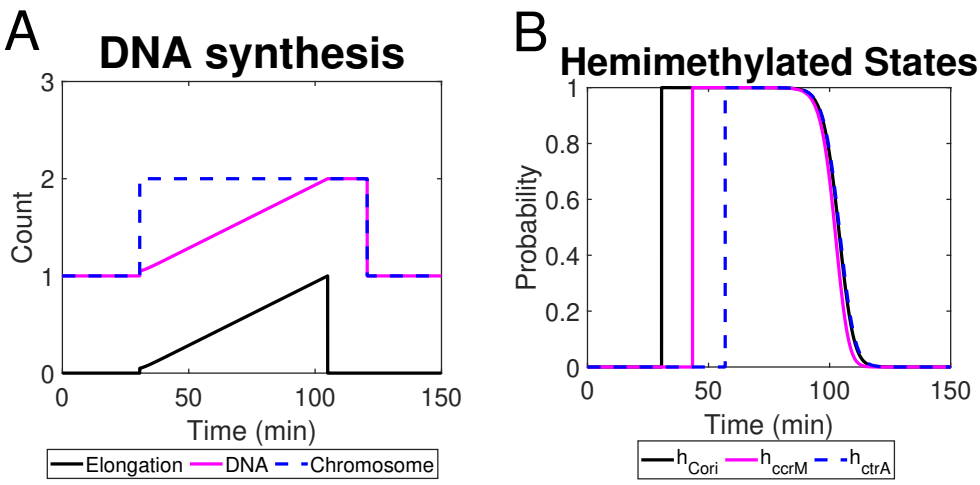

Figure 3.8: **Simulation of chromosome status.**
(A) Simulated chromosome/DNA replication and elongation process; (B) The probability of loci ($Cori, ccrM, ctrA$) being hemimethylated in a single cell cycle.

dition to replication and transcription, we investigate the proteolysis regulation of CtrA, the essential component of cell cycle control system, and explore the contribution of the conserved proteolysis module. Based on the hierarchical diagram of protease complexes (Fig 3.5), we use ODEs to simulate the temporal dynamics of three classes of protease complexes (Eqs. 20-29 of Table 3.1). Since there is no experimental data of protease complexes, we evaluate our simulations using western blots of CpdR, RcdA, PleD, PdeA, and cdG [90, 112, 61] (see Table B.2), where numerical values are extracted by ImageJ or GetData, shown as the red circles in Fig 3.9. Those proteins are essential components of ClpXP-dependent proteolysis system.

Our simulated CpdR, PleD and PdeA match well the experimental dynamics (see Fig 3.9). The general trend of modeled RcdA and cdG agrees with experiments, whereas cdG peaks a little bit late compared with experimental data. The discrepancy may derive from other regulatory enzymes of cdG or PleD which are not involved in our current model. As most proteins involved in protease complexes are modeled reasonably, We use the hierarchical model to simulate the cyclic proteolysis of CtrA (Eq. 17 of Table 3.1). In addition to degradation regulation, the hierarchical model influences the phosphorylation of CtrA via cdG and CckA, while phosphorylated CtrA in turn impacts the expression of components involved in degradation module, including *cpdR*, *rcdA*, and *pleD*.

Temporal dynamics of mRNA and master regulators. We convert the regulatory network diagram in Fig 3.3 into ODEs shown in Table 3.1 (Eqs. 7-18) to simulate the temporal dynamics of five master regulators and their mRNA. The proposed hierarchical protease complexes are applied to simulate the cyclic degradation of CtrA. Figure 3.10A-E and figure 3.10F-J exhibit the comparisons between simulations (black curves) in our

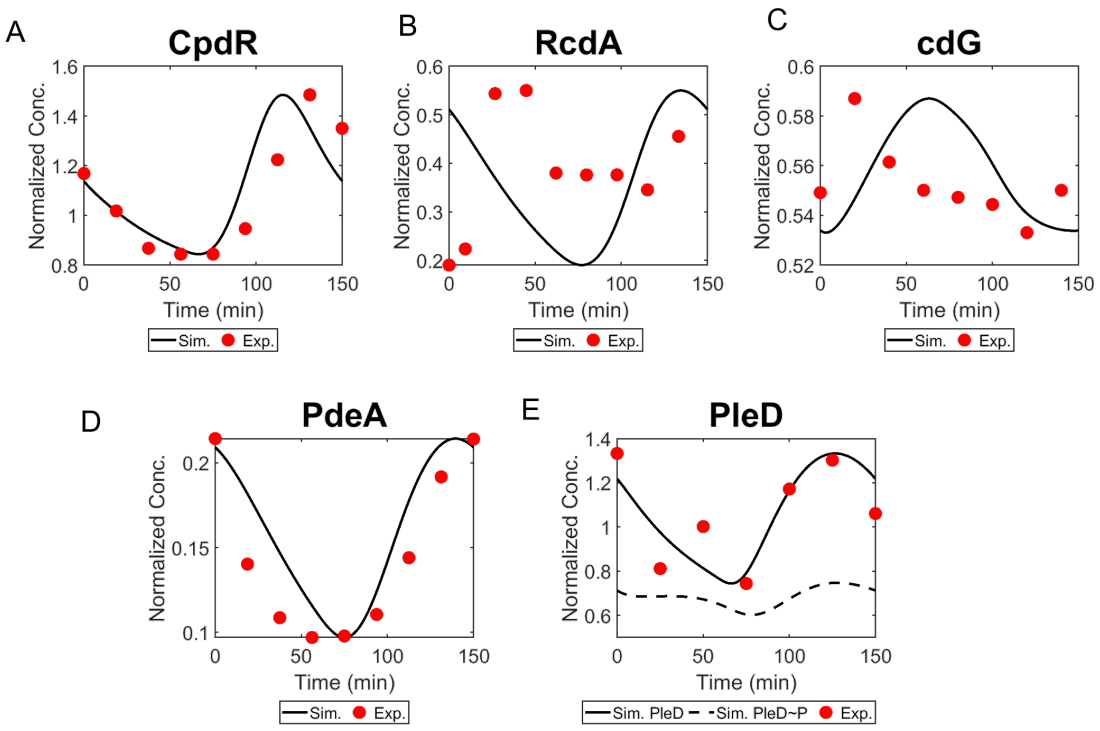

Figure 3.9: **The dynamics of total CpdR, RcdA, cdG, PdeA, total PleD, and PleD∼P in simulation with the corresponding experimental data.**
.Experimental data of CpdR is from Iniesta et al. [100], RcdA is from McGrath et al. [112], cdG is from Abel et al. [57], PdeA is from Abel et al. [61], and PleD is from Aldridge et al. [113].

model and experimental data (red circles and blue triangles) for mRNA (*dnaA*, *gcrA*, *ctrA*, *ccrM*, and *sciP*) and protein (DnaA, GcrA, CtrA, CcrM, and SciP) levels, respectively. In general, our simulations fit the experimental observations well. As we capture the genetic information flowing from mRNA to proteins, the protein concentration curves generally resemble the corresponding mRNA abundance curves. *dnaA* transcription is reduced by hemi-methylation state, which in part explains the dip in our simulation of *dnaA* during DNA replication ($t \in [30, 110]$ min in Fig 3.10A). Additionally, the expression of *dnaA* is activated by CtrA [83] and inhibited by GcrA [114]. Thus, the high levels of GcrA and low levels of CtrA during sw-to-stalk transition reinforce the decrease of *dnaA* expression (Fig 3.10A, G, H). When the replication fork passes *ccrM* and *ctrA* right before and after 50 min, h_{ccrM} and h_{ctrA} are switched from 0 to 1 (Fig 3.8), which explains the increase of CcrM (*ccrM*) and CtrA (*ctrA*) at the corresponding time (Fig 3.10B,D,I,H). Meanwhile, the high levels of activator GcrA and low levels of inhibitor SciP amplify the increase of *ctrA*. DnaA and CtrA collaborate to regulate the initiation of DNA replication: 1) during sw-to-st transition, initiator DnaA is high and suppressor CtrA is low, allowing the cell to initiate replication; 2) during DNA replication, DnaA keeps low and CtrA is high, avoiding another initiation of replication in the same cycle. Under the combined functions of DnaA and CtrA, the transcription of of *gcrA* increases in the beginning and decreases in the predivisional stage, which agrees with the observation of *gcrA* transcription (see Fig 3.10B). *sciP* expression is activated by CtrA, which is observed in our simulation as well (Fig 3.10E). We summarize the simulated and observed abundance of five master regulators in a single cell cycle in a bar chart (Fig 3.11B), where our simulation shows similar translation patterns with experiments. Fig 3.11A shows the maximum levels of our simulated master regulators, in which the relative scales agree with experiments [13]. Even though the experimental data comes from a variety of sources and experimental techniques, visual inspection suggests fair agreement between the timing of master regulator abundance in simulation and experimental data.

One objection worth noting is that some of our simulations deviate from the experimental data at the beginning or the end of the cell cycle. For example in Fig 3.10C, at the end of the cell cycle, the expression level of *ctrA* is considerably lower in our simulation than the experimental data suggest. Additionally, this type of discrepancy can be witnessed in the simulated GcrA, where the simulated level is lower than experimental observations after $t = 100$ min (Fig 3.10G). This disagreement stems from a limitation that the simulated endpoint has to be equal to the starting point ($t = 0$ min), because we do not model the asymmetrical heritage of two distinct daughter cells after progenies are completely separated. Although there are several mismatches between the simulation and experiments, our model fits most data points and captures key trends during cell cycle, such as the dynamics of regulators during sw-to-st transition. Our model exhibits that key regulators interact with each other through transcription, degradation, and phosphorylation regulations to determine the timing of cell differentiation and reproduction.

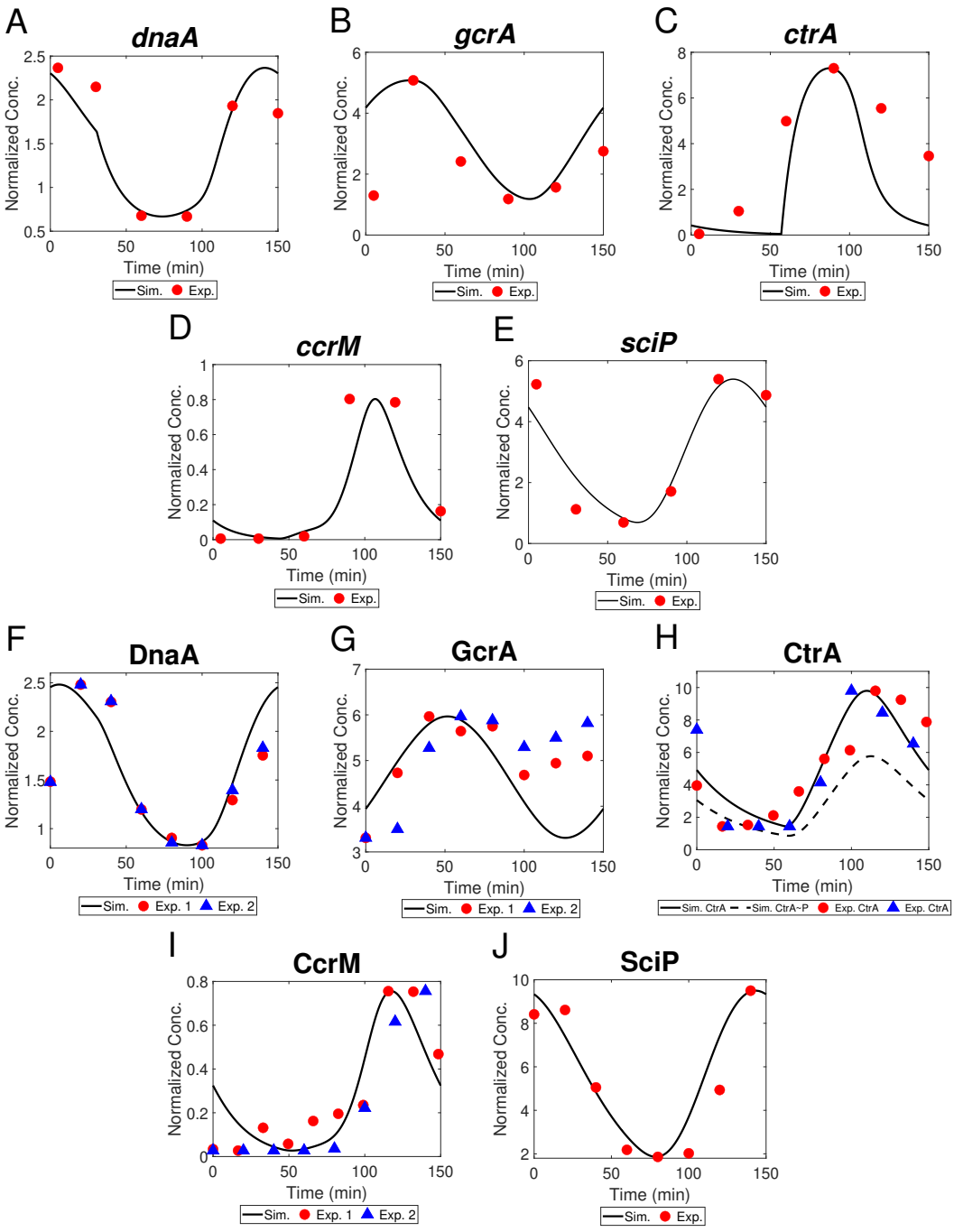

Figure 3.10: **Comparison of mRNA and proteins of master regulators in simulation with experimental data.**
(A-E) Experimental mRNA concentration of *dnaA*, *gcrA*, *ctrA*, *ccrM*, *sciP* (curves) with corresponding simulated data (red circles, from Schrader et al. [88]), and (F-J) simulated protein concentration of DnaA, GcrA, total CtrA (CtrA∼P), CcrM, SciP (curves) with experimental data (circles or triangles) over a single cell cycle. For the sources of experimental data, DnaA data is from Shen et al. [4] and Collier et al. [85]; GcrA data is from Collier et al. [85] and Tan et al. [81]; CtrA data and CcrM data are both from Reisenauer et al. [115] and Shen et al. [4]; and SciP data is from Tan et al. [81].

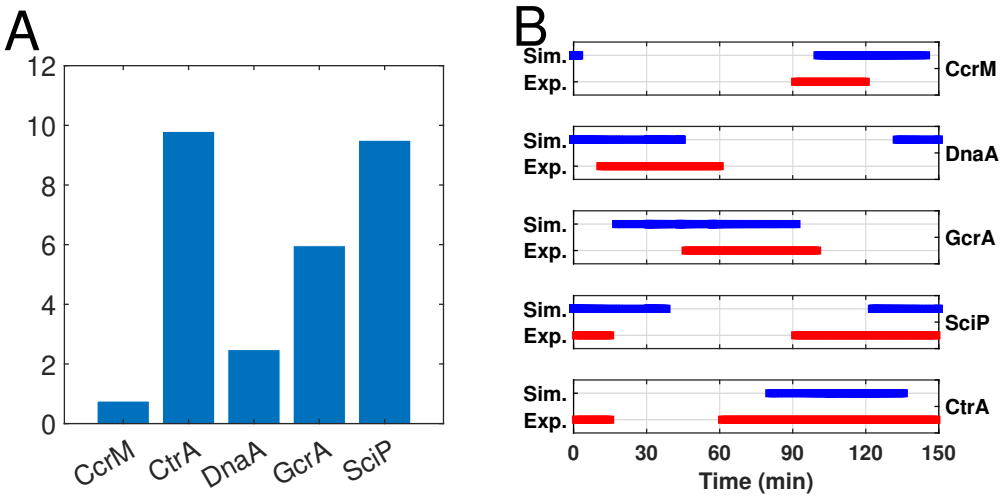

Figure 3.11: **Summary of the simulation results for the five regulators - CcrM, CtrA, DnaA, GcrA, and SciP.**
(A) Relative maximum concentrations of master regulators across one swarmer cell cycle. (B) Abundance of five master regulators (CcrM, CtrA, DnaA, GcrA, and SciP) from simulated results and experimental data. Horizontal bars represent the time periods of protein abundance across the swarmer cell cycle. Blue bars indicate the time frame where simulated protein levels are above the mid-range concentrations and red bars are the corresponding experimental data from [99].

3.4.2 Hierarchical protease complexes contribute to the timed cell cycle progression

Our modeled hierarchical cyclic proteolysis module performs well in the simulation of CtrA. Here, we explore the contribution of this module for cell development. We replace the cyclic proteolysis by a constant for CtrA, CpdR, and RcdA, separately, setting $J_{\mathrm{d,CtrA-ClpXP}}$, $J_{\mathrm{d,CpdR}}$, or $J_{\mathrm{d,RcdA}}$ as 0. In the simulation of $J_{\mathrm{d,CtrA-ClpXP}} = 0$, where the degradation rate of CtrA is constant, the system still oscillates during cell cycles whereas the amplitude of CtrA and SciP shows noteworthy reduces. The cycle time increases, resulting in delays of master regulators in simulation, including CtrA and CcrM (Fig 3.12A). With a constant degradation of CpdR or RcdA, simulations show severe defects, especially for the dynamics of CtrA. The oscillation of CtrA almost disappears and methylation states are abnormal under these conditions (Fig 3.12B,C). In summary, the cyclic proteolysis deriving from the hierarchical protease complexes shows significant impacts on the system. We further replace all cyclic complexes with constants, setting $J_{\mathrm{d,CtrA-ClpXP}}$, $J_{\mathrm{d,CpdR}}$, and $J_{\mathrm{d,RcdA}}$ as 0 simultaneously. The corresponding simulation is similar with the $J_{\mathrm{d,CtrA-ClpXP}} = 0$ mutant, which shows delayed cell cycles and reduced amplitudes of several species (Fig 3.12D). Simulations of these cyclic proteolysis mutants suggest the cyclic proteolysis of CtrA is key to regulate the entire system, because both deletion ($J_{\mathrm{d,CtrA-ClpXP}} = 0$) and changes ($J_{\mathrm{d,CpdR}} = 0$ and $J_{\mathrm{d,RcdA}} = 0$) of CtrA cyclic degradation would screw up the dynamics pattern of both master regulators and their mRNA. Moreover, the system is more sensitive without the cyclic proteolysis module. We increased the degradation rate of CtrA to 5-fold for system with and without the cyclic proteolysis module; wild type system still has an acceptable cell cycle while cyclic proteolysis mutant systems have severe deficiencies. Taken together, our model suggests the hierarchical cyclic proteolysis module contributes the timed cell cycle and robustness of the *Caulobacter* system.

3.4.3 Our model captures the phenotype of mutant strains

To further test the validity of our model, we use the same equations and initial values to simulate seven different mutant strains (Fig 3.13). Among these mutant strains, cell cycle of $\Delta dnaA$, where $dnaA$ is knocked out ($k_{\mathrm{s},dnaA} = 0$), is arrested. The other six mutant strains are all viable. Our mutant simulations correctly capture the viability of these seven mutant strains. To be more specific:

$\Delta ccrM$: $ccrM$ is verified to be dispensable for cell viability [19]. The doubling time is about 162±9 min, longer than that for WT. Our simulated $\Delta ccrM$ ($k_{\mathrm{s},ccrM} = 0$) has a 164 min cycle time, which fits the experimental observation well (Fig 3.13A). In our simulation, all h can not be returned to 0 because there is no CcrM re-methylating the chromosome. Additionally, experiments have suggested the cell cycle is also regulated by CcrM independent with GANTC motif. This study does not include the GANTC motif independent influence

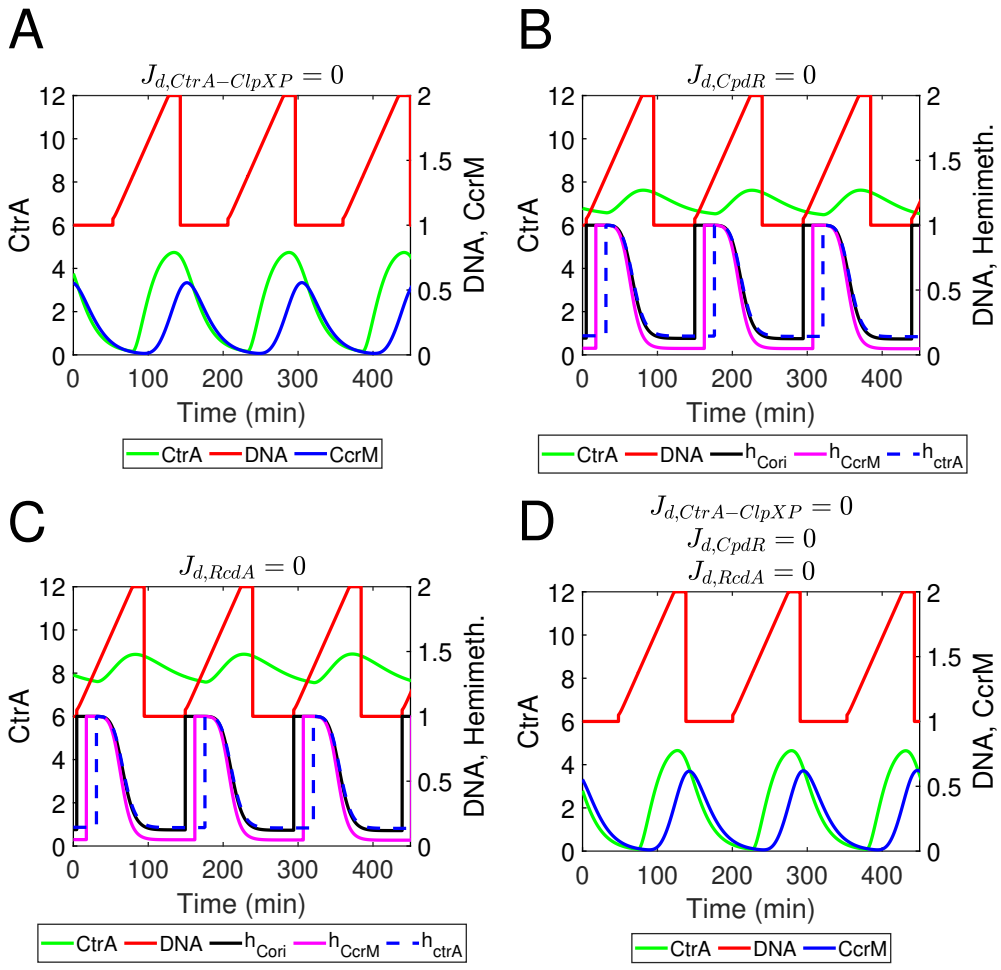

Figure 3.12: **Simulated results of mutating the cyclic proteolysis of CtrA, CpdR, or/and RcdA.**
(A). $J_{\mathrm{d,CtrA-ClpXP}} = 0$ indicates the cyclic proteolysis of CtrA is replaced by a constant. (B). $J_{\mathrm{d,CpdR}} = 0$ indicates the cyclic proteolysis of CpdR is replaced by a constant. (C). $J_{\mathrm{d,RcdA}} = 0$ indicates the cyclic proteolysis of RcdA is replaced by a constant. (D). The cyclic proteolysis of CtrA, CpdR, and RcdA are all mutated as constant degradation.

of CcrM, so the simulation of $\Delta ccrM$ only shows the potential of deleting methylation of GANTC motif by CcrM.

$\Delta gcrA$: In *gcrA* knocked out strain, the doubling time is 40% longer than for the WT [19]. Our simulated *gcrA* mutant ($k_{s,gcrA} = 0$) has approximately 10 min longer cell cycle compared with the WT simulation (Fig 3.13B), which less than the experimental observation. The gap is likely derived from the forced modeling of Z-ring constriction process, which is not explicitly modeled in this study.

$ctrA\Delta\Omega 3$: $ctrA\Delta\Omega 3$ contains modifications to the C-terminal amino acids of *ctrA*, resulting in a non-proteolizable CtrA allele [116]. Here, we decreases $k_{\mathrm{d,CtrA\text{-}ClpXP}}$ to 10% of WT in simulation. In Fig 3.13D, The average CtrA levels increase in simulation with less fluctuation because of the non-proteolizable CtrA allele. Our simulation suggests the proteolysis of CtrA is important for its cell cycle-dependent regulation. h in simulated $ctrA\Delta\Omega 3$ can not decrease to 0, suggesting the levels of CcrM in $ctrA\Delta\Omega 3$ are not sufficient to completely re-methylate chromosome, while the lower levels of CcrM is caused by higher levels of the inhibitor CtrA.

cdG related mutant strains: cdG^0 mutant strain has been verified to be viable, although it shows morphology defects [28]. In Fig 3.13E, our simulation of cdG^0 strain ($k_{\mathrm{s,cdG}} = 0$) is viable and shows a horizontal shift which may result in morphology defects. The CtrA levels increase with less fluctuation which is caused by the deletion of cdG. *pleD* knocked out mutant ($k_{\mathrm{s,PleD}} = 0$) results in a lower cdG levels (Fig 3.13G), which shows a similar phenotype with the simulation of cdG^0. *pdeA* mutant increases cdG levels in simulation (Fig 3.13F, $k_{\mathrm{s,PdeA}} = 0$). Both $\Delta pleD$ and $\Delta pdeA$ are viable in simulation, consistent with observations [28, 61]. Oscillations exist but shifts little bit in the simulations of these three cdG regulated mutants, as shown in Fig 3.13E-G.

3.5 Discussion

The five major regulators–DnaA, GcrA, CcrM, CtrA, and SciP–work in tandem to drive the cell cycle progression of *C. crescentus*. Here, we investigated the interactions among master regulators to study the underlying mechanisms of DNA replication, methylation, transcription, and proteolysis of cyclic regulators. We applied the central dogma of molecular biology to simulate the temporal dynamics of mRNAs and proteins. Furthermore, we mathematically built a hierarchical model to simulate protease complexes and apply this model to CtrA degradation. Two MOP approaches (NSGA-II and VTMOP) have been applied to estimate parameters in this complicated system.

In *C. crescentus*, the protease ClpXP primed by one assistant adaptor recruits additional adaptors in sequence [29]. The hierarchical adaptor assembly determines the time and location of the proteolysis of hierarchical substrates. Our hierarchical model correctly captures the key dynamics of CpdR, PleD, and PdeA; it shows fair agreement with the trend of RcdA and cdG. Additionally, the protease model performs well in modeling the proteolysis of CtrA.

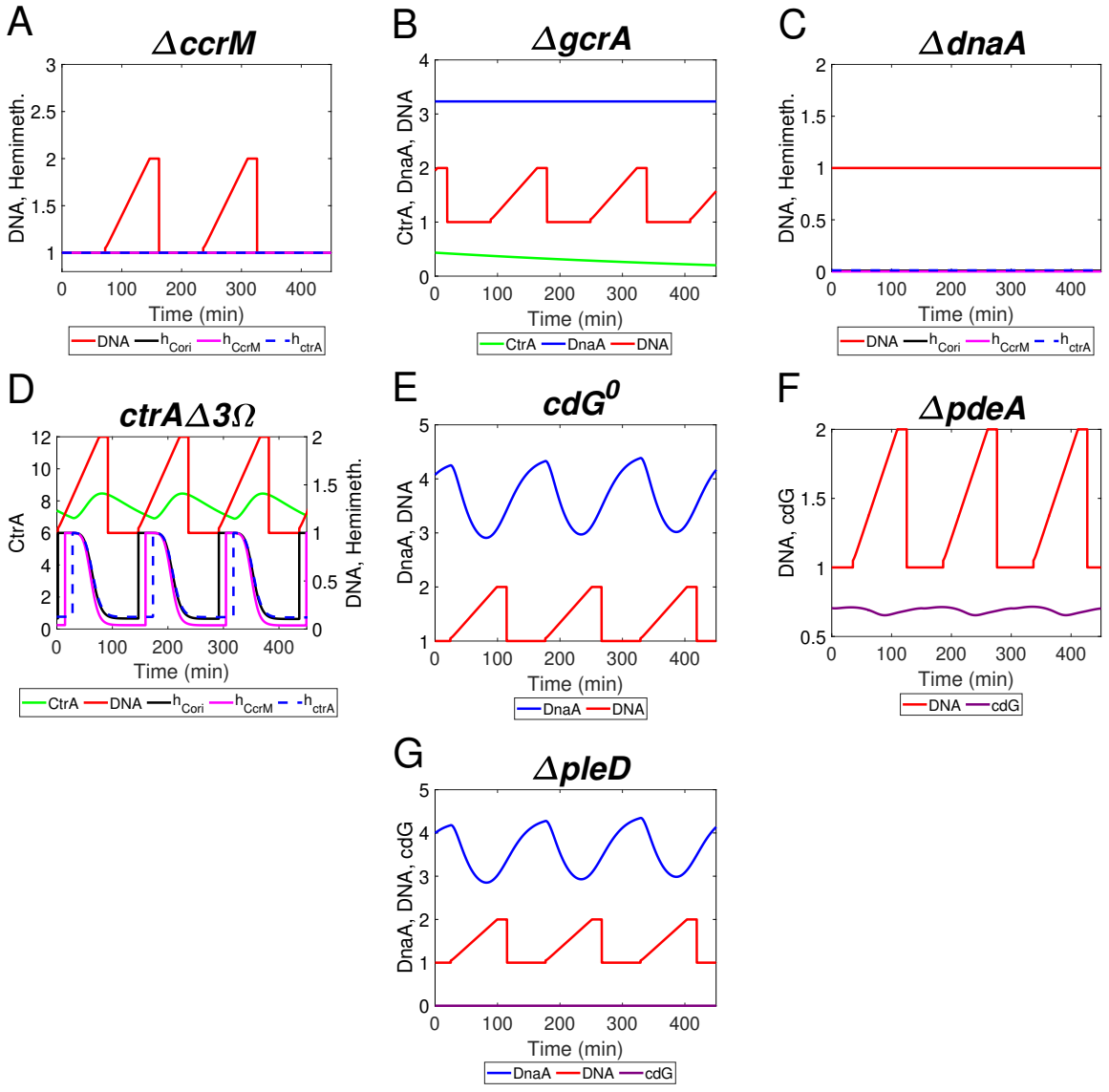

Figure 3.13: **Simulated results of mutant strains:** $\Delta ccrM$, $\Delta gcrA$, $\Delta dnaA$, $ctrA\Delta 3\Omega$, **cdG^0,** $\Delta pdeA$, **and** $\Delta pleD$.
In knock out mutant simulations, we set $k_{s,i} = 0$, where i indicates corresponding species including $ccrM$, $gcrA$, $dnaA$, cdG, PdeA, and PleD. In the simulation of $ctrA\Delta 3\Omega$, the cyclic proteolysis rate of CtrA is reduced to 10%.

Deleting the hierarchical protease module causes defects of cell cycle development and protein oscillations. Considering the fast formation of the protease Complex 3 (ClpXP bound with CpdR, RcdA, PopA, and cdG), we test the quasi-steady-state assumption (QSSA) for Complex 3. QSSA shows similar simulated results in both wild-type cells and mutant cases, suggesting QSSA might be a good approach in reducing model complexity of biological systems. As a wide range of proteins is degraded by ClpXP protease complex, our model provides a good quantitative tool to analyze the proteolysis of these proteins in *C. crescentus*, such as TacA and ShkA. As most components of the hierarchic protease complexes are conserved in bacterial species, our model has the potential for a wide range of applications. Moreover, cdG is a significant component of Complex 3 and participates in several essential pathways of cell cycle regulation in *C. crescentus*. For example, cdG binds to CckA and ShkA to induce phosphatase and kinase activity, respectively. While CckA controls the phosphorylation/dephosphorylation of several proteins, such as CtrA and CpdR, ShkA:cdG regulates the phosphorylation of TacA, which downregulates the stalked pole muramidase homolog SpmX and the stalk length regulator StaR [117]. Additionally, cdG has been verified to participate in the stress response, contributing to the survival of *Caulobacter* in oligotrophic environments [118] (Chapter 2). Due to the importance of cdG, our protease complex model is potentially a valuable tool for understanding the regulatory network of *C. crescentus*.

With the advances in experimental technologies, mRNA and protein abundance of master regulators have been monitored and measured throughout the cell cycle. However, there is a limited comparison between experiments and simulations. Our results align very well with the experimental data. Satisfactory simulation results of our model, as indicated by visual inspection, suggest that the proposed regulatory network appropriately characterizes the *Caulobacter* cell cycle progression. This study also suggests the cell cycle dependent proteolysis of CtrA is significant for the cell cycle regulations and robustness. Our model can capture major features of seven mutant strains, which has the potential to predict phenotypes of nonviable mutant strains and functions of involved proteins. As most molecules involved in our model (CtrA, CcrM, GcrA, DnaA, etc.) are conserved among proteobacteria [119, 120, 27], this framework could be applied to the study of other proteobacteria. Last but not least, this work is a successful application of multiobjective optimization problem, showing that MOP is a promising approach for handling conflicting objectives in biological modeling.

Table 3.1: Equations of replication and methylation, transcription, translation, and proteolysis.

	Equations of DNA
(1)	$\frac{dIni}{dt} = k_{\mathrm{s,Ini}} \cdot \frac{\left(\frac{[\mathrm{DnaA}]}{\Theta_{\mathrm{DnaA}}}\right)^4}{J_{\mathrm{a,Ini}}^4 + \left(\frac{[\mathrm{CtrA\sim P}]}{\Theta_{\mathrm{ctrA}}}\right)^4 + \left(\frac{[\mathrm{DnaA}]}{\Theta_{\mathrm{DnaA}}}\right)^4} \cdot \left(1 + \frac{1}{J_{\mathrm{i,Ini}}^4 + \left(\frac{h_{Cori}}{\Theta_{\mathrm{Cori}}}\right)^4}\right)$
(2)	$\frac{dElong}{dt} = k_{\mathrm{elong}} \cdot \frac{Elong^4}{Elong^4 + P_{\mathrm{elong}}^4} \times Count;$ (3) $\frac{dZring}{dt} = k_{s,Zring}$
(4)	$\frac{dh_{Cori}}{dt} = -k_{\mathrm{m},Cori} \cdot \frac{[\mathrm{CcrM}]^4}{J_{\mathrm{m},Cori}^4 + [\mathrm{CcrM}]^4} \cdot h_{Cori}$

Continued on next page

Table 3.1 – *Continued from previous page*

(5)	$\frac{dh_{ccrM}}{dt} = -k_{\mathrm{m},ccrM} \cdot \frac{[\mathrm{CcrM}]^4}{J^4_{\mathrm{m},ccrM}+[\mathrm{CcrM}]^4} \cdot h_{ccrM}$
(6)	$\frac{dh_{ctrA}}{dt} = -k_{\mathrm{m},ctrA} \cdot \frac{[\mathrm{CcrM}]^4}{J^4_{\mathrm{m},ctrA}+[\mathrm{CcrM}]^4} \cdot h_{ctrA}$
	Equations of mRNAs
(7)	$\frac{dI_{ccrM}}{dt} = k_{\mathrm{s},I_{ccrM}} \cdot \left(\frac{[\mathrm{CtrA}\sim\mathrm{P}]^2}{J^2_{\mathrm{a},ccrM\text{-}\mathrm{CtrA}}+[\mathrm{CtrA}\sim\mathrm{P}]^2} \cdot \frac{J^2_{\mathrm{i},ccrM\text{-}\mathrm{SciP}}}{J^2_{\mathrm{i},ccrM\text{-}\mathrm{SciP}}+[\mathrm{SciP}]^2} \right) \cdot h_{ccrM} - k_{\mathrm{d},I_{ccrM}} \cdot I_{ccrM}$
(8)	$\frac{dccrM}{dt} = k_{\mathrm{s},ccrM} \cdot I_{ccrM} - k_{\mathrm{d},ccrM} \cdot ccrM$
(9)	$\frac{ddnaA}{dt} = k_{\mathrm{s},dnaA} \cdot \left(\frac{J^2_{\mathrm{i},dnaA\text{-}\mathrm{GcrA}}}{J^2_{\mathrm{i},dnaA\text{-}\mathrm{GcrA}}+[\mathrm{GcrA}]^2} \right) \cdot (2 - h_{Cori}) - k_{\mathrm{d},dnaA} \cdot dnaA$
(10)	$\frac{dgcrA}{dt} = k_{\mathrm{s},gcrA} \cdot \left(\frac{[\mathrm{DnaA}]^2}{J^2_{\mathrm{a},gcrA\text{-}\mathrm{DnaA}}+[\mathrm{DnaA}]^2} \cdot \frac{J^2_{\mathrm{i},gcrA\text{-}\mathrm{CtrA}}}{J^2_{\mathrm{i},gcrA\text{-}\mathrm{CtrA}}+[\mathrm{CtrA}\sim\mathrm{P}]^2} \right) - k_{\mathrm{d},gcrA} \cdot gcrA$
(11)	$\frac{dsciP}{dt} = k_{\mathrm{s},sciP} \cdot \frac{[\mathrm{CtrA}\sim\mathrm{P}]^2}{J^2_{\mathrm{a},sciP\text{-}\mathrm{CtrA}}+[\mathrm{CtrA}\sim\mathrm{P}]^2} - k_{\mathrm{d},sciP} \cdot sciP$
(12)	$\frac{dctrA}{dt} = k_{\mathrm{s1},ctrA} \cdot \left(\frac{[\mathrm{GcrA}]^2}{J^2_{\mathrm{a},ctrA\text{-}\mathrm{GcrA}}+[\mathrm{GcrA}]^2} \cdot \frac{J^4_{\mathrm{i},ctrA\text{-}\mathrm{CtrA}}}{J^4_{\mathrm{i},ctrA\text{-}\mathrm{CtrA}}+[\mathrm{CtrA}\sim\mathrm{P}]^4} \cdot \frac{J^4_{\mathrm{i},ctrA\text{-}\mathrm{SciP}}}{J^4_{\mathrm{i},ctrA\text{-}\mathrm{SciP}}+[\mathrm{SciP}]^4} \right) \cdot h_{ctrA}$ $+k_{\mathrm{s2},ctrA} \cdot \frac{[\mathrm{CtrA}\sim\mathrm{P}]^2}{J^2_{\mathrm{a},ctrA\text{-}\mathrm{CtrA}}+[\mathrm{CtrA}\sim\mathrm{P}]^2} - k_{\mathrm{d},ctrA} \cdot ctrA$
	Equations of regulatory proteins
(13)	$\frac{d[\mathrm{CcrM}]}{dt} = k_{\mathrm{s},\mathrm{CcrM}} \cdot ccrM - k_{\mathrm{d},\mathrm{CcrM}} \cdot [\mathrm{CcrM}]$
(14)	$\frac{d[\mathrm{DnaA}]}{dt} = k_{\mathrm{s},\mathrm{DnaA}} \cdot dnaA - k_{\mathrm{d},\mathrm{DnaA}} \cdot [\mathrm{DnaA}]$
(15)	$\frac{d[\mathrm{GcrA}]}{dt} = k_{\mathrm{s},\mathrm{GcrA}} \cdot gcrA - k_{\mathrm{d},\mathrm{GcrA}} \cdot [\mathrm{GcrA}]$
(16)	$\frac{d[\mathrm{SciP}]}{dt} = k_{\mathrm{s},\mathrm{SciP}} \cdot sciP - k_{\mathrm{d},\mathrm{SciP}} \cdot [\mathrm{SciP}]$
(17)	$\frac{d[\mathrm{CtrA}]}{dt} = k_{\mathrm{s},\mathrm{CtrA}} \cdot ctrA - \left(k_{\mathrm{d},\mathrm{CtrA}} + \frac{k_{\mathrm{d},\mathrm{CtrA\text{-}ClpXP}} \cdot [\mathrm{Complex3}]^2}{J^2_{\mathrm{d},\mathrm{CtrA\text{-}CplXP}}+[\mathrm{Complex3}]^2} \right) \cdot [\mathrm{CtrA}]$ $-k_{\mathrm{phoCtrA}} \cdot [\mathrm{CckA}\sim\mathrm{P}] \cdot [\mathrm{CtrA}] + k_{\mathrm{dephoCtrA}} \cdot [\mathrm{CtrA}\sim\mathrm{P}]$
(18)	$\frac{d[\mathrm{CtrA}\sim\mathrm{P}]}{dt} = -\left(k_{\mathrm{d},\mathrm{CtrA}} + \frac{k_{\mathrm{d},\mathrm{CtrA\text{-}ClpXP}} \cdot [\mathrm{Complex3}]^2}{J^2_{\mathrm{d},\mathrm{CtrA\text{-}ClpXP}}+[\mathrm{Complex3}]^2} \right) \cdot [\mathrm{CtrA}\sim\mathrm{P}]$ $+k_{\mathrm{phoCtrA}} \cdot [\mathrm{CckA}\sim\mathrm{P}] \cdot [\mathrm{CtrA}] - k_{\mathrm{dephoCtrA}} \cdot [\mathrm{CtrA}\sim\mathrm{P}]$
	Equations of protease complexes
(19)	$\frac{d[\mathrm{CckA}\sim\mathrm{P}]}{dt} = k_{\mathrm{phoCckA}} \cdot (\mathrm{CckAT} - [\mathrm{CckA}\sim\mathrm{P}]) - k_{\mathrm{dephoCckA}} \cdot (1 + \alpha_{\mathrm{cdG}} \cdot [\mathrm{cdG}]) \cdot [\mathrm{CckA}\sim\mathrm{P}]$
(20)	$\frac{d[\mathrm{Complex1}]}{dt} = k_1^+ \cdot [\mathrm{ClpXP}] \cdot [\mathrm{CpdR}] - k_1^- \cdot [\mathrm{Complex1}] - k_2^+ \cdot [\mathrm{Complex1}] \cdot [\mathrm{RcdA}] + k_2^- \cdot [\mathrm{Complex2}]$
(21)	$\frac{d[\mathrm{CpdR}]}{dt} = k_{\mathrm{s},\mathrm{CpdR}} \cdot \frac{[\mathrm{CtrA}\sim\mathrm{P}]^2}{J^2_{\mathrm{a},\mathrm{CpdR\text{-}CtrA}}+[\mathrm{CtrA}\sim\mathrm{P}]^2} - k_{\mathrm{d},\mathrm{CpdR}} \cdot [\mathrm{CpdR}] \cdot \frac{[\mathrm{Complex1}]}{J_{\mathrm{d},\mathrm{CpdR}}+[\mathrm{Complex1}]} + k_1^- \cdot [\mathrm{Complex1}]$ $-k_1^+ \cdot [\mathrm{ClpXP}] \cdot [\mathrm{CpdR}] + k_{\mathrm{dephos},\mathrm{CpdR}} \cdot [\mathrm{CpdR}\sim\mathrm{P}] - k_{\mathrm{phos},\mathrm{CpdR}} \cdot [\mathrm{CckA}\sim\mathrm{P}] \cdot [\mathrm{CpdR}]$
(22)	$\frac{d[\mathrm{CpdR}\sim\mathrm{P}]}{dt} = -k_{\mathrm{d},\mathrm{CpdR}} \cdot [\mathrm{CpdR}\sim\mathrm{P}] \cdot \frac{[\mathrm{Complex1}]}{J_{\mathrm{d},\mathrm{CpdR}}+[\mathrm{Complex1}]} + k_{\mathrm{phos},\mathrm{CpdR}} \cdot [\mathrm{CckA}\sim\mathrm{P}] \cdot [\mathrm{CpdR}]$ $-k_{\mathrm{dephos},\mathrm{CpdR}} \cdot [\mathrm{CpdR}\sim\mathrm{P}]$

Continued on next page

Table 3.1 – *Continued from previous page*

(23) $\frac{d[\text{Complex2}]}{dt} = k_2^+ \cdot [\text{Complex1}] \cdot [\text{RcdA}] - k_2^- \cdot [\text{Complex2}]$
$+k_3^- \cdot [\text{Complex3}] - k_3^+ \cdot [\text{cdG}]^2 \cdot [\text{Complex2}]$

(24) $\frac{d[\text{RcdA}]}{dt} = k_{\text{s,RcdA}} \cdot \frac{[\text{CtrA}\sim\text{P}]^2}{J^2_{\text{a,RcdA-CtrA}}+[\text{CtrA}\sim\text{P}]^2} - k_{\text{d,RcdA}} \cdot [\text{RcdA}] \cdot \frac{[\text{Complex1}]}{J_{\text{d,RcdA}}+[\text{Complex1}]}$

(25) $\frac{d[\text{Complex3}]}{dt} = k_3^+ \cdot [\text{cdG}]^2 \cdot [\text{Complex2}] - k_3^- \cdot [\text{Complex3}]$

(26) $\frac{d[\text{PleD}]}{dt} = k_{\text{s,PleD}} \cdot \frac{[\text{CtrA}\sim\text{P}]^2}{J^2_{\text{a,PleD-CtrA}}+[\text{CtrA}\sim\text{P}]^2} - k_{\text{d,PleD}} \cdot [\text{PleD}] - k_{\text{phosPleD}} \cdot [\text{PleD}] + k_{\text{dephoPleD}} \cdot [\text{PleC}] \cdot [\text{PleD} \sim \text{P}]$

(27) $\frac{d[\text{PleD}\sim\text{P}]}{dt} = k_{\text{phosPleD}} \cdot [\text{PleD}] - k_{\text{dephoPleD}} \cdot [\text{PleC}] \cdot [\text{PleD} \sim \text{P}]$

(28) $\frac{d[\text{PdeA}]}{dt} = k_{\text{s,PdeA}} \cdot \frac{[\text{CtrA}\sim\text{P}]^2}{J^2_{\text{a,PdeA-CtrA}}+[\text{CtrA}\sim\text{P}]^2} - k_{\text{d,PdeA}} \cdot [\text{PdeA}] \cdot \frac{[\text{Complex1}]}{J_{\text{d,PdeA}}+[\text{Complex1}]}$

(29) $\frac{d[\text{cdG}]}{dt} = k_{\text{s,cdG}} \cdot (1 + \alpha_{\text{PleD}} \cdot [\text{PleD}]) \cdot \frac{J^2_{\text{i,cdG-cdG}}}{J^2_{\text{i,cdG-cdG}}+[\text{cdG}]^2} - k_{\text{d,cdG}} \cdot (1 + \alpha_{\text{PdeA}} \cdot [\text{PdeA}]) \cdot [\text{cdG}]$
$+k_3^- \cdot [\text{Complex3}] - k_3^+ \cdot [\text{cdG}]^2 \cdot [\text{Complex2}]$

Table 3.2: Event list.

Event description	**Condition**	**Change(s)**
DNA replication initiates	$Ini = P_{\text{elong}}$	$Ini = 0, \quad Elong = 0.05, \quad DNA = 1.05,$ $k_{\text{s,Zring}} = 0.011, \quad h_{Cori} = 1 \quad Count = 2$
replication fork passes *ccrM* locus	$Elong = 0.2$	$h_{ccrM} = 1$
replication fork passes *ctrA* locus	$Elong = 0.375$	$h_{ctrA} = 1$
DNA elongation terminates	$Elong = 1$	$Elong = 0$
Z-ring constriction	$Zring = 1$	$Zring = 0, \quad k_{s,Zring} = 0, \quad DNA = 1$ $Count = 1$

Table 3.3: Parameter values. (Parameters marked with $*$ are obtained from publications.)

Parameters of DNA
Rate constants, units = $\min^{-1}$
$k_{\text{s,Ini}} = 3.104\text{e-}4$, $k^*_{\text{elong}} = 6.53\text{e-}3$ [20], $P_{\text{elong}^*} = 0.05$ [20],
$k_{\text{m},Cori} = 1.5637$, $k_{\text{m},ccrM} = 2.2763$, $k_{\text{m},ctrA} = 1.4645$
Binding constants (dimensionless)
$J_{\text{a, Ini}} = 1$, $J_{\text{i, Ini}} = 1.4565$, $J_{\text{m},Cori} = 0.95$, $J_{\text{m},ccrM} = 0.95$, $J_{\text{m},ctrA} = 0.95$
Scaling variables (dimensionless)
$\Theta_{\text{CtrA}} = 6.0$, $\Theta_{\text{DnaA}} = 0.5$, $\Theta_{\text{Cori}} = 0.308$
Parameters of mRNAs
Rate constants, units = $\min^{-1}$
$k_{\text{s},I_{ccrM}} = 0.1105$, $k_{\text{d},I_{ccrM}} = 0.0696$, $k_{\text{s},ccrM} = 0.2557$, $k_{\text{d},ccrM} = 0.1005$,
$k_{\text{s},dnaA} = 0.199$, $k_{\text{d},dnaA} = 0.0693$, $k_{\text{s},gcrA} = 5.4235$, $k_{\text{d},gcrA} = 0.7342$,
$k_{\text{s1},ctrA} = 1.0035$, $k_{\text{s2},ctrA} = 0.0937$, $k_{\text{d},ctrA} = 0.0983$, $k_{\text{s},sciP} = 0.583$, $k_{\text{d},sciP} = 0.0523$,
Binding constants (dimensionless)
$J_{\text{a},ccrM\text{-CtrA}} = 5$, $J_{\text{i},ccrM\text{-SciP}} = 6$, $J_{\text{i},dnaA\text{-GcrA}} = 3$, $J_{\text{a},gcrA\text{-DnaA}} = 1.25$, $J_{\text{i},gcrA\text{-CtrA}} = 5$,
$J_{\text{a},ctrA\text{-CtrA}} = 5$, $J_{\text{a},ctrA\text{-GcrA}} = 3$, $J_{\text{i},ctrA\text{-CtrA}} = 8$, $J_{\text{i},ctrA\text{-SciP}} = 8$, $J_{\text{a},sciP\text{-CtrA}} = 5$
Parameters of master regulators
Rate constants, units = $\min^{-1}$
$k_{\text{s,DnaA}} = 0.0787$, $k^*_{\text{d,DnaA}} = 0.07$ [121], $k_{\text{s,GcrA}} = 0.032$, $k^*_{\text{d,GcrA}} = 0.022$ [20],
$k_{\text{s,CcrM}} = 0.0834$, $k^*_{\text{d,CcrM}} = 0.07$ [122], $k_{\text{s,SciP}} = 0.1294$, $k_{\text{d,SciP}} = 0.0673$,
$k_{\text{s,CtrA}} = 0.0404$, $k^*_{\text{d,CtrA}} = 0.002$ [20], $k_{\text{d,CtrA-ClpXP}} = 0.053$
Phosphorylation constant, units=$\min^{-1}$
$k_{\text{phos,CtrA}} = 4.2919$, $k_{\text{dephos,CtrA}} = 0.113$, $k_{\text{phos,CckA}} = 1.027$, $k_{\text{dephos,CckA}} = 0.9242$
Binding constants (dimensionless)
$J_{\text{d,CtrA-ClpXP}} = 4$
Parameters of protease complexes
Rate constants, units = $\min^{-1}$
$k_1^+ = 0.6072$, $k_2^+ = 1.4375$, $k_3^+ = 170.4913$, $k_1^- = 3.3013$, $k_2^- = 0.8164$, $k_3^- = 2.3133$,
$k_{\text{phos,PleD}} = 0.046$, $k_{\text{dephos,PleD}} = 0.0414$, $k_{\text{s,CpdR}} = 1.2227$, $k_{\text{d,CpdR}} = 1.6152$,
$k_{\text{pho,CpdR}} = 1.1239$, $k_{\text{depho,CpdR}} = 1.3854$, $k_{\text{s,RcdA}} = 0.1642$, $k_{\text{d,RcdA}} = 0.2323$,
$k_{\text{s,cdG}} = 0.0099$, $k_{\text{d,cdG}} = 0.9893$,
$k_{\text{s,PleD}} = 0.0956$, $k_{\text{d,PleD}} = 0.1314$, $k_{\text{s,PdeA}} = 0.012$, $k_{\text{d,PdeA}} = 0.5161$
Binding constants (dimensionless)
$J_{\text{a,CpdR-CtrA}} = 15$, $J_{\text{d,CpdR}} = 6$, $J_{\text{a,RcdA-CtrA}} = 15$, $J_{\text{d,RcdA}} = 2$
$J_{\text{a,PdeA-CtrA}} = 5$, $J_{\text{d,PdeA}} = 5$, $J_{\text{a,PleD-CtrA}} = 2.5$, $J^*_{\text{i,cdG-cdG}} = 0.2$ [118]
Constants (dimensionless)
CckAT=0.3, [ClpXP]=1, $\alpha_{\text{PdeA}} = 7$, $\alpha_{\text{PleD}} = 1500$, $\alpha_{cdG} = 10$

Chapter 4

Molecular mechanisms of cell cycle arrest in carbon and nitrogen starved *Caulobacter* populations

Bronson R. Weston[1*], Chunrui Xu[1*], John J. Tyson[2], Yang Cao[3]

1 Genetics, Bioinformatics, and Computational Biology, Virginia Tech, Blacksburg, VA, USA
2 Department of Biological Science, Virginia Tech, Blacksburg, VA, USA
3 Department of Computer Science, Virginia Tech, Blacksburg, VA, USA
* Equal contributor

4.1 Abstract

Caulobacter crescentus inhabits aquatic environments, which can thrive with poor nutrients. it divides asymmetrically during the cell cycle, producing two distinct daughter cells. The "stalked" cell utilizes a stalk to attach to surfaces in its environment, while the "swarmer" cell utilizes a flagellum to move and search for more favorable environmental conditions. Given satisfactory conditions, the swarmer cell differentiates into the stalked morphology and proceeds with the cell cycle. The molecular mechanism underlying this intriguing behavior is well studied under nutrient-rich conditions, however, the mechanism of responding to nitrogen and carbon starvation is unclear. Here we present a mathematical model to capture the dynamics of the control mechanism driving the *C. crescentus* cell cycle. We investigate known carbon and nitrogen signaling pathways. We demonstrate that these pathways are

sufficient to explain experimental observations of rapid, robust arrest in swarmer cell populations. However, the reduced CtrA expression because of starvation introduced should be determined by other independent pathways. We find that the cdG-dependent starvation response is significant for the immediate G1 arrest, while it is not sufficient to arrest cells. We demonstrate that the reduced DnaA responding to starvation is essential for the G1 arrest for both swarmer and stalked cells. Our simulations also suggest that the reduction of DivK and PleD levels may stimulate the G1 arrest of starved cells.

4.2 Introduction

Caulobacter crescentus is a ubiquitous Gram-negative bacterium colonizing freshwater and certain kinds of soils. It utilizes a dimorphic lifestyle to survive in nutrient-poor environments [8, 15, 123]. In the G1 phase, the bacterium expresses pili and a flagellum, referred to as a "swarmer" cell. The pili and flagellum enable the swarmer cell to move and search for nutrients in its environments [15]. Given suitable environmental conditions, the swarmer cell will differentiate into a "stalked" cell by releasing its flagellum and synthesizing a stalk [24]. During this differentiation stage, *Caulobacter* simultaneously initiates chromosome replication, progressing into the S phase of the cell cycle. The bacterium continues to grow and synthesizes a new flagellum at the pole opposite to the stalk and assembles a Z-ring near the middle point. Finally, the cell divides into two progenies with different morphologies [99]. Unlike swarmer cell, the stalked daughter cell is non-motile and reproducible, remaining attached to the environmental surface.

The asymmetrical cell cycle of *Caulobacter* requires complex coordination of genetic expression, proteolysis, phosphorylation, and second messenger signaling. System biologists have proposed a series of mathematical models to study the temporal regulations of chromosome replication and cell differentiation of *Caulobacter*. Li et al. [20, 89] and Weston et al. [22] have utilized a core cell cycle regulatory network, consisting of four master regulators CtrA, DnaA, GcrA, and CcrM, to investigate the mechanisms and capture the behaviors of the cell cycle development in wild type and novel mutant cells. Subramanian et al. [124, 125] have demonstrated how *Caulobacter* utilizes the bistability and phosphotransfer of regulatory proteins to navigate the cell cycle. Xu et al. have preliminarily explored how second messengers detect and respond to the environmental nutrition changes through PTS systems [118] (Chapter 2). However, how *Caulobacter* cell cycle responds to starvation and the corresponding detailed mechanisms are yet elucidated. In this study, we are motivated to develop a mathematical model to explore the cell cycle mechanism in the context of nutrient stress.

Starvation behaviors of *Caulobacter* cells. Under carbon or nitrogen starved conditions, *C. crescentus* arrests its cell cycle, however, the details of arrest are a bit controversial. Swarmer cells that are introduced to carbon or nitrogen depleted medium immediately arrest at G1. It was thought that swarmer cells arrest and keep their swarmer morphology

unless the environmental nutrient is replenished [75, 126, 6]. However, Britos et al. [127] observed that 65% of carbon starved swarmer cells develop stalks and only 11% initiate DNA replication after 2 hours. Therefore, there is an agreement on the G1 arrest of starved swarmer populations, but whether swarmer cells develop stalks or remain in the swarmer morphology is debatable. Gorbatyuk et al. [75] observed that most stalked cells remain in the pre-divisional phase after 180 min of carbon starvation. However, Ronneau et al. [6] suggested that starved stalked cells demonstrated delays in S phase and cytokinesis, but eventually divide and arrest at G1 after 200-260 min. To summarize, these experiments suggest that carbon or nitrogen starved swarmer populations immediately arrest in G1 phase while starved stalked populations go through a significant delay in cell division and arrest in G1 phase (Fig. 4.1C).

Response to nutrition signals by second messengers in *Caulobacter*. Guanine-based second messengers, (p)ppGpp and cdG, have been reported to influence the cell cycle behavior under nitrogen and carbon starvation conditions [6, 40]. As mentioned in Chapter 2, (p)ppGpp is synthesized from GDP and GTP by the synthetase form of the bifunctional enzyme, SpoT, in *Caulobacter* [44], while the hydrolase form of SpoT converts (p)ppGpp back into GDP/GTP. The conformation exchange between the SpoT synthetase and hydrolase state is regulated by the phosphorylation state of enzymes involved in the nitrogen Phosphotransferase System (PTS^{Ntr}) [6]. Carbon and nitrogen starvation signals are detected by the PTS^{Ntr} system through changes of intracellular concentrations of glutamine, pyruvate (Pyr) and phosphoenolpyruvate (PEP). These molecules directly influence the phosphate transfer within the PTS^{Ntr} system, which downstream determines the activity of SpoT. We have developed a mathematical model involving the PTS^{Ntr} and guanine-based secondary messenger network (Chapter 2). Our model captures the dramatic increase of (p)ppGpp level and decreases of GTP and cdG levels under carbon and/or nitrogen starvation [118], which is consistent with experimental observations [6, 40]. In addition to PTS^{Ntr}, the carbon PTS system, which is conserved in many bacteria types, may influence SpoT activities by detecting carbon starvation signals - the concentration of PEP and Pyr. Moreover, the carbon PTS likely interacts with PTS^{Ntr} through phosphate transfer because their enzymes share some conserved domains [128, 129]. However, the mechanisms underlying the crosstalk between carbon PTS and PTS^{Ntr} are not fully investigated.

***Caulobacter* cell cycle response to nutrition changes.** The depletion of environmental nutrients targets *Caulobacter* regulatory proteins to arrest the cell cycle and to conserve energy to survive [130]. Here, we refer to carbon and nitrogen starvation as "starvation" unless otherwise stated, because these pathways mostly rely on the same signaling mechanisms.

The proteolysis of master regulator CtrA is inhibited by a SpoT-dependent pathway under starvation condition [131]. It was previously thought the CtrA is stabilized by (p)ppGpp, the downstream second messengers regulated by SpoT. However, our second messenger model (Chapter 2) demonstrated that starvation-induced SpoT activity leads to reduced GTP and cdG levels. As cdG participates in CtrA proteolysis, it is more likely that SpoT impairs CtrA proteolysis through the decrease of cdG levels. Despite being stabilized, CtrA levels are still

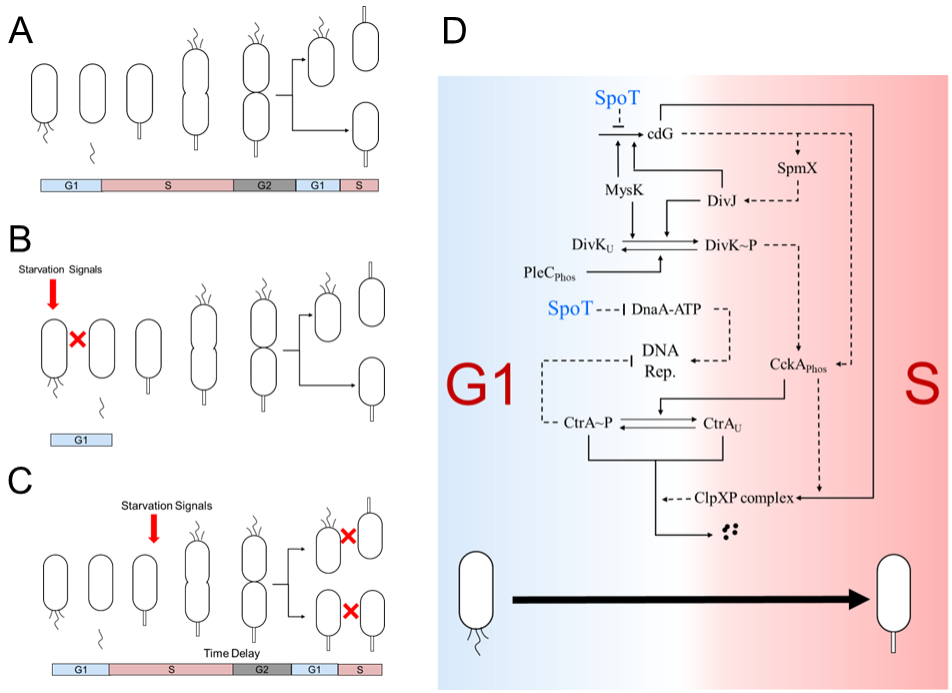

Figure 4.1: **Nitrogen/Carbon starvation leads to G1 arrest.**
(A) In nutrient rich conditions, C. crescentus undergoes an asymmetrical cell cycle. Upon cytokinesis, the stalked daughter cell immediately enters S phase while the swarmer cell delays chromosome replication and enters G1. (B) Starved swarmer populations exhibit immediate G1 arrest. (C) Starved stalked populations show delays in S phase and cytokinesis followed by G1 arrest. (D) The G1-S transition is dependent on regulations of CtrA∼P and DnaA (DnaA-ATP), which directly inhibit and promote DNA replication, respectively. In G1, levels of PleC phosphatase (PleCphos), unphosphorylated DivK ($DivK_U$) and CtrA∼P are high. During the G1-S transition, PleC levels decrease with the increased levels of kinase DivJ and cdG, leading to accumulation of SpmX, DivK∼P and CckA phosphatase. As a result, CtrA∼P levels decrease, chromosome replication initiates, and cells enter S phase. Solid lines indicate metabolisms, including conversion between two species, synthesis, and degradation. Dashed lines indicate influential interactions, where an arrowhead indicates a positive influence and a flat head indicates inhibition.

reduced to approximately 30% of normal levels in starved cells [127]. It is suggested that the decrease of CtrA levels is partially dependent on SigT, however the detailed mechanism has not been determined [127].

Additionally, levels of cell cycle regulator DnaA are rapidly reduced under starvation conditions due to decreased dnaA translation efficiency and constitutive proteolysis by Lon protease [121]. It has been demonstrated that the depletion of DnaA is dependent on (p)ppGpp [75], however the mechanism is yet to be elucidated.

Because CtrA and DnaA suppress and activate the initiation of chromosome replication, respectively, the starvation signaling likely induces the G1 arrest via regulating CtrA and DnaA stability [131]. However, the detailed mechanism of this possibility is not clear and should be further explored. First, the half-life of DnaA protein under starvation condition is 16-20 minutes [126, 121]. It has been reported that 50% of observed swarmer cells enter S phase around 22 min after synchronization under rich medium [84]. Therefore, there should be mechanism(s) independent of DnaA to halt DNA replication in starved swarmer cells, resulting in the G1 arrest. Moreover, while CtrA is first stabilized when starvation is introduced, only the phosphorylated form (CtrA$\sim$P) can inhibit chromosome replication and it is unclear whether CtrA remains phosphorylated under starvation.

The phosphorylation status of CtrA is regulated by CckA kinase and phosphatase. As discussed in Chapter 2, cdG decreases under starvation, which should also reduce CckA phosphatase activity, promoting dephosphorylation and inactivation of CtrA; however, the cdG0 strain (deleting cdG) can navigate through the cell cycle without arrest [57]. It demonstrates that cdG is not sufficient to halt DNA replication. Additionally, the regulator DivK binds to DivL to switch CckA from kinase to phosphatase [132]. A previous study indicates that strains depleted of DivK result in G1 arrest [133], which suggests that DivK likely plays an important role in response to starvation signaling.

Under starvation conditions, DivJ does not localize to the old pole as it typically does under nutrient-rich conditions [59]. The delocalization of DivJ is likely caused by the decrease of SpmX, the scaffolding protein that localizes DivJ at the old pole [18], as cdG influences SpmX levels through a ShkA-ShpT-TacA signaling pathway at the G1 to S transition [94]. cdG is understood to activate the phosphorylation of TacA, which improves the transcription of spmX [94]. Importantly, SpmX also increases the activity of DivJ kinase.

Figure 3.1D summarizes how the nutrient-regulated SpoT signaling controls the G1-S transition. However, the underlying nutrient signaling mechanisms and details need further studies. In this chapter, we integrate our second messenger model [118] into a temporal cell cycle regulatory network [22] to analyze the molecular mechanisms of nutrition starvation. We find that the identified signaling pathways can explain many biological observations, but are not sufficient to explain the delayed cytokinesis of stalked cell populations. A cdG-independent regulatory pathway has the potential to reduce the levels of CtrA under starvation, causing the significant delay of cytokinesis in stalked cells. Additionally, we demonstrate that the cdG-involved second messenger network and DnaA expression both play important roles in

the G1 arrest of swarmer cells, while both are not sufficient to arrest cells under starvation conditions. The 'protection' of CtrA∼P from cdG at the initial stage of starvation is required for the G1 arrest. Our analysis also reveals both DivK and PleD activities contribute to the G1 arrest of starved cells.

4.3 Methods

In this study, we integrate our second messenger model [118] (see Chapter 2) into Weston et al.'s temporal model [22] with the newly modelled connections between second messengers and key regulators such as CtrA and CckA. Additionally, we modified and improved Weston et al.'s model with newly investigated pathways to enhance the biological accuracy. Here we specify our modifications. The full list of equations is provided in Appendix C1, where modifications are indicated in the red font.

4.3.1 Modeling PTS$^{\mathrm{Ntr}}$/SpoT nutrient signaling cascade through cdG:

In chapter 2, we modeled the response of secondary messengers - (p)ppGpp, GTP, and cdG - to starvation signals in *Caulobacter* [118]. We found that the SpoT enzyme dramatically influences GTP levels through conversion into (p)ppGpp, which leads to reduced cdG synthesis. On the contrary, we find that cdG synthesis and hydrolysis rates make a negligible impact on GTP and (p)ppGpp levels because cdG concentrations are negligible compared to GTP concentrations in *C. crescentus* [57] and other bacteria species [134]. Based on this observation, we import GTP levels from the second messenger model [118] (Chapter 2) under normal and starvation conditions and adjust the synthesis rate of cdG such that:

$$\begin{aligned}\frac{d[\mathrm{cdG}]}{dt} =&(k_{\mathrm{s,cdG1}}\cdot[\mathrm{PleD}\sim\mathrm{P}]+k_{\mathrm{s,cdG2}}\cdot[\mathrm{DgcB}]_{\mathrm{a}})\cdot\frac{[\mathrm{GTP}]^2}{[\mathrm{GTP}]^2+J_{\mathrm{s,cdG}}^2}-k_{\mathrm{d,cdG1}}\\&\cdot([\mathrm{PdeA}]+PDE)\cdot[\mathrm{cdG}]-\mu\cdot[\mathrm{cdG}]+2\cdot(-k^{+}_{\mathrm{PopAcdG}}\cdot[\mathrm{PopA}]\cdot[\mathrm{cdG}]^2\\&+(k^{-}_{\mathrm{XcdG}}+K_{\mathrm{d,PopA}})\cdot[\mathrm{PopA:cdG_2}])+2\cdot(-k^{+}_{\mathrm{PleDcdG}}\cdot[\mathrm{PleD}]_{\mathrm{T}}\cdot[\mathrm{cdG}]^2\\&+(k^{-}_{\mathrm{XcdG}}+K_{\mathrm{d,PleD}})\cdot[\mathrm{PleD:cdG_2}]_{\mathrm{T}})-k^{+}_{\mathrm{CckAcdG}}\cdot([\mathrm{CckA}]_{\mathrm{T}}-[\mathrm{CckA:cdG}])\\&\cdot[\mathrm{cdG}]+k^{-}_{\mathrm{CckAcdG}}\cdot[\mathrm{CckA:cdG}]+2\cdot(-k^{+}_{\mathrm{DgcBcdG}}\cdot(DgcB-[\mathrm{DgcB:cdG_2}]))\\&\cdot[\mathrm{cdG}]^2+k^{-}_{\mathrm{XcdG}}\cdot[\mathrm{DgcB:cdG_2}],\end{aligned}\tag{4.1}$$

where the red text highlights the change made to the cdG differential equation from Weston et al's model. Here, $J_{\mathrm{s,cdG}}$ indicates the concentration of GTP corresponding to half maximal synthesis. We input different GTP levels to adjust the synthesis of cdG under normal and

starved conditions in this study, where $J_{\mathrm{s,cdG}} = 1500\mu M$, [GTP]=$1221\mu M$ for nutrient rich condition and $227\mu M$ for starved condition (obtained from Xu et al. [118] or Chapter 2). Therefore, the fractional term $\frac{[\mathrm{GTP}]^2}{[\mathrm{GTP}]^2+J_{\mathrm{s,cdG}}^2}$ is reduced to 5.6%-fold under starvation.

4.3.2 cdG regulates the morphogenesis of *Caulobacter* through ShkA-TacA-SpmX pathway

cdG regulates SpmX accumulation, which recruits DivJ to the old pole, at the G1-S transition [7]. cdG synthesis is impaired from starvation [118] and DivJ delocalization has been observed in starved Caulobacter cells [59, 94], which suggests that SpmX synthesis is dramatically reduced under such conditions. In weston et al's model [22] SpmX is modelled via a simplistic function to reduce model complexity. In order to accurately capture the molecular mechanism of starvation signaling in *Caulobacter*, we modify the modeling of SpmX with its transcription regulation.

cdG controls the expression of *spmX* through the ShkA-TacA pathway. Phosphorylated TacA controls the transcription of SpmX [18, 94], which recruits and activates DivJ at the stalked pole [135] (see Fig. 4.1). TacA is activated by a phosphorelay system, including a hybrid histidine kinase ShkA and a phosphotransferase protein ShpA [94]. cdG binds to ShkA to induce the kinase activity of ShkA [133, 136]. ShkA kinase transfers phosphates to a His residue of the phosphotransferase ShpA, which are then received by the receiver domain of TacA in sequence [133, 94]. Additionally, a few HisKA-family kinases, such as ShkA, EnvZ [137], and WalK [138], share a conserved HXXXT domain. As EnvZ and WalK are reported as bifunctional enzymes [139, 140], we assume ShkA is also bifunctional, where ShkA is the phosphatase form and ShkA:cdG is the active kinase form.

We were unable to find information regarding temporal regulation of ShpA in the literature. Thus, we turn to a similar CckA-ChpT-CtrA pathway, where ChpT concentrations are stable throughout the cell cycle [30]. We assume that ShpA level is constant throughout the cell cycle; thus, the kinetics of ShpA transfer can be collapsed into the transfer of phosphates between ShkA and TacA directly, to simplify the model.

CtrA∼P directly promotes the expression of *shkA* [141] and *tacA* [94]. Additionally, ShkA and TacA are both proteolyzed by ClpXP, but depend on different arrangements of adaptor molecules [94]. The proteolysis of ShkA requires the adaptors PopA, cdG, RcdA and CpdR, while TacA proteolysis only requires CpdR and RcdA [94]. Therefore, the ShkA-TacA pathway includes both cdG-mediated activation and cdG-dependent degradation. We model the ShkA-TacA pathway as follows:

$$\begin{aligned}
\frac{d[\mathrm{ShkA}]}{dt} &= k_{\mathrm{s,ShkA}} \cdot \frac{[\mathrm{CtrA}\sim\mathrm{P}]}{[\mathrm{CtrA}\sim\mathrm{P}] + J_{\mathrm{a,ShkACtrA}}} - (k_{\mathrm{d,ShkA1}} + \mu) \cdot [\mathrm{ShkA}] \\
&\quad - k_{\mathrm{d,ShkA2}} \cdot [\mathrm{ClpXP}]_{\mathrm{Complex}} \cdot \frac{[\mathrm{ShkA}]}{[\mathrm{ShkA}]_{\mathrm{T}} + J_{\mathrm{d,ShkA}}} \\
&\quad - k^{+}_{\mathrm{ShkAcdG}} \cdot [\mathrm{cdG}] \cdot [\mathrm{ShkA}] + k^{-}_{\mathrm{ShkAcdG}}, \\
\frac{d[\mathrm{ShkA:cdG}]}{dt} &= -(\mu + k_{\mathrm{d,ShkA1}}) \cdot [\mathrm{ShkA:cdG}] \\
&\quad - k_{\mathrm{d,ShkA2}} \cdot [\mathrm{ClpXP}]_{\mathrm{Complex}} \cdot \frac{[\mathrm{ShkA:cdG}]}{[\mathrm{ShkA}]_{\mathrm{T}} + J_{\mathrm{d,ShkA}}} \\
&\quad + k^{+}_{\mathrm{ShkAcdG}} \cdot [\mathrm{cdG}] \cdot [\mathrm{ShkA}] - k^{-}_{\mathrm{ShkAcdG}},
\end{aligned} \tag{4.2}$$

where $k_{\mathrm{s,ShkA}}$ is the synthesis rate of ShkA and $J_{\mathrm{a,ShkACtrA}}$ indicates the dissociation constant between CtrA∼P and the *shkA* promoter. $k_{\mathrm{d,ShkA1}}$ and $k_{\mathrm{d,ShkA2}}$ represent the basal degradation rate and ClpXP-dependent degradation rate, respectively. $[\mathrm{ClpXP}]_{\mathrm{complex}}$ is the complex of ClpXP, cdG, RcdA and CpdR, as described later. $J_{\mathrm{d,ShkA}}$ is the dissociation constant between ShkA and the ClpXP complex. k^{+}_{ShkAcdG} and k^{-}_{ShkAcdG} represent binding and unbinding rates between ShkA and cdG, respectively.

Regulation of TacA is described as:

$$\begin{aligned}
\frac{d[\mathrm{TacA}]}{dt} &= k_{\mathrm{s,TacA}} \cdot \frac{[\mathrm{CtrA}\sim\mathrm{P}]}{[\mathrm{CtrA}\sim\mathrm{P}] + J_{\mathrm{a,TacACtrA}}} - (k_{\mathrm{d,TacA1}} + \mu) \cdot [\mathrm{TacA}] \\
&\quad - k_{\mathrm{d,TacA2}} \cdot [\mathrm{RcdA:CpdR}] \cdot \frac{[\mathrm{TacA}]}{[\mathrm{TacA}]_{\mathrm{T}} + J_{\mathrm{d,TacA}}} \\
&\quad - k_{\mathrm{phos,TacA}} \cdot [\mathrm{ShkA:cdG}] \cdot [\mathrm{TacA}] + k_{\mathrm{dephos,TacA}} \cdot [\mathrm{ShkA}] \cdot [\mathrm{TacA}\sim\mathrm{P}], \\
\frac{d[\mathrm{TacA}\sim\mathrm{P}]}{dt} &= -k_{\mathrm{d,TacA2}} \cdot [\mathrm{RcdA:CpdR}] \cdot \frac{[\mathrm{TacA}\sim\mathrm{P}]}{[\mathrm{TacA}]_{\mathrm{T}} + J_{\mathrm{d,TacA}}} + k_{\mathrm{phos,TacA}} \cdot [\mathrm{ShkA:cdG}] \cdot [\mathrm{TacA}] \\
&\quad - (\mu + k_{\mathrm{d,TacA1}} + k_{\mathrm{dephos,TacA}} \cdot [\mathrm{ShkA}]) \cdot [\mathrm{TacA}\sim\mathrm{P}],
\end{aligned} \tag{4.3}$$

where $k_{\mathrm{s,TacA}}$ represents the synthesis rate of TacA. $k_{\mathrm{d,TacA1}}$ and $k_{\mathrm{d,TacA2}}$ indicate the rates of basal degradation and degradation catalyzed by the protease complex, ClpXP:CpdR:RcdA, respectively. $k_{\mathrm{phos,TacA}}$ and $k_{\mathrm{dephos,TacA}}$ indicate the phosphorylation and dephosphorylation constants of TacA, respectively.

The modified equation of SpmX is given by:

$$\frac{d[\mathrm{SpmX}]}{dt} = k_{\mathrm{s,SpmX}} \cdot \frac{[\mathrm{TacA}\sim\mathrm{P}]}{[\mathrm{TacA}\sim\mathrm{P}] + J_{\mathrm{a,SpmXTacA}}} - (k_{\mathrm{d,SpmX}} + \mu) \cdot [\mathrm{SpmX}], \tag{4.4}$$

where $k_{\mathrm{s,SpmX}}$ and $k_{\mathrm{d,SpmX}}$ represent the synthesis and proteolysis rates of SpmX, respectively. $J_{\mathrm{a,SpmXTacA}}$ indicates the binding affinity between TacA∼P and *spmX* promoter.

In addition to recruiting DivJ, SpmX stimulates the kinase activity of DivJ. DivJ kinase activity is upregulated by interacting DivK as well. However, it is unclear how much the activity is influenced when DivJ is bound to just SpmX, just DivK, or both molecules. For simplicity, we assume that DivJ activity is negligible when not bound by either SpmX or DivK, and that DivJ is at 100% activity when bound by both, DivK and SpmX. We further assume that the phosphorylated and unphosphorylated forms of DivK impact the DivJ activity to a similar degree. Hence, we model the active DivJ kinase as follows:

$$\begin{aligned}[\text{DivJ}]_{\text{A}} = &([\text{DivJ} : \text{DivK} \sim \text{P}] + [\text{DivJ} : \text{DivK}]) \\ &\cdot ((1 - \epsilon_{\text{DivJDivK}}) \cdot (\frac{\min([\text{SpmX}], [\text{DivJ}]_{\text{T}})}{[\text{DivJ}]_{\text{T}}}) + \epsilon_{\text{DivJDivK}}) \\ &+ \epsilon_{\text{DivJSpmX}} \cdot [\text{DivJ}] \cdot \frac{\min([\text{SpmX}], [\text{DivJ}]_{\text{T}})}{[\text{DivJ}]_{\text{T}}},\end{aligned} \tag{4.5}$$

where $\epsilon_{\text{DivJSpmX}}$ dictates the fraction of activity DivJ has when only bound to SpmX and $\epsilon_{\text{DivJDivK}}$ is the fraction of DivJ activity when only bound to DivK. The function $\min([\text{SpmX}], [\text{DivJ}]_{\text{T}})$ represents the fraction of DivJ bound by SpmX.

4.3.3 Modifications to modeling the ClpXP and adaptor complex

The degradation of TacA is dependent on the ClpXP:CpdR:RcdA complex, where the independent interaction between RcdA and CpdR:ClpXP was not considered in Weston et al's model [22]. Here, we assume that RcdA may interact with CpdR independently of its phosphorylated state, and therefore we define the concentration of the RcdA:CpdR complex as:

$$[\text{RcdA} : \text{CpdR}]_{\text{T}} = \frac{[\text{CpdR}]_{\text{T}} + [\text{RcdA}] + K_{\text{RcdACpdR}} - \sqrt{([\text{CpdR}]_{\text{T}} + [\text{RcdA}] + K_{\text{RcdACpdR}})^2 - 4 \cdot [\text{CpdR}]_{\text{T}} \cdot [\text{RcdA}]}}{2} \tag{4.6}$$

where K_{RcdACpdR} is the dissociation constant for the RcdA:CpdR complex. As only unphosphorylated CpdR interacts with the ClpXP complex to catalyze proteolysis [27], we calculate the concentration of RcdA bound to unphosphorylated CpdR such that:

$$[\text{RcdA} : \text{CpdR}] = [\text{RcdA} : \text{CpdR}]_{\text{T}} \cdot \frac{[\text{CpdR}]}{[\text{CpdR}]_{\text{T}}}$$

Additionally, it was shown that the proteolysis of RcdA adaptor is targeted by the CpdR:ClpXP complex [95], which was modelled in Weston et al. [22]; however, *in vivo* expression patterns

of RcdA do not reflect significant proteolysis at the timing of CpdR expression [142, 143]. Therefore, we have removed this insignificant interaction in our model and obtain the following differential equation for RcdA:

$$\frac{d[\mathrm{RcdA}]}{dt} = k_{\mathrm{s,RcdA}} \cdot \frac{[\mathrm{CtrA} \sim \mathrm{P}]^2}{[\mathrm{CtrA} \sim \mathrm{P}]^2 + J^2_{\mathrm{a,RcdACtrA}}} - (\mu + k_{\mathrm{d,RcdA}}) \cdot [\mathrm{RcdA}], \tag{4.7}$$

where $k_{\mathrm{s,RcdA}}$ and $k_{\mathrm{d,RcdA}}$ are the synthesis and degradation rates, respectively, and $J^2_{\mathrm{a,RcdACtrA}}$ corresponds to concentration of CtrA∼P that leads to half-maximal rates of synthesis of RcdA.

4.3.4 An unknown kinase phosphorylating PleD and DivK and a newly identified phosphatase CckN dephosphorylating DivK∼P are introduced

PleD, the primary synthetase of cdG, is active in its phosphorylated form (PleD∼P) and is regulated by DivJ kinase and PleC phosphatase [113]. Previous experiments have measured that SpmX is expressed in Δ*divJ* and double mutant Δ*divJ*Δ*pleC* strains, while transcription of *spmX* decreases to 1/4 of wild type cells in Δ*pleD* [94]. Together with the cdG-ShkA-TacA-SpmX pathway introduced in Section 4.3.2, these results indicate that PleD is phosphorylated and active in Δ*divJ* and Δ*divJ*Δ*pleC* strains. Therefore, there must be an unknown kinase responsible for the phosphorylation of PleD independently of DivJ and PleC. Moreover, significant levels of phosphorylated DivK have been identified in Δ*divJ* and double mutant Δ*divJ*&*pleC* :: Tn5 strains [14]. As DivJ and PleC are the only known kinases of DivK, this result indicates that an unknown kinase must regulate DivK as well. These observations suggest that there is at least one unknown kinase acting on DivK and PleD. We assume the unknown kinase regulating PleD and DivK is the same one and name this mystery kinase 'MysK' for short. Here, we include 'MysK' as an independent parameter in the phosphorylation reaction of DivK and PleD (see Appendix C1).

As the Δ*divJ*&*pleC* :: Tn5 strain expresses DivK∼P at ∼27% of WT levels [14], we also justify that DivK∼P must have a significant basil rate of hydrolysis relative to MysK activity, otherwise DivK∼P levels should be much greater than 27% of WT in the presence of a sufficient kinase. In support of an additional phosphatase, CckN has been identified as a phosphatase for DivK. Furthermore, it was shown that CckN makes little impact on the phosphorylation of DivK in the presence of DivJ and PleC, but makes a profound impact in their absence [104]. Additionally, the expression of *cckN* is induced in stationary phase, depending on the accumulation of (p)ppGpp [104]. As (p)ppGpp increases in responding to starvation signals, CckN likely increases under starvation conditions.

The transcription of *cckN* is stimulated by CtrA∼P, while its degradation depends on ClpX with unknown adaptor(s) [104]. The observation of CckN abundance over cell cycle time

indicates that CckN is quickly and dramatically degraded during the G1-to-S transition, faster than the degradation of CtrA. We speculate that the unknown adaptor(s) in CckN-specific protease complex likely behave similarly with PopA:cdG$_2$ although it is independent with PopA based on mutant analyses [104]. Here, we borrow PopA:cdG$_2$ to simulate the degradation of CckN and model the phosphatase CckN as follows:

$$\begin{aligned}\frac{d[\mathrm{CckN}]}{dt} &= k_{\mathrm{s,CckN}} \cdot \frac{[\mathrm{CtrA} \sim \mathrm{P}]^4}{[\mathrm{CtrA} \sim \mathrm{P}]^4 + J^4_{\mathrm{a,CckNCtrA}}} - (\mu + k_{\mathrm{d,CckN1}}) \cdot [\mathrm{CckN}] \\ &\quad - k_{\mathrm{d,CckN2}} \cdot [\mathrm{PopA} : \mathrm{cdG_2}] \cdot \frac{[\mathrm{CckN}]}{[\mathrm{CckN}] + J_{\mathrm{d,CckN}}},\end{aligned} \tag{4.8}$$

CckN is integrated into the dephosphorylation reaction of DivK (See Appendix C1).

4.3.5 RpoD-regulated transcriptions are affected by starvation

The sigma factor RpoD (σ^{70}) in *Caulobacter* directly mediates the transcription of house-keeping genes, while sigma factors are observed to respond to stresses and influence down-stream gene transcriptions in other bacteria, such as *E. coli* and *B. subtilis* [144]. RpoD levels are reduced to 78% in 30 min after carbon starvation in *Caulobacter*, suggesting a RpoD-dependent pathway of stringent response [144]. RpoD targets the promoter of many genes, including *ctrA*, *divK*, *pleC*, *pleD*, *rcdA*, and so on [141]. Moreover, high-throughput proteome analyses show that DivK levels, CtrA levels, and PleD levels decrease to 70%, 40%, and 10% in wild type cells upon 60 min carbon deprivation, respectively; while the rest RpoD-downstream proteins do not significantly shift under starvation [127]. Considering the importance of CtrA, DivK, and PleD in cell cycle regulation, we take RpoD-regulated pathways into our model. We introduce 'RpoD' as an adjustable parameter, being 1 in nutrient-rich condition and 0.1 in starved condition, into the modeling of synthesis of DivK, CtrA, and PleD (See Appendix C1).

4.3.6 Modelling other starvation signaling pathways

(p)ppGpp influences numerous other molecules in response to starvation. SpoT is required for the rapid proteolysis of DnaA upon starvation, which is confirmed by Δ*spoT* mutant analysis [126]. We reduce DnaA synthesis ($k_{\mathrm{s,DnaA}}$) in our model to simulate the inhibition of DnaA translation efficiency under stress. (p)ppGpp constrains cell size and slows down cell growth under starvation, where the underlying mechanisms have not been identified [59, 131]. In this study, we reduce the average cell growth rate from normal conditions by 1/3 to capture decreased growth rates under starvation. While evidence suggests that there is no significant growth in *Caulobacter* colonies after 8 hrs of monitoring starvation [75], we assume that there

must be some growth in the initial stages of starvation response as stalked cells continue to proceed through their cell cycle slowly and divide before G1 arrest [6].

4.3.7 Improvement to SciP modeling

As SciP binds to several genes targeted by CtrA to perturb promoter activity, including the *ctrA* promoter [81]. Meanwhile, CtrA in turn activates expression of *sciP* through the *sciP* promoter. The interaction between SciP and CtrA is essential for the robustness of DNA replication regulation, which is involved in Chapter 3 and Weston et al.'s model [22]. Here, we incorporate the observation that SciP binds to its own promoter to impair transcription [141]. The improved equation of SciP is as follows:

$$\frac{d[\text{SciP}]}{dt} = k_{\text{s,SciP}} \cdot \frac{[\text{CtrA} \sim \text{P}]^2}{[\text{CtrA} \sim \text{P}]^2 + J^2_{\text{a,SciPCtrA}}} \cdot \frac{J^2_{\text{i,SciPSciP}}}{J^2_{\text{i,SciPSciP}} + [\text{SciP}]^2} - (\mu + k_{\text{d,SciP}}) \cdot [\text{SciP}], \quad (4.9)$$

where $k_{\text{s,SciP}}$ and $k_{\text{d,SciP}}$ are the synthesis rate and degradation rate, respectively. μ indicates the dilution rate due to C. crescentus cell growth. $J_{\text{a,SciPCtrA}}$ and $J_{\text{i,SciPSciP}}$ describe the affinity of CtrA:*sciP*-promoter and SciP:*sciP*-promoter binding, respectively.

4.3.8 Deriving parameter sets

In general, we use the same parameterization algorithm, the Monte-Carlo Markov-Chain method, as described in Weston et al's model [22]. However, different list of mutant strains are used for estimating parameters in this research as follows: P*pleC*::Tn, Δ*ccrM*, Δ*gcrA*, Δ*pleD*, *divL*A601L, *ctrA*Δ3Ω, *ctrA*D51E, P*pleC*::Tn&Δ*divJ*, Δ*divJ*.

To be specific, we start from a seed parameter set $\mathbf{P}=(p_1, p_2, ..., p_n)$. A temporary parameter set, $\mathbf{P}' = (p_1', p_2', ..., p_n')$, is generated as follows:

$$p_i' = p_i(1 + \xi_i \cdot N(0, \sigma)),$$

where ξ_i is a Boolean variable, either 0 or 1, which is randomly determined by a MATLAB built-in function. $N(0, \sigma)$ is a normal distribution with a mean of 0 and a standard deviation of σ.

Whether $\mathbf{P}'$ replaces $\mathbf{P}$ as the new parameter set is determined by the following algorithm (same in Weston et al's model [22]):

$$\mathbf{P} = \mathbf{P}' \text{if} \quad g \leqslant T,$$

Table 4.1: Signaling targets and arrest statistics.

Paradigm	Description	Parameters changes		Fractional Arrested*			
				1^{st}G1	2^{nd}G1	1^{st}G2	2^{nd}G2
Signal 1	Introducing stress response through cdG-dependent pathway. Inhibiting DnaA synthesis. Decreasing all RpoD-dependent transcriptions increasing CckN synthesis	$k_{s,DnaA} = 0$ $k_{s,cdG1} = 0.056k_{s,cdG1}$ $k_{s,cdG2} = 0.056k_{s,cdG2}$ $\mu = 0.0018$ RpoD=0.1 $k_{s,CckN} = 1.5k_{s,CckN}$	**SW**	100%	0	0	0
			ST	2.1%	96.9%	0.5%	0
Signal 2	Introducing stress response through cdG-dependent pathway. Inhibiting DnaA synthesis. Decreasing all RpoD-dependent transcriptions increasing CckN synthesis Decreasing CtrA.	$k_{s,DnaA} = 0$ $k_{s,cdG1} = 0.056k_{s,cdG1}$ $k_{s,cdG2} = 0.056k_{s,cdG2}$ $\mu = 0.0018$ RpoD=0.1 $k_{s,CckN} = 1.5k_{s,CckN}$ $k_{s,CtrA1} = k_{s,CtrA1}/30$ $k_{s,CtrA1} = k_{s,CtrA1}/30$	**SW**	100%	0	0	0
			ST	3.1%	96.4%	0	0
Signal 3	Inhibiting DnaA synthesis. Decreasing all RpoD-dependent transcriptions increasing CckN synthesis Decreasing CtrA.	$k_{s,DnaA} = 0$ $\mu = 0.0018$ RpoD=0.1 $k_{s,CckN} = 1.5k_{s,CckN}$ $k_{s,CtrA1} = k_{s,CtrA1}/30$ $k_{s,CtrA1} = k_{s,CtrA1}/30$	**SW**	13.3%	86.7%	0	0
			ST	0.5%	99%	0	0
Signal 4	Introducing stress response through cdG-dependent pathway.	$k_{s,cdG1} = 0.056k_{s,cdG1}$ $k_{s,cdG2} = 0.056k_{s,cdG2}$ $\mu = 0.0018$	**SW**	10.2%	0	0	0
			ST	0.6%	0	0	0

* 1^{st} G1 corresponds to cells with immediate G1 arrest (no chromosome replication). 2^{nd} G1 corresponds to cells that divide and then arrest at G1. 1^{st} G2 corresponds to cells that initiate chromosome replication but never divide. 2^{nd} G2 corresponds to cells that replicate DNA twice but only divide once.

$$T = \min(\exp(\frac{f(\mathbf{P}) - f(\mathbf{P}')}{\tau}), 1),$$

where g is a random number between 0 and 1. f represents the cost function. The cost function in this research is determined in Appendix C2.

4.4 Results

4.4.1 Investigating performance of model

To study the response of *Caulobacter*, we first improve Weston et al's model [22] and integrate the network with our second messenger network (Chapter 2), the ShkA-TacA-SpmX pathway, mystery kinase, CckN phosphatase, RpoD-related transcription, and several signaling mechanisms (Figure 4.2).

To ensure our new model and parameter sets are in sufficient agreement with experimentally observed behavior, we analyze the prediction of mutant strain viability by the new model (Fig, 4.3A). The success rate in predicting the viability of 35 mutant strains, 70 types of cell populations (SW and ST) in total, is about 80%, which is reasonable considering the complexity of our model and the large number of predicted strains. Additionally, we compare the temporal dynamics of key regulators in WT swarmer cell in simulation with this in experiments (Fig. 4.3B), which matches very well with the experimental observations.

Given that Caulobacter arrests at G1 under starvation and CtrA∼P regulates the G1-S transition, we conduct further analysis to ensure that our model can accurately capture the regulation of CtrA phosphorylation. CckA is regulated by DivK and cdG [28]. The model in Chapter 2 suggests that cdG should be depleted due to SpoT activity in starvation conditions [118], but the behavior of DivK phosphorylation has not been investigated, to the best of our knowledge, under carbon or nitrogen stress. To ensure our model can predict DivK∼P levels reliably, we evaluate DivK∼P levels measured in mutants from two different papers: 1) Wheeler and Shapiro (1999) [14]; 2) Radhakrishnan et al. (2008) [18]. We conduct our own quantitative analysis of the Western blots provided by Wheeler and Shapiro and Radhakrishnan et al. utilizing ImageJ software (Table 4.2). Our simulation of DivK(∼P) shows reasonable agreement with experimental analysis.

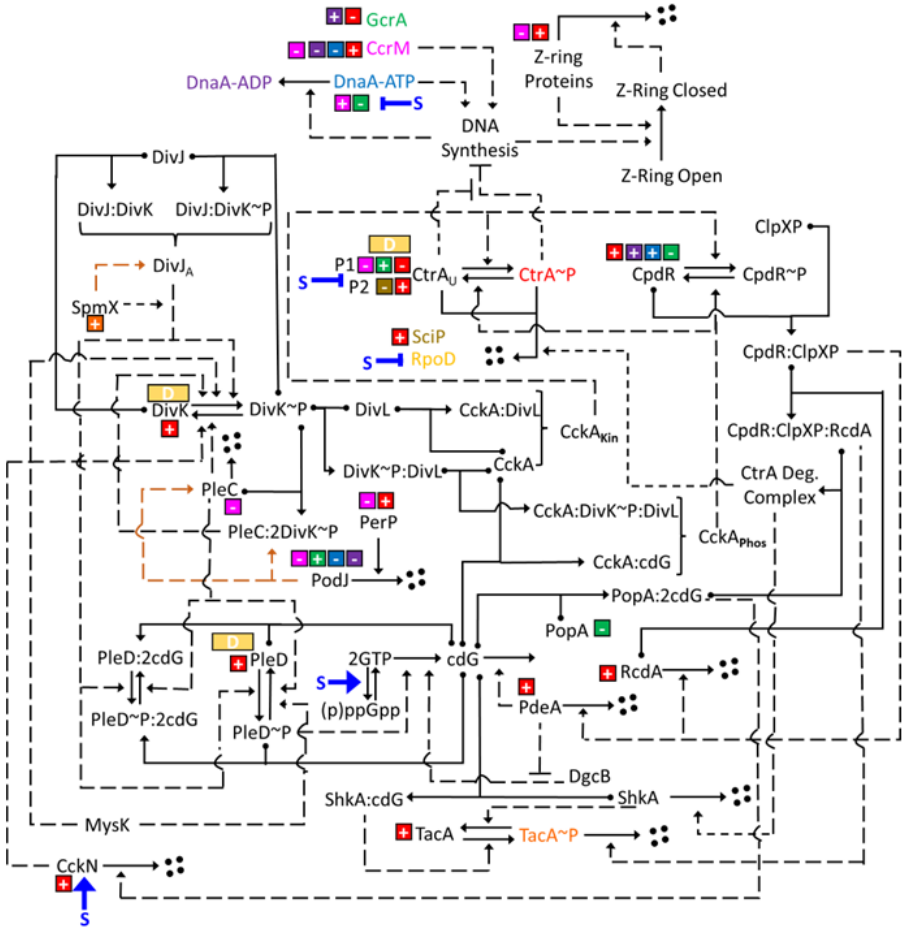

Figure 4.2: **Wiring diagram of regulatory interactions captured by the model.** A box with a plus or minus sign indicates whether the protein indicated by the same color (e.g., green = GcrA) activates or inhibits expression of the gene. The sigma factor RpoD is indicated as yellow where its promoter regulation is indicated in yellow box. Dot-headed solid line indicates the binding of species (e.g., PopA and RcdA form the PopA:RcdA complex). Chemical conversion of one molecular species to another is indicated by an arrow. Proteolysis is depicted by an arrow from a protein to four black circles. Dashed arrows indicate an 'influence' (e.g., catalysis) of a protein on a chemical reaction. A dashed orange arrow indicates spatial influence. A bright blue S indicates an element of starvation signaling, where arrow represents activation and bar represents inhibition influence (see Table 4.1).

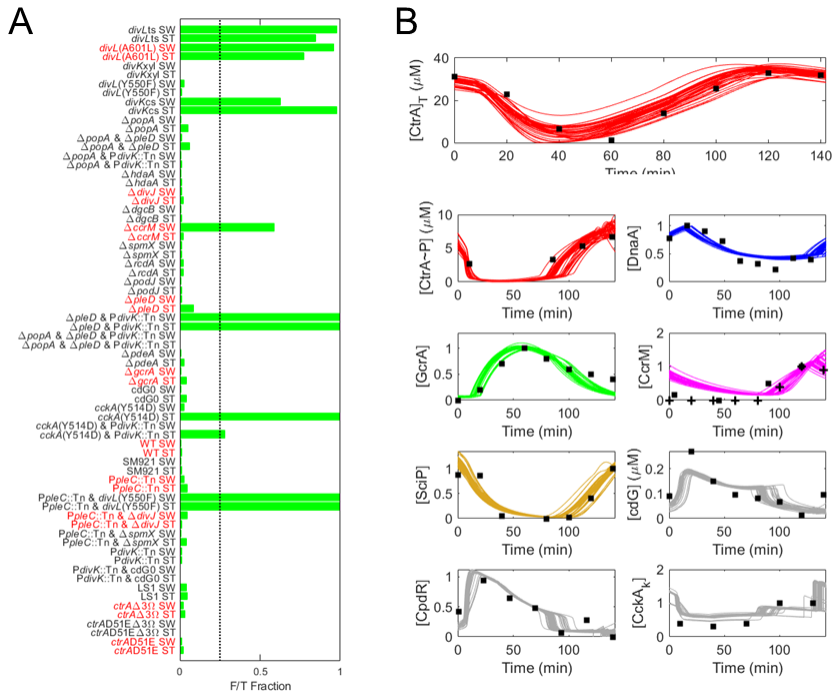

Figure 4.3: **Model and parameter sets fit experimental data reasonably well.** (A) The fraction of total simulations that failed (F/T fraction) is plotted for each mutant case. A simulation is considered as 'failed' if it predicts cell cycle arrest when experimental observations report a viable cell cycle, or vice versa. Mutant simulations in this chapter have the same parameter setting with Weston et al. [22]. 150 parameter sets were chosen at random from the parameter set collection and simulated for both swarmer cell (SW) and stalked cell (ST). The black dashed line corresponds to an arbitrary threshold (25%) that we use to compute the success rate of strain prediction. Strains labeled with red font were included in the parameterization cost function (see Method). (B) For 50 randomly selected parameter sets, we plot swarmer-cell simulations in comparison to experimental data. Data collected as follows: [$CckA_K$]: Jacobs et al. [145]; [CpdR]: Iniesta et al. [143]; [cdG]: Abel et al. [57]; [SciP]: Tan et al. [81]; [CcrM]:+, Zhou and Shapiro [146]; [CcrM]: solid square, Grunenfelder et al. [147]; [GcrA]: Holtzendorff et al. [114]; [DnaA]: Cheng and Keiler [148]; [CtrA∼P]: Jacobs et al. [145]; $[CtrA]_T$: Mcgrath et al. [142]. In all plots except [cdG], $[CtrA]_T$ and [CtrA∼P], concentrations are unitless and normalized to the experimental data, which predict relative concentrations over time are normalized to one. $[CtrA]_T$ and [CtrA∼P] experimental data are also unitless, however, absolute CtrA concentrations in our model are a prediction and therefore the data is normalized to the simulation output. The absolute concentration of cdG is quantified from the source of the data, and the simulation of cdG is not normalized.

Table 4.2: DivK∼P levels in various mutant strains.

	Normailzed DivK∼P (%)			Normailzed Ratio $\frac{\text{DivK}\sim\text{P}}{\text{DivKT}}$ (%)		
Source of Data	Ref [14]	Ref [18]	Model Results	Ref [18]	Ref [14]	Model Results
Source of Analysis	This study*	This study*	This study	This study*	This study*	This study
WT	100	100	100	100	100	100
Δ*spmX*	-	36	46	36	-	43
Δ*divJ*	8	4	0.1	4	7	0.1
Δ*pleC*	142	179	160	225	170	185
Δ*spmX*&Δ*pleC*	-	187	147	222	-	169
Δ*divJ*&Δ*pleC*	7	-	27	-	7	28

* Analysis conducted using ImageJ software.

4.4.2 Introducing known signaling mechanisms of starvation (Signal 1) successfully captures the first G1 arrest of swarmer population and the secondary G1 arrest of stalked population

Given reasonable agreement of our model with experimental data, we proceed to investigate how our model responds to environmental signals. The exact mechanism of nutrient signaling is not clear in many cases. For instance, it is observed that GcrA levels decrease significantly under carbon starvation [141], but whether this is a downstream consequence of shifts in transcription factor activity (e.g. due to shifts in CtrA activity) or due to an independent signaling mechanism is unclear. Here, we first introduce a signal that we define as 'Signal 1' (Table 4.1) of starvation and compare simulations with observations. Signal 1 composes of 1) inhibition to the translation of *dnaA*; 2) impaired synthesis of cdG due to the response of the PTS^{Ntr}-SpoT pathway [118]; 3) reduced growth rate; 4) decreased RpoD-dependent transcription of *ctrA*, *divK*, and *pleD*; and 5) increased CckN.

When introducing Signal 1 at t=0 (G1 phase/swarmer cell), we find that the cell cycle arrests immediately (Figure 4.4A and Table 4.1), which is observed by experiments [75, 126, 6]. We call this the first G1 arrest. When introducing Signal 1 at t=45 (S phase/stalked cell), the cell cycle appears to be relatively unhindered but arrests at the G1 stage after cytokinesis (Figure 4.4B and Table 4.1). We call this the secondary G1 arrest. Although the secondary G1 arrest is observed in experiments, stalked cells introduced to starvation should also exhibit significant delays in cytokinesis [6]. Therefore, Signal 1 can explain the G1 arrest of starved cells, while the stalked cycle-cycle delay is not captured.

To identify whether or not Signal 1 can adequately explain DnaA and CtrA expression patterns, we plot simulations against temporal protein expression data from a population of nitrogen starved swarmer cells, retrieved from Gorbatyuk et al. [75] (Figure 4.4C and D). We find that Signal 1 adequately explains DnaA expression but does not capture the

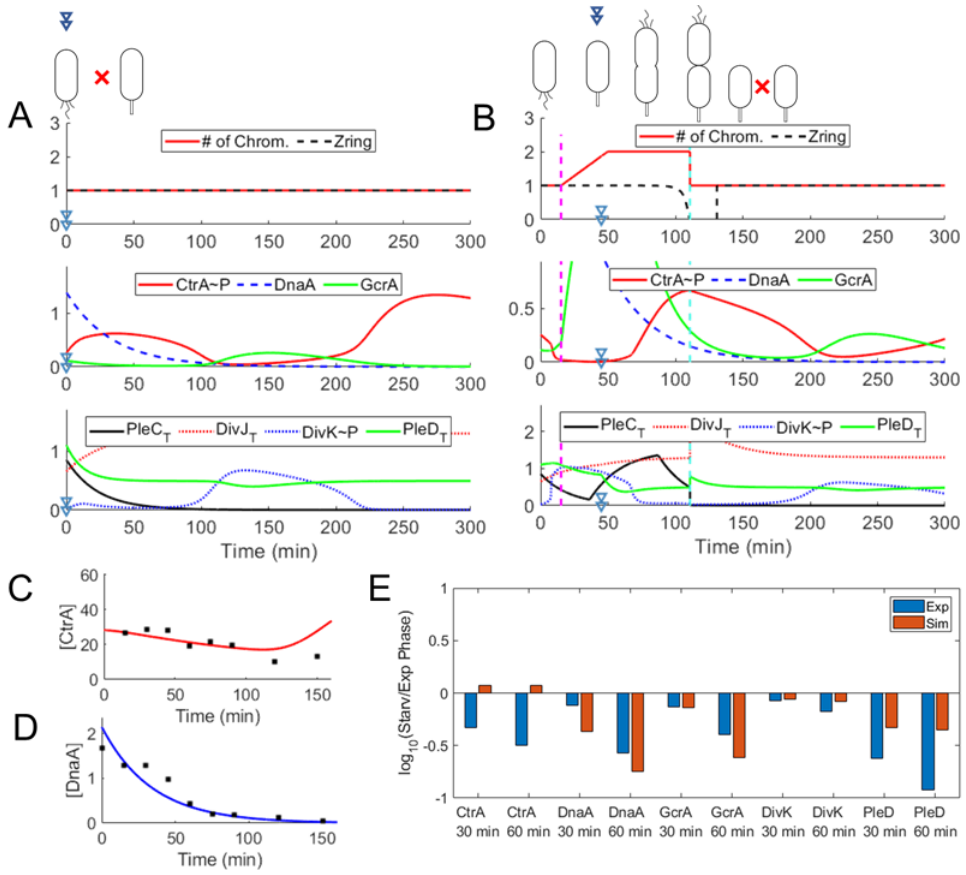

Figure 4.4: **Cell cycle response of starvation Signal 1.**
(A) Swarmer cell simulation of Signal 1 response. Plot of chromosome count and Z-ring constriction (first panel) and select normalized protein concentrations (second and third panel). Concentrations are normalized to average WT expression. When the Zring variable is equal to 1, the Z-ring is fully open. It is closed when Zring is equal to 0. The corresponding position in the cell cycle is indicated in the illustration above. A double arrow indicates when the nutrient signal is introduced. A red "X" represents that swarmer cells arrest in the stage indicated (G1 phase for this figure). (B) Stalked cell simulation of Signal 1 response. Stalked cells arrest at the secondary G1 as indicated in the illustration. All other details are the same as in "A". (C) CtrA expression levels in swarmer cell simulations relative to normalized data extracted from Gorbatyuk et al. [75]. (D) DnaA expression levels in swarmer cell simulations relative to normalized data extracted from Gorbatyuk et al. [75]. (E) Protein expression levels 30 and 60 minutes after nutrient depletion relative to nutrient rich conditions. 'Exp' indicates experimental observations from Britos et al. [127]. 'Sim' indicates average simulation values from 30 and 60 minutes into simulations of swarmer, stalked and pre-divisional cells.

pattern of CtrA. Additionally, we compare the simulated abundance of CtrA, DnaA, DivK, and PleC under Signal 1 with their experimental measurements under carbon starvation conditions (30 min and 60 min after starvation was introduced) [127] in Fig. 4.4E. We find Signal 1 can capture the general response of most indicated proteins except for CtrA. Our simulation results suggest the decrease of RpoD-regulated *ctrA* expression in our model is not sufficient to overcome the initial stabilization of CtrA caused by the cdG shift. As CtrA levels are eventually reduced under starvation, there should be cdG-independent and might be RpoD-independent pathways controlling the response to starvation. Moreover, the successful prediction of GcrA response to starvation indicates the current pathways are substantially sufficient to reduce GcrA in starved cells, so we do not need to introduce independent GcrA pathways to simulate the starvation response in *Caulobacter*.

4.4.3 The decreased expression of CtrA contributes to observed delays in cytokinesis of starved stalked cells

In the simulation with Signal 1, the CtrA levels do not reduce as low as Britos et al indicates [127], which suggests that there are likely unknown pathways controlling CtrA under starvation condition. Moreover, Signal 1 can not explain the obvious delay in cytokinesis observed in starved stalked cells.

Here, we introduce Signal 2 (Table 4.1), integrating the enforced reduction of CtrA expression with Signal 1, to investigate the influence of reduced CtrA. Not surprisingly, Signal 2 still performs well in the simulation of starved swarmer cells and DnaA expression pattern under starvation conditions (Fig. 4.5A and D). Additionally, the expression pattern of CtrA and its abundance changes under starvation are accurately captured by simulations with Signal 2 (Fig. 4.5C and E). Importantly, Signal 2 can explain the delayed cytokinesis of starved stalked cells (Fig. 4.5B), which suggests the reduced CtrA contributes to the observed delay in cytokinesis for stalked cells under starvation condition. Moreover, the simulation of $[\mathrm{CtrA}]_\mathrm{T}$ and [CtrA∼P] in swarmer cell (Fig. 4.5A and C) suggests that phosphorylated CtrA levels are relatively high at the initial stage of starvation introduction to inhibit the initiation of chromosome replication, although the total levels of CtrA reduce.

4.4.4 cdG-dependent pathways play important roles in the response to starvation signals

cdG shifts dramatically under different concentrations of environmental nutrients, and it regulates the activity and abundance of the master regulator CtrA through several pathways [118]. Here, we delete the cdG-dependent pathways from Signal 2, calling it Signal 3 (Table 4.1), to study the contribution of cdG in the response to starvation.

Without the cdG-dependent pathways, our simulated swarmer population exhibits the sec-

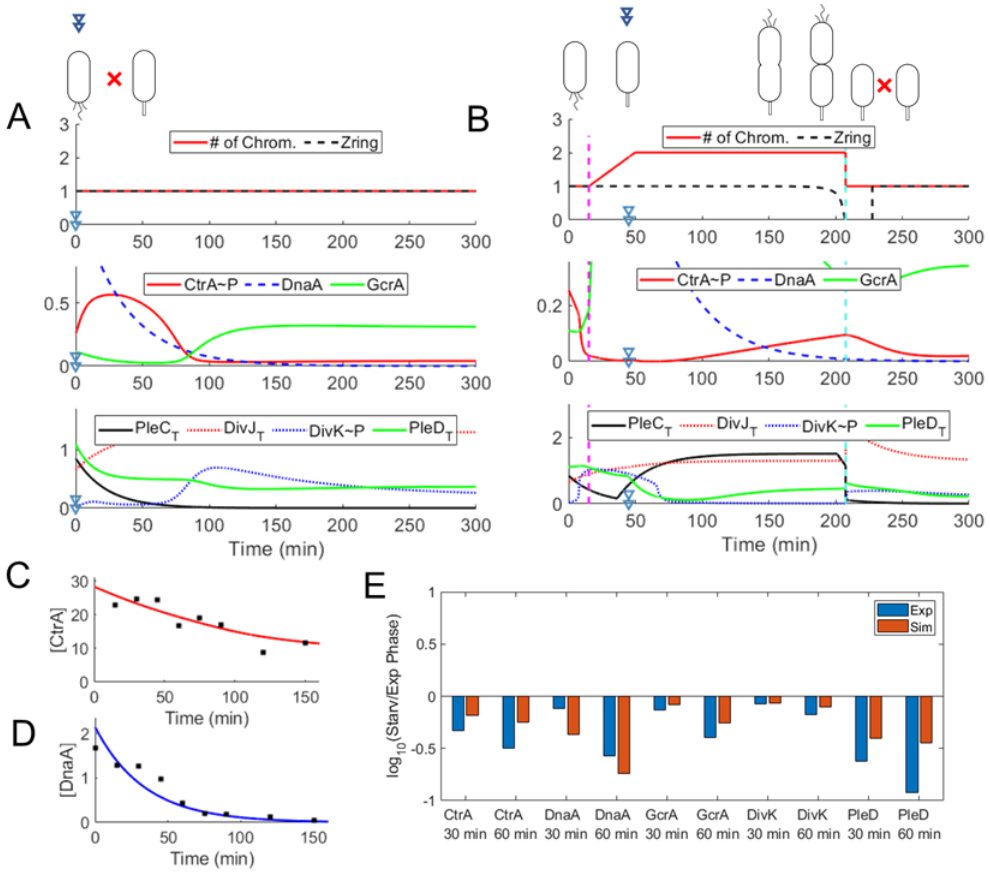

Figure 4.5: **Starvation Signal 2 simulations fit experimental observations well with the exception of CtrA expression.**
(A) Swarmer cell simulation of Signal 2 response. Red "X" indicates immediate G1 arrest. Other details are identical to Figure 4.4A. (B) Stalked cell simulation of Signal 2 response. Red "X" indicates the secondary G1 arrest in stalked daughter cell. Other details are identical to Figure 4.4A. (C) CtrA expression levels in swarmer cell simulations relative to normalized data extracted from Gorbatyuk et al. [75]. (D) DnaA expression levels in swarmer cell simulations relative to normalized data extracted from Gorbatyuk et al. [75]. (E) Protein expression levels 30 and 60 minutes after nutrient depletion relative to nutrient rich conditions. Details specified in Figure 4.4E.

ondary G1 arrest in 86.7% of our parameter sets, while only 13.3% of our parameter sets indicate immediate cell cycle arrest at G1 for swarmer cells (Table 4.1). Our research suggests the cdG-involved second messenger network proposed in Chapter 2 is significant for the immediate G1 arrest of swarmer cells in starved environments. Additionally, although the simulation with Signal 3 performs well in predicting shifts of key proteins including CtrA after 30 min and 60 min of starvation introduced (Fig. 4.6E), it can not exactly capture the expression pattern of CtrA under starvation condition (Fig. 4.6C). Taken the simulation of Signal 3 and previous simulations with Signal 1 and Signal 2 together, our model suggests that the immediate G1 of swarmer cells results from a relatively high level of CtrA∼P inhibiting the DNA replication. Our simulation further suggests that cdG decreases under starvation condition to 'protect' CtrA∼P and inhibits the S-entry.

Additionally, the simulation with starvation Signal 3 together with previous starvation Signal 1 indicates that the decrease of DnaA in swarmer cells under starvation is not sufficient to prevent chromosome replication. A closer investigation reveals that DnaA levels are about 35-45% of peak levels at the timing of chromosome replication. Leslie et al. showed that *Caulobacter* cells in stationary phase have DnaA levels that are approximately 10-18% of exponential phase [121]. Furthermore, since cells still divide, albeit slowly, in stationary phase, this suggests that 10-18% of typical DnaA levels (compared to a nutrient rich simulation) should be sufficient for chromosome replication. Altogether, these investigations suggest that the rate of DnaA depletion is not fast enough to explain G1 arrest from starvation signaling. Therefore, the reason of G1 arrest under starvation is that CtrA∼P remains sufficiently high to inhibit chromosome replication, at least until DnaA can be sufficiently depleted.

4.4.5 cdG-dependent pathways are not sufficient to arrest cells

We keep the reduced growth rate and cdG-dependent pathways in Signal 4 to investigate whether the important cdG-related response is sufficient to capture observations of starved cells. We find neither swarmer cells nor stalked cells arrest as experiments suggest in the simulation with Signal 4 via most parameter sets (Table 4.1, Fig. 4.7A and B). Our simulation agrees with the experimental observation that cdG0 strain (deleting cdG) is not arrested.

We also try other combinations of starvation response pathways shown in Table C3.1. When adding reduced DnaA expression into Signal 4, calling it Signal 5a, the simulated swarmer cells with 92.3% parameter sets can arrest at the first G1 stage, while the simulated stalked cells with 98.4% parameter sets can arrest at the secondary G1 stage. Therefore, our model suggests that the reduced level of DnaA is essential for the cell cycle response to starvation, although it is not enough to stimulate the rapid G1 arrest of swarmer cells. We further explore the significance of RpoD-dependent transcription of *ctrA*, *divK*, and *pleD* with Signal 5b-5d (Table C3.1). Signal 5c (adding decreased RpoD-regulated *divK* expression) increases the fraction of first G1 arrest of swarmer cells from 92% to 100%, while Signal 5d (adding decreased RpoD-regulated *pleD* expression) improves this index to 97%.

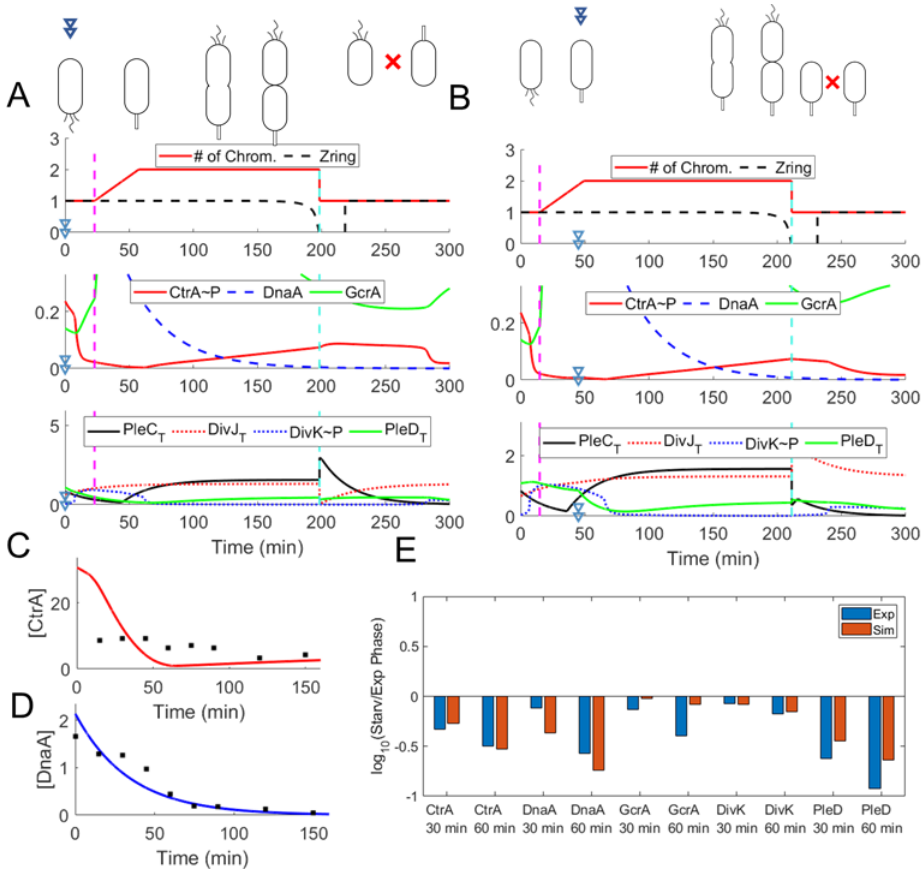

Figure 4.6: **Starvation Signal 3 is not sufficient to arrest swarmer cells in the first G1 stage.**
(A) Swarmer cell simulation of Signal 3 response. Swarmer cell is not arrested at the first G1 phase. Other details are identical to Figure 4.4A. (B) Stalked cell simulation of Signal 3 response. Red "X" indicates the secondary G1 arrest in the stalked daughter cell. Other details are identical to Figure 4.4A. (C) CtrA expression levels in swarmer cell simulations relative to normalized data extracted from Gorbatyuk et al. [75]. (D) DnaA expression levels in swarmer cell simulations relative to normalized data extracted from Gorbatyuk et al. [75]. (E) Protein expression levels 30 and 60 minutes after nutrient depletion relative to nutrient-rich conditions. Details specified in Figure 4.4E.

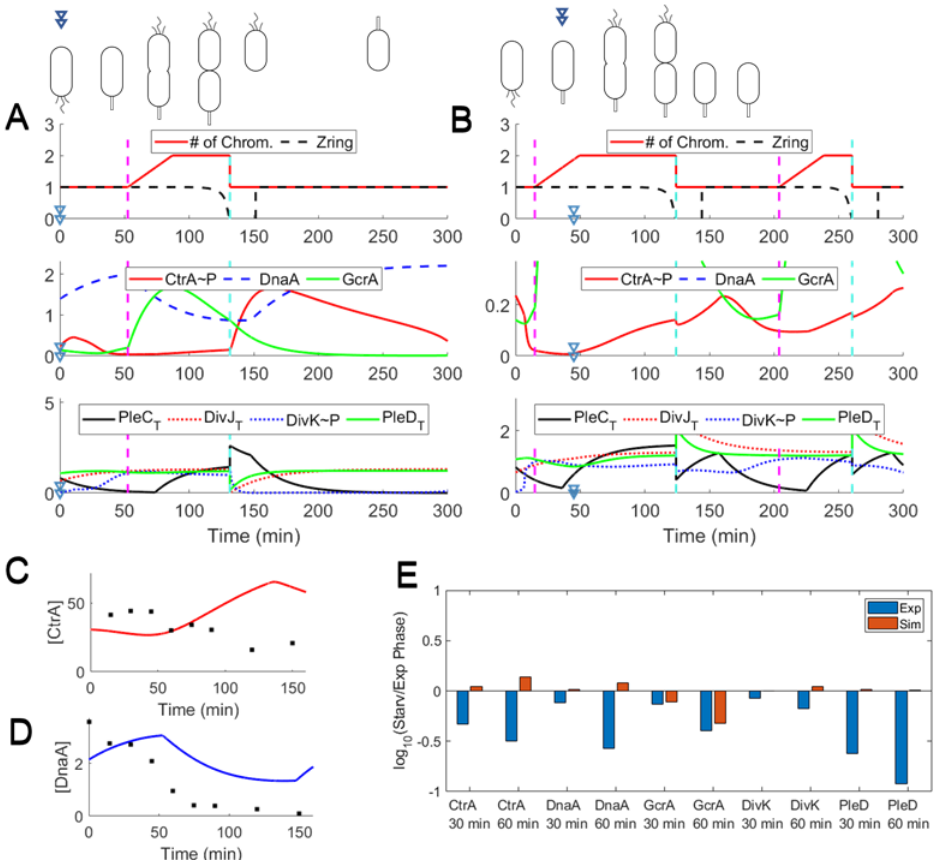

Figure 4.7: **Starvation Signal 4 is not sufficient to arrest cells.**
(A) Swarmer cell simulation of Signal 4 response. Swarmer cell is not arrested in this case. Other details are identical to Figure 4.4A. (B) Stalked cell simulation of Signal 4 response. Stalked cell is not arrested in this case. Other details are identical to Figure 4.4A. (C) CtrA expression levels in swarmer cell simulations relative to normalized data extracted from Gorbatyuk et al. [75]. (D) DnaA expression levels in swarmer cell simulations relative to normalized data extracted from Gorbatyuk et al. [75]. (E) Protein expression levels 30 and 60 minutes after nutrient depletion relative to nutrient rich conditions. Details specified in Figure 4.4E.

Both reduced *divK* expression and reduced *pleD* expression help to improve the simulation performance of swarmer population arrest, while the *divK* expression plays more important roles.

4.5 Discussion

In this study, we investigate the molecular mechanism behind *Caulobacter* cell cycle arrest from nutrient starvation. Our model has good agreement with experimental observations in the phenotypes of WT and mutant cells under nutrient-rich condition (Fig. 4.3, Table. 4.2). Based on the rationality of this model, we further explore the contribution of known starvation-relevant pathways (Signal 1) and find that these pathways are sufficient to capture most characteristics of starved cells except for two observed phenomena: 1) the delayed cytokinesis of stalked cells and 2) the expression pattern of CtrA which does not reduce to a low level which experiments suggest. Therefore, we enforce the reduction of CtrA level in Signal 2, which solves the above two problems. This suggests that nutrient signals must influence CtrA via additional mechanisms to explain reduced CtrA expression under carbon and nitrogen starvation. The delayed cytokinesis in starved stalked cells seems to be a consequence of the slowed synthesis of Z-ring proteins which are controlled by CtrA∼P. Altogether, CtrA∼P remains high at the initial starvation stage because cdG is reduced, and it is required to decrease to delay the cytokinesis in starved stalked populations.

In previous work (Chapter 2) [118], Xu et al. demonstrated that cdG levels are likely depleted due to the accumulation of (p)ppGpp, thus providing a link between (p)ppGpp regulation and CtrA proteolysis. cdG is also responsible for the accumulation of SpmX at the G1-S transition via TacA and ShkA [94]. Modelling the ShkA-TacA-SpmX pathway reinforces the relationship between cdG and phosphorylation state of CtrA. We expand on this work here and find that the sole cdG response is not sufficient for cell cycle arrest (Table 4.1, Signal 4). However, when we remove the impaired cdG from the starvation signal (Signal 3), we find that immediate G1 arrest in swarmer cells is heavily compromised. Thus, while the proposed signal from Chapter 2 is not sufficient on its own to explain starvation response behavior, it is an essential component of the starvation response. Our simulation results suggest that the cdG-dependent stabilization of phosphorylated CtrA is essential for the G1 arrest of starved cells, while the following reduction of total CtrA levels is caused by unclear control mechanisms. Similarly, our simulations with Signal 5a and Signal 3 suggest the reduced expression of DnaA is essential but not sufficient for the rapid G1 arrest of swarmer cells population. Our model suggests that the *Caulobacter* response to starvation signals is under multifaceted regulations and interactions.

In addition to essential players in starvation response control, such as cdG and DnaA, there are a few regulators that contribute to the robust and rapid G1 arrest. We individually introduce the RpoD-regulated expression of *divK* and *pleD* in starvation signals, which play roles in phospho-signaling. DivK affects the phosphorylation of CtrA and CpdR through

switching CckA from kinase to phosphatase state, while PleD is the major synthetase producing cdG from GTP molecules. The simulation results suggest that the reduced expression of both *divK* and *pleD* stimulate the G1 arrest, where *divK* is more powerful than *pleD*. Additionally, a newly discovered DivK phosphatase CckN has demonstrated elevation in response of (p)ppGpp [104]. Comparing the simulation result of Signal 1 and Signal 5d, with and without the shift of CckN, we find that the CckN-pathway also helps cells to arrest at G1 when nutrition is depleted.

In summary, our results indicate that numerous aspects of the cell cycle machinery are targets of starvation signals. The phosphorylation of CtrA together with DnaA determine the G1 arrest, while CtrA also influences the cytokinesis delay under starvation. Although second messengers are small molecules with relatively low levels in *Caulobacter* cells compared with proteins, they play key roles in detecting and responding to starvation signals.

Chapter 5

Turing-pattern model of scaffolding proteins that establishes spatial asymmetry during the cell cycle of *Caulobacter crescentus*

Chunrui Xu[1], John J. Tyson[2], Yang Cao[3]

1 Genetics, Bioinformatics, and Computational Biology, Virginia Tech, Blacksburg, VA, USA
2 Department of Biological Science, Virginia Tech, Blacksburg, VA, USA
3 Department of Computer Science, Virginia Tech, Blacksburg, VA, USA

5.1 Abstract

Caulobacter crescentus is a model organism to investigate the spatial asymmetry of prokaryotes. The dimorphic cell division cycle of *Caulobacter crescentus* is driven by the asymmetrical localization and periodical appearance of key regulatory proteins that control cell fate, such as the master regulator CtrA. The spatial regulations of phosphotransfer and proteolysis of CtrA are characterized by two distinct signaling hubs at opposite poles of the *Caulobacter* cell, where the scaffolding protein PodJ and PopZ work as the central organizer at the flagellated pole and the stalked pole respectively. In this study, we use a modified Turing-pattern mechanism to simulate the spatiotemporal dynamics of scaffolding proteins, accounting for the initial arrangement at distinct poles. Additionally, the non-uniform distributions of key regulators involved in two phosphotransfer modules, DivJ/PleC-DivK and DivL-CckA-CtrA, are investigated based on the network of scaffolding proteins. Our math-

ematical model captures key features of wild-type and mutant strains, and we predict the distribution of CtrA∼P in mutant strains.

5.2 Introduction

The asymmetrical distribution of proteins in prokaryotic cells contributes to diverse biological processes, including morphogenesis, stress response, and signal transduction [149, 150]. The oligotrophic aquatic bacterium, *Caulobacter crescentus* (*Caulobacter*), is a model organism for investigating the bacterial cellular asymmetry, in which at least 10% of proteins are non-uniformly distributed across cells [149, 151]. *Caulobacter* undergoes a dimorphic cell cycle regulated by asymmetrically distributed proteins, such as the master cell cycle regulator CtrA, producing two distinct progenies: a motile non-replicable swarmer cell with a high level of phosphorylated CtrA (CtrA∼P) and a sessile replicable stalked cell with a low level of CtrA∼P [125] (Fig. 5.1). As phosphorylated CtrA inhibits the initiation of DNA replication by targeting the chromosome replication origin (*Cori*) in *Caulobacter*, the swarmer daughter cell is required to reduce the CtrA∼P level to reproduce. The nascent swarmer cell goes through a phase named swarmer-to-stalked (sw-to-st) transition given suitable environments, reducing the level of CtrA∼P and differentiating into the stalked morphology, whereas the stalked cell can immediately enter the next replication cycle [152, 3, 15]. The predivisional cell, with a flagellum at the 'new' pole and a stalk at the 'old' pole, establishes a spatial gradient of CtrA∼P, with high levels near the flagellated end and low levels near the stalked end (Fig. 5.1). Then, the cell divide asymmetrically producing distinct daughters, where the new swarmer cell enters the sw-to-st transition stage and the new stalked cell re-commences DNA replication (Fig. 5.1). Additionally, CtrA is an essential transcriptional factor controlling the expression of over 90 genes in *C,crescentus* [153, 25]. During the sw-to-st transition, the flagellum of swarmer cell is shed and replaced by a stalk and holdfast, which is also regulated by the level of CtrA∼P.

As CtrA is of great importance for DNA replication, gene transcription, and cell cycle regulation, its spatial concentration gradient is a decisive factor for the establishment of asymmetry in *Caulobacter*. The abundance of active CtrA is determined through three pathways: synthesis, proteolysis, and phospho-signaling. The temporal regulation of CtrA synthesis has been well studied [20]. There are two *ctrA* promoters: the weaker promoter (P1) is inhibited by CtrA∼P and the stronger promoter (P2) is activated by CtrA∼P. Additionally, three other major regulators - DnaA, GcrA, and CcrM - collaborate with CtrA constituting a pivotal regulatory network to orchestrate the cell cycle and ensure the robustness of *Caulobacter* [22, 20, 89]. Li et al. [20, 89] converted the regulatory network into quantitative models, investigating the mechanisms underlying cell-cycle-based DNA replication, methylation, and protein metabolism. Simulation results of Li's model reproduced the temporal dynamics of key regulators in wild type (WT) and relevant mutant cells, and predicted the phenotype of novel mutants. Murray et al. proposed a simplified mathematical model

involving GcrA, CtrA, and CcrM in the cell cycle regulatory network in *Caulobacter* [19]. Weston et al. constructed a CtrA-centric temporal mathematical model, suggesting that the unphosphorylated CtrA competes with the phosphorylated form for binding to the *Cori* [22]. However, these models fail to account for the localization of essential regulators, which are fundamental to the polar morphogenesis and asymmetry establishment in *Caulobacter*.

The phosphorylation state of CtrA is regulated by two phosphotransfer modules: DivL-CckA-CtrA and DivJ/PleC-DivK (Fig. 5.2, yellow and green boxes), where CckA and PleC are bifunctional histidine kinases working as either a kinase or phosphatase for their response regulators - CtrA and DivK, respectively [125, 154, 30, 124]. CckA mediates the phosphorylation/dephosphorylation of CtrA and CpdR via a phosphotransferase ChpT, while unphosphorylated CpdR is an essential component of the ClpXP protease complex specifically responsible for the proteolysis of CtrA [155]. Thus, CckA regulates the activity of CtrA through both phosphotransfer and proteolysis. Although CckA level remains constant throughout the cell cycle, its subcellular localization varies [156]. Time-lapse microscopy indicates that CckA has no preferential localization in swarmer stage and accumulates at the flagellated pole (new pole) during stalked and predivisional stages (Fig. 5.1, fluorescent yellow). Around 30% observed WT cells have a strong old-polar accumulation of CckA during the stalked stage, which suggests that the old pole may serve as a depot for surplus CckA, and CckA localized at the old pole is dispensable for normal cell cycle development [155, 30]. The switch between kinase and phosphatase of CckA is allosterically mediated by DivL and cyclic-di-GMP (cdG) [157]. DivL stimulates the kinase activity of CckA, whereas CckA binding with cdG or DivL:DivK∼P complex leads to the increase of CckA phosphatase activity [157, 132, 151]. Therefore, DivL connects the two phosphotransfer modules by interacting with DivK and CckA. Additionally, DivL is required for the new-polar localization of CckA [157, 158]. Another binding partner of CckA which may contribute to its localization is PopZ [159].

DivJ functions as a kinase phosphorylating DivK whereas PleC is the major phosphatase of DivK [160, 149]. In addition, PleC can function as a kinase of DivK in a specific state which is stimulated by DivK∼P [154]. Experiments have indicated that phosphorylated DivK accumulates at the old pole during most time of the cell cycle, while it is temporarily localized at the new pole in the predivisional stage and released from the new pole after cytokinesis [160] (Fig. 5.1, red). Interestingly, DivJ and PleC are localized at opposite poles during the cell cycle of *Caulobacter*: DivJ is localized at the old pole and PleC is localized at the new pole [14, 18] (Fig. 5.1, orange and purple). The function and polar localization of DivJ and PleC regulate the spatial phosphorylation and dephosphorylation of DivK. Therefore, DivK is phosphorylated at the old pole and dephosphorylated at the new pole, resulting in a lower level of DivK∼P in the swarmer compartment after cytokinesis [149].

Chen et al. [151] and Tropini et al. [149] have constructed mathematical models to simulate the development of CtrA∼P gradient in predivisional cells via CckA-relevant and DivK-relevant reactions, respectively. Their models account for the phenotype of relevant mutants and suggest that *Caulobacter* establishes robust asymmetry before cytokinesis. Subramanian

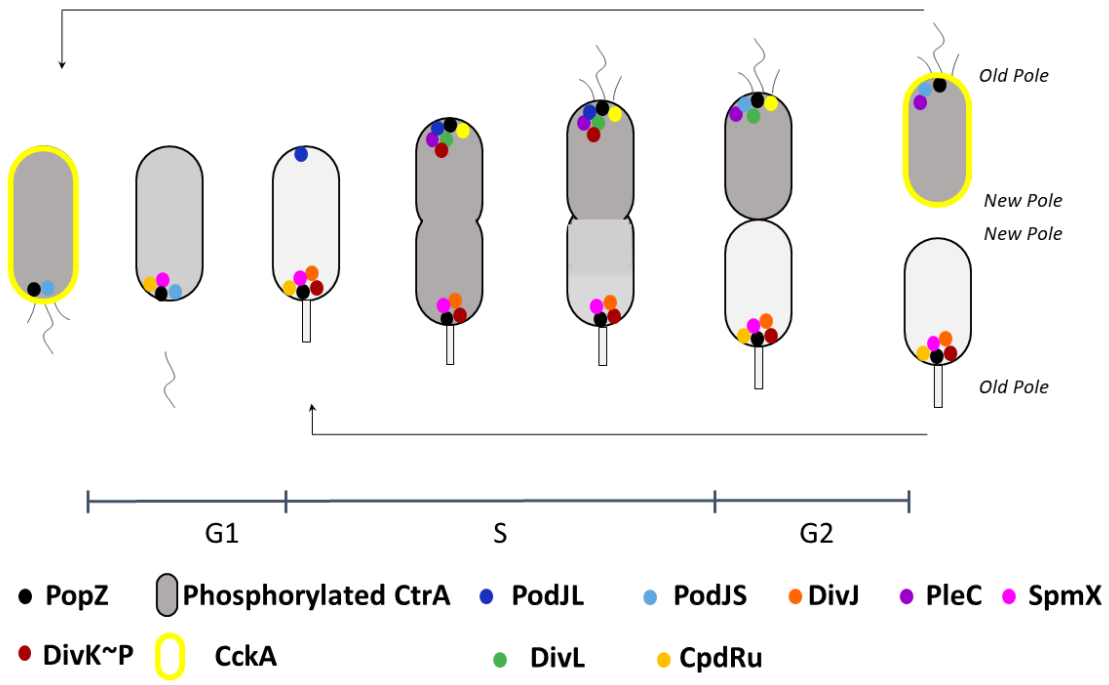

Figure 5.1: **Dynamic localization of key proteins over the cell cycle of *C. crescentus*.**
CtrA∼P develops a spatial concentration gradient during the cell cycle (gray). The three scaffolding proteins, PopZ, PodJ, and SpmX, interact with each other and recruit (directly or indirectly) client proteins at specific poles, including DivJ [18], PleC [7], DivK [18], CckA [159], DivL [159], and CpdR [159].

et al. [125] proposed an 'inhibitor-sequestration' model, suggesting that new-polar DivK∼P is sequestrated by PleC kinase, so that CckA can retain its kinase activity at the new pole in the predivisional stage.

These spatial modelling work provided certain insights into mechanisms of spatial regulations and morphogenesis of bacteria; however, in these models, initial non-uniform localizations were enforced and the source of localization could not be well explained. Normally, spatial orchestration is fulfilled by scaffolding proteins which initially occupy particular areas and recruit binding partners to the same or neighbouring area [161]. The localization and activity of several key regulators involved in the CtrA-centric network are dependent on the localization and interactions of three scaffolding proteins - PodJ, PopZ, and SpmX in *C. crescentus* [161, 18]. PodJ is localized at the flagellated pole, SpmX at the stalked pole, and PopZ at both poles during the cell cycle of *Caulobacter* [161, 18] (Fig. 5.1, blue, violet, and black). PodJ and SpmX directly bind to PleC and DivJ respectively, causing the new-polar PleC and old-polar DivJ [7, 18]. Additionally, the localization of DivK, DivL, CckA and CpdR are dependent on PopZ [159, 18, 162]. Mutant analysis indicates the new-polar DivL

is determined by PodJ [135]. As PleC and DivL, recruited by PodJ at the new pole, are binding partners of DivK, PodJ likely influences the localization of DivK as well.

Several hypotheses have been proposed for the initial polar localization of scaffolding proteins [161]. One suggests the nucleoid occlusion may result in polar distributions because poles, which are devoid of chromosomes, can provide sufficient space for the assembly of proteins [163]. Other suggestions indicate some unique elements of poles, such as the negative polar curvature [164, 165], lipid [165, 166] or peptidoglycan [167] composition, may cause polar accumulation of scaffolding proteins.

Chen et al. [92] and Subramanian et al. [168, 21] utilized the Turing-pattern mechanism to investigate the spatial dynamics of PopZ. The PopZ model suggests there is an unknown nucleating factor at the new pole recruiting PopZ to stabilize the bipolar accumulation. In this study, we use a similar reaction-diffusion mechanism to investigate the initial localization of three scaffolding proteins - PopZ, PodJ, and SpmX. We use protein-protein interactions together with Turing-pattern to simulate the temporal and spatial dynamics of scaffolding proteins and their client proteins. In our study, PodJ functions as a nucleating factor recruiting PopZ, which is sufficient to ensure the bipolar pattern of PopZ. Moreover, we apply the scaffolding protein network to explore the non-uniform distribution of CtrA, DivK, and CckA. Our mathematical model correctly reproduces two signaling hubs at two poles of a wild type cell and the phosphorylation state of DivK of mutant cells. Additionally, we predict the distribution of DivK$\sim$P and CtrA$\sim$P in mutant cases.

5.3 Methods

5.3.1 Reaction-diffusion equations and compartment-based discretization

We apply a reaction-diffusion model to capture the spatiotemporal dynamics of proteins. The governing partial differential equation (PDE) for a generic protein S is as follows (Eq. 5.1):

$$\frac{\partial C}{\partial t} = \text{Chemical Reaction Rates} + D\frac{\partial^2 C}{\partial x^2}, \tag{5.1}$$

where $C(x,t)$ is the concentration of protein S. D denotes the diffusion coefficient of S.

We use a compartment-based scheme to convert continuous equations to discrete compartments to solve PDEs. In addition, the compartment-based method allows us to extend the determined model to its stochastic version in our future work. Here, the total cell length (L) is divided into 10 even compartments of length $l = L/10$. Therefore, we convert the PDE into 10 ODEs as follows:

$$\begin{cases} \frac{dC_1}{dt} = \mathrm{CR} + \frac{D(C_2 - C_1)}{l^2} \\ \frac{dC_i}{dt} = \mathrm{CR} + \frac{D(C_{i+1} - C_i)}{l^2} + \frac{D(C_{i-1} - C_i)}{l^2},\ i = 2 - 9 \\ \frac{dC_{10}}{dt} = \mathrm{CR} + \frac{D(C_9 - C_{10})}{l^2} \end{cases} \tag{5.2}$$

The first compartment represents the new pole of *Caulobacter* cell and the tenth compartment is the old pole.

The number of compartments influences the computational complexity of the model. To initially test the rationality of our work and efficiently search parameter space, we used a four-compartment model at the first stage shown in Appendix D 3. The four-compartment model makes the computation simple enough yet still provides sufficient spatial information. Moreover, it is more efficient to search the parameter space through a model with a small number of compartments. After the model is initially verified and parameters estimated, we extended the four-compartment scheme to a ten-compartment model to provide more accurate simulations, as described above. In principle, the compartment-based model can be extended to greater numbers of compartments.

As the *Caulobacter* cell is growing as a result of new cell wall materials being added uniformly along the long axis [169], we assume each compartment grows exponentially with time (Eq. 5.3).

$$\frac{dl}{dt} = \mu l. \tag{5.3}$$

During the swarmer cell cycle, a swarmer cell grows, over the course of 150 min, from ∼2 μm at birth to ∼4.4 μm at separation [170, 171], so we calculate $\mu = \frac{1}{150\,\mathrm{min}} \log\left(\frac{4.4}{2}\right) \approx 0.0053$ min^{-1}.

Localizations of PodJ, PopZ, and SpmX based on an activator-substrate depletion (A-SD) type of Turing pattern

Turing Pattern [172] has often been used to explain periodic patterns in space, such as spots and stripes on coats of animals, bacterial colony formation, and the MinCD system in *E. coli* [21]. The stable formation of A-SD type Turing Pattern requires two criteria [21, 93]:

1. the activator species is formed from the substrate by an autocatalytic reaction;
2. the substrate species diffuses significantly faster than the activator [173, 21].

In the *Caulobacter* system, the three scaffolding proteins (PodJ, PopZ, and SpmX) satisfy the two criteria of A-SD Turing-pattern formation. These proteins have monomeric and polymeric forms in cells, while the monomer diffuses much faster because of lower molecular mass [7, 174, 21]. PodJ, PopZ, and SpmX self-assemble *in vitro* and *in vivo* [161]. Furthermore, these proteins show branched accumulations in overexpressed and filamentous conditions [175, 176, 21, 7, 174], implying autocatalytic polymerization processes. A-SD Turing pattern has the potential to exhibit unipolar, central, and bipolar accumulations of product corresponding to various Turing wavelengths [21]. The characteristics of Turing pattern fits well with the observation of PopZ localization that PopZ has an old-polar focus in shorter nascent swarmer cells (Fig. 5.1) and accumulates at both poles in longer stalked cells and predivisional cells (Fig. 5.1). Therefore, we utilize a Turing pattern model to explain the spatial dynamics of PopZ. In order to stabilize the bipolar pattern for PopZ, we also include its interaction with PodJ, a nucleating factor biasing PopZ localization to poles [7] (Eq. 5.4).

$$\begin{aligned}
\frac{d[\mathrm{PopZ_m}]}{dt} &= k_{\mathrm{s,PopZ}} - (k_{\mathrm{d,PopZ}} + \mu)\cdot[\mathrm{PopZ_m}] + k_{\mathrm{depol,PopZ}}\cdot[\mathrm{PopZ_p}] \\
&\quad - k_{\mathrm{dnv,PopZ}}\cdot(1+\alpha_{\mathrm{PopZPodJ}}\cdot[\mathrm{PodJL_T}])\cdot[\mathrm{PopZ_m}] \\
&\quad - k_{\mathrm{aut,PopZ}}\cdot[\mathrm{PopZ_m}]\cdot[\mathrm{PopZ_p}]^2 + D_{\mathrm{PopZm}}\cdot\frac{\partial^2[\mathrm{PopZ_m}]}{\partial x^2} \\
\frac{d[\mathrm{PopZ_p}]}{dt} &= -(k_{\mathrm{d,PopZ}} + \mu)\cdot[\mathrm{PopZ_p}] - k_{\mathrm{depol,PopZ}}\cdot[\mathrm{PopZ_p}] \\
&\quad + k_{\mathrm{dnv,PopZ}}\cdot(1+\alpha_{\mathrm{PopZPodJ}}\cdot[\mathrm{PodJL_T}])\cdot[\mathrm{PopZ_m}] \\
&\quad + k_{\mathrm{aut,PopZ}}\cdot[\mathrm{PopZ_m}]\cdot[\mathrm{PopZ_p}]^2 + D_{\mathrm{PopZp}}\cdot\frac{\partial^2[\mathrm{PopZ_p}]}{\partial x^2}
\end{aligned} \tag{5.4}$$

where $[\mathrm{PopZ_m}]$ and $[\mathrm{PopZ_p}]$ are the concentrations of PopZ monomer and polymer, respectively. $[\mathrm{PodJL_T}]$ denotes the total concentration of long form PodJ ($[\mathrm{PodJL_m}] + [\mathrm{PodJL_p}]$). $k_{\mathrm{s,PopZ}}$ and $k_{\mathrm{d,PopZ}}$ represent the synthesis and degradation rate of PopZ. $k_{\mathrm{depol,PopZ}}$ indicates the rate constant of de-polymerization, while $k_{\mathrm{dnv,PopZ}}$ and $k_{\mathrm{aut,PopZ}}$ are the rate constants for the *de novo* and autocatalytic polymerization of PopZ, respectively. $\alpha_{\mathrm{PopZPodJ}}$ describes the recruitment by PodJ. D_{PopZm} and D_{PopZp} are the diffusion coefficients of monomer and polymer of PopZ respectively, where $D_{\mathrm{PopZm}} \ll D_{\mathrm{PopZp}}$. The diffusion coefficients of species except for polymers in this study are estimated by an empirical function in *E.coli* (Eq. 5.5) [177].

$$D = \alpha(MW)^{-2} + D_0, \tag{5.5}$$

where $\alpha = 4.3\times10^3 \mu\mathrm{m^2 s^{-1} kDa^2}$, $D_0 = 0.65\mu\mathrm{m^2 s^{-1}}$ and MW is for the molecular weight of the protein.

In addition, PopZ at the old pole recruits SpmX, which inhibits the localization of PodJ [7, 93]. Thus, we take interactions of PopZ-SpmX and SpmX-PodJ into our Turing pattern

model to explain the periodical localizations of PodJ and SpmX (Fig. 5.2 blue box, Eq. 5.6, Table. D1.1 Eq. (1)). PodJ shows bipolar localization when it is expressed alone in *E. coli*, suggesting that PodJ itself has an intrinsically high affinity with poles [7]. Furthermore, co-expressed SpmX and PodJ in *E. coli* results in dispersed PodJ [7]. Additionally, PodJ accumulates at both poles in Δ*spmX* mutant strains, while accumulation of PodJ is reduced in SpmX overexpressed strains [7]. Taken together, these experiments suggest that SpmX suppresses the assembly of PodJ (Fig. 5.2 blue box). Here, the inhibition effect of SpmX on PodJ is modeled in Eq. 5.6.

$$
\begin{aligned}
\frac{d[\mathrm{PodJL_m}]}{dt} &= k_{\mathrm{s,PodJ}} \cdot ((1-\epsilon)\cdot S_{podJ} + \epsilon) + k_{\mathrm{s,PodJ2}} \cdot \frac{J^2_{\mathrm{i,PodJCtrA}}}{J^2_{\mathrm{i,PodJCtrA}} + [\mathrm{CtrA}\sim\mathrm{P}]^2} \\
&\quad - (k_{\mathrm{d,PodJ1}} + k_{\mathrm{d,PodJ2}} \cdot [\mathrm{PerP}] + \mu) \cdot [\mathrm{PodJL_m}] + k_{\mathrm{depol,PodJ}} \cdot [\mathrm{PodJL_p}] \\
&\quad - k_{\mathrm{dnv,PodJ}} \cdot [\mathrm{PodJL_m}] - \frac{k_{\mathrm{aut,PodJ}}}{1 + \alpha_{\mathrm{PodJSpmX}} \cdot [\mathrm{SpmX_T}]} \cdot [\mathrm{PodJL_m}] \cdot [\mathrm{PodJL_p}]^2 \\
&\quad + D_{\mathrm{PodJLm}} \cdot \frac{\partial^2 [\mathrm{PodJL_m}]}{\partial x^2} \\
\frac{d[\mathrm{PodJL_p}]}{dt} &= -(k_{\mathrm{d,PodJ1}} + k_{\mathrm{d,PodJ2}} \cdot [\mathrm{PerP}] + \mu) \cdot [\mathrm{PodJL_p}] - k_{\mathrm{depol,PodJ}} \cdot [\mathrm{PodJL_p}] \\
&\quad + k_{\mathrm{dnv,PodJ}} \cdot [\mathrm{PodJL_m}] + \frac{k_{\mathrm{aut,PodJ}}}{1 + \alpha_{\mathrm{PodJSpmX}} \cdot [\mathrm{SpmX_T}]} \cdot [\mathrm{PodJL_m}] \cdot [\mathrm{PodJL_p}]^2 \\
&\quad + D_{\mathrm{PodJLp}} \cdot \frac{\partial^2 [\mathrm{PodJL_p}]}{\partial x^2}
\end{aligned}
\tag{5.6}
$$

where $\alpha_{\mathrm{PodJSpmX}}$ indicates the inhibition from SpmX on the polymerization of PodJ proteins. $J_{\mathrm{i,PodJCtrA}}$ describes the binding affinity between CtrA∼P and *podJ* promoter, which models the suppression of *podJ* expression by transcriptional factor CtrA∼P [130]. $((1-\epsilon)\cdot S_{podJ}+\epsilon)$ represents the methylation regulation of *podJ* expression, which is explained in next section (see 'Chromosome replication, methylation, and cell division').

5.3.2 Chromosome replication, methylation, and cell division

In addition to CtrA, other regulators control the chromosome replication to ensure the robustness of *Caulobacter* system. One key regulator is DnaA, which activates the initiation of replication by binding to *Cori* [85]. During DNA replication, fully-methylated chromosome turns into hemi-methylated. CcrM, a conserved DNA methyltransferase that methylates promoters with methylation sites, is turned on around the completion of replication [79]. In this study, we do not explicitly model chromosome replication and methylation because these processes are not closely associated with spatial regulations, although they are vital to temporal checkpoints of cell cycle. As increased DnaA and reduced CtrA∼P levels of initiating the DNA replication are concurrent, we take a threshold of [CtrA∼P] as an event

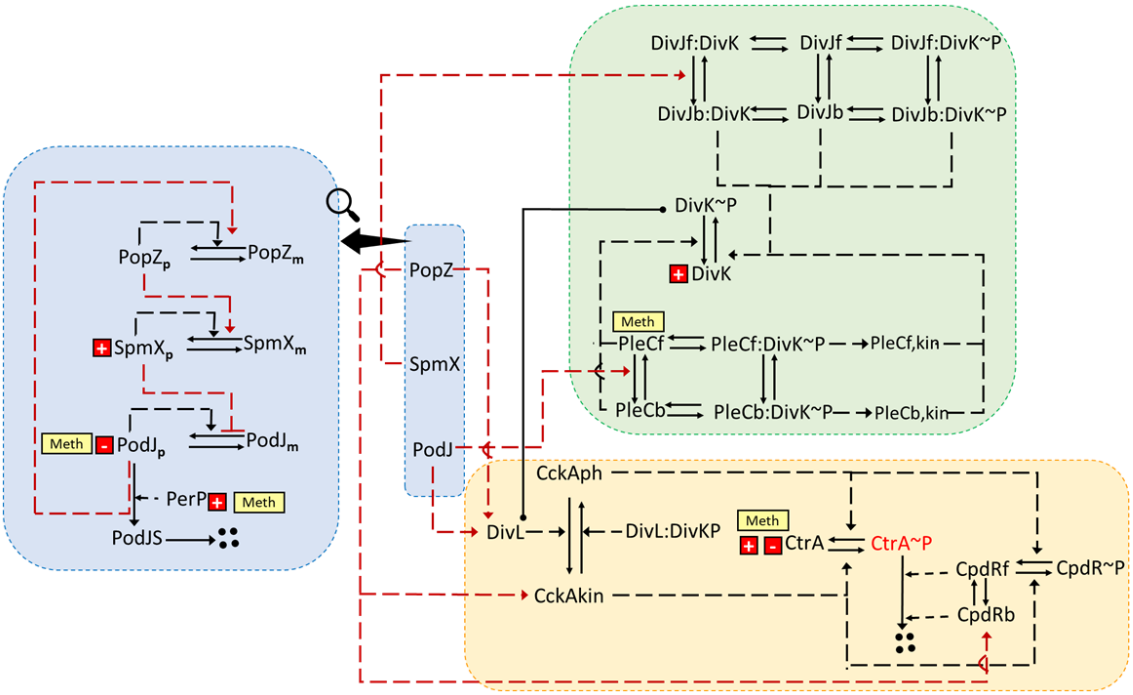

Figure 5.2: **A schematic diagram of the spatiotemporal regulatory network.** Red dashed lines indicate the localization effects by scaffolding proteins. Black dashed lines indicate the metabolism effects. Arrows are for activation and bars are for inhibition effect. 'Meth' indicates methylation-controlled transcription. The red square with minus or plus represent CtrA-regulated inhibition or activation of transcriptions. Four black spots represent the products of degradation. The line with solid circles at ends describes the binding reaction.

to initiate the DNA replication [19] (Table 5.1). When [CtrA∼P] is reduced to a level lower than the threshold (Θ), replication initiates and that time is recorded as $T_{\rm ini}$. The replication period time (S-phase) of WT cells is approximately 90 min [84]. Here we do not explicitly model the signal for replication termination. Instead, we set replication termination time, $T_{\rm term} = T_{\rm ini}$+90 min. For promoters with methylation sites (*ctrA*, *pleC*, *perP*, and *podJ*), we use $(1-\epsilon)\mathrm{S}+\epsilon$ to model the methylation regulation by CcrM (see yellow rectangles with 'Meth' in Fig. 5.2):

- S=0: fully-methylated promoters with lower rate of transcription.
- S=1: hemi-methylated promoters.

where ϵ is a small number indicating the suppressed expression of genes when fully methylated (Eq. 5.6, Table D1.1). Experiments suggest that the bacterial chromosome arrangement likely preserve the linear order of genes [178]. Therefore, we calculate the approximate time

when replication fork passes the corresponding gene based on its genome coordinate [179, 141]. When the replication fork passes the gene, S is set to 1; when replication terminates, S is set back to 0. All switching parameters for these events are listed in Table 5.1.

Z-ring closure is not modelled in this study. Here, we assume that the completion time of compartmentalization (z-ring closed) is 5 min after DNA replication terminates, formulated as $t = T_{\text{term}}$+5 min. The simulated cycle completes about 25 min after the compartmentalization. Then the two daughter cells are assumed to be completely separated. The cycle timeline is shown in Fig. 5.3. Note that the assumptions of time for specific events, such as the Z-ring closure and progenies separation, come from experimental observations of WT cells. For mutant cases where the levels of CtrA∼P are either too low or too high to trigger the 'DNA replication' event (Table 5.1), we enforce we enforce following operations:

1. if the average [CtrA∼P] is already lower than the threshold Θ (Table 5.1) at t=15 min, T_{ini}=15 min;
2. if the average [CtrA∼P] has never been lower than Θ until t=300 min, the simulation is forced to stop.

Table 5.1: Events and switches of parameters.

event description	condition	change at the event
replication initiation	average [CtrA∼P] changes from $>$ to $<\Theta$	$T_{\text{ini}} = t$
replication fork passes *ctrA*	t>90×37%+T_{ini}	S_{ctrA}=1
replication fork passes *pleC*	t>90×65%+T_{ini}	S_{pleC}=1
replication fork passes *perP*	t>90×74%+T_{ini}	S_{perP}=1
replication fork passes *podJ*	t>90×87%+T_{ini}	S_{podJ}=1
replication termination	t>T_{term}	All 'S's are switched to 0

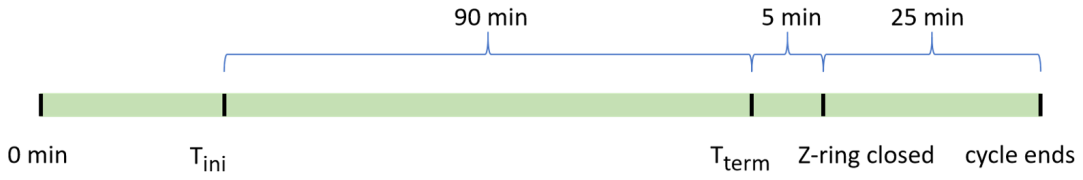

Figure 5.3: **Schematic simulated cell cycle timeline for a WT cell.** The DNA replication initiates when the average [CtrA∼P] changes from higher than Θ to lower than Θ. DNA replication needs 90 min to terminate, where T_{term}=T_{ini}+90 min. Z-ring is completely closed 5 min after the replication termination, and the daughter cells need 25 min to completely separate.

In addition to methylation, transcription of certain genes is regulated by CtrA∼P (see red squares with plus and minus in Fig. 5.2). We use Hill functions to describe transcriptional activation and inhibition by CtrA∼P as follows:

$$\mathrm{H_a}(\mathrm{CtrA}\sim\mathrm{P}) = \frac{[\mathrm{CtrA}\sim\mathrm{P}]^n}{J^n_{\mathrm{a,CtrAP}} + [\mathrm{CtrA}\sim\mathrm{P}]^n}, \tag{5.7}$$

$$\mathrm{H_i}(\mathrm{CtrA}\sim\mathrm{P}) = \frac{J^n_{\mathrm{i,CtrAP}}}{J^n_{\mathrm{i,CtrAP}} + [\mathrm{CtrA}\sim\mathrm{P}]^n}. \tag{5.8}$$

where the subscripts a and i denote activation and inhibition. n is the Hill coefficient and J is the dissociation constant between CtrA∼P and the corresponding promoter.

Finally, because mRNAs in *Caulobacter* diffuse slowly ($\approx 0.03\,\mu\mathrm{m}^2\mathrm{min}$) [180] and poles are void of chromosome [163], we assume that the translation of proteins only take place in central compartments. Thus, the synthesis rate (k_s) is set as 0 in polar compartments.

5.3.3 Multiobjective optimization

We use MATLAB's built-in multiobjective genetic algorithm to estimate parameters. There are in total 110 parameters in this model. Parameters are split into two groups: fixed and optimized parameters. 69 parameters are fixed, including 1) 33 parameters that are estimated from experimental or mathematical publications, and 2) 36 parameters that were initially estimated from our preliminary trials of scaffolding protein models, such as the model included in Xu et al. [93], and tuned slightly and manually in this study. The remaining 41 parameters are chosen for optimization. Let $\chi \in \mathbb{R}^{41}$ be the vector of estimated parameters. We define two objective functions as follows:

$$f_1(\chi) = \sum_{\mathrm{cycle2}}^{\mathrm{cycle3}} \Big(\sum_{\mathrm{CtrA}}^{\mathrm{PodJ}} \sum_{i}^{n} (x_i - y_i)^2 + \max(0, |\mathrm{T_{ini}} - 25| - 5)^2, \tag{5.9}$$

$$f_2(\chi) = \sum_{\mathrm{cycle2}}^{\mathrm{cycle3}} \mathrm{SpatialCost}, \tag{5.10}$$

where x_i indicates the simulated value at time i and y_i indicates the experimental data point at time point i of WT cells. n varies for different species. We compare simulation results for the second and the third cycle so that we may avoid bias in initial values. The first objective function include the temporal fitting cost of two species: PodJ and CtrA, as well as the initiation time fitting cost for DNA replication in the WT simulation. The second objective function indicates the spatial fitting cost of WT simulation that includes three types of penalties to ensure experiment-similar simulation of spatial dynamics for DivK and PopZ:

1. PopZ concentration in new-polar compartment is less than in central compartments,
2. PopZ concentration in old-polar compartment is less than in new-polar compartment,
3. DivK∼P concentration in new-polar compartment is less than in central compartments.

Details of objective functions are in our codes at https://github.com/chunruixu/Turing-pattern-model-of-scaffolding-proteins.git. Note that these objective functions only include temporal data of PodJ and CtrA, the spatial observations of PopZ and DivK; and the initiation time of DNA replication. Other WT observations and mutant phenotypes are not included in parameter optimization and are used to validate our model.

Additionally, to improve the efficiency of searching parameters, we first apply the optimization to the four-compartment model described in Appendix D3. The parameters derived from the optimized four-compartment model are used as the seed to search for optimized parameters in the ten-compartment model.

5.4 Results

To simulate mutant cells, we make appropriate changes to some of the parameters, as specified in Table S1.4. For WT cell type the simulation is run for three cell cycles and we plot results of the third cycle. For mutant cells that DNA replication initiates before 300 min in our simulation, we plot results of the second cycle. For mutant cells that DNA replication does not initiates before 300 min, we plot simulated results of 0-300 min.

5.4.1 A-SD Turing-pattern accurately captures the spatiotemporal dynamics of scaffolding proteins

The simulated spatial dynamics of scaffolding proteins in wild type swarmer cells are shown in heat-maps (Fig. 5.4), where the top line indicates the new pole and the bottom line indicates the old pole. PopZ simulation shows stable bipolar localization over the cell cycle. To be specific, the second focus of PopZ starts to present at approximately 60 min, matching with experimental data [7] (Fig. 5.4(a)). SpmX, recruited by PopZ, sharply accumulates at the old pole at approximately 10-20 min in our simulation, which also agrees with experimental data (Fig. 5.4(b)) [18]. Full PodJ (the long form PodJ indicated as PodJL) is localized at the new pole and is truncated by the protease PerP to turn into a short form PodJ (PodJS) (Fig. 5.1, blue) [7, 181]. PodJS remains at the flagellated pole until it is degraded during the sw-to-st transition of the next cell cycle, where the new flagellated pole of the previous cycle turns into the old pole (Fig. 5.1). Later, PodJL is newly synthesized and localized at the new pole of the new cycle (Fig. 5.4(c)) because old polar SpmX inhibits the polymerization of PodJL. The simulation results of PodJL and PodJS are consistent with experiments. To

specify, PodJL proteins occupy the new pole during the S-phase in simulation, while PodJS proteins are localized at the old pole at the beginning of cell cycle, which are inherited from the mother cell (Fig. 5.4(c)(d)). In the predivisional stage, PodJS proteins re-accumulate at the new pole (Fig. 5.4(d)). The assumption that synthesis of proteins only takes place in central compartments impairs the polar localization of Turing pattern; however, our system is robust enough to reproduce polar localizations of scaffolding proteins in wild type cells.

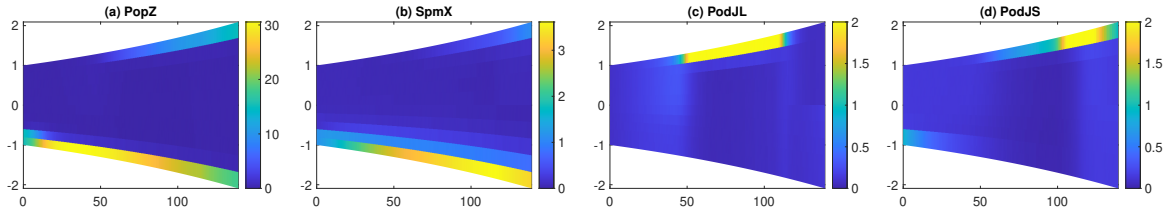

Figure 5.4: **The spatial dynamics of scaffolding proteins in ten-compartment spatial simulations over one cell cycle of the *Caulobacter* swarmer cell.**
(a-d)PopZ, SpmX, long form PodJ, and short form PodJ. X-asix indicates time of cycle, while Y-axis represents the distance to the midpoint of long-axis of cells. Top and bottom compartment indicates the new pole and old pole, respectively. Color denotes the scaled concentration of indicated species.

5.4.2 The spatial gradients of CtrA∼P and DivK∼P are reproduced by our model

With the mechanisms of A-SD Turing pattern formation, the three scaffolding proteins - PodJ, PopZ, and SpmX - can initially occupy specific polar areas through polymerization and protein-protein interactions. Here, we build a spatiotemporal regulatory network for the asymmetry development over the cell cycle on the basis of scaffolding proteins network (Fig. 5.2). In addition to the three scaffolding proteins, we include key enzymes DivJ, PleC, DivL, DivK, CckA, the master regulator CtrA and its proteolysis promoter CpdR (Fig. 5.2, green and yellow boxes).

DivJ and PleC are recruited by scaffolding proteins to localize at the old pole and new pole, respectively, to function as a major kinase and phosphatase of DivK. The opposite localizations of DivJ and PleC provide the foundation of spatial gradient for DivK∼P. DivK∼P binds to DivL to control the switch of CckA phosphatase and kinase [182, 183]. As CckA kinase and phosphatase regulate the phosphorylation state of CtrA and CpdR, the distribution of DivK∼P likely influences the distribution of CtrA∼P. Additionally, PopZ has been reported to directly bind to DivL and CpdR [159], and PodJ participates in the localization of DivL [135, 184]. Therefore, the spatial regulation of scaffolding proteins is multifaceted. Detailed molecular mechanisms involved in the three modules, scaffolding proteins module (blue box in Fig. 5.2), phosphotransfer module of DivJ/PleC-DivK (green box), and phos-

photransfer module DivL-CckA-CtrA (yellow box), are explained in Appendix D 2. We convert the diagram in Fig. 5.2 into a set of PDEs shown in Table. D1.1, and then convert the PDEs into a system of ODEs using the compartment-based discretization explained in Methods.

Fig. 5.5 shows the simulated spatial dynamics of proteins involved in the two phosphotransfer modules. Overall, the simulations of proteins shown in Fig. 5.5 match well with experimental observations. In Fig. 5.5(c), phosphorylated DivK accumulates in the stalked compartment after the cell division, which is consistent with experiments (Fig. 5.1) [160]. In detail, DivK∼P is not only localized at the old pole over the cell cycle, but also shows a temporary accumulation at the new pole in the predivisional stage, which has been observed in experiments [160]. The general asymmetrical distribution of DivK in simulation is caused by the new polar PleC and old polar DivJ, because DivJ and PleC regulate the phosphorylation state of DivK and bind to DivK to influence its localization (Fig. 5.2 and Fig. 5.5(a-b)).

Experiments show that DivL is stably localized at the new pole during S phase and less frequently localized at the old pole (Fig. 5.1, olive) [185]. Our model captures the new-polar accumulation of DivL, which is mainly recruited by PodJ (Fig. 5.5(d)). CckA is dispersed in the nascent swarmer cell and shows a strong new-polar accumulation later (Fig. 5.5(f)), which agree with experiments (Fig. 5.1) [30, 155]. Following cell division, simulations exhibit a higher level of unphosphorylated CpdR in the stalked compartment (Fig. 5.5(g)) and a higher level of phosphorylated CtrA in the swarmer compartment (Fig. 5.5(h)), which are consistent with the asymmetrical life-cycle of *Caulobacter*. Furthermore, the mechanism that unphosphorylated CpdR promotes the proteolysis of CtrA reinforces the reduced levels of CtrA∼P in the stalked compartment.

5.4.3 The consistency in temporal dynamics between our simulation and experiments further demonstrates the rationality of this model

We further compare the temporal dynamics of PodJL, PodJS, SpmX, DivJ, PleC, DivK, and CtrA in model simulation and experiments (Fig. 5.6). Generally, our temporal simulation fits well with experimental data although there are some minor mismatches. PodJS is degraded at the beginning of the cell cycle,while PodJL keeps increasing until PerP is expressed in the late S-phase, which converts PodJL into PodJS (Fig. 5.6(a)). SpmX levels grow slowly, while most of SpmX at the end of cycle is in the stalked compartment, which explains the low levels of SpmX at the birth of a swarmer cell (Fig. 5.6(b)). Similarly, because most of DivJ is localized at the old pole, the nascent swarmer cell inherits less DivJ, which explains the lower level of DivJ at t=0 min (Fig. 5.6(c)). Compared with experimental data, the simulated PleC shows a slightly delayed turning point, but it still catches the general trend (Fig. 5.6(d)). The decrease of CtrA (Fig. 5.6(f)) during the sw-to-st transition is used to signal the initiation

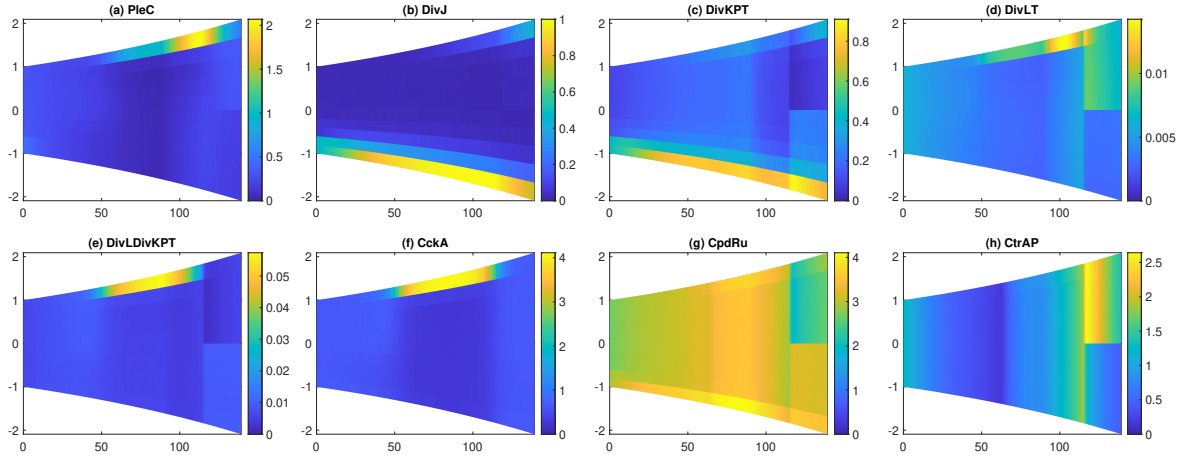

Figure 5.5: **Spatial dynamics of client proteins (or complex) in ten-compartment simulations, including PleC, DivJ, DivK∼P, DivL without binding to DivK∼P, DivL:DivK∼P complex, CckA, unphosphorylated CpdR, and CtrA∼P.**

time of DNA replication and methylation-regulated synthesis in this model (see 'Methods', Table 5.1). The simulated initiation time of DNA replication is approximately 29 min after previous cell separation. This is reasonable and works well in simulating the timing of cell cycle.

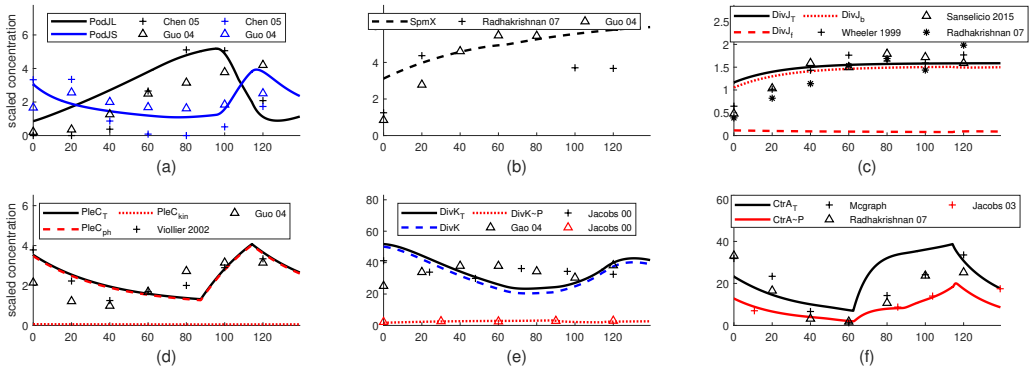

Figure 5.6: **Comparison of simulated temporal dynamics with corresponding experimental observations over one cell cycle of a *Caulobacter* swarmer cell.** X-asix indicates time of simulated cell cycle. Y-axis represents the scaled concentration of proteins. Triangle, plus, and asterisk represent data points from indicated publications.

5.4.4 Interactions among scaffolding proteins and higher polar affinity are required for their proper localization patterns

PopZ is a critical scaffolding protein recruiting core regulators of CtrA, such as SpmX, DivL, and CpdR [159]. Therefore, it is imperative to look into the mechanisms underlying the localization of PopZ [7]. While PopZ stably shows bipolar accumulation in wild type cells, no detectable PopZ accumulates at the new pole in the Δ*podJ* mutant, suggesting the recruitment by PodJ is required for the stable second focus of PopZ [7]. Here, we model the Δ*podJ* mutant by setting the synthesis rate of PodJ as 0, in which *podJ* expression is completely deleted (Table. D1.3). In the wild type simulation, PodJ works as the factor biasing PopZ from the monopolar accumulation to the bipolar accumulation. When the biasing effect of PodJ disappears, PopZ can not ensure its polar localization. There are other candidate factors reinforcing the new polar accumulation of PopZ, such as ParA, TipN and ZitP, which interact with PopZ at the new pole [7, 21, 186]. Additionally, unique characteristics of poles, such as curvature and composition of polar cell walls, may provide a higher affinity for scaffolding proteins like PopZ [161]. As the specific mechanism of polar affinity independent of PodJ is unclear, we assume a higher polymerization rate of PopZ at poles to enforce the polar affinity in our model. Specifically, auto-catalytic polymerization rate of PopZ ($k_{\mathrm{aut,PopZ}}$) is 25% higher in polar compartments than in central compartments. Likewise, the auto-catalytic polymerization rate of PodJ is 25% higher in polar compartments.

With the assumption of higher polar affinity, our model reproduces the phenotype of Δ*podJ* that PopZ localizes at the old pole without PodJ, while PleC is dispersed across the cell (Fig. 5.7(a)). Our model indicates that PodJ is required for the new polar focus of PopZ and PleC. Additionally, SpmX and DivJ keep co-localized with PopZ in the Δ*podJ* simulation.

Next, we investigate the spatial regulation of PopZ via Δ*popZ* mutant ($k_{\mathrm{s,PopZ}} = 0$). Instead of accumulate at one pole, PodJ shows bipolar pattern but less accumulation in the Δ*popZ* simulation, which is consistent with experiments (Fig. 5.7(b)) [7, 162]. Our simulation also captures the features of Δ*popZ* observed in experiments that the polar localizations of SpmX, DivJ, CpdR and DivK are severely impaired (Fig. 5.7(b) and Fig. D4.1) [162]. The delocalization of DivJ is likely caused by the delocalization of SpmX. Moreover, the bipolar localization of PodJ is likely a result of delocalized SpmX because SpmX works as an inhibitor of PodJ localization [7, 93].

To further investigate the function of SpmX, we set $k_{\mathrm{s,SpmX}} = 0$ to simulate Δ*spmX* strains (Table.D1.3). In our simulation, PodJ exhibits bipolar localization, while DivJ is dispersed. The new-polar localization of PopZ is weakened, which is likely caused by two pathways: 1) partial PodJ is localized at the old pole, which means that the new-polar recruitment by PodJ is reduced; 2) The absence of SpmX results in weaker kinase activity of DivJ, so that DivK∼P level decreases, CtrA∼P level increases, PodJ level is reduced because of higher inhibition by CtrA∼P (Fig. 5.2), and less PopZ is polymerized at the new pole in sequence. Experiments of Δ*spmX* indicate that the number of cells with bipolar PodJ and ectopic

midcell PodJ increases [7]. Thus, our model can capture certain behavior of Δ*spmX* cells.

Taken together, our A-SD Turing model can reproduce most phenotypes of deleted mutant cases relevant to scaffolding proteins. Our work suggests that interactions among PopZ, PodJ, and SpmX are indispensable for their correct localization. Additionally, there should be a higher polar affinity for PopZ and PodJ.

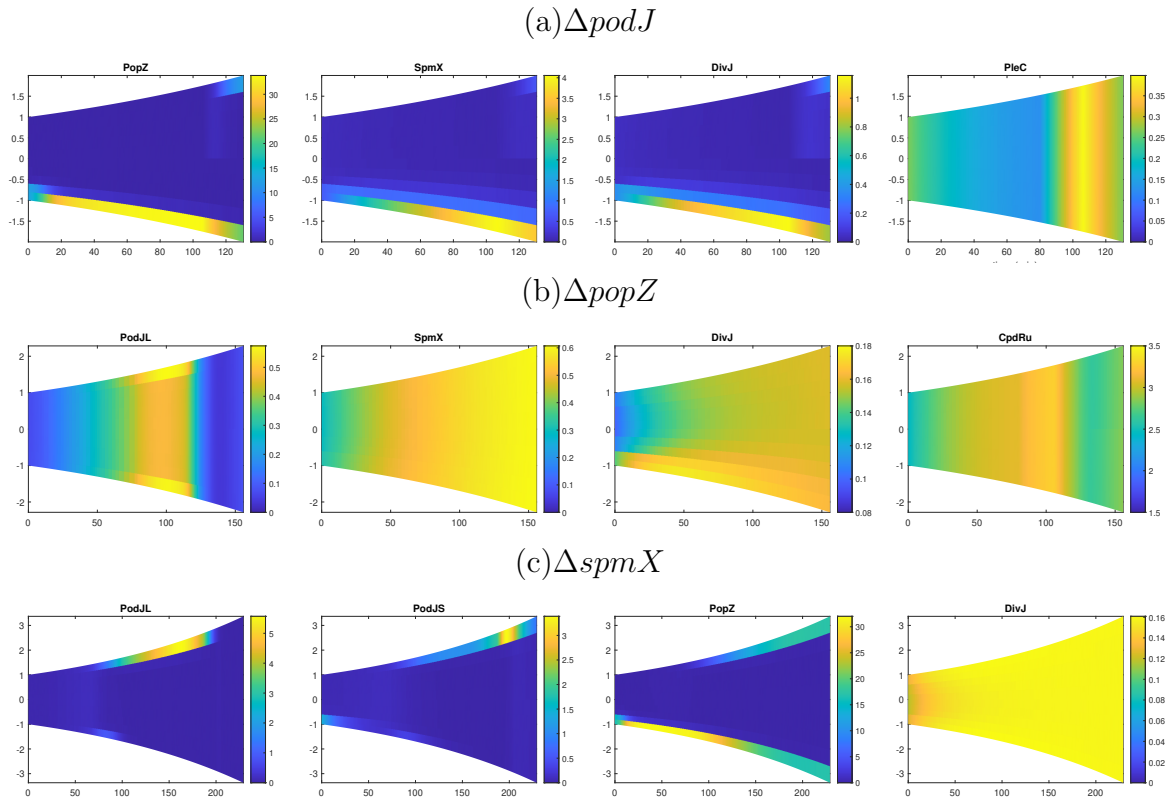

Figure 5.7: **Spatial simulations of Δ*podJ*, Δ*popZ*, and Δ*spmX*.**

5.4.5 DivL determines the new-polar localization of DivK in the predivisional stage

A previous study has shown that the phosphorylated form of DivK preferentially localizes at the cell poles [150]. Among the currently known binding partners of DivK, PleC and DivL show significantly higher affinity with DivK∼P *in vivo*, whereas DivJ can bind to both phosphorylated and non-phosphorylated forms [182]. Therefore, we consider the following complexes of DivK in our model: PleC:DivK∼P, DivL:DivK∼P, DivJ:DivK∼P, and DivJ:DivKu (DivKu denotes unphosphorylated DivK, see Appendix D2). Our model can

reproduce the phenotype of DivK spatial dynamics in DivJ and PleC mutants, as described below.

DivJ is necessary for the polar localization of DivK. DivJ binds to DivK and functions as the major kinase phosphorylating DivK [150]. Without DivJ (see the Δ*divJ* mutant, Table. D1.3), DivK∼P levels drop dramatically and DivK is delocalized [150, 187, 15]. DivK in the kinase-defective DivJ strain (DivJ-H338A) can localize at the old pole but fails to localize at the new pole [150]. Our simulations of Δ*divJ* and DivJ-H338A (Fig. 5.8(a)(b)) are consistent with experimental observations, which agree that DivJ determines the old polar localization of DivK and DivJ kinase activity is required for the new polar accumulation of DivK. PleC has been reported to determine the new polar release rather than the localization of DivK, because DivK∼P keeps occupying the new pole after z-ring closure in Δ*pleC* and PleC-H610A mutant strains [150, 160, 22]. Here, we simulate Δ*pleC* and PleC-H610A (inactive kinase and phosphatase PleC mutation) in Fig. 5.8(c)-(d), where DivK∼P fails to release from the new pole after cell division. We also check the function of kinase activity of PleC in the simulation of PleC-F778L (kinase-defective pleC strain), where DivK shows WT like dynamics, consistent with experiments (Fig. 5.8(e)) [160]. Therefore, our model together with experimental observations suggests that the kinase activity of PleC is dispensable for the transient new polar accumulation of DivK in the predivisional stage.

Based on these results, we speculate that either the localized PleC or DivL or both function as the physical binding partner to recruit DivK∼P at the new pole, which requires the kinase activity of DivJ. We utilize Our spatial model to explore two hypothetical mutant cases, 'delocalized PleC' mutant ($k_{\mathrm{fb,PleC}} = 0$) and 'delocalized DivL' mutant ($\alpha_{\mathrm{b,DivLPodJ}} = 0$, deleting the recruitment of PleC by PodJ), to further study the effects of PleC and DivL. DivK fails to accumulate at the new pole in delocalized DivL mutant, while delocalized PleC mutant exhibits WT similar dynamics in simulation (Fig. 5.8(f)(g)). Therefore, we suggest that DivL plays a more important role in recruiting DivK∼P at the new pole in the predivisional stage.

To sum up, our model agrees with experimental observations that the DivJ kinase activity is required for the new-polar accumulation of DivK, while PleC is required for the timely release from the new pole [150]. Additionally, our mutant simulations suggest that PleC localization and kinase activity are not necessary for the localization of DivK, while DivL is required for the new polar localization of DivK.

5.4.6 Our model captures key characteristics of phosphotransfer processes

In Δ*divJ* strain, the level of DivK∼P is reduced and CtrA-dependent transcriptions increase [188, 15]. The observed phenotype of Δ*divJ* is successfully captured by our model (Fig. 5.8(a)). The simulation of Δ*pleC* shows increased levels of DivK∼P and reduced lev-

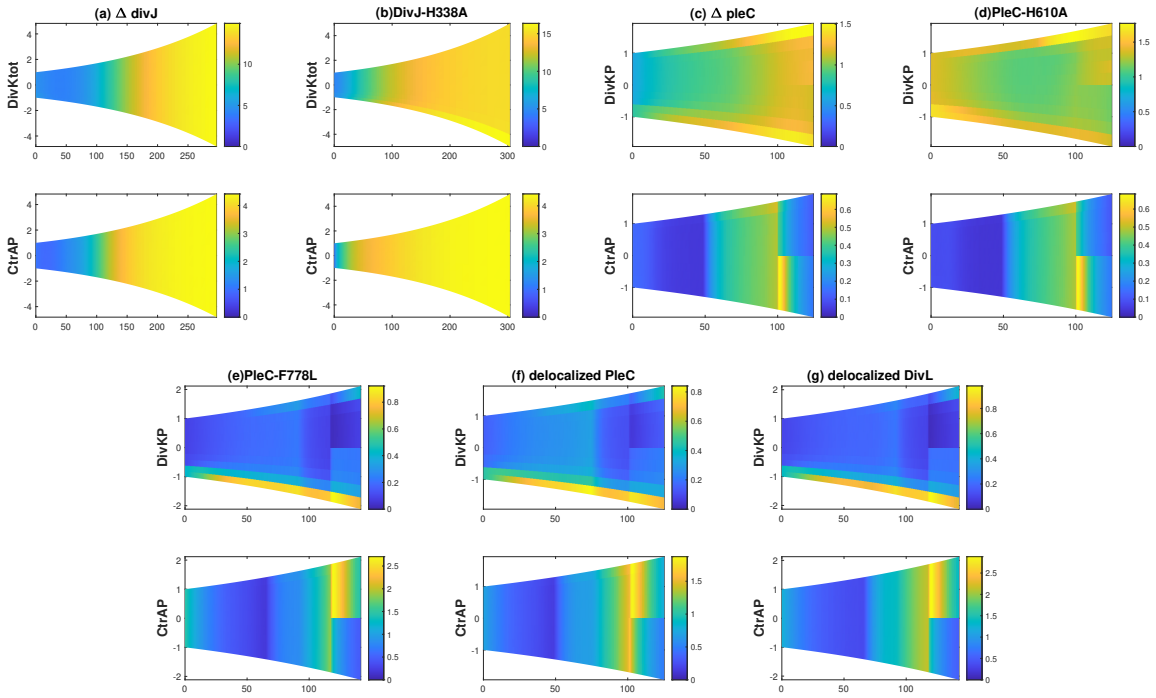

Figure 5.8: **DivK(∼P) and CtrA∼P dynamics in Δ*divJ*, DivJ-H338A, Δ*pleC*, PleC-H610A, PleC-F778L, delocalized PleC, and delocalized DivL mutant strains.** The total DivK rather than DivK∼P is observed in two DivJ mutant cases because DivJ can bind to unphosphorylated DivK while PleC and DivL prefer to bind to phosphorylated DivK. In 'delocalized PleC' and 'delocalized DivL' mutant simulation, the recruitment by PodJ on PleC and DivL is deleted, respectively.

Table 5.2: Phosphorylation state of DivK in mutant strains.

mutant		WT	Δ*spmX*	Δ*divJ*	Δ*pleC*	Δ*podJ*
DivK∼P[1]	Exp[2]	1	0.36 [18]	0.04 [18]	1.79 [18]	1.50 [5]
	Sim	1	0.28	0.09	4.02	1.27

[1] DivK∼P levels are normalized with respect to the level in wild-type cells.
[2] Experimental data in Radhakrishnan et al. [18] is quantified using ImageJ.

els of CtrA∼P, which is consistent with experiments as well (Fig. 5.8(c)) [188, 124]. We further quantitatively compare the simulated levels of DivK∼P in four mutant cases with the corresponding experimental measurements in Table 5.2. Numbers in Table 5.2 indicate normalized levels with respect to WT cells (both for simulation and experiment). Our simulation captures the key trends of DivK∼P level in mutant cases and matches with experimental data. DivK∼P level dramatically decreases in Δ*spmX* and Δ*divJ* because the kinase activity of DivJ is largely impaired or deleted (Table 5.2, Fig. D4.1, Fig. 5.8(a)). As PleC mainly functions to dephosphorylate DivK, Δ*pleC* mutation results in the increased DivK∼P (Table 5.2, Fig. 5.8(c)). In addition, the higher level of DivK∼P in Δ*podJ* suggests that PodJ likely inhibits rather than activates the kinase activity of PleC, which is a debatable issue in Kowallis et al. [161].

Because DivK∼P inhibits the phosphotransfer to CtrA∼P through interacting with DivL, mutations that impact the localization or/and abundance of DivK∼P should affect the establishment of CtrA∼P spatial gradient by amount or degree.

Here, our model provides predictions of CtrA spatial dynamics for some relevant mutant strains (Fig. 5.8, Fig. D4.1). Δ*pleC* and PleC-H610A mutant strains, failing to release DivK∼P from the new pole, exhibit severe reverse distribution of CtrA∼P in simulation (Fig. 5.8(c) and (d)). Our model predicts the spatial gradient of CtrA∼P almost disappears in Δ*divJ*, DivJ-H338A, and Δ*popZ* mutant cases. Our model predicts the spatial gradient of CtrA∼P almost disappears in Δ*divJ*, *divJ-H338A* and Δ*popZ* mutant strains. All other mutant simulations in this study show higher levels of CtrA∼P in the swarmer compartment, but the 'delocalized PleC' and Δ*podJ* mutant simulations display shallower CtrA∼P gradient (Fig. 5.8, Fig. D4.1). These predictions suggest that mutations in activity of key enzymes, such as the DivJ kinase and PleC phosphatase, seem to have more severe phenotypes than localization mutations.

5.5 Discussion

In this study, we integrate the Turing-pattern mechanism with protein-protein interactions of scaffolding proteins to study polarity establishment in *C. crescentus*. The mutant analysis of scaffolding proteins indicates that PopZ and PodJ should have a higher affinity with poles. Jacob et al. has proposed a hypothesis that the cell membrane only grows in a central zone

of bacterial cells [189], which has been supported by subsequent evidences [190, 191, 192]. Therefore, the unique curvature and less new wall insertion of cell poles may cause the higher affinity of PodJ and PopZ with poles suggested in this study. In addition to using different auto-catalytic polymerization rates in different types of compartments (this study), it is reasonable to apply different growth rates in polar and central compartments in modeling. We tried a different-growth-rate model with an assumption that the growth rate of poles is half of the growth rate of centers (with the difference of auto-catalytic polymerization rates of PodJ and PopZ being removed). The different-growth-rate model successfully reproduced the polar accumulation of WT, $\Delta podJ$ and $\Delta spmX$ mutant simulations, while PodJ failed to localize at the pole in $\Delta popZ$ simulation. Our trial verified that the slower growth rate of pole contributed to at least part of the polar localization of scaffolding proteins. Chen et al. [92] has constructed a two-dimensional model to describe the poles and central zones of *C. crescentus* cells with different shapes, which provides an idea to differentiate poles from middle areas. Additionally, other proteins, such as ZitP and TipN, has the potential to stabilize the polar accumulation of PopZ. They are not currently modelled in this study yet [186].

We model the CtrA-relevant phosphotransfer cascades based on a scaffolding protein network to investigate the relationships among localization, activity and asymmetry within *Caulobacter* cells. The activities of proteins are closely associated with localization. We directly include the activation of DivJ kinase by SpmX, the activation of PleC kinase by DivK∼P, and the inhibition of PleC kinase by PodJ in this model, where the activation or inhibition is influenced by the spatial distribution of corresponding proteins. Moreover, the spatial regulation of phosphorylation/dephosphorylation and proteolysis affects the activity and abundance of key regulators. The activation of DivJ kinase by DivK∼P is ignored for simplification at this stage. Our model reproduces the asymmetry establishment over the cell cycle and captures the key characteristics of phosphotransfer cascades (Fig. 5.5, Fig. 5.8, Table. 5.2), while more associations between localization and activity can be discussed in the future.

We apply the multi-objective optimization genetic algorithm (GA) in this spatiotemporal model to estimate parameters. Objective functions of spatial dynamics and temporal dynamics of two species, and timing of replication initiation in WT cells are used to minimize the disparity between simulations and experiments. To increase the efficiency, we first apply the GA optimization in the four-compartment model and get a bundle of parameter sets that work well (Fig. D4.2). We next apply the parameter set optimized by the four-compartment model as the seed set of parameters to search the parameter space in the ten-compartment model with the same set of PDEs. With a set of parameters that was already selected based on a coarse discretization, it is easier to reach a set of parameters that enable the ten-compartment model to capture phenotypes of WT cells. To verify the feasibility and efficiency of starting from a model with less number of compartment, we further run this model with the same set of parameters and different numbers of compartments (Fig. 5.9). The simulation time is approximately a quadratic function of the compartment number.

Thus, this trial suggests that using a small number of compartment helps to improve the efficiency of searching parameters.

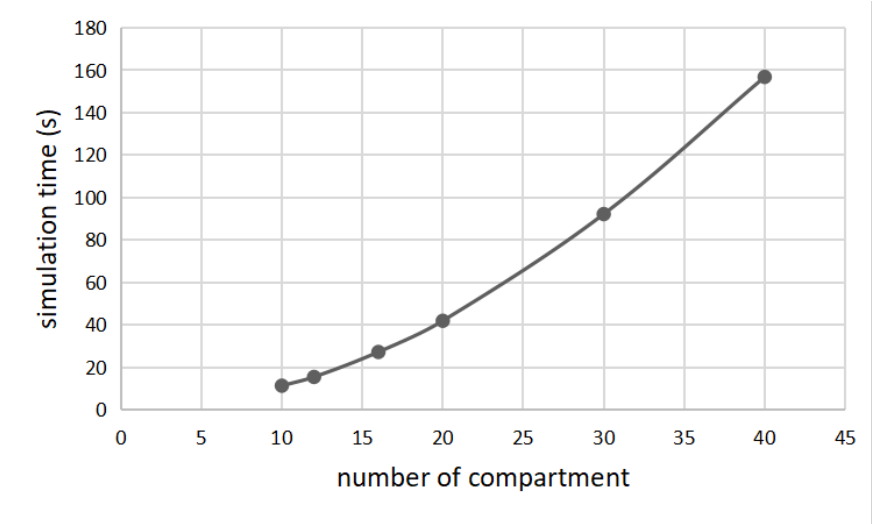

Figure 5.9: **The simulation time increases with the number of compartment as a quadratic function.**
x-axis indicates the number of compartment, and the y-axis indicates the simulation time of one cell cycle in this spatial model. The quadratic function is estimated by the built-in tool of MATLAB as: $y = 0.097x^2 + 2.216$, where the R-square is approaching 1.

To summarize, our spatiotemporal model is built on the foundation of the A-SD Turing model to explain the asymmetrical localization of regulators and the establishment of polarity. It captures the phenotypes of WT and mutant strains and provides predictions in mutant cases that are not experimentally observed and in hypothetical mutant cells that can be experimentally tested (Table. 5.3). This work investigates the functions and associations of localizing and phosphotransfer reactions during the cell development, which can be utilized to predict the behavior of bacterial mutant cases that are difficult to be cultivated or operated.

Table 5.3: Predictions provided by the spatiotemporal model

predictions	**cell types**
higher polar affinity for PodJ and PopZ	all cell types
distributions of SpmX and DivJ	Δ*podJ* (Fig. 5.7(a))
distribution of PopZ	Δ*spmX* (Fig. 5.7(c))
DivK∼P spatial gradient	'delocalized PleC' and 'delocalized DivL' (Fig. 5.8(f)(g)); Δ*podJ*, Δ*popZ*, and Δ*spmX* (Fig. D4.1)
CtrA∼P spatial gradient	delocalized PleC' and 'delocalized DivL' (Fig. 5.8(f)(g)); Δ*podJ*, Δ*popZ*, and Δ*spmX* (Fig. D4.1) Δ*divJ*, *divJ-H338A*, Δ*pleC*, *pleC-H610A*, *pleC-F778L* (Fig. 5.8)

Chapter 6

Summary and future directions

6.1 Overview of this dissertation

In this dissertation, we have applied mathematical models to investigate control mechanisms of stressful responses and spatial cell cycle regulations in *Caulobacter crescentus*.

Chapters 2-4 were motivated by the important roles of cdG in controlling the cell cycle of *C. crescentus*, especially in influencing the master cell cycle regulator CtrA. The intracellular levels of cdG and its antagonists (p)ppGpp fluctuate during the cell cycle progression and under stressful conditions, influencing the synthesis and proteolysis of key regulators in *C. crescentus* [31]. As the stress signaling pathways are relatively conserved in prokaryotes and regulate the bacterial interactions with host cells, it is attractive to study the underlying mechanisms of stressful responses starting from cdG-relative networks. cdG regulates the activity of CtrA through two pathways - proteolysis and phospho-signaling. cdG is a significant component of ClpXP protease complex, where the conserved protease ClpXP hierarchically recruits adaptors to specifically degrade substrates [29]. The hierarchical assembly of ClpXP complex determines the degradation of different substrates in time and space. The proteolysis of CtrA requires ClpXP to recruit CpdR, RcdA and cdG bound PopA in sequence. Thus, the dynamics of involved adaptors, including cdG, spatiotemporally mediate the abundance of CtrA [27, 29]. Additionally, cdG mediates the switch between kinase and phosphatase state of the histidine kinase CckA [157, 193] and ShkA [133], which control the phosphorylation and dephosphorylation of CtrA. Thus, cdG plays an important role in the phosphorylation state of CtrA [124, 155]. Although cdG has been verified to regulate the cell cycle progression and environmental responses of *C. crescentus*, the detailed relationships between environmental cues and cdG as well as downstream pathways are not clear. In Chapter 2, we propose a temporal model of the cdG-centered second messenger network to study how second messengers respond to external changes. The hierarchical assembly of ClpXP protease complex is modelled in Chapter 3 and Chapter 4 to improve the simulation

of proteolysis of CtrA and other regulators such as PdeA and TacA. Moreover, we have introduced known targets of starvation signals in the temporal model in Chapter 4 and provided predictions of stress response and cell cycle arrest to different signals in *C. crescentus*.

Chapter 5 was motivated by Subramanian et al's spatial models, which include spatial regulatory networks of scaffolding protein PopZ, Z-ring mediator FtsZ, and proteins involved in phosphotransfer modules [21, 125]. Their spatial models explained the dynamic localization of some key regulators; however, some sources of localization are missing and individual spatial model can not be integrated into one system because of these absent factors. In Chapter 5, we propose a Turing pattern model integrated with the interactive network of three scaffolding proteins - PopZ, PodJ, and SpmX. Our model provides a reasonable explanation of stable localization of scaffolding proteins and downstream client proteins, which fills in gaps of Subramanian et al's work. Additionally, we provide a simple temporal frame for the spatial regulatory network, integrating the control mechanisms of DNA replication and methylation in Chapter 5. Thus, spatial studies can be combined with temporal perspectives to investigate the bacterial cell cycle control from a comprehensive viewpoint.

6.2 Future directions

Although our work can answer a series of questions for environmental responses and spatial regulations in *C. crescentus*, there are still several unclear and exciting directions that can be further investigated.

6.2.1 Other pathways of environmental responses

phosphoenolpyruvate:sugar phosphotransferase system

In Chapter 2, we investigated the response to carbon and nitrogen starvation through the nitrogen phosphoenolpyruvate phosphotransferase system (PTS^{Ntr}), where we took [PEP], [Pyr] and [Gln] as adjustable carbon and nitrogen signals. In addition to detecting nutrition signals through PTS^{Ntr}, many bacteria can incorporate carbohydrates via the phosphoenolpyruvate:sugar phosphotransferase system (PTS) [194, 195]. Similarly with PTS^{Ntr}, the Enzyme I (EI) of PTS accepts the phosphoryl group from PEP and transfers the phosphoryl group to downstream enzymes HPr and EIIs (EIIA, EIIB, etc) [68]. Interestingly, PTS and PTS^{Ntr} in the same bacterium likely share a number of functional motifs, which enables the cross-talk between different phosphotransferase systems [129]. The exchange of high-energy phosphates between separate phosphotransferase systems has been observed *in vivo* and *in vitro* [129, 196]; however, the biological significance and mechanisms of the cross-talk are not clear. Therefore, for the response to nutrition signals, our work can be extended by 1). introducing [PEP] and [Pyr] as dynamical variables rather than adjustable parameters,

and 2). including carbohydrate PTS into our system to globally understand environmental responses for both carbon and nitrogen shifts.

UV Radiation and extreme abundance of salt and ethanol

Our work already included multiple-faceted regulatory networks and it has the potential to integrate separate modules into one comprehensive system in the cell cycle progression of *Caulobacter*. It is efficient to utilize our model to study the responses to different environmental cues, such as ultra-violet (UV) lights, heat shock, salt and Ethanol stresses and so on.

UV light waves have the ability to cause mutations in DNA [197]. When a DNA mutation occurs, a cell must repair the DNA before the chromosome(s) replicate and duplicate the mutation. However, in *Caulobacter*, the cell cycle is arrested in the predivisional stage [198], which is typically associated with the completion of chromosome replication. Therefore, there must be repair pathways to avoid inheriting a mass of mutations during the DNA replication in *Caulobacter* cells. One known pathway of response to DNA mutations in *Caulobacter* is the SOS response regulon. In normal cells, the SOS repair is repressed by the LexA protein, which binds to the 'SOS box' of targeted DNA; when the cell detects DNA damages, LexA is released from SOS box, thus the genes of the SOS response regulon can be transcribed [198, 199]. SidA is the primary SOS-induced division inhibitor in *Caulobacter*. Besides SidA, there is a second division inhibitor, DidA, which is induced by DNA damage but independent with SOS system [198]. Both SidA and DidA target Z-ring proteins to block cytokinesis in response to DNA mutations [198, 199]. Additionally, CtrA is inhibited in response to light-induced DNA mutations independent of the SOS regulon, although the mechanism is unknown [2, 198].

Ethanol and salt concentrations impair bacterial function as they can damage proteins [200]. Under such stressful conditions, the bacteria must conserve their resources towards repairing their cell walls and therefore will arrest their cell cycle to conserve energy. *Caulobacter* cells respond to salt and Ethanol stress by arresting the cell cycle at the S to G2 transition, likely by shifting the activity of CckA towards the phosphatase state [201]. While the mechanism that results in the shift of CckA activity is unknown, it is hypothesized that it responds directly to external stimulation by the stressors. Because CckA phosphatase drives dephosphorylation and proteolysis of CtrA, the stimulation of CckA phosphatase likely targets CtrA activity to arrest the cell cycle.

While some aspects of the stress signalling pathways have been elucidated, it is unknown whether these pathways are sufficient to explain corresponding experimental observations. Additionally, some detailed mechanisms are missing. Our model can be extended by integrating these known pathways and applied to identify the mechanisms and the contribution of these mechanisms of responding to different stress signals.

6.2.2 A comprehensive spatiotemporal model

Chapters 2-4 and Chapter 5 respectively offered temporal and spatial insights on how the *Caulobacter* cells navigate the asymmetrical cell cycle. One future goal is to integrate more distinct modules and construct a comprehensive deterministic model to thoroughly study the control mechanisms of *Caulobacter* cell cycle.

Integration of temporal regulations with spatial networks

In Chapter 5, to concentrate on the study of spatial control mechanisms, we simplified the modeling of DNA replication initiation, elongation, segregation and the Z-ring closure during cell division. A CtrA-determined replication initiation and a fixed duration of replication and cell separation were applied. For future research, our model can be extended by integrating the temporal work in Chapter 4 with the spatial model in Chapter 5. To be specific, the core regulatory network with DnaA and GcrA, two major transcriptional factors collaborating with CtrA to regulate the chromosome duplication, can be integrated into the spatial model. CtrA-regulated and DnaA-regulated pathways both control *Caulobacter* cell development and improve the robustness of *Caulobacter* system. Including both pathways in modeling DNA replication can improve the accuracy of our model and its tolerance to disturbance. Another improvement is to integrate the temporal regulation of Z-ring development. The Z-ring formation is highly regulated by a series of Z-ring proteins, while many of these proteins are controlled by CtrA∼P [141, 202, 203]. The shift of [CtrA∼P] should influence the timing of cell division. Hence, including the CtrA-regulated Z-ring dynamics will further improve our model and help in analyzing and predicting the viability and arrest of mutant strains.

Spatial regulations of chromosome replication, separation, and Z-ring formation

In Chapter 5, the model suggested PopZ and PodJ have higher affinity with poles, where the underlying mechanisms are unknown. In addition to a slower growth rate of poles and potential nucleating factors ZitP and TipN that had been discussed in Chapter 5, the biased location of genes likely contributes to the polar localization of PopZ and PodJ. Although bacterial chromosome is folded and dynamically distributed, experimental visualizations suggest that gene locations are linearly consistent with their genome coordinates [178]. Instead of simply assuming the synthesis of proteins only takes place in middle compartments as defined in Chapter 5, the spatial dynamics of genes can be modelled by the genome coordinates and the movement rate of replication forks.

The segregation of chromosomes is also involved in the spatial regulatory network. The scaffolding protein PopZ binds to *parS*/ParB centromeric complex, which captures the migration of one chromosome from one pole to the other [21, 204]. Additionally, ParA interacts with PopZ and DNA, the asymmetrical distribution of which is required in the chromosome

migration [204]. The detailed mechanisms underlying the ParA-ParB regulatory system are still being debated and need further studies.

The Z-ring construction is spatially regulated by FtsZ, which forms polymers and recruits other Z-ring proteins for Z-ring development [205, 206, 207]. The midcell localization of FtsZ is a consequence of chromosome segregation. MipZ, a protein promoting the depolymerization of FtsZ, forms a complex with ParB. Hence, MipZ is localized at two poles with the segregation of chromosome [21, 208]. As a result, the maximum concentration of FtsZ is near the midpoint of the cell, where [MipZ] is very low. Our previous model provided the foundation of investigating and integrating the spatial dynamics of chromosome and Z-ring complex, which likely in turn influences the localization of scaffolding proteins [209].

6.2.3 Stochastic version of the spatiotemporal model

This dissertation focused on the deterministic simulations of cell cycle control in *Caulobacter*, which is to predict average behaviors at the population level. However, deterministic models can not answer questions related to inherent noise and randomness in cells [210]. Our plan is to convert the deterministic model into a stochastic version to capture the variations of cell development. One concerned point of the stochastic model is the computational complexity. For the current version of our deterministic spatial model, the parameterization is already highly time-consuming. The computational time will dramatically increase with the consideration of randomness [211]. Hence, it is imperative to improve the efficiency of stochastic simulation in future work.

Appendix A. Supplementary Material for Chapter 2

A1. Calculations for ODEs

A set of equations in Table 2.1 in the main text of Chapter 2 can be simplified further.

From Equation 8 and Equation 9, we can get the relationship between [EI] and [EI$^{\mathrm{PEP}}$], as well as [EI $\sim$ P] and [EI $\sim$ P$^{\mathrm{Pyr}}$]:

$$\begin{aligned} [\mathrm{EI}^{\mathrm{PEP}}] &= \tfrac{[\mathrm{PEP}][\mathrm{EI}]}{K_{\mathrm{d1}}} \\ [\mathrm{EI} \sim \mathrm{P}^{\mathrm{Pyr}}] &= \tfrac{[\mathrm{Pyr}][\mathrm{EI} \sim \mathrm{P}]}{K_{\mathrm{d2}}} \end{aligned} \tag{A1.1}$$

We plug Equation A1.1 and Equation 10 into Equation 5 and write the expression as follows:

$$\begin{aligned} \frac{d[\mathrm{EI} \sim \mathrm{P}]_{\mathrm{tot}}}{dt} &= k_1 \cdot \tfrac{K_4 + \epsilon[\mathrm{Gln}]}{K_4 + [\mathrm{Gln}]} \cdot \tfrac{[\mathrm{PEP}][\mathrm{EI}]}{K_{\mathrm{d1}}} - k_{-1} \cdot \tfrac{[\mathrm{Pyr}][\mathrm{EI} \sim \mathrm{P}]}{K_{\mathrm{d2}}} \\ &- k_2 \cdot [\mathrm{EI} \sim \mathrm{P}]_{\mathrm{tot}}[\mathrm{NPr}] + k_{-2} \cdot [\mathrm{NPr} \sim \mathrm{P}][\mathrm{EI}]_{\mathrm{tot}} \end{aligned} \tag{A1.2}$$

where $[\mathrm{EI}] = \frac{[\mathrm{EI}]_{\mathrm{T}} - [\mathrm{EI} \sim \mathrm{P}](1 + \frac{[\mathrm{Pyr}]}{K_{\mathrm{d2}}})}{1 + \frac{[\mathrm{PEP}]}{K_{\mathrm{d1}}}}$; $[\mathrm{EI}]_{\mathrm{tot}} = [\mathrm{EI}]_{\mathrm{T}} - [\mathrm{EI} \sim \mathrm{P}]_{\mathrm{tot}}$, $[\mathrm{EI} \sim \mathrm{P}]_{\mathrm{tot}} = [\mathrm{EI} \sim \mathrm{P}](1 + \frac{[\mathrm{Pyr}]}{K_{\mathrm{d2}}})$.

With the same method, we plug Equation 11 and Equation 12 into Equation 6 and Equation 7. Then we can rewrite Equation A1.2, 6, and 7 as follows:

$$\begin{aligned} \frac{d[\mathrm{EI} \sim \mathrm{P}]_{\mathrm{tot}}}{dt} &= k_1 \cdot \tfrac{K_4 + \epsilon[\mathrm{Gln}]}{K_4 + [\mathrm{Gln}]} \cdot \tfrac{[\mathrm{PEP}][\mathrm{EI}]}{K_{\mathrm{d1}}} - k_{-1} \cdot \tfrac{[\mathrm{Pyr}][\mathrm{EI} \sim \mathrm{P}]}{K_{\mathrm{d2}}} \\ &- k_2 \cdot [\mathrm{EI} \sim \mathrm{P}]_{\mathrm{tot}}([\mathrm{NPr}]_{\mathrm{T}} - [\mathrm{NPr} \sim \mathrm{P}]) + k_{-2} \cdot [\mathrm{NPr} \sim \mathrm{P}][\mathrm{EI}]_{\mathrm{tot}} \\ \\ \frac{d[\mathrm{NPr} \sim \mathrm{P}]}{dt} &= k_2 \cdot [\mathrm{EI} \sim \mathrm{P}]_{\mathrm{tot}}([\mathrm{NPr}]_{\mathrm{T}} - [\mathrm{NPr} \sim \mathrm{P}]) \\ &- k_{-2} \cdot [\mathrm{NPr} \sim \mathrm{P}][\mathrm{EI}]_{\mathrm{tot}} \\ &- k_3 \cdot [\mathrm{NPr} \sim \mathrm{P}]([\mathrm{EIIA}]_{\mathrm{T}} - [\mathrm{EIIA} \sim \mathrm{P}]) \\ &+ k_{-3} \cdot ([\mathrm{NPr}]_{\mathrm{T}} - [\mathrm{NPr} \sim \mathrm{P}])[\mathrm{EIIA} \sim \mathrm{P}] \\ \frac{d[\mathrm{EIIA} \sim \mathrm{P}]}{dt} &= k_3 \cdot [\mathrm{NPr} \sim \mathrm{P}]([\mathrm{EIIA}]_{\mathrm{T}} - [\mathrm{EIIA} \sim \mathrm{P}]) \\ &- k_{-3} \cdot ([\mathrm{NPr}]_{\mathrm{T}} - [\mathrm{NPr} \sim \mathrm{P}])[\mathrm{EIIA} \sim \mathrm{P}] \end{aligned} \tag{A1.3}$$

In this manner, the seven ODEs and five algebraic equations in Table 2.1 can be rewritten rewritten as seven ODEs:

$$
\begin{aligned}
\frac{d[\mathrm{cdG}]}{dt} &= k_{\mathrm{s.cdG}} \cdot [\mathrm{DGC}] \cdot \frac{K_1^2}{K_1^2+[\mathrm{cdG}]^2} \cdot \frac{[\mathrm{GTP}]^2}{[\mathrm{GTP}]^2+K_{\mathrm{m1}}^2} \\
&- -k_{\mathrm{d.cdG}} \cdot [\mathrm{PDE}] \cdot \frac{[\mathrm{cdG}]}{[\mathrm{cdG}]+K_{\mathrm{m2}}} \\
\frac{d[\mathrm{(p)ppGpp}]}{dt} &= k_{\mathrm{s.(p)ppGpp}} \cdot \{\mathrm{SpoT_{sd}}\} \cdot \frac{[\mathrm{GTP}]}{[\mathrm{GTP}]+K_{\mathrm{m3}}} \\
&- k_{\mathrm{d.(p)ppGpp}} \cdot \{\mathrm{SpoT_{hd}}\} \cdot \frac{[\mathrm{(p)ppGpp}]}{[\mathrm{(p)ppGpp}]+K_{\mathrm{m4}}} \\
\frac{d[\mathrm{GTP}]}{dt} &= k_{\mathrm{s.GTP}} \cdot [\mathrm{GMP}] - k_{\mathrm{d.GTP}} \cdot [\mathrm{GTP}] - 2 \cdot k_{\mathrm{s.cdG}} \cdot [\mathrm{DGC}] \cdot \frac{K_1^2}{K_1^2+[\mathrm{cdG}]^2} \cdot \frac{[\mathrm{GTP}]^2}{[\mathrm{GTP}]^2+K_{\mathrm{m1}}^2} \\
&+ k_{\mathrm{d.(p)ppGpp}} \cdot \{\mathrm{SpoT_{hd}}\} \cdot \frac{[\mathrm{(p)ppGpp}]}{[\mathrm{(p)ppGpp}]+K_{\mathrm{m4}}} - k_{\mathrm{s.(p)ppGpp}} \cdot \{\mathrm{SpoT_{sd}}\} \cdot \frac{[\mathrm{GTP}]}{[\mathrm{GTP}]+K_{\mathrm{m3}}} \\
\frac{d[\mathrm{GMP}]}{dt} &= 2 \cdot k_{\mathrm{d.cdG}} \cdot [\mathrm{PDE}] \cdot \frac{[\mathrm{cdG}]}{[\mathrm{cdG}]+K_{\mathrm{m2}}} \\
&+ k_{\mathrm{d.GTP}} \cdot [\mathrm{GTP}] - k_{\mathrm{s.GTP}} \cdot [\mathrm{GMP}] \\
\frac{d[\mathrm{EI} \sim \mathrm{P}]_{\mathrm{tot}}}{dt} &= k_1 \cdot \frac{K_4+\epsilon[\mathrm{Gln}]}{K_4+[\mathrm{Gln}]} \cdot \frac{[\mathrm{PEP}][\mathrm{EI}]}{K_{\mathrm{d1}}} - k_{-1} \cdot \frac{[\mathrm{Pyr}][\mathrm{EI} \sim \mathrm{P}]}{K_{\mathrm{d2}}} \\
&- k_2 \cdot [\mathrm{EI} \sim \mathrm{P}]_{\mathrm{tot}}([\mathrm{NPr}]_{\mathrm{T}} - [\mathrm{NPr} \sim \mathrm{P}]) + k_{-2} \cdot [\mathrm{NPr} \sim \mathrm{P}][\mathrm{EI}]_{\mathrm{tot}} \\
\frac{d[\mathrm{NPr} \sim \mathrm{P}]}{dt} &= k_2 \cdot [\mathrm{EI} \sim \mathrm{P}]_{\mathrm{tot}}([\mathrm{NPr}]_{\mathrm{T}} - [\mathrm{NPr} \sim \mathrm{P}]) \\
&- k_{-2} \cdot [\mathrm{NPr} \sim \mathrm{P}][\mathrm{EI}]_{\mathrm{tot}} \\
&- k_3 \cdot [\mathrm{NPr} \sim \mathrm{P}]([\mathrm{EIIA}]_{\mathrm{T}} - [\mathrm{EIIA} \sim \mathrm{P}]) \\
&+ k_{-3} \cdot ([\mathrm{NPr}]_{\mathrm{T}} - [\mathrm{NPr} \sim \mathrm{P}])[\mathrm{EIIA} \sim \mathrm{P}] \\
\frac{d[\mathrm{EIIA} \sim \mathrm{P}]}{dt} &= k_3 \cdot [\mathrm{NPr} \sim \mathrm{P}]([\mathrm{EIIA}]_{\mathrm{T}} - [\mathrm{EIIA} \sim \mathrm{P}]) \\
&- k_{-3} \cdot ([\mathrm{NPr}]_{\mathrm{T}} - [\mathrm{NPr} \sim \mathrm{P}])[\mathrm{EIIA} \sim \mathrm{P}]
\end{aligned}
\tag{A1.4}
$$

A2. Phosphorylation of PTS^{Ntr} is non-linearly dependent on the [PEP]:[Pyr] ratio in simulation.

We simulate EIIA^{Ntr} ∼P under various PEP and Pyr levels in Table A2.1 to investigate how [PEP], [Pyr], and [PEP]:[Pyr] ratio affect phosphorylation of PTS^{Ntr} proteins.

Table A2.1: Effect of [PEP]:[Pyr] ratio on phosphorylation of EIIA^{Ntr} in simulation.

[EIIA^{Ntr} ∼P]μM [PEP] \ [Pyr]	500μM	1000μM	1500μM	2000μM
500μM	3.1	2.3	2.0	1.8
1000μM	3.8	2.8	2.5	2.3
1500μM	4.1	3.0	2.7	2.5
2000μM	4.3	3.2	2.8	2.6

Based on steady state analysis of ODEs, $\frac{[\text{EIIA}\sim\text{P}]}{[\text{EIIA}]}$, $\frac{[\text{NPr}\sim\text{P}]}{[\text{NPr}]}$, and $\frac{[\text{EI}\sim\text{P}]_{\text{tot}}}{[\text{EI}]_{\text{tot}}}$ are dependent on $\frac{[\text{PEP}]^2(K_{\text{d2}}+[\text{Pyr}])}{[\text{Pyr}]^2(K_{\text{d1}}+[\text{PEP}])}$ in our model, which means the phosphorylation fraction of PTS^{Ntr} proteins is non-linearly dependent with [PEP]:[Pyr] ratio.

Appendix B. Supplementary Material for Chapter 3

Table B.1: Initial values of model variables.

DNA variables	**Initial values**	**Master regulator vars.**	**Initial values**
Ini	0.0383	CcrM	0.435
$Elong$	0	DnaA	2.638
DNA	1	GcrA	3.841
$Count$	1	SciP	12.485
$Zring$	0	CtrA	1.973
h_{Cori}	0	CtrA∼P	3.960
h_{ccrM}	0		
h_{ctrA}	0		
mRNA variables	**Initial values**	**Protease complex vars.**	**Initial values**
$ccrM$	0.173	Complex 1	0.211
$dnaA$	3.154	CpdR	1.045
$gcrA$	4.525	CpdR∼P	0.042
$sciP$	6.335	Complex 2	0.187
$ctrA$	0.658	RcdA	0.789
		Complex 3	3.407
		CckAP	0.042
		cdG	0.511
		PleD	0.526
		PleD∼P	0.663
		PdeA	0.228

Table B.2: Sources for experimental data used to evaluate our models.

Species	**Data source**	**Species**	**Data source**
ccrM	[88]	CcrM	[115, 4]
dnaA	[88]	DnaA	[4, 85]
gcrA	[88]	GcrA	[85, 81]
sciP	[88]	SciP	[81]
ctrA	[88]	CtrA	[115, 4]
CpdR	[100]	RcdA	[112]
PleD	[113]	PdeA	[61]
cdG	[57]		

Table B.3: Parameter optimization with lower and upper bounds and starting point.

Parameter	**[L,U]**	**Starting**	**Parameter**	**[L,U]**	**Starting**
$k_{\mathrm{m,Cori}}$	[0.35, 5.6]	1.4	$k_{\mathrm{m,ccrM}}$	[0.35, 5.6]	1.4
$k_{\mathrm{m,ctrA}}$	[0.35, 5.6]	1.4	$k_{\mathrm{s},I_{ccrM}}$	[0.025 0.4]	0.1
$k_{\mathrm{d},I_{ccrM}}$	[0.016675, 0.2668]	0.0667	$k_{\mathrm{s,ccrM}}$	[0.064, 1.024]	0.256
$k_{\mathrm{d,ccrM}}$	[0.02, 0.32]	0.08	$k_{\mathrm{s,dnaA}}$	[0.0605,0.968]	0.242
$k_{\mathrm{d,dnaA}}$	[0.015, 0.24]	0.06	$k_{\mathrm{s,gcrA}}$	[1.4, 22.4]	5.6
$k_{\mathrm{d,gcrA}}$	[0.15, 2.4]	0.6	$k_{\mathrm{s,sciP}}$	[0.125, 2]	0.5
$k_{\mathrm{d,sciP}}$	[0.01, 0.16]	0.04	$k_{\mathrm{s1,ctrA}}$	[0.2475, 3.96]	0.99
$k_{\mathrm{s2,ctrA}}$	[0.0225, 0.36]	0.09	$k_{\mathrm{d,ctrA}}$	[0.02075, 0.332]	0.083
$k_{\mathrm{s,DnaA}}$	[0.01625, 0.26]	0.065	$k_{\mathrm{s,GcrA}}$	[0.007, 0.112]	0.028
$k_{\mathrm{s,CcrM}}$	[0.02125, 0.34]	0.085	$k_{\mathrm{s,SciP}}$	[0.0295, 0.472]	0.1183
$k_{\mathrm{d,SciP}}$	[0.015, 0.24]	0.06	$k_{\mathrm{s,CtrA}}$	[0.0108, 0.1728]	0.0432
$k_{\mathrm{d,CtrA\text{-}ClpXP}}$	[0.015, 0.24]	0.06	k_1^+	[0.15, 2.4]	0.6
k_1^-	[0.75, 12]	3	$k_{\mathrm{s,CpdR}}$	[0.175, 2.8]	0.7
$k_{\mathrm{d,CpdR}}$	[0.375, 6]	1.5	$k_{\mathrm{dephos,CpdR}}$	[0.25, 4]	1
$k_{\mathrm{phos,CpdR}}$	[0.25, 4]	1	k_2^+	[0.275, 4.4]	1.1
k_2^-	[0.25, 4]	1	$k_{\mathrm{s,RcdA}}$	[0.0375, 0.6]	0.15
$k_{\mathrm{d,RcdA}}$	[0.05, 0.8]	0.2	k_3^+	[35, 560]	140
k_3^-	[0.5, 8]	2	$k_{\mathrm{s,cdG}}$	[0.0025, 0.04]	0.01
$k_{\mathrm{d,cdG}}$	[0.25, 4]	1	$k_{\mathrm{s,PleD}}$	[0.025, 0.4]	0.1
$k_{\mathrm{d,PleD}}$	[0.0375, 0.6]	0.15	k_{phosPleD}	[0.01, 0.16]	0.04
$k_{\mathrm{dephosPleD}}$	[0.01, 0.16]	0.04	$k_{\mathrm{s,PdeA}}$	[0.0025, 0.04]	0.01
$k_{\mathrm{d,PdeA}}$	[0.125, 2]	0.5	k_{phoCtrA}	[1.25, 20]	5
$k_{\mathrm{dephoCckA}}$	[0.25, 4]	1	$k_{\mathrm{dephoCtrA}}$	[0.025, 0.4]	0.1
k_{phoCckA}	[0.25, 4]	1			

Appendix C. Supplementary Material for Chapter 4

C1. New Equations

Here, we provide equations of the model in Chapter 4 and compare with Weston et al.'s model [22]. New equations and terms are shown in red font.

Table C1.1: Equations.

(1) $\frac{d[\mathrm{CtrA_U}]}{dt} = \mathit{RpoD_{ctrA}} \cdot k_{\mathrm{s,CtrA1}} \cdot (1 - m_{\mathrm{CtrA}} \cdot (2M_{\mathrm{ctrA}} - 1)) \cdot \frac{\epsilon_{CtrA-GcrA} \cdot J_{\mathrm{a,CtrAGcrA}} + [\mathrm{GcrA}]}{J_{\mathrm{a,CtrAGcrA}} + [\mathrm{GcrA}]} \cdot (1 - \frac{[\mathrm{CtrA{\sim}P}]}{J_{\mathrm{i,CtrACtrA}} + [\mathrm{CtrA_U}] + [\mathrm{CtrA{\sim}P}]})$
$+k_{\mathrm{s,CtrA2}} \cdot \frac{\epsilon_{\mathrm{CtrACtrA}} \cdot J^2_{\mathrm{a,CtrACtrA_{\sim P}}} + [\mathrm{CtrA{\sim}P}]^2}{J^2_{\mathrm{a,CtrACtrA_{\sim P}}} + [\mathrm{CtrA_U}]^2 + [\mathrm{CtrA{\sim}P}]^2} \cdot \frac{J^2_{\mathrm{i,CtrASciP}}}{J^2_{\mathrm{i,CtrASciP}} + [\mathrm{SciP}]^2} - (\mu + k_{\mathrm{d,CtrA1}} + k_{\mathrm{d,CtrA2}} \cdot \frac{[\mathrm{ClpXP}]_{\mathrm{complex}}}{J_{\mathrm{d,CtrA}} + [\mathrm{CtrA{\sim}P}] + [\mathrm{CtrA_U}]}) \cdot [\mathrm{CtrA_U}]$
$+k_{\mathrm{dephos,CtrA}} \cdot [\mathrm{CckA_P}] \cdot [\mathrm{CtrA} \sim \mathrm{P}] - k_{\mathrm{phos,CtrA}} \cdot [\mathrm{CtrA_U}] \cdot [\mathrm{CckA_K}]$

(2) $\frac{d[\mathrm{CtrA{\sim}P}]}{dt} = -(\mu + k_{\mathrm{d,CtrA1}} + k_{\mathrm{d,CtrA2}} \cdot \frac{[\mathrm{ClpXP}]_{\mathrm{complex}}}{J_{\mathrm{d,CtrA}} + [\mathrm{CtrA{\sim}P}] + [\mathrm{CtrA_U}]}) \cdot [\mathrm{CtrA} \sim \mathrm{P}] - k_{\mathrm{dephos,CtrA}} \cdot [\mathrm{CckA_P}] \cdot [\mathrm{CtrA} \sim \mathrm{P}]$
$+k_{\mathrm{phos,CtrA}} \cdot [\mathrm{CtrA_U}] \cdot [\mathrm{CckA_K}]$

(3) $\frac{d[\mathrm{DnaA}]_{\mathrm{T}}}{dt} = k_{\mathrm{s,DnaA}} \cdot \frac{J_{\mathrm{i,DnaAGcrA}}}{J_{\mathrm{i,DnaAGcrA}} + [\mathrm{GcrA}]} \cdot (1 - 2 \cdot m_{\mathrm{DnaA}} \cdot (1 - M_{\mathrm{dnaA}})) - (\mu + k_{\mathrm{d,DnaA}}) \cdot [\mathrm{DnaA}]_{\mathrm{t}}$

(4) $\frac{d[\mathrm{DnaA{\sim}ATP}]}{dt} = k_{\mathrm{s,DnaA}} \cdot \frac{J_{\mathrm{i,DnaAGcrA}}}{J_{\mathrm{i,DnaAGcrA}} + [\mathrm{GcrA}]} \cdot (1 - 2 \cdot m_{\mathrm{DnaA}} \cdot (1 - M_{\mathrm{dnaA}}))$
$-(\mu + k_{\mathrm{d,DnaA}} + \mathrm{RepSwitch}) \cdot [\mathrm{DnaA} \sim \mathrm{ATP}]$

(5) $\frac{d[\mathrm{GcrA}]}{dt} = k_{\mathrm{s,GcrA}} \cdot \frac{\epsilon_{\mathrm{GcrADnaA}} \cdot J_{\mathrm{a,GcrADnaA}} + ([\mathrm{DnaA}]_{\mathrm{T}} - [\mathrm{DnaA{\sim}ATP}])}{J_{\mathrm{a,GcrADnaA}} + ([\mathrm{DnaA}]_{\mathrm{T}} - [\mathrm{DnaA{\sim}ATP}])} \cdot \frac{J^2_{\mathrm{i,GcrACtrA}}}{J^2_{\mathrm{i,GcrACtrA}} + [\mathrm{CtrA{\sim}P}]^2} - (\mu + k_{\mathrm{d,GcrA}}) \cdot [\mathrm{GcrA}]$

(6) $\frac{d[\mathrm{SciP}]}{dt} = k_{\mathrm{s,SciP}} \cdot \frac{[\mathrm{CtrA{\sim}P}]^2}{[\mathrm{CtrA{\sim}P}]^2 + J^2_{\mathrm{a,SciPCtrA}}} \cdot \frac{J^2_{\mathrm{i,SciPSciP}}}{J^2_{\mathrm{i,SciPSciP}} + [\mathrm{SciP}]^2} - (\mu + k_{\mathrm{d,SciP}}) \cdot [\mathrm{SciP}]$

(7) $\frac{d[\mathrm{DivK}]}{dt} = \mathit{RpoD_{divK}} \cdot k_{\mathrm{s,DivK1}} + k_{\mathrm{s,DivK2}} \cdot \frac{[\mathrm{CtrA{\sim}P}]^2}{J^2_{\mathrm{a,DivKCtrA}} + [\mathrm{CtrA{\sim}P}]^2} - (\mu + k_{\mathrm{d,DivK}}) \cdot [\mathrm{DivK}] - (k_{\mathrm{phos,DivK1}} \cdot [\mathrm{DivJ}]_{\mathrm{A}}$
$+k_{\mathrm{phos,DivK2}} \cdot [\mathrm{PleC}]_{\mathrm{K}} + k_{\mathrm{phos,DivK3}} \cdot \mathit{MysK}) \cdot [\mathrm{DivK}] + (k_{\mathrm{dephos,DivK1}} \cdot [\mathrm{PleC}] + k_{\mathrm{dephos,DivK2}} \cdot [\mathrm{CckN}]) \cdot [\mathrm{DivK} \sim \mathrm{P}]$
$-k_{\mathrm{b,DivJDivK}} \cdot [\mathrm{DivJ}] \cdot [\mathrm{DivK}] + (k_{\mathrm{ub,DivJDivK}} + k_{\mathrm{d,DivJ}}) \cdot [\mathrm{DivJ} : \mathrm{DivK}] - k_{\mathrm{b,DivLDivK}} \cdot [\mathrm{DivL}] \cdot [\mathrm{DivK}]$
$+(k_{\mathrm{ub,DivLDivK}} + k_{\mathrm{d,DivL}}) \cdot [\mathrm{DivL} : \mathrm{DivK}]$

(8) $\frac{d[\mathrm{DivK{\sim}P}]}{dt} = -(\mu + k_{\mathrm{d,DivK}}) \cdot [\mathrm{DivK}] - (k_{\mathrm{dephos,DivK1}} \cdot [\mathrm{PleC}] + k_{\mathrm{dephos,DivK2}} \cdot [\mathrm{CckN}]) \cdot [\mathrm{DivK} \sim \mathrm{P}]$
$+(k_{\mathrm{phos,DivK1}} \cdot [\mathrm{DivJ}]_{\mathrm{A}} + k_{\mathrm{phos,DivK2}} \cdot [\mathrm{PleC}]_{\mathrm{K}} + k_{\mathrm{phos,DivK3}} \cdot \mathit{MysK}) \cdot [\mathrm{DivK}]$
$+2 \cdot ((k_{\mathrm{ub,PleCDivKP}} + k_{\mathrm{d,PleC}} + k_{\mathrm{d,DivK}}) \cdot [\mathrm{PleC} : \mathrm{DivK} \sim \mathrm{P}_2] - k_{\mathrm{b,PleCDivKP}} \cdot [\mathrm{PleC}] \cdot [\mathrm{DivK} \sim \mathrm{P}]^2)$
$-k_{\mathrm{b,DivJDivKP}} \cdot [\mathrm{DivJ}] \cdot [\mathrm{DivK} \sim \mathrm{P}] + (k_{\mathrm{ub,DivJDivKP}} + k_{\mathrm{d,DivJ}}) \cdot [\mathrm{DivJ} : \mathrm{DivK} \sim \mathrm{P}]$

Continued on next page

Table A.1. – *Continued from previous page*

$-k_{\mathrm{b,DivLDivKP}} \cdot [\mathrm{DivL}] \cdot [\mathrm{DivK} \sim \mathrm{P}] + (k_{\mathrm{ub,DivLDivKP}} + k_{\mathrm{d,DivL}}) \cdot [\mathrm{DivL} : \mathrm{DivK} \sim \mathrm{P}]$

(9) $\frac{d[\mathrm{CckN}]}{dt} = k_{\mathrm{s,CckN}} \cdot \frac{[\mathrm{CtrA}\sim\mathrm{P}]^4}{[\mathrm{CtrA}\sim\mathrm{P}]^4 + J_{\mathrm{a,CckNCtrA}}^4} - (\mu + k_{\mathrm{d,CckN1}}) \cdot [\mathrm{CckN}] - k_{\mathrm{d,CckN2}} \cdot [\mathrm{PopA} : \mathrm{cdG_2}] \cdot \frac{[\mathrm{CckN}]}{[\mathrm{CckN}] + J_{\mathrm{d,CckN}}}$

(10) $\frac{[\mathrm{DivJ}]}{dt} = k_{\mathrm{s,DivJ}} - (\mu + k_{\mathrm{d,DivJ}}) \cdot [\mathrm{DivJ}] - k_{\mathrm{b,DivJDivKP}} \cdot [\mathrm{DivJ}] \cdot [\mathrm{DivK} \sim \mathrm{P}] + (k_{\mathrm{ub,DivJDivKP}} + k_{\mathrm{d,DivK}})$
$\cdot [\mathrm{DivJ} : \mathrm{DivK} \sim \mathrm{P}] - k_{\mathrm{b,DivJDivK}} \cdot [\mathrm{DivJ}] \cdot [\mathrm{DivK}] + (k_{\mathrm{ub,DivJDivK}} + k_{\mathrm{d,DivK}}) \cdot [\mathrm{DivJ} : \mathrm{DivK}]$

(11) $\frac{d[\mathrm{DivJ:DivK}]}{dt} = k_{\mathrm{b,DivJDivK}} \cdot [\mathrm{DivJ}] \cdot [\mathrm{DivK}] - (k_{\mathrm{ub,DivJDivK}} + k_{\mathrm{d,DivK}} + +k_{\mathrm{d,DivJ}} + \mu) \cdot [\mathrm{DivJ} : \mathrm{DivK}]$

(11) $\frac{d[\mathrm{DivJ:DivK\sim P}]}{dt} = k_{\mathrm{b,DivJDivK\sim P}} \cdot [\mathrm{DivJ}] \cdot [\mathrm{DivK} \sim \mathrm{P}] - (k_{\mathrm{ub,DivJDivK\sim P}} + k_{\mathrm{d,DivK}} + +k_{\mathrm{d,DivJ}} + \mu) \cdot [\mathrm{DivJ} : \mathrm{DivK} \sim \mathrm{P}]$

(12) $[\mathrm{DivJ}]_{\mathrm{A}} = ([\mathrm{DivJ} : \mathrm{DivK} \sim \mathrm{P}] + [\mathrm{DivJ} : \mathrm{DivK}]) \cdot ((1 - \epsilon_{\mathrm{DivJDivK}}) \cdot (\frac{\min([\mathrm{SpmX}], [\mathrm{DivJ}]_{\mathrm{T}})}{[\mathrm{DivJ}]_{\mathrm{T}}}) + \epsilon_{\mathrm{DivJDivK}})$
$+\epsilon_{\mathrm{DivJSpmX}} \cdot [\mathrm{DivJ}] \cdot \frac{\min([\mathrm{SpmX}], [\mathrm{DivJ}]_{\mathrm{T}})}{[\mathrm{DivJ}]_{\mathrm{T}}}$

(13) $\frac{[\mathrm{DivL}]}{dt} = k_{\mathrm{s,DivL}} - (\mu + k_{\mathrm{d,DivL}}) \cdot [\mathrm{DivL}] - k_{\mathrm{b,DivLDivK\sim P}} \cdot [\mathrm{DivL}] \cdot [\mathrm{DivK} \sim \mathrm{P}]$
$+(k_{\mathrm{ub,DivLDivK\sim P}} + k_{\mathrm{d,DivK}}) \cdot [\mathrm{DivL} : \mathrm{DivK} \sim \mathrm{P}]$

(14) $\frac{d[\mathrm{DivL:DivK\sim P}]}{dt} = k_{\mathrm{b,DivLDivK\sim P}} \cdot [\mathrm{DivL}] \cdot [\mathrm{DivK} \sim \mathrm{P}] - (k_{\mathrm{ub,DivLDivK\sim P}} + k_{\mathrm{d,DivK}} + k_{\mathrm{d,DivL}} + \mu) \cdot [\mathrm{DivL} : \mathrm{DivK} \sim \mathrm{P}]$

(15) $\frac{[\mathrm{CckA}]_{\mathrm{T}}}{dt} = k_{\mathrm{s,CckA}} - (\mu + k_{\mathrm{d,CckA}}) \cdot [\mathrm{CckA}]_{\mathrm{T}}$

(16) $\frac{d[\mathrm{CckA:cdG}]}{dt} = k_{\mathrm{b,CckAcdG}} \cdot [\mathrm{cdG}] \cdot ([\mathrm{CckA}]_{\mathrm{T}} - [\mathrm{CckA} : \mathrm{cdG}]) - (k_{\mathrm{ub,CckAcdG}} + k_{\mathrm{d,CckA}} + \mu) \cdot [\mathrm{CckA} : \mathrm{cdG}]$

(17) $[\mathrm{CckA} : \mathrm{DivL}]_{\mathrm{T}} = \frac{[\mathrm{CckA}]_{\mathrm{T}} + [\mathrm{DivL}]_{\mathrm{T}} + K_{\mathrm{CckADivL}} - \sqrt{([\mathrm{CckA}]_{\mathrm{T}} + [\mathrm{DivL}]_{\mathrm{T}} + \mathrm{K_{CckADivL}})^2 - 4 \cdot [\mathrm{CckA}]_{\mathrm{T}} \cdot [\mathrm{DivL}]_{\mathrm{T}}}}{2}$

(18) $[\mathrm{CckA}]_{\mathrm{P}} = \frac{[\mathrm{CckA:DivL}]_{\mathrm{T}} \cdot [\mathrm{DivL:DivK\sim P}]}{[\mathrm{DivL}]_{\mathrm{T}}} + [\mathrm{CckA} : \mathrm{cdG}] - \frac{[\mathrm{CckA:cdG}] \cdot \frac{[\mathrm{CckA:DivL}]_{\mathrm{T}} \cdot [\mathrm{DivL:DivK\sim P}]}{[\mathrm{DivL}]_{\mathrm{T}}}}{[\mathrm{CckA}]_{\mathrm{T}}}$

(19) $[\mathrm{CckA}]_{\mathrm{K}} = [\mathrm{CckA}]_{\mathrm{T}} - [\mathrm{CckA}]_{\mathrm{P}}$

(20) $\frac{d[\mathrm{PleC}]}{dt} = k_{\mathrm{s,PleC}} \cdot (2 - 2 \cdot M_{\mathrm{PleC}}) - (\mu + k_{\mathrm{d,PleC}}) \cdot [\mathrm{PleC}] - k_{\mathrm{b,PleCDivKP}} \cdot [\mathrm{PleC}] \cdot [\mathrm{DivK} \sim \mathrm{P}]^2 + (k_{\mathrm{ub,PleCDivKP}}$
$+2 \cdot k_{\mathrm{d,DivK}}) \cdot [\mathrm{PleC} : \mathrm{DivK} \sim \mathrm{P_2}]$

(21) $\frac{d[\mathrm{PleC:DivK\sim P_2}]}{dt} = k_{\mathrm{b,PleCDivKP}} \cdot [\mathrm{PleC}] \cdot [\mathrm{DivK} \sim \mathrm{P}]^2 - (k_{\mathrm{ub,PleCDivKP}} + 2 \cdot k_{\mathrm{d,DivK}} + k_{\mathrm{d,PleC}} + \mu)$
$\cdot [\mathrm{PleC} : \mathrm{DivK} \sim \mathrm{P_2}]$

(22) $\frac{d[\mathrm{PleC}]_{\mathrm{pole}}}{dt} = k_{\mathrm{PleCbinding}} \cdot ([\mathrm{PleC}]_{\mathrm{T}} - [\mathrm{PleC}]_{\mathrm{pole}}) \cdot \frac{[\mathrm{PodJ}]}{[\mathrm{PodJ}] \cdot V + J_{\mathrm{PleCPodJ}}} - (k_{\mathrm{PleCbinding}} + k_{\mathrm{d,PleC}} + \mu) \cdot [\mathrm{PleC}]_{\mathrm{pole}}$

(23) $\frac{d[\mathrm{PodJ}]}{dt} = k_{\mathrm{s,PodJ}} \cdot \frac{[\mathrm{GcrA}]}{[\mathrm{GcrA}] + J_{\mathrm{a,PodJGcrA}}} \cdot \frac{J_{\mathrm{i,PodJDnaA}}}{J_{\mathrm{i,PodJDnaA}} + [\mathrm{PodJ}]} \cdot (2 - 2 \cdot M_{\mathrm{PodJ}}) - (\mu + k_{\mathrm{d,PodJ1}} + k_{\mathrm{d,PodJ2}} \cdot [\mathrm{PerP}]) \cdot [\mathrm{PodJ}]$

(24) $\frac{d[\mathrm{PerP}]}{dt} = k_{\mathrm{s,PerP}} \cdot \frac{[\mathrm{CtrA}]^2}{[\mathrm{CtrA}]^2 + J_{\mathrm{a,PerPCtrA}}^2} \cdot (2 - 2 \cdot M_{\mathrm{PerP}}) - (\mu + k_{\mathrm{d,PerP}}) \cdot [\mathrm{PerP}]$

(25) $\frac{d[\mathrm{Ini}]}{dt} = (1 - 2 \cdot m_{\mathrm{ini}} \cdot (1 - M_{\mathrm{Ini}})) \cdot (1 - [\mathrm{DNA} : \mathrm{CtrA} \sim \mathrm{P_2}])^5 \cdot (\frac{[\mathrm{DNA}\sim\mathrm{ATP}]}{[\mathrm{DNA}\sim\mathrm{ATP}] + J_{\mathrm{a,IniDnaA}}})^2 - k_{\mathrm{d,Ini}} \cdot [\mathrm{Ini}]$

(26) $[\mathrm{DNA}]_{\mathrm{F}} = \frac{K_{\mathrm{d1}}}{K_{\mathrm{d1}} + 2 \cdot \mathrm{CtrA}\sim\mathrm{P} + (1 - \sigma_{\mathrm{CtrAU:}Cori}) \cdot (2 \cdot [\mathrm{CtrA_U}] + \frac{[\mathrm{CtrA_U}]^2}{K_{\mathrm{d2}}} + \frac{[\mathrm{CtrA_U}] + [\mathrm{CtrA}\sim\mathrm{P}]}{K_{\mathrm{d2}}})}$

(27) $[\mathrm{DNA} : \mathrm{CtrA} \sim \mathrm{P_2}] = \frac{[\mathrm{CtrA}\sim\mathrm{P}]^2 \cdot [\mathrm{DNA}]_{\mathrm{F}}}{K_{\mathrm{d1}} \cdot K_{\mathrm{d3}}}$

(28) $\frac{d[\mathrm{Elong}]}{dt} = k_{\mathrm{elong}} \cdot \mathit{RepSwitch}$

(29) $\frac{d[\mathrm{CcrM}]}{dt} = k_{\mathrm{s,CcrM}} \cdot \frac{[\mathrm{CtrA}]^2}{[\mathrm{CtrA}]^2 + J_{\mathrm{a,CcrMCtrA}}^2} \cdot \frac{J_{\mathrm{i,CcrMDnaA}}}{J_{\mathrm{i,CcrMDnaA}} + [\mathrm{DnaA}]} \cdot (2 - 2 \cdot M_{\mathrm{CcrM}}) - (\mu + k_{\mathrm{d,CcrM}}) \cdot [\mathrm{CcrM}]$

(30) $\frac{d[\mathrm{TacA}]}{dt} = k_{\mathrm{s,TacA}} \cdot \frac{[\mathrm{CtrA}\sim\mathrm{P}]}{[\mathrm{CtrA}\sim\mathrm{P}] + J_{\mathrm{a,TacACtrA}}} - (k_{\mathrm{d,TacA1}} + \mu) \cdot [\mathrm{TacA}] - k_{\mathrm{d,TacA2}} \cdot [\mathrm{RcdA} : \mathrm{CpdR}] \cdot \frac{[\mathrm{TacA}]}{[\mathrm{TacA}]_{\mathrm{T}} + J_{\mathrm{d,TacA}}}$
$-k_{\mathrm{phos,TacA}} \cdot [\mathrm{ShkA} : \mathrm{cdG}] \cdot [\mathrm{TacA}] + k_{\mathrm{dephos,TacA}} \cdot [\mathrm{ShkA}] \cdot [\mathrm{TacA} \sim \mathrm{P}]$

(31) $\frac{d[\mathrm{TacA\sim P}]}{dt} = -k_{\mathrm{d,TacA2}} \cdot [\mathrm{RcdA} : \mathrm{CpdR}] \cdot \frac{[\mathrm{TacA}\sim\mathrm{P}]}{[\mathrm{TacA}]_{\mathrm{T}} + J_{\mathrm{d,TacA}}} + k_{\mathrm{phos,TacA}} \cdot [\mathrm{ShkA} : \mathrm{cdG}] \cdot [\mathrm{TacA}]$
$-(\mu + k_{\mathrm{d,TacA1}} + k_{\mathrm{dephos,TacA}} \cdot [\mathrm{ShkA}]) \cdot [\mathrm{TacA} \sim \mathrm{P}]$

(32) $\frac{d[\mathrm{SpmX}]}{dt} = k_{\mathrm{s,SpmX}} \cdot \frac{[\mathrm{TacA}\sim\mathrm{P}]}{[\mathrm{TacA}\sim\mathrm{P}] + J_{\mathrm{a,SpmXTacA}}} - (k_{\mathrm{d,SpmX}} + \mu) \cdot [\mathrm{SpmX}]$

(33) $\frac{d[\mathrm{ShkA}]}{dt} = k_{\mathrm{s,ShkA}} \cdot \frac{[\mathrm{CtrA}\sim\mathrm{P}]}{[\mathrm{CtrA}\sim\mathrm{P}] + J_{\mathrm{a,ShkACtrA}}} - (k_{\mathrm{d,ShkA1}} + \mu) \cdot [\mathrm{ShkA}] - k_{\mathrm{d,ShkA2}} \cdot [\mathrm{ClpXP}]_{\mathrm{Complex}} \cdot \frac{[\mathrm{ShkA}]}{[\mathrm{ShkA}]_{\mathrm{T}} + J_{\mathrm{d,ShkA}}}$

Continued on next page

Table A.1. – *Continued from previous page*

$-k_{\mathrm{b,ShkAcdG}} \cdot [\mathrm{cdG}] \cdot [\mathrm{ShkA}] + k_{\mathrm{ub,ShkAcdG}} \cdot [\mathrm{ShkA : cdG}]$

(34) $\frac{d[\mathrm{ShkA:cdG}]}{dt} = -(\mu + k_{\mathrm{d,ShkA1}}) \cdot [\mathrm{ShkA : cdG}] - k_{\mathrm{d,ShkA2}} \cdot [\mathrm{ClpXP}]_{\mathrm{Complex}} \cdot \frac{[\mathrm{ShkA:cdG}]}{[\mathrm{ShkA}]_{\mathrm{T}} + J_{\mathrm{d,ShkA}}}$
$+k_{\mathrm{b,ShkAcdG}} \cdot [\mathrm{cdG}] \cdot [\mathrm{ShkA}] - k_{\mathrm{ub,ShkAcdG}} \cdot [\mathrm{ShkA : cdG}]$

(35) $\frac{d\mathrm{Zproteins}}{dt} = k_{\mathrm{s,Zp}} \cdot \frac{[\mathrm{CtrA}]^2}{[\mathrm{CtrA}]^2 + J^2_{\mathrm{a,ZpCtrA}}} - (\mu + k_{\mathrm{d,Zp1}} + k_{\mathrm{d,Zp2}} \cdot [\mathrm{ClpAP}]) \cdot [\mathrm{Zproteins}]$

(36) $\frac{d[\mathrm{Zring}]}{dt} = -k_{\mathrm{Zconstrict}} \cdot MipZswitch \cdot \frac{[\mathrm{Zproteins}]^5}{(J_{\mathrm{Zring}} + \theta_{\mathrm{Z}} \cdot [\mathrm{Zring}])^5 + [\mathrm{Zproteins}]^5}$

(37) $\frac{dV}{dt} = \mu V$

(38) $\mu = T_{-1} \cdot ln \frac{V_{\mathrm{div}}}{V_{\mathrm{birth}}}$

(39) $\frac{d[\mathrm{CpdR}]}{dt} = k_{\mathrm{s,CpdR}} \cdot \frac{\epsilon_{\mathrm{CpdRDnaA}} \cdot J_{\mathrm{a,CpdRDnaA}} + [\mathrm{DnaA}]_{\mathrm{T}}}{J_{\mathrm{a,CpdRDnaA}} + [\mathrm{DnaA}]_{\mathrm{T}}} \cdot \frac{[\mathrm{CtrA}]^2}{[\mathrm{CtrA}]^2 + J^2_{\mathrm{a,CpdRCtrA}}} \cdot \frac{J_{\mathrm{i,CpdRGcrA}}}{J_{\mathrm{i,CpdRGcrA}} + [\mathrm{GcrA}]} - (\mu + k_{\mathrm{d,CpdR}}) \cdot [\mathrm{CpdR}]$
$+k_{\mathrm{dephos,CpdR}} \cdot [\mathrm{CpdR} \sim \mathrm{P}] \cdot [\mathrm{CckA}]_{\mathrm{P}} - k_{\mathrm{phos,CpdR}} \cdot [\mathrm{CpdR}] \cdot [\mathrm{CckA}]_{\mathrm{K}}$

(40) $\frac{d[\mathrm{CpdR\sim P}]}{dt} = -k_{\mathrm{dephos,CpdR}} \cdot [\mathrm{CpdR} \sim \mathrm{P}] \cdot [\mathrm{CckA}]_{\mathrm{P}} + k_{\mathrm{phos,CpdR}} \cdot [\mathrm{CpdR}] \cdot [\mathrm{CckA}]_{\mathrm{K}}$

(41) $\frac{d[\mathrm{RcdA}]}{dt} = k_{\mathrm{s,RcdA}} \cdot \frac{[\mathrm{CtrA\sim P}]^2}{[\mathrm{CtrA\sim P}]^2 + J^2_{\mathrm{a,RcdACtrA}}} - (\mu + k_{\mathrm{d,RcdA}}) \cdot [\mathrm{RcdA}]$

(42) $\frac{d[\mathrm{cdG}]}{dt} = (k_{\mathrm{s,cdG1}} \cdot [\mathrm{PleC} \sim \mathrm{P}] + k_{\mathrm{s,cdG2}} \cdot [\mathrm{DgcB}]_{\mathrm{a}}) \cdot \frac{[\mathrm{GTP}]^2}{[\mathrm{GTP}]^2 + J^2_{\mathrm{s,cdG}}} - k_{\mathrm{d,cdG1}} \cdot ([\mathrm{PdeA}] + PDE) \cdot [\mathrm{cdG}]$
$-\mu \cdot [\mathrm{cdG}] + 2 \cdot (-k^+_{\mathrm{PopAcdG}} \cdot [\mathrm{PopA}] \cdot [\mathrm{cdG}]^2 + (k^-_{\mathrm{XcdG}} + K_{\mathrm{d,PopA}}) \cdot [\mathrm{PopA : cdG_2}])$
$+2 \cdot (-k^+_{\mathrm{PleDcdG}} \cdot [\mathrm{PleD}]_{\mathrm{T}} \cdot [\mathrm{cdG}]^2 + (k^-_{\mathrm{XcdG}} + K_{\mathrm{d,PleD}}) \cdot [\mathrm{PleD : cdG_2}]_{\mathrm{T}}) - k^+_{\mathrm{CckAcdG}}$
$\cdot([\mathrm{CckA}]_{\mathrm{T}} - [\mathrm{CckA : cdG}]) \cdot [\mathrm{cdG}] + k^-_{\mathrm{CckAcdG}} \cdot [\mathrm{CckA : cdG}]$
$+2 \cdot (-k^+_{\mathrm{DgcBcdG}} \cdot (DgcB - [\mathrm{DgcB : cdG_2}])) \cdot [\mathrm{cdG}]^2 + k^-_{\mathrm{XcdG}} \cdot [\mathrm{DgcB : cdG_2}]$

(43) $\frac{d[\mathrm{PopA}]}{dt} = k_{\mathrm{s,PopA}} \cdot \frac{J_{\mathrm{i,PopAGcrA}}}{J_{\mathrm{i,PopAGcrA}} + [\mathrm{GcrA}]} - (\mu + k_{\mathrm{d,PopA}}) \cdot [\mathrm{PopA}] - k_{\mathrm{b,PopAcdG}} \cdot [\mathrm{PopA}] \cdot [\mathrm{cdG}]^2$
$+k_{\mathrm{ub,PopAcdG}} \cdot [\mathrm{PopA : cdG_2}]$

(44) $\frac{d[\mathrm{PopA:cdG_2}]}{dt} = k_{\mathrm{b,PopAcdG}} \cdot [\mathrm{PopA}] \cdot [\mathrm{cdG}]^2 - (\mu + k_{\mathrm{d,PopA}} + k_{\mathrm{ub,PopAcdG}}) \cdot [\mathrm{PopA : cdG_2}]$

(45) $[\mathrm{RcdA : CpdR}]_{\mathrm{T}} = \frac{[\mathrm{CpdR}]_{\mathrm{T}} + [\mathrm{RcdA}] + K_{\mathrm{RcdACpdR}} - \sqrt{([\mathrm{CpdR}]_{\mathrm{T}} + [\mathrm{RcdA}] + K_{\mathrm{RcdACpdR}})^2 - 4 \cdot [\mathrm{CpdR}]_{\mathrm{T}} \cdot [\mathrm{RcdA}]}}{2}$

(46) $[\mathrm{RcdA : CpdR}] = [\mathrm{RcdA : CpdR}]_{\mathrm{T}} \cdot \frac{[\mathrm{CpdR}]}{[\mathrm{CpdR}]_{\mathrm{T}}}$

(47) $[\mathrm{ClpXP}]_{\mathrm{Complex}} = \frac{[\mathrm{RcdA:CpdR}]}{[\mathrm{RcdA:CpdR}] + \frac{K_{\mathrm{ClpXPCpdR}}}{V}} \cdot [\mathrm{PopA : cdG_2}]$

(48) $\frac{d[\mathrm{PdeA}]}{dt} = k_{\mathrm{s,PdeA}} \cdot \frac{[\mathrm{CtrA\sim P}]}{[\mathrm{CtrA\sim P}] + J_{\mathrm{a,PdeACtrA}}} - (\mu + k_{\mathrm{d,PdeA1}}) \cdot [\mathrm{PdeA}] - k_{\mathrm{d,PdeA2}} \cdot \frac{[\mathrm{PdeA}]}{[\mathrm{PdeA}] + J_{\mathrm{d,PdeA}}}$

(49) $[\mathrm{DgcB}]_{\mathrm{a}} = \max(DgcB - \mathrm{PdeA}, 0) \cdot \frac{DgcB - [\mathrm{DgcB:cdG_2}]}{DgcB}$

(50) $\frac{[\mathrm{DgcB:cdG_2}]}{dt} = k_{\mathrm{b,DgcBcdG}} \cdot (DgcB - [\mathrm{DgcB : cdG_2}]) \cdot [\mathrm{cdG}]^2 - (\mu + k_{\mathrm{ub,XcdG}}) \cdot [\mathrm{DgcB : cdG_2}]$

(51) $\frac{d[\mathrm{PleD}]}{dt} = k_{\mathrm{s,PleD1}} \cdot \frac{[\mathrm{CtrA\sim P}]^2}{[\mathrm{CtrA\sim P}]^2 + J^2_{\mathrm{a,PleDCtrA}}} + k_{\mathrm{s,PleD2}} \cdot RpoD_{pleD} - (\mu + k_{\mathrm{d,PleD}}) \cdot [\mathrm{PleD}] - k_{\mathrm{phos,PleD}} \cdot ([\mathrm{DivJ}]_{\mathrm{A}} + MysK)$
$\cdot[\mathrm{PleD}] + (\frac{1}{10} + \frac{9}{10} \cdot \frac{[\mathrm{PleC}]_{\mathrm{tot}} - [\mathrm{PleC}]_{\mathrm{pole}}}{[\mathrm{PleC}]_{\mathrm{tot}}}) \cdot k_{\mathrm{dephos,PleCPleD}} \cdot [\mathrm{PleC}] \cdot [\mathrm{PleD} \sim \mathrm{P}] + k_{\mathrm{dephos,CckNPleD}} \cdot [\mathrm{CckN}]$
$-k_{\mathrm{b,PleDcdG}} \cdot [\mathrm{PleD}] \cdot [\mathrm{cdG}]^2 + k_{\mathrm{ub,PleDcdG}} \cdot [\mathrm{PleD : cdG_2}]$

(52) $\frac{d[\mathrm{PleD\sim P}]}{dt} = -(\mu + k_{\mathrm{d,PleD}}) \cdot [\mathrm{PleD}] + k_{\mathrm{phos,PleD}} \cdot ([\mathrm{DivJ}]_{\mathrm{A}} + MysK) \cdot [\mathrm{PleD}] - (\frac{1}{10} + \frac{9}{10} \cdot \frac{[\mathrm{PleC}]_{\mathrm{tot}} - [\mathrm{PleC}]_{\mathrm{pole}}}{[\mathrm{PleC}]_{\mathrm{tot}}})$
$\cdot k_{\mathrm{dephos,PleCPleD}} \cdot [\mathrm{PleC}] \cdot [\mathrm{PleD} \sim \mathrm{P}] - k_{\mathrm{dephos,CckNPleD}} \cdot [\mathrm{CckN}] \cdot [\mathrm{PleD} \sim \mathrm{P}] - k_{\mathrm{b,PleDcdG}} \cdot [\mathrm{PleD} \sim \mathrm{P}] \cdot [\mathrm{cdG}]^2$
$+k_{\mathrm{ub,PleDcdG}} \cdot [\mathrm{PleD} \sim \mathrm{P : cdG_2}]$

(53) $\frac{d[\mathrm{PleD:cdG_2}]}{dt} = -(\mu + k_{\mathrm{d,PleD}}) \cdot [\mathrm{PleD : cdG_2}] - k_{\mathrm{phos,PleD}} \cdot ([\mathrm{DivJ}]_{\mathrm{A}} + MysK) \cdot [\mathrm{PleD : cdG_2}]$
$+(\frac{1}{10} + \frac{9}{10} \cdot \frac{[\mathrm{PleC}]_{\mathrm{tot}} - [\mathrm{PleC}]_{\mathrm{pole}}}{[\mathrm{PleC}]_{\mathrm{tot}}}) \cdot k_{\mathrm{dephos,PleCPleD}} \cdot [\mathrm{PleC}] \cdot [\mathrm{PleD} \sim \mathrm{P : cdG_2}] + k_{\mathrm{dephos,CckNPleD}} \cdot [\mathrm{CckN}]$
$\cdot[\mathrm{PleD} \sim \mathrm{P : cdG_2}] + k_{\mathrm{b,PleDcdG}} \cdot [\mathrm{PleD}] \cdot [\mathrm{cdG}]^2 - k_{\mathrm{ub,PleDcdG}} \cdot [\mathrm{PleD : cdG_2}]$

Continued on next page

Table A.1. – *Continued from previous page*

(54)	$\frac{d[\text{PleD}\sim\text{P:cdG}_2]}{dt} = -(\mu + k_{\text{d,PleD}}) \cdot [\text{PleD} \sim \text{P} : \text{cdG}_2] + k_{\text{phos,PleD}} \cdot ([\text{DivJ}]_{\text{A}} + MysK) \cdot [\text{PleD} : \text{cdG}_2]$
	$-(\frac{1}{10} + \frac{9}{10} \cdot \frac{[\text{PleC}]_{\text{tot}} - [\text{PleC}]_{\text{pole}}}{[\text{PleC}]_{\text{tot}}}) \cdot k_{\text{dephos,PleCPleD}} \cdot [\text{PleC}] \cdot [\text{PleD} \sim \text{P} : \text{cdG}_2] - k_{\text{dephos,CckNPleD}} \cdot [\text{CckN}]$
	$\cdot[\text{PleD} \sim \text{P} : \text{cdG}_2] + k_{\text{b,PleDcdG}} \cdot [\text{PleD} \sim \text{P}] \cdot [\text{cdG}]^2 - k_{\text{ub,PleDcdG}} \cdot [\text{PleD} \sim \text{P} : \text{cdG}_2]$

C3. Other starvation signals

Table C3.1: Additional signaling targets and arrest statistics.

Paradigm	Description	Parameters changes		Fractional Arrested*			
				1^{st}G1	2^{nd}G1	1^{st}G2	2^{nd}G2
Signal 5a	Introducing stress response through cdG-dependent pathway. Inhibiting DnaA synthesis.	$\mu = 0.0018$ $k_{s,cdG1} = 0.056k_{s,cdG1}$ $k_{s,cdG2} = 0.056k_{s,cdG2}$ $k_{s,DnaA} = 0$	**SW**	92.3%	6%	1.7%	0
			ST	1%	98.4%	0	0
Signal 5b	Introducing stress response through cdG-dependent pathway. Inhibiting DnaA synthesis. Decreasing RpoD-dependent *ctrA* transcription	$\mu = 0.0018$ $k_{s,cdG1} = 0.056k_{s,cdG1}$ $k_{s,cdG2} = 0.056k_{s,cdG2}$ $k_{s,DnaA} = 0$ $RpoD_{ctrA}$=0.1	**SW**	92.3%	7.1%	0.5%	0
			ST	1%	98.4%	0	0
Signal 5c	Introducing stress response through cdG-dependent pathway. Inhibiting DnaA synthesis. Decreasing RpoD-dependent *divK* transcription	$\mu = 0.0018$ $k_{s,cdG1} = 0.056k_{s,cdG1}$ $k_{s,cdG2} = 0.056k_{s,cdG2}$ $k_{s,DnaA} = 0$ $RpoD_{divK}$=0.1	**SW**	100%	0	0	0
			ST	1.6%	96.9%	0/5%	0/5%
Signal 5d	Introducing stress response through cdG-dependent pathway. Inhibiting DnaA synthesis. Decreasing RpoD-dependent *pleD* transcription	$\mu = 0.0018$ $k_{s,cdG1} = 0.056k_{s,cdG1}$ $k_{s,cdG2} = 0.056k_{s,cdG2}$ $k_{s,DnaA} = 0$ $RpoD_{pleD}$=0.1	**SW**	97.3%	2.8%	0	0
			ST	1%	97.4%	1%	0

* Same definitions with Table 4.1.

Appendix D. Supplementary Material for Chapter 5

D1. Equations, parameters, initial conditions, and mutant lists

Table D1.1: PDEs of the spatiotemporal model (Equations of PopZ and PodJL are shown in the main text)

(1) $\frac{d[\mathrm{PodJS}]}{dt} = (k_{\mathrm{d,PodJ1}} + k_{\mathrm{d,PodJ2}} \cdot [\mathrm{PerP}]) \cdot ([\mathrm{PodJL_m}] + [\mathrm{PodJL_p}]) - (\mu + k_{\mathrm{d,PodJS}}) \cdot [\mathrm{PodJS}]$

(2) $\frac{d[\mathrm{SpmX_m}]}{dt} = k_{\mathrm{s,SpmX}} \cdot \frac{[\mathrm{CtrA{\sim}P}]^2}{[\mathrm{CtrA{\sim}P}]^2 + J_{\mathrm{a,SpmXCtrA}}^2} - (k_{\mathrm{d,SpmX}} + \mu) \cdot [\mathrm{SpmX_m}] - k_{\mathrm{dnv,SpmX}} \cdot (1 + \alpha_{\mathrm{SpmXPopZ}} \cdot \mathrm{PopZ_T}) \cdot [\mathrm{SpmX_m}]$
$-k_{\mathrm{aut,SpmX}} \cdot [\mathrm{SpmX_m}] \cdot [\mathrm{SpmX_p}]^2 + k_{\mathrm{depol,SpmX}} \cdot [\mathrm{SpmX_p}] + D_{\mathrm{SpmX_m}} \cdot \frac{\partial^2 [\mathrm{SpmX_m}]}{\partial x^2}$

(3) $\frac{d[\mathrm{SpmX_p}]}{dt} = -(k_{\mathrm{d,SpmX}} + \mu) \cdot [\mathrm{SpmX_p}] + k_{\mathrm{dnv,SpmX}} \cdot (1 + \alpha_{\mathrm{SpmXPopZ}} \cdot [\mathrm{PopZ_T}]) \cdot [\mathrm{SpmX_m}]$
$+k_{\mathrm{aut,SpmX}} \cdot [\mathrm{SpmX_m}] \cdot [\mathrm{SpmX_p}]^2 - k_{\mathrm{depol,SpmX}} \cdot [\mathrm{SpmX_p}] + D_{\mathrm{SpmX_p}} \cdot \frac{\partial^2 [\mathrm{SpmX_p}]}{\partial x^2}$

(4) $\frac{d[\mathrm{CtrA_u}]}{dt} = k_{\mathrm{s,CtrA1}} \cdot (1 - \frac{[\mathrm{CtrA{\sim}P}]}{J_{\mathrm{i,CtrACtrA}} + [\mathrm{CtrA_T}]}) \cdot ((1-\epsilon) \cdot S_{ctrA} + \epsilon) + k_{\mathrm{s,CtrA2}} \cdot \frac{[\mathrm{CtrA{\sim}P}]}{J_{\mathrm{a,CtrACtrA}} + [\mathrm{CtrA_T}]}$
$-(k_{\mathrm{d,CtrA1}} + k_{\mathrm{d,CtrA2}} \cdot \frac{[\mathrm{CpdRu_T}]}{J_{\mathrm{d,CtrA}} + [\mathrm{CpdRu_T}]} + \mu) \cdot [\mathrm{CtrA_u}] - k_{\mathrm{b,CtrAuCckAkin}} \cdot ([\mathrm{CckA_{f,kin}}] + [\mathrm{CckA_{b,kin}}]) \cdot [\mathrm{CtrA_u}]$
$+(k_{\mathrm{ub,CtrAuCckAkin}} + k_{\mathrm{d,CckA}}) \cdot ([\mathrm{CtrAu : CckA_{f,kin}}] + [\mathrm{CtrAu : CckA_{b,kin}}])$
$+k_{\mathrm{dephoCtrA}} \cdot ([\mathrm{CtrAP : CckA_{f,ph}}] + [\mathrm{CtrAP : CckA_{b,ph}}]) + D_{\mathrm{CtrA}} \cdot \frac{\partial^2 [\mathrm{CtrAu}]}{\partial x^2}$

(5) $\frac{d[\mathrm{CtrA{\sim}P}]}{dt} = -(k_{\mathrm{d,CtrA1}} + k_{\mathrm{d,CtrA2}} \cdot \frac{[\mathrm{CpdRu_T}]}{J_{\mathrm{d,CtrA}} + [\mathrm{CpdRu_T}]} + \mu) \cdot [\mathrm{CtrA \sim P}]$
$-k_{\mathrm{b,CtrAPCckAph}} \cdot ([\mathrm{CckA_{f,ph}}] + [\mathrm{CckA_{b,ph}}]) \cdot [\mathrm{CtrA \sim P}] + k_{\mathrm{phoCtrA}} \cdot ([\mathrm{CtrA_u : CckA_{f,kin}}] + [\mathrm{CtrA_u : CckA_{b,kin}}])$
$+(k_{\mathrm{ub,CtrAPCckAph}} + k_{\mathrm{d,CckA}}) \cdot ([\mathrm{CtrAP : CckA_{f,ph}}] + [\mathrm{CtrAP : CckA_{b,ph}}]) + D_{\mathrm{CtrA}} \cdot \frac{\partial^2 [\mathrm{CtrA{\sim}P}]}{\partial x^2}$

(6) $\frac{d[\mathrm{PleC_f}]}{dt} = k_{\mathrm{s,PleC}} \cdot ((1 - \epsilon_{pleC}) \cdot S_{pleC} + \epsilon_{pleC}) - (k_{\mathrm{d,PleC}} + \mu) \cdot [\mathrm{PleC_f}] - k_{\mathrm{fb,PleC}} \cdot [\mathrm{PodJ_p}] \cdot [\mathrm{PleC_f}] + k_{\mathrm{bf,PleC}} \cdot [\mathrm{PleC_b}]$
$-k_{\mathrm{b,PleCDivKP}} \cdot [\mathrm{PleC_f}] \cdot [\mathrm{DivK \sim P}] + (k_{\mathrm{ub,PleCDivKP}} + k_{\mathrm{d,DivK}} + k_{\mathrm{dephoDivK}}) \cdot [\mathrm{PleC_f : DivKP}]$
$+D_{\mathrm{PleC}} \cdot \frac{\partial^2 [\mathrm{PleC_f}]}{\partial x^2}$

(7) $\frac{d[\mathrm{PleC_b}]}{dt} = -(k_{\mathrm{d,PleC}} + \mu) \cdot [\mathrm{PleC_b}] + k_{\mathrm{fb,PleC}} \cdot [\mathrm{PodJ_p}] \cdot [\mathrm{PleC_f}] - k_{\mathrm{bf,PleC}} \cdot [\mathrm{PleC_b}]$
$-k_{\mathrm{b,PleCDivKP}} \cdot [\mathrm{PleC_b}] \cdot [\mathrm{DivK \sim P}] + (k_{\mathrm{ub,PleCDivKP}} + k_{\mathrm{d,DivK}} + k_{\mathrm{dephoDivK}}) \cdot [\mathrm{PleC_b : DivKP}]$

(8) $\frac{d[\mathrm{PleC_f{:}DivKP}]}{dt} = -(k_{\mathrm{d,PleC}} + k_{\mathrm{d,DivK}} + k_{\mathrm{ub,PleCDivKP}} + k_{\mathrm{dephoDivK}} + k_{\mathrm{ph2kin,PleC1}} + \mu) \cdot [\mathrm{PleC_f : DivKP}]$

Continued on next page

Table. D1.1 – *Continued from previous page*

$$+k_{\mathrm{b,PleCDivKP}}\cdot[\mathrm{PleC_f}]\cdot[\mathrm{DivK}\sim\mathrm{P}]-k_{\mathrm{fb,PleC}}\cdot[\mathrm{PodJ_p}]\cdot[\mathrm{PleC_f}:\mathrm{DivKP}]$$

$$+k_{\mathrm{bf,PleC}}\cdot[\mathrm{PleC_b}:\mathrm{DivKP}]+D_{\mathrm{PleCDivKP}}\cdot\frac{\partial^2[\mathrm{PleC_f}:\mathrm{DivKP}]}{\partial x^2}$$

(9) $$\frac{d[\mathrm{PleC_b}:\mathrm{DivKP}]}{dt}=-(k_{\mathrm{d,PleC}}+k_{\mathrm{d,DivK}}+k_{\mathrm{ub,PleCDivKP}}+k_{\mathrm{dephoDivK}}+k_{\mathrm{ph2kin,PleC2}}+\mu)\cdot[\mathrm{PleC_b}:\mathrm{DivKP}]$$

$$+k_{\mathrm{b,PleCDivKP}}\cdot[\mathrm{PleC_b}]\cdot[\mathrm{DivK}\sim\mathrm{P}]+k_{\mathrm{fb,PleC}}\cdot[\mathrm{PodJ_p}]\cdot[\mathrm{PleC_f}:\mathrm{DivKP}]$$

$$-k_{\mathrm{bf,PleC}}\cdot[\mathrm{PleC_b}:\mathrm{DivKP}]$$

(10) $$\frac{d[\mathrm{PleC_{f,kin}}]}{dt}=-(k_{\mathrm{d,PleC}}+\mu)\cdot[\mathrm{PleC_{f,kin}}]-k_{\mathrm{fb,PleC}}\cdot[\mathrm{PodJ_p}]\cdot[\mathrm{PleC_{f,kin}}]+k_{\mathrm{bf,PleC}}\cdot[\mathrm{PleC_{b,kin}}]$$

$$+k_{\mathrm{ph2kin,PleC1}}\cdot[\mathrm{PleC_f}:\mathrm{DivKP}]+D_{\mathrm{PleC}}\cdot\frac{\partial^2[\mathrm{PleC_{f,kin}}]}{\partial x^2}$$

(11) $$\frac{d[\mathrm{PleC_{b,kin}}]}{dt}=-(k_{\mathrm{d,PleC}}+\mu)\cdot[\mathrm{PleC_{b,kin}}]+k_{\mathrm{fb,PleC}}\cdot[\mathrm{PodJ_p}]\cdot[\mathrm{PleC_{f,kin}}]-k_{\mathrm{bf,PleC}}\cdot[\mathrm{PleC_{b,kin}}]$$

$$+k_{\mathrm{ph2kin,PleC2}}\cdot[\mathrm{PleC_b}:\mathrm{DivKP}]$$

(12) $$\frac{d[\mathrm{DivJ_f}]}{dt}=k_{\mathrm{s,DivJ}}-(k_{\mathrm{d,DivJ}}+\mu)\cdot[\mathrm{DivJ_f}]-k_{\mathrm{fb,DivJ}}\cdot[\mathrm{SpmX_p}]\cdot[\mathrm{DivJ_f}]+k_{\mathrm{bf,DivJ}}\cdot[\mathrm{DivJ_b}]$$

$$-k_{\mathrm{b,DivJDivKP}}\cdot[\mathrm{DivJ_f}]\cdot[\mathrm{DivK}\sim\mathrm{P}]+(k_{\mathrm{ub,DivJDivKP}}+k_{\mathrm{d,DivK}})\cdot[\mathrm{DivJ_f}:\mathrm{DivKP}]$$

$$-k_{\mathrm{b,DivJDivKu}}\cdot[\mathrm{DivJ_f}]\cdot[\mathrm{DivKu}]+(k_{\mathrm{ub,DivJDivKu}}+k_{\mathrm{d,DivK}})\cdot[\mathrm{DivJ_f}:\mathrm{DivKu}]+D_{\mathrm{DivJ}}\cdot\frac{\partial^2[\mathrm{DivJ_f}]}{\partial x^2}$$

(13) $$\frac{d[\mathrm{DivJ_b}]}{dt}=-(k_{\mathrm{d,DivJ}}+\mu)\cdot[\mathrm{DivJ_b}]+k_{\mathrm{fb,DivJ}}\cdot[\mathrm{SpmX_p}]\cdot[\mathrm{DivJ_f}]-k_{\mathrm{bf,DivJ}}\cdot[\mathrm{DivJ_b}]$$

$$-k_{\mathrm{b,DivJDivKP}}\cdot[\mathrm{DivJ_b}]\cdot[\mathrm{DivK}\sim\mathrm{P}]+(k_{\mathrm{ub,DivJDivKP}}+k_{\mathrm{d,DivK}})\cdot[\mathrm{DivJ_b}:\mathrm{DivKP}]$$

$$-k_{\mathrm{b,DivJDivKu}}\cdot[\mathrm{DivJ_b}]\cdot[\mathrm{DivKu}]+(k_{\mathrm{ub,DivJDivKu}}+k_{\mathrm{d,DivK}})\cdot[\mathrm{DivJ_b}:\mathrm{DivKu}]$$

(14) $$\frac{d[\mathrm{DivJ_f}:\mathrm{DivKu}]}{dt}=-(k_{\mathrm{d,DivJ}}+k_{\mathrm{d,DivK}}+k_{\mathrm{ub,DivJDivKu}}+k_{\mathrm{phoDivK,DivJ_f}}+\mu)\cdot[\mathrm{DivJ_f}:\mathrm{DivKu}]$$

$$+k_{\mathrm{b,DivJDivKu}}\cdot[\mathrm{DivJ_f}]\cdot[\mathrm{DivKu}]-k_{\mathrm{fb,DivJ}}\cdot[\mathrm{SpmX_p}]\cdot[\mathrm{DivJ_f}:\mathrm{DivKu}]+k_{\mathrm{bf,DivJ}}\cdot[\mathrm{DivJ_b}:\mathrm{DivKu}]$$

$$+D_{\mathrm{DivJDivK}}\cdot\frac{\partial^2[\mathrm{DivJ_f}:\mathrm{DivKu}]}{\partial x^2}$$

(15) $$\frac{d[\mathrm{DivJ_b}:\mathrm{DivKu}]}{dt}=-(k_{\mathrm{d,DivJ}}+k_{\mathrm{d,DivK}}+k_{\mathrm{ub,DivJDivKu}}+k_{\mathrm{phoDivK,DivJ_b}}+\mu)\cdot[\mathrm{DivJ_b}:\mathrm{DivKu}]$$

$$+k_{\mathrm{b,DivJDivKu}}\cdot[\mathrm{DivJ_b}]\cdot[\mathrm{DivKu}]+k_{\mathrm{fb,DivJ}}\cdot[\mathrm{SpmX_p}]\cdot[\mathrm{DivJ_f}:\mathrm{DivKu}]-k_{\mathrm{bf,DivJ}}\cdot[\mathrm{DivJ_b}:\mathrm{DivKu}]$$

(16) $$\frac{d[\mathrm{DivJ_f}:\mathrm{DivKP}]}{dt}=-(k_{\mathrm{d,DivJ}}+k_{\mathrm{d,DivK}}+k_{\mathrm{ub,DivJDivKP}}+\mu)\cdot[\mathrm{DivJ_f}:\mathrm{DivKP}]+k_{\mathrm{phoDivK,DivJ_f}}\cdot[\mathrm{DivJ_f}:\mathrm{DivKu}]$$

$$+k_{\mathrm{b,DivJDivKP}}\cdot[\mathrm{DivJ_f}]\cdot[\mathrm{DivK}\sim\mathrm{P}]-k_{\mathrm{fb,DivJ}}\cdot[\mathrm{SpmX_p}]\cdot[\mathrm{DivJ_f}:\mathrm{DivKP}]+k_{\mathrm{bf,DivJ}}\cdot[\mathrm{DivJ_b}:\mathrm{DivKP}]$$

$$+D_{\mathrm{DivJDivK}}\cdot\frac{\partial^2[\mathrm{DivJ_f}:\mathrm{DivKP}]}{\partial x^2}$$

(17) $$\frac{d[\mathrm{DivJ_b}:\mathrm{DivKP}]}{dt}=-(k_{\mathrm{d,DivJ}}+k_{\mathrm{d,DivK}}+k_{\mathrm{ub,DivJDivKP}}+\mu)\cdot[\mathrm{DivJ_b}:\mathrm{DivKP}]+k_{\mathrm{phoDivK,DivJ_b}}\cdot[\mathrm{DivJ_b}:\mathrm{DivKu}]$$

$$+k_{\mathrm{b,DivJDivKP}}\cdot[\mathrm{DivJ_b}]\cdot[\mathrm{DivK}\sim\mathrm{P}]+k_{\mathrm{fb,DivJ}}\cdot[\mathrm{SpmX_p}]\cdot[\mathrm{DivJ_f}:\mathrm{DivKP}]-k_{\mathrm{bf,DivJ}}\cdot[\mathrm{DivJ_b}:\mathrm{DivKP}]$$

(18) $$\frac{d[\mathrm{PerP}]}{dt}=k_{\mathrm{s,PerP}}\cdot((1-\epsilon)\cdot S_{perP}+\epsilon)\cdot\frac{[\mathrm{CtrA}\sim\mathrm{P}]^2}{J^2_{\mathrm{a,PerPCtrA}}+[\mathrm{CtrA}\sim\mathrm{P}]^2}-(k_{\mathrm{d,PerP}}+\mu)\cdot[\mathrm{PerP}]+D_{\mathrm{PerP}}\cdot\frac{\partial^2[\mathrm{PerP}]}{\partial x^2}$$

(19) $$\frac{d[\mathrm{DivKu}]}{dt}=k_{\mathrm{s,DivK1}}+k_{\mathrm{s,DivK2}}\cdot\frac{[\mathrm{CtrA}\sim\mathrm{P}]^2}{J^2_{\mathrm{a,DivKCtrA}}+[\mathrm{CtrA}\sim\mathrm{P}]^2}-(k_{\mathrm{d,DivK}}+\mu)\cdot[\mathrm{DivKu}]$$

$$-k_{\mathrm{phoDivK,PleC_{kin}}}\cdot([\mathrm{PleC_{f,kin}}]+[\mathrm{PleC_{b,kin}}])\cdot[\mathrm{DivKu}]+k_{\mathrm{dephoDivK}}\cdot([\mathrm{PleC_f}:\mathrm{DivKP}]+[\mathrm{PleC_b}:\mathrm{DivKP}])$$

$$-k_{\mathrm{b,DivJDivKu}}\cdot([\mathrm{DivJ_f}]+[\mathrm{DivJ_b}])\cdot[\mathrm{DivKu}]+(k_{\mathrm{ub,DivJDivKu}}+k_{\mathrm{d,DivJ}})\cdot([\mathrm{DivJ_f}:\mathrm{DivKu}]+[\mathrm{DivJ_b}:\mathrm{DivKu}])$$

$$+D_{\mathrm{DivK}}\cdot\frac{\partial^2[\mathrm{DivKu}]}{\partial x^2}$$

(20) $$\frac{d[\mathrm{DivK}\sim\mathrm{P}]}{dt}=-(k_{\mathrm{d,DivK}}+\mu)\cdot[\mathrm{DivK}\sim\mathrm{P}]+k_{\mathrm{phoDivK,PleC_{kin}}}\cdot([\mathrm{PleC_{f,kin}}]+[\mathrm{PleC_{b,kin}}])\cdot[\mathrm{DivKu}]$$

$$-k_{\mathrm{b,PleCDivKP}}\cdot([\mathrm{PleC_f}]+[\mathrm{PleC_b}])\cdot[\mathrm{DivK}\sim\mathrm{P}]+(k_{\mathrm{ub,PleCDivKP}}+k_{\mathrm{d,PleC}})\cdot([\mathrm{PleC_f}:\mathrm{DivKP}]+[\mathrm{PleC_b}:\mathrm{DivKP}])$$

Continued on next page

Table. D1.1 – *Continued from previous page*

$$-k_{\mathrm{b,DivJDivKP}}\cdot([\mathrm{DivJ_f}]+[\mathrm{DivJ_b}])\cdot[\mathrm{DivK}\sim\mathrm{P}]+(k_{\mathrm{ub,DivJDivKP}}+k_{\mathrm{d,DivJ}})\cdot([\mathrm{DivJ_f}:\mathrm{DivKP}]+[\mathrm{DivJ_b}:\mathrm{DivKP}])$$

$$-k_{\mathrm{b,DivLDivKP}}\cdot([\mathrm{DivL_f}]+[\mathrm{DivL_b}])\cdot[\mathrm{DivK}\sim\mathrm{P}]+(k_{\mathrm{ub,DivLDivKP}}+k_{\mathrm{d,DivL}})\cdot([\mathrm{DivL_f}:\mathrm{DivKP}]+[\mathrm{DivL_b}:\mathrm{DivKP}])$$

$$+k_{\mathrm{ph2kin,PleC1}}\cdot[\mathrm{PleC_f}:\mathrm{DivKP}]+k_{\mathrm{ph2kin,PleC2}}\cdot[\mathrm{PleC_b}:\mathrm{DivKP}]+D_{\mathrm{DivK}}\cdot\frac{\partial^2[\mathrm{DivK}\sim\mathrm{P}]}{\partial x^2}$$

(21) $$\frac{d[\mathrm{DivL_f}]}{dt}=k_{\mathrm{s,divL}}-(k_{\mathrm{d,DivL}}+\mu)\cdot[\mathrm{DivL_f}]-k_{\mathrm{fb,DivL}}\cdot(\alpha_{\mathrm{DivLPopZ}}\cdot[\mathrm{PopZ_p}]+\alpha_{\mathrm{DivLPodJ}}\cdot[\mathrm{PodJ_p}])\cdot[\mathrm{DivL_f}]$$

$$+k_{\mathrm{bf,DivJ}}\cdot[\mathrm{DivL_b}]-k_{\mathrm{b,DivLDivKP}}\cdot[\mathrm{DivL_f}]\cdot[\mathrm{DivK}\sim\mathrm{P}]+(k_{\mathrm{ub,DivLDivKP}}+k_{\mathrm{d,DivK}})\cdot[\mathrm{DivL_f}:\mathrm{DivKP}]$$

$$+D_{\mathrm{DivL}}\cdot\frac{\partial^2[\mathrm{DivL_f}]}{\partial x^2}$$

(22) $$\frac{d[\mathrm{DivL_b}]}{dt}=-(k_{\mathrm{d,DivL}}+\mu)\cdot[\mathrm{DivL_b}]+k_{\mathrm{fb,DivL}}\cdot(\alpha_{\mathrm{DivLPopZ}}\cdot[\mathrm{PopZ_p}]+\alpha_{\mathrm{DivLPodJ}}\cdot[\mathrm{PodJ_p}])\cdot[\mathrm{DivL_f}]-k_{\mathrm{bf,DivJ}}\cdot[\mathrm{DivL_b}]$$

$$-k_{\mathrm{b,DivLDivKP}}\cdot[\mathrm{DivL_b}]\cdot[\mathrm{DivK}\sim\mathrm{P}]+(k_{\mathrm{ub,DivLDivKP}}+k_{\mathrm{d,DivK}})\cdot[\mathrm{DivL_b}:\mathrm{DivKP}]$$

(23) $$\frac{d[\mathrm{DivL_f}:\mathrm{DivKP}]}{dt}=-(k_{\mathrm{d,DivL}}+k_{\mathrm{d,DivK}}+k_{\mathrm{ub,DivLDivKP}}+\mu)\cdot[\mathrm{DivL_f}:\mathrm{DivKP}]+k_{\mathrm{b,DivLDivKP}}\cdot[\mathrm{DivL_f}]\cdot[\mathrm{DivK}\sim\mathrm{P}]$$

$$-k_{\mathrm{fb,DivL}}\cdot(\alpha_{\mathrm{DivLPopZ}}\cdot[\mathrm{PopZ_p}]+\alpha_{\mathrm{DivLPodJ}}\cdot[\mathrm{PodJ_p}])\cdot[\mathrm{DivL_f}:\mathrm{DivKP}]+k_{\mathrm{bf,DivJ}}\cdot[\mathrm{DivL_b}:\mathrm{DivKP}]$$

$$+D_{\mathrm{DivLDivKP}}\cdot\frac{\partial^2[\mathrm{DivL_f}:\mathrm{DivKP}]}{\partial x^2}$$

(24) $$\frac{d[\mathrm{DivL_b}:\mathrm{DivKP}]}{dt}=-(k_{\mathrm{d,DivL}}+k_{\mathrm{d,DivK}}+k_{\mathrm{ub,DivLDivKP}}+\mu)\cdot[\mathrm{DivL_b}:\mathrm{DivKP}]+k_{\mathrm{b,DivLDivKP}}\cdot[\mathrm{DivL_b}]\cdot[\mathrm{DivK}\sim\mathrm{P}]$$

$$+k_{\mathrm{fb,DivL}}\cdot(\alpha_{\mathrm{DivLPopZ}}\cdot[\mathrm{PopZ_p}]+\alpha_{\mathrm{DivLPodJ}}\cdot[\mathrm{PodJ_p}])\cdot[\mathrm{DivL_f}:\mathrm{DivKP}]-k_{\mathrm{bf,DivJ}}\cdot[\mathrm{DivL_b}:\mathrm{DivKP}]$$

(25) $$\frac{d[\mathrm{CckA_{f,kin}}]}{dt}=k_{\mathrm{s,CckA}}-(k_{\mathrm{d,CckA}}+\mu)\cdot[\mathrm{CckA_{f,kin}}]+k_{\mathrm{bf,CckA}}\cdot[\mathrm{CckA_{b,kin}}]$$

$$-k_{\mathrm{fb,CckA}}\cdot(\alpha_{\mathrm{CckAPopZ}}\cdot[\mathrm{PopZ_p}]+\alpha_{\mathrm{CckADivL}}\cdot[\mathrm{DivL_{bT}}]\cdot\frac{\alpha_{\mathrm{DivLPodJ}}\cdot[\mathrm{PodJ_p}]}{\alpha_{\mathrm{DivLPopZ}}\cdot[\mathrm{PopZ_p}]+\alpha_{\mathrm{DivLPodJ}}\cdot[\mathrm{PodJ_p}]})\cdot[\mathrm{CckA_{f,kin}}]$$

$$+(k_{\mathrm{pk,CckA1}}+k_{\mathrm{pk,CckA2}}\cdot([\mathrm{DivL_f}]+[\mathrm{DivL_b}]))\cdot[\mathrm{CckA_{f,ph}}]$$

$$-(k_{\mathrm{kp,CckA1}}+k_{\mathrm{kp,CckA2}}\cdot([\mathrm{DivL_f}:\mathrm{DivKP}]+[\mathrm{DivL_b}:\mathrm{DivKP}]))\cdot[\mathrm{CckA_{f,kin}}]$$

$$-k_{\mathrm{b,CtrACckAkin}}\cdot[\mathrm{CckA_{f,kin}}]\cdot[\mathrm{CtrAu}]+(k_{\mathrm{d,CtrA1}}+k_{\mathrm{d,CtrA2}}\cdot\frac{[\mathrm{CpdRu_T}]}{J_{\mathrm{d,CtrA}}+[\mathrm{CpdRu_T}]}+k_{\mathrm{ub,CtrACckAkin}}+k_{\mathrm{phoCtrA}})\cdot$$

$$[\mathrm{CtrAu}:\mathrm{CckA_{f,kin}}]+D_{\mathrm{CckA}}\cdot\frac{\partial^2[\mathrm{CckA_{f,kin}}]}{\partial x^2}$$

(26) $$\frac{d[\mathrm{CckA_{b,kin}}]}{dt}=-(k_{\mathrm{d,CckA}}+\mu)\cdot[\mathrm{CckA_{b,kin}}]-k_{\mathrm{bf,CckA}}\cdot[\mathrm{CckA_{b,kin}}]$$

$$+k_{\mathrm{fb,CckA}}\cdot(\alpha_{\mathrm{CckAPopZ}}\cdot[\mathrm{PopZ_p}]+\alpha_{\mathrm{CckADivL}}\cdot[\mathrm{DivL_{bT}}]\cdot\frac{\alpha_{\mathrm{DivLPodJ}}\cdot[\mathrm{PodJ_p}]}{\alpha_{\mathrm{DivLPopZ}}\cdot[\mathrm{PopZ_p}]+\alpha_{\mathrm{DivLPodJ}}\cdot[\mathrm{PodJ_p}]})\cdot[\mathrm{CckA_{f,kin}}]$$

$$+(k_{\mathrm{pk,CckA1}}+k_{\mathrm{pk,CckA2}}\cdot([\mathrm{DivL_f}]+[\mathrm{DivL_b}]))\cdot[\mathrm{CckA_{b,ph}}]$$

$$-(k_{\mathrm{kp,CckA1}}+k_{\mathrm{kp,CckA2}}\cdot([\mathrm{DivL_f}:\mathrm{DivKP}]+[\mathrm{DivL_b}:\mathrm{DivKP}]))\cdot[\mathrm{CckA_{b,kin}}]$$

$$-k_{\mathrm{b,CtrACckAkin}}\cdot[\mathrm{CckA_{b,kin}}]\cdot[\mathrm{CtrAu}]+(k_{\mathrm{d,CtrA1}}+k_{\mathrm{d,CtrA2}}\cdot\frac{[\mathrm{CpdRu_T}]}{J_{\mathrm{d,CtrA}}+[\mathrm{CpdRu_T}]}+k_{\mathrm{ub,CtrACckAkin}}+k_{\mathrm{phoCtrA}})\cdot$$

$$[\mathrm{CtrAu}:\mathrm{CckA_{b,kin}}]$$

(27) $$\frac{d[\mathrm{CckA_{f,ph}}]}{dt}=-(k_{\mathrm{d,CckA}}+\mu)\cdot[\mathrm{CckA_{f,ph}}]+k_{\mathrm{bf,CckA}}\cdot[\mathrm{CckA_{b,ph}}]$$

$$-k_{\mathrm{fb,CckA}}\cdot(\alpha_{\mathrm{CckAPopZ}}\cdot[\mathrm{PopZ_p}]+\alpha_{\mathrm{CckADivL}}\cdot[\mathrm{DivL_{bT}}]\cdot\frac{\alpha_{\mathrm{DivLPodJ}}\cdot[\mathrm{PodJ_p}]}{\alpha_{\mathrm{DivLPopZ}}\cdot[\mathrm{PopZ_p}]+\alpha_{\mathrm{DivLPodJ}}\cdot[\mathrm{PodJ_p}]})\cdot[\mathrm{CckA_{f,ph}}]$$

$$-(k_{\mathrm{pk,CckA1}}+k_{\mathrm{pk,CckA2}}\cdot([\mathrm{DivL_f}]+[\mathrm{DivL_b}]))\cdot[\mathrm{CckA_{f,ph}}]$$

$$+(k_{\mathrm{kp,CckA1}}+k_{\mathrm{kp,CckA2}}\cdot([\mathrm{DivL_f}:\mathrm{DivKP}]+[\mathrm{DivL_b}:\mathrm{DivKP}]))\cdot[\mathrm{CckA_{f,kin}}]-k_{\mathrm{b,CtrAPCckAph}}\cdot[\mathrm{CckA_{f,ph}}]\cdot$$

$$[\mathrm{CtrA}\sim\mathrm{P}]+(k_{\mathrm{d,CtrA1}}+k_{\mathrm{d,CtrA2}}\cdot\frac{[\mathrm{CpdRu_T}]}{J_{\mathrm{d,CtrA}}+[\mathrm{CpdRu_T}]}+k_{\mathrm{ub,CtrAPCckAph}}+k_{\mathrm{dephoCtrA}})\cdot$$

$$[\mathrm{CtrAP}:\mathrm{CckA_{f,ph}}]+D_{\mathrm{CckA}}\cdot\frac{\partial^2[\mathrm{CckA_{f,ph}}]}{\partial x^2}$$

(28) $$\frac{d[\mathrm{CckA_{b,ph}}]}{dt}=-(k_{\mathrm{d,CckA}}+\mu)\cdot[\mathrm{CckA_{b,ph}}]-k_{\mathrm{bf,CckA}}\cdot[\mathrm{CckA_{b,ph}}]$$

Continued on next page

Table. D1.1 – *Continued from previous page*

$$+k_{\mathrm{fb,CckA}}\cdot(\alpha_{\mathrm{CckAPopZ}}\cdot[\mathrm{PopZ_p}]+\alpha_{\mathrm{CckADivL}}\cdot[\mathrm{DivL_{bT}}]\cdot\frac{\alpha_{\mathrm{DivLPodJ}\cdot[\mathrm{PodJ_p}]}}{\alpha_{\mathrm{DivLPopZ}\cdot[\mathrm{PopZ_p}]}+\alpha_{\mathrm{DivLPodJ}\cdot[\mathrm{PodJ_p}]}})\cdot[\mathrm{CckA_{f,ph}}]$$

$$-(k_{\mathrm{pk,CckA1}}+k_{\mathrm{pk,CckA2}}\cdot([\mathrm{DivL_f}]+[\mathrm{DivL_b}]))\cdot[\mathrm{CckA_{b,ph}}]$$

$$+(k_{\mathrm{kp,CckA1}}+k_{\mathrm{kp,CckA2}}\cdot([\mathrm{DivL_f}:\mathrm{DivKP}]+[\mathrm{DivL_b}:\mathrm{DivKP}]))\cdot[\mathrm{CckA_{b,kin}}]-k_{\mathrm{b,CtrAPCckAph}}\cdot[\mathrm{CckA_{b,ph}}]\cdot$$

$$[\mathrm{CtrA}\sim\mathrm{P}]+(k_{\mathrm{d,CtrA1}}+k_{\mathrm{d,CtrA2}}\cdot\frac{[\mathrm{CpdRu_T}]}{J_{\mathrm{d,CtrA}}+[\mathrm{CpdRu_T}]}+k_{\mathrm{ub,CtrAPCckAph}}+k_{\mathrm{dephoCtrA}})\cdot[\mathrm{CtrAP}:\mathrm{CckA_{b,ph}}]$$

(29) $$\frac{d[\mathrm{CtrAP:CckA_{f,ph}}]}{dt}=-(k_{\mathrm{d,CckA}}+k_{\mathrm{d,CtrA1}}+k_{\mathrm{d,CtrA2}}\cdot\frac{[\mathrm{CpdRu_T}]}{J_{\mathrm{d,CtrA}}+[\mathrm{CpdRu_T}]}+k_{\mathrm{ub,CtrAPCckAph}}+k_{\mathrm{dephoCtrA}}+\mu)\cdot$$

$$[\mathrm{CtrAP}:\mathrm{CckA_{f,ph}}]+k_{\mathrm{b,CtrACPckAph}}\cdot[\mathrm{CckA_{f,ph}}]\cdot[\mathrm{CtrA}\sim\mathrm{P}]+k_{\mathrm{bf,CckA}}\cdot[\mathrm{CtrAP}:\mathrm{CckA_{b,ph}}]$$

$$-k_{\mathrm{fb,CckA}}\cdot(\alpha_{\mathrm{CckAPopZ}}\cdot[\mathrm{PopZ_p}]+\alpha_{\mathrm{CckADivL}}\cdot[\mathrm{DivL_{bT}}]\cdot\frac{\alpha_{\mathrm{DivLPodJ}\cdot[\mathrm{PodJ_p}]}}{\alpha_{\mathrm{DivLPopZ}\cdot[\mathrm{PopZ_p}]}+\alpha_{\mathrm{DivLPodJ}\cdot[\mathrm{PodJ_p}]}})\cdot[\mathrm{CtrAP}:\mathrm{CckA_{f,ph}}]$$

$$+D_{\mathrm{CtrACckA}}\cdot\frac{\partial^2[\mathrm{CtrAP:CckA_{f,ph}}]}{\partial x^2}$$

(30) $$\frac{d[\mathrm{CtrAP:CckA_{b,ph}}]}{dt}=-(k_{\mathrm{d,CckA}}+k_{\mathrm{d,CtrA1}}+k_{\mathrm{d,CtrA2}}\cdot\frac{[\mathrm{CpdRu_T}]}{J_{\mathrm{d,CtrA}}+[\mathrm{CpdRu_T}]}+k_{\mathrm{ub,CtrAPCckAph}}+k_{\mathrm{dephoCtrA}}+\mu)\cdot$$

$$[\mathrm{CtrAP}:\mathrm{CckA_{b,ph}}]+k_{\mathrm{b,CtrAPCckAph}}\cdot[\mathrm{CckA_{b,ph}}]\cdot[\mathrm{CtrA}\sim\mathrm{P}]-k_{\mathrm{bf,CckA}}\cdot[\mathrm{CtrAP}:\mathrm{CckA_{b,ph}}]$$

$$+k_{\mathrm{fb,CckA}}\cdot(\alpha_{\mathrm{CckAPopZ}}\cdot[\mathrm{PopZ_p}]+\alpha_{\mathrm{CckADivL}}\cdot[\mathrm{DivL_{bT}}]\cdot\frac{\alpha_{\mathrm{DivLPodJ}\cdot[\mathrm{PodJ_p}]}}{\alpha_{\mathrm{DivLPopZ}\cdot[\mathrm{PopZ_p}]}+\alpha_{\mathrm{DivLPodJ}\cdot[\mathrm{PodJ_p}]}})\cdot[\mathrm{CtrAP}:\mathrm{CckA_{f,ph}}]$$

(31) $$\frac{d[\mathrm{CtrAu:CckA_{f,kin}}]}{dt}=-(k_{\mathrm{d,CckA}}+k_{\mathrm{d,CtrA1}}+k_{\mathrm{d,CtrA2}}\cdot\frac{[\mathrm{CpdRu_T}]}{J_{\mathrm{d,CtrA}}+[\mathrm{CpdRu_T}]}+k_{\mathrm{ub,CtrAuCckAkin}}+k_{\mathrm{phoCtrA}}+\mu)\cdot$$

$$[\mathrm{CtrAu}:\mathrm{CckA_{f,kin}}]+k_{\mathrm{b,CtrAuCckAkin}}\cdot[\mathrm{CckA_{f,kin}}]\cdot[\mathrm{CtrAu}]+k_{\mathrm{bf,CckA}}\cdot[\mathrm{CtrAu}:\mathrm{CckA_{b,kin}}]$$

$$-k_{\mathrm{fb,CckA}}\cdot(\alpha_{\mathrm{CckAPopZ}}\cdot[\mathrm{PopZ_p}]+\alpha_{\mathrm{CckADivL}}\cdot[\mathrm{DivL_{bT}}]\cdot\frac{\alpha_{\mathrm{DivLPodJ}\cdot[\mathrm{PodJ_p}]}}{\alpha_{\mathrm{DivLPopZ}\cdot[\mathrm{PopZ_p}]}+\alpha_{\mathrm{DivLPodJ}\cdot[\mathrm{PodJ_p}]}})\cdot[\mathrm{CtrAu}:\mathrm{CckA_{f,kin}}]$$

$$+D_{\mathrm{CtrACckA}}\cdot\frac{\partial^2[\mathrm{CtrAu:CckA_{f,kin}}]}{\partial x^2}$$

(32) $$\frac{d[\mathrm{CtrAu:CckA_{b,kin}}]}{dt}=-(k_{\mathrm{d,CckA}}+k_{\mathrm{d,CtrA1}}+k_{\mathrm{d,CtrA2}}\cdot\frac{[\mathrm{CpdRu_T}]}{J_{\mathrm{d,CtrA}}+[\mathrm{CpdRu_T}]}+k_{\mathrm{ub,CtrAuCckAkin}}+k_{\mathrm{phoCtrA}}+\mu)\cdot$$

$$[\mathrm{CtrAu}:\mathrm{CckA_{b,kin}}]+k_{\mathrm{b,CtrAuCckAkin}}\cdot[\mathrm{CckA_{b,kin}}]\cdot[\mathrm{CtrAu}]-k_{\mathrm{bf,CckA}}\cdot[\mathrm{CtrAu}:\mathrm{CckA_{b,kin}}]$$

$$+k_{\mathrm{fb,CckA}}\cdot(\alpha_{\mathrm{CckAPopZ}}\cdot[\mathrm{PopZ_p}]+\alpha_{\mathrm{CckADivL}}\cdot[\mathrm{DivL_{bT}}]\cdot\frac{\alpha_{\mathrm{DivLPodJ}\cdot[\mathrm{PodJ_p}]}}{\alpha_{\mathrm{DivLPopZ}\cdot[\mathrm{PopZ_p}]}+\alpha_{\mathrm{DivLPodJ}\cdot[\mathrm{PodJ_p}]}})\cdot[\mathrm{CtrAu}:\mathrm{CckA_{f,kin}}]$$

(33) $$\frac{d[\mathrm{CpdR_f}]}{dt}=k_{\mathrm{s,CpdR}}\cdot\frac{[\mathrm{CtrA}\sim\mathrm{P}]^2}{J^2_{\mathrm{a,CpdRCtrA}}+[\mathrm{CtrA}\sim\mathrm{P}]^2}-(k_{\mathrm{d,CpdR}}+\mu)\cdot[\mathrm{CpdR_f}]-k_{\mathrm{fb,CpdR}}\cdot[\mathrm{PopZ_p}]\cdot[\mathrm{CpdR_f}]+k_{\mathrm{bf,CpdR}}\cdot[\mathrm{CpdR_b}]$$

$$-k_{\mathrm{phoCpdR}}\cdot([\mathrm{CckA_{f,kin}}]+[\mathrm{CckA_{b,kin}}])\cdot[\mathrm{CpdR_f}]+k_{\mathrm{dephoCpdR}}\cdot([\mathrm{CckA_{f,ph}}]+[\mathrm{CckA_{b,ph}}])\cdot[\mathrm{CpdR}\sim\mathrm{P}]$$

$$+D_{\mathrm{CpdR}}\cdot\frac{\partial^2[\mathrm{CpdR_f}]}{\partial x^2}$$

(34) $$\frac{d[\mathrm{CpdR_b}]}{dt}=-(k_{\mathrm{d,CpdR}}+\mu)\cdot[\mathrm{CpdR_b}]+k_{\mathrm{fb,CpdR}}\cdot[\mathrm{PopZ_p}]\cdot[\mathrm{CpdR_f}]-k_{\mathrm{bf,CpdR}}\cdot[\mathrm{CpdR_b}]$$

(35) $$\frac{d[\mathrm{CpdR}\sim\mathrm{P}]}{dt}=-(k_{\mathrm{d,CpdR}}+\mu)\cdot[\mathrm{CpdR}\sim\mathrm{P}]+k_{\mathrm{phoCpdR}}\cdot([\mathrm{CckA_{f,kin}}]+[\mathrm{CckA_{b,kin}}])\cdot[\mathrm{CpdR_f}]$$

$$-k_{\mathrm{dephoCpdR}}\cdot([\mathrm{CckA_{f,ph}}]+[\mathrm{CckA_{b,ph}}])\cdot[\mathrm{CpdR}\sim\mathrm{P}]+D_{\mathrm{CpdR}}\cdot\frac{\partial^2[\mathrm{CpdR}\sim\mathrm{P}]}{\partial x^2}$$

Table D1.2: Parameters of the ten-compartment simulation*.

parameter	source	parameter	source
$k_{\mathrm{s,PopZ}}$=0.24	this study, [21]	$k_{\mathrm{d,PopZ}}$=0.05	[21]
$k_{\mathrm{depol,PopZ}}=0.15$	this study	$k_{\mathrm{aut,PopZ}}=15$(pole)	this study, [21]
$k_{\mathrm{dnv,PopZ}}=2.5$	this study, [21]	$\alpha_{\mathrm{PopZPodJ}}=100$	this study
$D_{\mathrm{PopZ_m}}=835$	[212]	$D_{\mathrm{PopZ_p}}=0.0005$	[21], this study
$k_{\mathrm{s,PodJ}}=0.01$	this study	ϵ=0.1	[19]

Continued on next page

Table D1.2 – *Continued from previous page*

$k_{s,PodJ2} = 0.0154$	GA	$J_{i,PodJCtrA} = 1.7634$	GA
$k_{d,PodJ1} = 0.007$	[181]	$k_{d,PodJ2} = 0.05$	[181]
μ=0.0053	[171]	$k_{depol,PodJ} = 0.2$	this study
$k_{aut,PodJ} = 90$(pole)	this study, [21]	$k_{dnv,PodJ} = 2$	this study, [21]
$\alpha_{PodJSpmX} = 30$	this study	$D_{PodJ_m} = 100$	[7]
$D_{PodJ_p} = 0.0005$	[21], this study	$k_{deg,PodJS}$=0.05	[?]
$k_{s,SpmX} = 0.0123$	GA	$J_{a,SpmXCtrA} = 0.082$	GA
$k_{d,SpmX} = 0.01$	this study	$k_{dnv,SpmX}$ =1E-3	this study
$\alpha_{SpmXPopZ} = 50$	this study	$k_{aut,SpmX} = 0.1$	this study
$k_{depol,SpmX}$ =4E-4	this study	$D_{SpmX_m} = 200$	[174]
$D_{SpmX_p} = 0.0005$	[21], this study	$k_{s,CtrA1} = 0.5444$	GA
$k_{s,CtrA2} = 1.9193$	GA	$J_{a,CtrACtrA} = 5.8361$	GA
$J_{i,CtrACtrA} = 1$	this study	$k_{d,CtrA1} = 0.0038$	[116]
$k_{d,CtrA2} = 0.1306$	GA	$J_{d,CtrA} = 0.024$	GA
$k_{b,CtrAuCckAkin} = 3$	this study	$k_{ub,CtrAuCckAkin} = 0.6563$	GA
$k_{d,CckA} = 0.2$	this study	$k_{depho,CtrA} = 140$	[19, 151], this study
$D_{CtrA} = 427$	[213]	$k_{b,CtrAPCckAph} = 3$	this study
$k_{ub,CtrAPCckAph} = 1.0807$	GA	$k_{s,PleC} = 0.0219$	GA
$\epsilon_{pleC} = 0.15$	this study	$k_{d,PleC} = 0.02$	this study
$k_{fb,PleC} = 572.1086$	GA	$k_{bf,PleC} = 0.1$	this study
$k_{b,PleCDivKP} = 4.9589$	GA	$k_{ub,PleCDivKP} = 1.2$	this study
$k_{d,DivK} = 0.014$	this study	$k_{dephoDivK} = 165.7573$	GA
$D_{PleC} = 71$	[213]	$k_{ph2kin,PleC1} = 1.5149$	GA
$D_{PleCDivKP} = 63$	[213]	$k_{ph2kin,PleC2} = 0.1515$	this study
$k_{s,DivJ} = 0.008$	this study	$k_{d,DivJ} = 0.035$	[22]
$k_{fb,DivJ} = 20$	this study	$k_{bf,DivJ} = 0.5$	this study
$k_{b,DivJDivKP} = 1$	this study	$k_{ub,DivJDivKP} = 1.3254$	GA
$k_{b,DivJDivKu} = 1$	this study	$k_{ub,DivJDivKu} = 1.0009$	GA
$D_{DivJ} = 108$	[213]	$k_{phoDivK,DivJf} = 0.18.7$	GA
$D_{DivJDivK} = 84.5$	[213]	$k_{phoDivK,DivJb} = 176.0863$	GA
$k_{s,PerP} = 1.2112$	GA	$J_{a,PerPCtrA} = 2.5841$	GA
$k_{d,PerP} = 0.04$	[22]	$D_{PerP} = 853$	[213]
$k_{s,DivK1} = 0.001$	this study	$k_{s,DivK2} = 0.4682$	GA
$J_{a,DivKCtrA} = 2.2878$	GA	$k_{phoDivK,PleC_{kin}} = 0.2086$	GA
$D_{DivJDivK} = 1319$	[213]	$k_{b,DivLDivKP} = 89.7649$	GA
$k_{ub,DivLDivKP} = 1.1$	this study	$k_{d,DivL} = 5.5412$	GA
$k_{s,DivL} = 0.0846$	GA	$k_{fb,DivL} = 1$	this study
$k_{bf,DivL} = 1$	this study	$\alpha_{DivLPopZ} = 0.0039$	GA
$\alpha_{DivLPodJ} = 9.5636$	GA	$D_{DivL} = 76.6$	[213]
$D_{DivLDivK} = 66.4$	[213]	$k_{s,CckA} = 0.1714$	GA

Continued on next page

Table D1.2 – *Continued from previous page*

$k_{\mathrm{d,CckA}} = 0.2$	this study	$k_{\mathrm{fb,CckA}} = 1$	this study
$k_{\mathrm{bf,CckA}} = 0.5$	this study	$\alpha_{\mathrm{CckAPopZ}} = 0.0034$	GA
$\alpha_{\mathrm{CckADivL}} = 213.2857$	GA	$k_{\mathrm{pk,CckA1}} = 2.0784$	GA
$k_{\mathrm{pk,CckA2}} = 644.8741$	GA	$k_{\mathrm{kp,CckA1}} = 0$	this study
$k_{\mathrm{kp,CckA2}} = 563.2248$	this study	$D_{\mathrm{CckA}} = 87.3$	[213]
$D_{\mathrm{CtrACckA}} = 65$	[213]	$k_{\mathrm{s,CpdR}} = 2.3443$	GA
$j_{\mathrm{a,CpdRCtrA}} = 0.0596$	GA	$k_{\mathrm{d,CpdR}} = 0.4298$	GA
$k_{\mathrm{fb,CpdR}} = 0.0785$	GA	$k_{\mathrm{bf,CpdR}} = 12$	this study
$k_{\mathrm{phoCpdR}} = 3.1971$	GA	$k_{\mathrm{dephoCpdR}} = 4$	this study
$D_{\mathrm{CtrACckA}} = 1638.6$	[143]	Θ=0.517	GA

*Units: all protein 'concentrations' in this model are dimensionless; all diffusion coefficients have units $\mu m^2 min^{-1}$; all α's are dimensionless; all other parameters are rate constants with units min^{-1}.

'GA' indicates the parameter is estimated by genetic algorithm; 'this study' denotes the parameter is tuned manually; 'this study' with specific reference indicates the parameter is first obtained from publications and tuned slightly.

Table D1.3: Mutant Simulations

mutant	setting	mutant	setting
$\Delta podJ$	$k_{\mathrm{s,PodJ}} = 0$, $k_{\mathrm{s,PodJ2}} = 0$	$\Delta popZ$	$k_{\mathrm{s,PopZ}} = 0$
$\Delta spmX$	$k_{\mathrm{s,SpmX}} = 0$	$\Delta divJ$	$k_{\mathrm{s,divJ}} = 0$
DivJ-H336A	$k_{\mathrm{phoDivK,DivJ_f}} = 0$, $k_{\mathrm{phoDivK,DivJ_b}} = 0$	$\Delta pleC$	$k_{\mathrm{s,PleC}} = 0$
PleC-F778L	$k_{\mathrm{phoDivK,PleC_{kin}}} = 0$	delocalized PleC	$k_{\mathrm{fb,PleC}} = 0$
PleC-H610A	$k_{\mathrm{dephoDivK}} = 0, k_{\mathrm{phoDivK,PleC_{kin}}} = 0$	delocalized DivL	$\alpha_{\mathrm{DivLPodJ}} = 0$

D2. Statements of detailed mechanisms and diagram.

DivJ/PleC-DivK module

DivJ is a principal kinase of DivK while PleC mainly works as a phosphatase to dephosphorylate DivK∼P [149]. DivJ and PleC are binding partners of SpmX and PodJ, respectively, while SpmX activates the kinase activity of DivJ [18]. In this study, we introduce X_f and X_b to indicate free protein and protein bound to anchor(s). For example, $DivJ_b$ represents DivJ bound to SpmX, where SpmX is the anchor of DivJ (Fig. 5.2). Because bound DivJ is a more active kinase than free DivJ, we set $k_{\text{phoDivK,DivJ}_b}$ is significantly larger than $k_{\text{phoDivK,DivJ}_f}$ (Table. D1.1).

In addition to phosphatase, PleC can function as a kinase with specific conformation, while the kinase activity of PleC is stimulated by DivK∼P [154]. Therefore, we include the transition from PleC phosphatase ($PleC_f$:DivK∼P and $PleC_b$:DivK∼P) to kinase ($PleC_{f,kin}$ and $PleC_{b,kin}$) (Fig. D2.1). We describe the detailed reactions among DivJ, PleC and DivK in the green box of Fig. D2.1.

DivL-CckA-CtrA/CpdR module

In addition to binding with DivJ and PleC, the spatial distribution of DivK is regulated by binding to DivL [182, 183]. DivL is a binding partner of PopZ [159] and indirectly anchored to PodJ [135, 184]. Here, we introduce α_{DivLPodJ} and α_{DivLPopZ} to describe the recruitment of DivL by PodJ and PopZ, respectively (Table. D1.1, Fig. D2.1). In summary, the spatial regulatory network indicates the scaffolding protein PodJ impacts DivK distribution through PleC-dependent and DivL-dependent pathways.

DivL, the connector between the two phosphotransfer modules, has been reported to directly control the kinase and phosphatase switch of CckA by varying conformations [158]. The binding between DivL and DivK∼P inhibits the kinase activity of CckA [132, 182]. Here, we construct a simplified model for the kinase-phosphatase switch of CckA: the complex DivL:DivK∼P promotes the conversion of CckA from kinase into phosphatase state, while DivL without binding to DivK∼P stimulates the kinase activity of CckA (Yellow module in Fig. 5.2, Table. D1.1, Fig. D2.1). DivL is also suggested to regulate the localization of CckA [130, 214, 132, 158], while CckA is a binding partner of PopZ [159]. To simplify the modelling of CckA, we assume CckA has two types of binding sites: a localization site that binds to DivL or PopZ to decide the location of CckA, and a catalytic regulatory site that binds to DivL or DivL:DivK∼P complex to decide the conformation and activity of CckA. The two sites are assumed to be independent (Fig. D2.1).

Moreover, CpdR is a binding partner of the scaffolding protein PopZ. We introduce $CpdR_f$ and $CpdR_b$ to indicate the recruitment by PopZ. To simplify the model, we assume unphos-

phorylated CpdR binds to PopZ, while phosphorylation only takes place in the free form of CpdR.

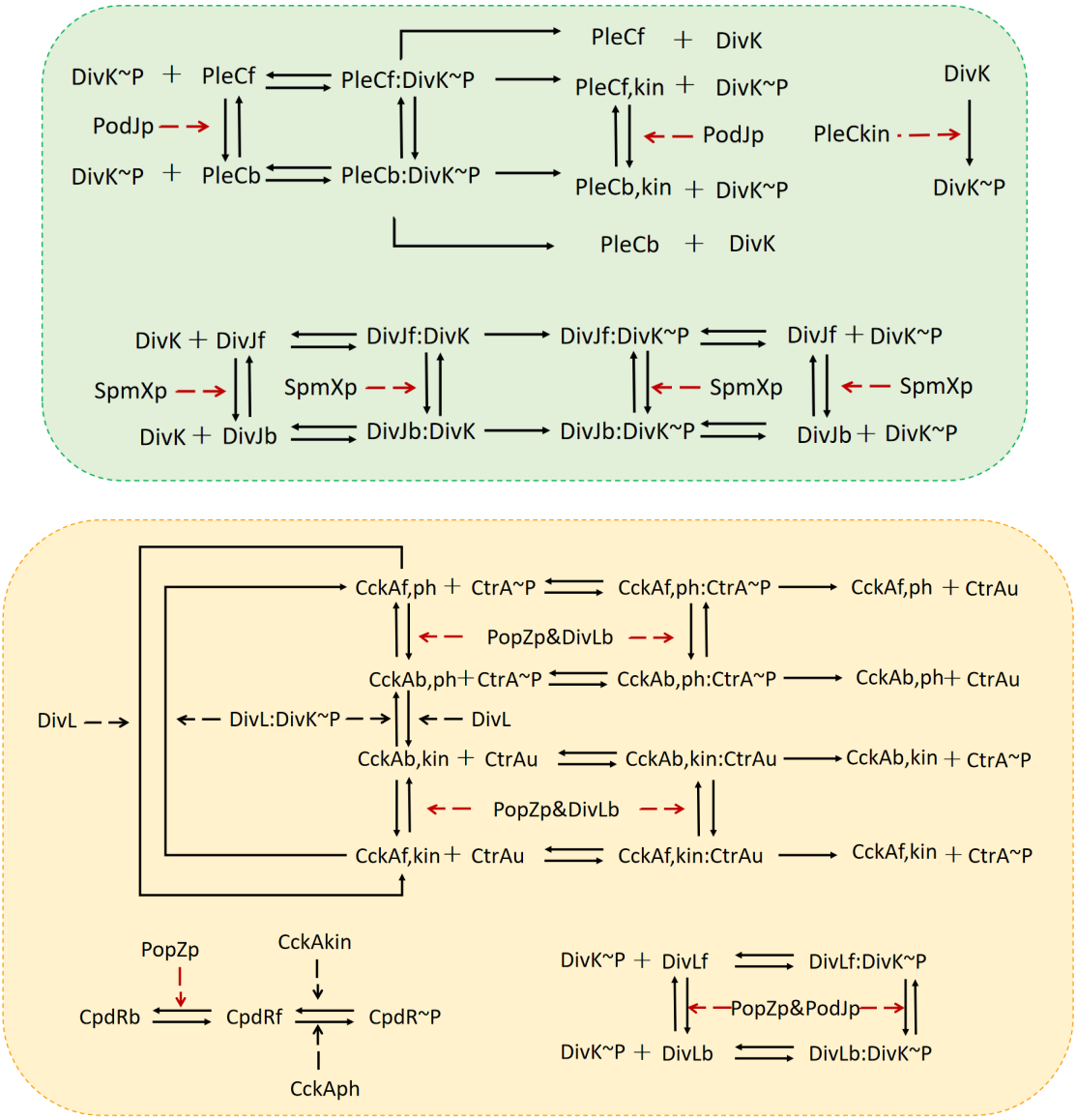

Figure D2.1: **Details of reactions involved in the DivJ/PleC-DivK and DivL-CckA-CtrA modules.**
Red dashed lines with arrows are recruitments by indicated scaffolding proteins.

D3. The four-compartment model.

In the four-compartment model, the total cell length (L) is divided into four compartments, with two poles of length $0.2L$ each and two central compartments of length $0.3L$ each. Diffusion across the boundary between neighbouring compartments causes compensatory changes in the concentrations of the diffusing species within each compartment. Hence, we describe the reaction and diffusion of protein S in a four-compartment model by a set of four ODEs for $C_i(t)$, the concentration of S in compartment i at time t [93]:

$$\begin{cases} \frac{dC_1}{dt} = \mathrm{CR} + \frac{4D(C_2-C_1)}{(l_1+l_2)^2} \\ \frac{dC_i}{dt} = \mathrm{CR} + \frac{4D(C_{i+1}-C_i)}{(l_{i+1}+l_i)^2} + \frac{4D(C_{i-1}-C_i)}{(l_{i-1}+l_i)^2},\ i = 2,3 \\ \frac{dC_4}{dt} = \mathrm{CR} + \frac{4D(C_3-C_4)}{(l_3+l_4)^2} \end{cases} \tag{D3.1}$$

where l_i indicates the length of compartment i.

D4. Supplementary results of spatial model.

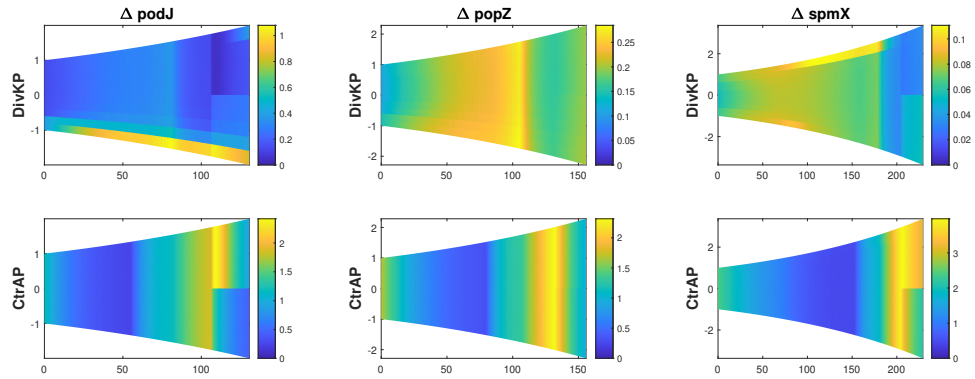

Figure D4.1: **DivK∼P and CtrA∼P dynamics in the simulation of Δ*podJ*, Δ*popZ*, and Δ*spmX*.**

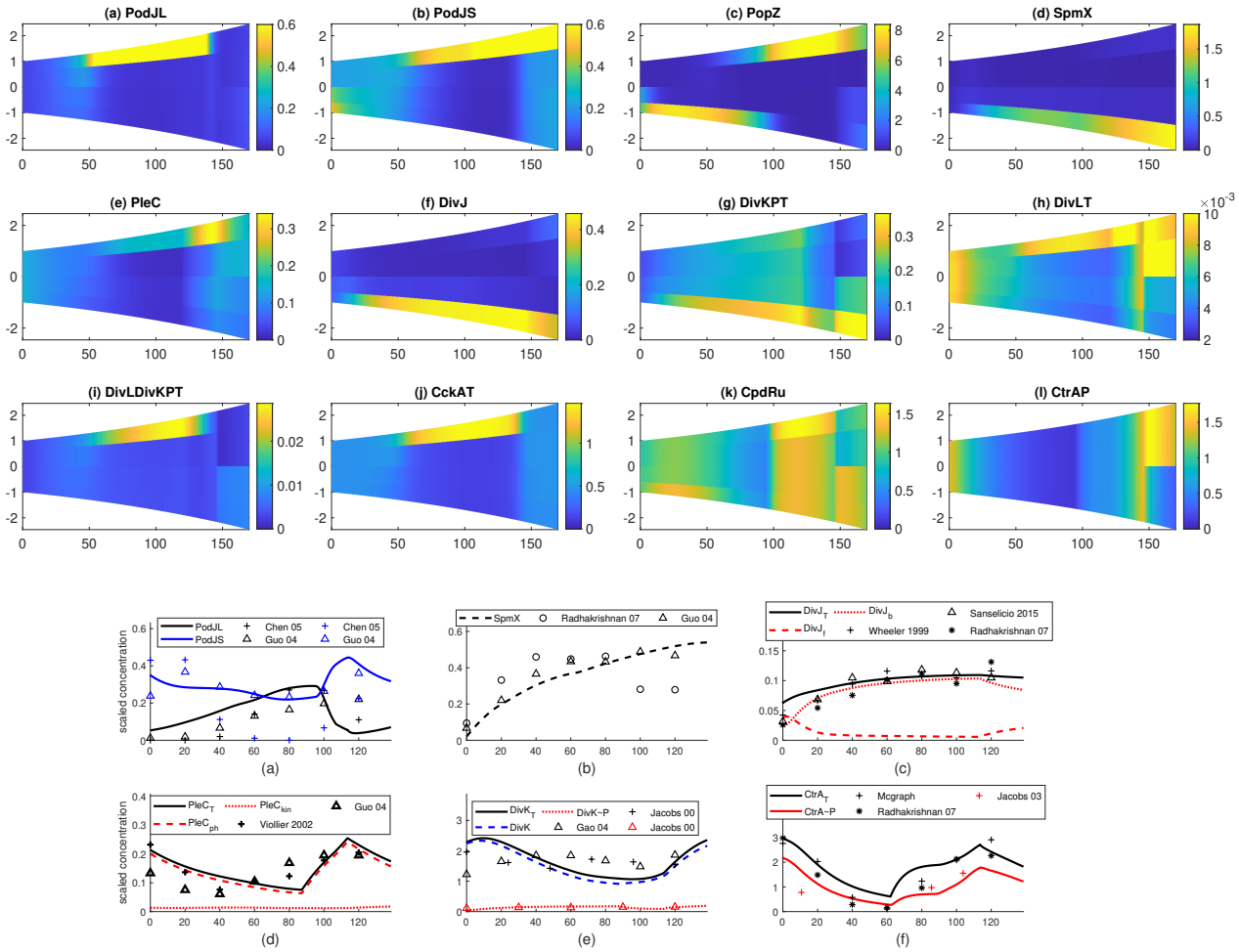

Figure D4.2: **WT simulation of the four-compartment model.**
The upper (a)-(l) spatial figures indicate the spatial dynamics over one replication cell cycle of long form PodJ, short form PodJ, PopZ, SpmX, PleC, DivJ, phosphorylated free DivK, free DivL, DivL:DivKP complex, CckA, unphosphorylated CpdR, and phosphorylated CtrA. The lower (a)-(f) indicate the temporal dynamics over one replication cell cycle. Other details are identical to Figure 5.6.

Bibliography

[1] Rodrigo Reyes-Lamothe and David J Sherratt. The bacterial cell cycle, chromosome inheritance and cell growth. *Nature Reviews Microbiology*, 17(8):467–478, 2019.

[2] Kristina Jonas. To divide or not to divide: control of the bacterial cell cycle by environmental cues. *Current Opinion in Microbiology*, 18:54–60, 2014.

[3] Harley H McAdams and Lucy Shapiro. A bacterial cell-cycle regulatory network operating in time and space. *Science*, 301(5641):1874–1877, 2003.

[4] Xiling Shen, Justine Collier, David Dill, Lucy Shapiro, Mark Horowitz, and Harley H McAdams. Architecture and inherent robustness of a bacterial cell-cycle control system. *Proceedings of the National Academy of Sciences*, 105(32):11340–11345, 2008.

[5] Xiaoyun Guo. *A bacterial scaffolding protein keeps the cell cycle and differentiation in check by regulating histidine kinase activity.* PhD thesis, Indiana University, 2014.

[6] Séverin Ronneau, Kenny Petit, Xavier De Bolle, and Régis Hallez. Phosphotransferase-dependent accumulation of (p) ppgpp in response to glutamine deprivation in caulobacter crescentus. *Nature Communications*, 7(1):1–12, 2016.

[7] Wei Zhao, Samuel W Duvall, Kimberly A Kowallis, Dylan T Tomares, Haley N Petitjean, and W Seth Childers. A circuit of protein-protein regulatory interactions enables polarity establishment in a bacterium. *BioRxiv*, page 503250, 2018.

[8] Jeanne Stove Poindexter. The caulobacters: ubiquitous unusual bacteria. *Microbiological Reviews*, 45(1):123–179, 1981.

[9] Roland C Wilhelm. Following the terrestrial tracks of caulobacter-redefining the ecology of a reputed aquatic oligotroph. *The ISME Journal*, 12(12):3025–3037, 2018.

[10] Jared M Schrader and Lucy Shapiro. Synchronization of caulobacter crescentus for investigation of the bacterial cell cycle. *JoVE (Journal of Visualized Experiments)*, (98):e52633, 2015.

[11] Peter H Tsang, Guanglai Li, Yves V Brun, L Ben Freund, and Jay X Tang. Adhesion of single bacterial cells in the micronewton range. *Proceedings of the National Academy of Sciences*, 103(15):5764–5768, 2006.

[12] Jigar Patel, Qiong Zhang, R Michael L McKay, Robert Vincent, and Zhaohui Xu. Genetic engineering of caulobacter crescentus for removal of cadmium from water. *Applied Biochemistry and Biotechnology*, 160(1):232–243, 2010.

[13] James R. Aretakis, Alisa Gega, and Jared M. Schrader. Absolute measurements of mrna translation in *Caulobacter crescentus* reveal important fitness costs of vitamin b12 scavenging. *mSystems*, 4(4):e00170–19, 2019.

[14] Robert T Wheeler and Lucy Shapiro. Differential localization of two histidine kinases controlling bacterial cell differentiation. *Molecular Cell*, 4(5):683–694, 1999.

[15] Nora Ausmees and Christine Jacobs-Wagner. Spatial and temporal control of differentiation and cell cycle progression in caulobacter crescentus. *Annual Reviews in Microbiology*, 57(1):225–247, 2003.

[16] Santo Motta and Francesco Pappalardo. Mathematical modeling of biological systems. *Briefings in Bioinformatics*, 14(4):411–422, 2013.

[17] Matteo Osella, Sander J Tans, and Marco Cosentino Lagomarsino. Step by step, cell by cell: quantification of the bacterial cell cycle. *Trends in Microbiology*, 25(4):250–256, 2017.

[18] Sunish Kumar Radhakrishnan, Martin Thanbichler, and Patrick H Viollier. The dynamic interplay between a cell fate determinant and a lysozyme homolog drives the asymmetric division cycle of caulobacter crescentus. *Genes & Development*, 22(2):212–225, 2008.

[19] Seán M Murray, Gaël Panis, Coralie Fumeaux, Patrick H Viollier, and Martin Howard. Computational and genetic reduction of a cell cycle to its simplest, primordial components. *PLoS Biology*, 11(12):e1001749, 2013.

[20] Shenghua Li, Paul Brazhnik, Bruno Sobral, and John J Tyson. A quantitative study of the division cycle of caulobacter crescentus stalked cells. *PLoS Computational Biology*, 4(1):e9, 2008.

[21] Kartik Subramanian. *Spatiotemporal model of the asymmetric division cycle of Caulobacter crescentus*. PhD thesis, Virginia Polytechnic Institute and State University, 2014.

[22] Bronson R Weston, John J Tyson, and Yang Cao. Computational modeling of unphosphorylated ctra: Cori binding in the caulobacter cell cycle. *iScience*, 24(12):103413, 2021.

[23] Ismael Sánchez-Osorio, Carlos A Hernández-Martínez, and Agustino Martínez-Antonio. Modeling asymmetric cell division in caulobacter crescentus using a boolean logic approach. In *Asymmetric Cell Division in Development, Differentiation and Cancer*, pages 1–21. Springer, 2017.

[24] Urs Jenal. The role of proteolysis in the caulobacter crescentus cell cycle and development. *Research in Microbiology*, 160(9):687–695, 2009.

[25] Michael T Laub, Swaine L Chen, Lucy Shapiro, and Harley H McAdams. Genes directly controlled by ctra, a master regulator of the caulobacter cell cycle. *Proceedings of the National Academy of Sciences*, 99(7):4632–4637, 2002.

[26] Kathleen R Ryan, Ellen M Judd, and Lucy Shapiro. The ctra response regulator essential for caulobacter crescentus cell-cycle progression requires a bipartite degradation signal for temporally controlled proteolysis. *Journal of Molecular Biology*, 324(3):443–455, 2002.

[27] Stephen C Smith, Kamal K Joshi, Justin J Zik, Katherine Trinh, Aron Kamajaya, Peter Chien, and Kathleen R Ryan. Cell cycle-dependent adaptor complex for clpxp-mediated proteolysis directly integrates phosphorylation and second messenger signals. *Proceedings of the National Academy of Sciences*, 111(39):14229–14234, 2014.

[28] Christian Lori, Shogo Ozaki, Samuel Steiner, Raphael Böhm, Sören Abel, Badri N Dubey, Tilman Schirmer, Sebastian Hiller, and Urs Jenal. Cyclic di-gmp acts as a cell cycle oscillator to drive chromosome replication. *Nature*, 523(7559):236–239, 2015.

[29] Kamal Kishore Joshi, Matthieu Bergé, Sunish Kumar Radhakrishnan, Patrick Henri Viollier, and Peter Chien. An adaptor hierarchy regulates proteolysis during a bacterial cell cycle. *Cell*, 163(2):419–431, 2015.

[30] Y Erin Chen, Christos G Tsokos, Emanuele G Biondi, Barrett S Perchuk, and Michael T Laub. Dynamics of two phosphorelays controlling cell cycle progression in caulobacter crescentus. *Journal of Bacteriology*, 191(24):7417–7429, 2009.

[31] Regis Hallez, Marie Delaby, Stefano Sanselicio, and Patrick H Viollier. Hit the right spots: cell cycle control by phosphorylated guanosines in alphaproteobacteria. *Nature Reviews Microbiology*, 15(3):137–148, 2017.

[32] Dimpy Kalia, Gökçe Merey, Shizuka Nakayama, Yue Zheng, Jie Zhou, Yiling Luo, Min Guo, Benjamin T Roembke, and Herman O Sintim. Nucleotide, c-di-gmp, c-di-amp, cgmp, camp,(p) ppgpp signaling in bacteria and implications in pathogenesis. *Chemical Society Reviews*, 42(1):305–341, 2013.

[33] Urs Jenal and Jacob Malone. Mechanisms of cyclic-di-gmp signaling in bacteria. *Annu. Rev. Genet.*, 40:385–407, 2006.

[34] Tilman Schirmer and Urs Jenal. Structural and mechanistic determinants of c-di-gmp signalling. *Nature Reviews Microbiology*, 7(10):724–735, 2009.

[35] Matthias Christen, Beat Christen, Marc Folcher, Alexandra Schauerte, and Urs Jenal. Identification and characterization of a cyclic di-gmp-specific phosphodiesterase and its allosteric control by gtp. *Journal of Biological Chemistry*, 280(35):30829–30837, 2005.

[36] Rebecca M Corrigan, Lauren E Bellows, Alison Wood, and Angelika Gründling. ppgpp negatively impacts ribosome assembly affecting growth and antimicrobial tolerance in gram-positive bacteria. *Proceedings of the National Academy of Sciences*, 113(12):E1710–E1719, 2016.

[37] Junutula R Jagath, Marina V Rodnina, and Wolfgang Wintermeyer. Conformational changes in the bacterial srp receptor ftsy upon binding of guanine nucleotides and srp. *Journal of Molecular Biology*, 295(4):745–753, 2000.

[38] Manoja Ratnayake-Lecamwasam, Pascale Serror, Ka-Wing Wong, and Abraham L Sonenshein. Bacillus subtilis cody represses early-stationary-phase genes by sensing gtp levels. *Genes & Development*, 15(9):1093–1103, 2001.

[39] Vasili Hauryliuk, Gemma C Atkinson, Katsuhiko S Murakami, Tanel Tenson, and Kenn Gerdes. Recent functional insights into the role of (p) ppgpp in bacterial physiology. *Nature Reviews Microbiology*, 13(5):298–309, 2015.

[40] Cara C Boutte and Sean Crosson. The complex logic of stringent response regulation in caulobacter crescentus: starvation signalling in an oligotrophic environment. *Molecular Microbiology*, 80(3):695–714, 2011.

[41] Allison Kriel, Alycia N Bittner, Sok Ho Kim, Kuanqing Liu, Ashley K Tehranchi, Winnie Y Zou, Samantha Rendon, Rui Chen, Benjamin P Tu, and Jue D Wang. Direct regulation of gtp homeostasis by (p) ppgpp: a critical component of viability and stress resistance. *Molecular Cell*, 48(2):231–241, 2012.

[42] Brent W Anderson, Kuanqing Liu, Christine Wolak, Katarzyna Dubiel, Fukang She, Kenneth A Satyshur, James L Keck, and Jue D Wang. Evolution of (p) ppgpp-hprt regulation through diversification of an allosteric oligomeric interaction. *eLife*, 8:e47534, 2019.

[43] Katharina Pflüger-Grau, Max Chavarría, and Víctor de Lorenzo. The interplay of the eiiantr component of the nitrogen-related phosphotransferase system (ptsntr) of pseudomonas putida with pyruvate dehydrogenase. *Biochimica et Biophysica Acta (BBA)-General Subjects*, 1810(10):995–1005, 2011.

[44] Tanis Hogg, Undine Mechold, Horst Malke, Mike Cashel, and Rolf Hilgenfeld. Conformational antagonism between opposing active sites in a bifunctional rela/spot homolog modulates (p) ppgpp metabolism during the stringent response. *Cell*, 117(1):57–68, 2004.

[45] Moises Santillán. On the use of the hill functions in mathematical models of gene regulatory networks. *Mathematical Modelling of Natural Phenomena*, 3(2):85–97, 2008.

[46] Tatiana A Karelina, Hongwu Ma, Igor Goryanin, and Oleg V Demin. Ei of the phosphotransferase system of escherichia coli: mathematical modeling approach to analysis of its kinetic properties. *Journal of Biophysics*, 2011, 2011.

[47] N Weigel, MA Kukuruzinska, A Nakazawa, EB Waygood, and S Roseman. Sugar transport by the bacterial phosphotransferase system. phosphoryl transfer reactions catalyzed by enzyme i of salmonella typhimurium. *Journal of Biological Chemistry*, 257(23):14477–14491, 1982.

[48] Katharina Pfluger and Victor de Lorenzo. Evidence of in vivo cross talk between the nitrogen-related and fructose-related branches of the carbohydrate phosphotransferase system of pseudomonas putida. *Journal of Bacteriology*, 190(9):3374–3380, 2008.

[49] BERT Ely, AB Amarasinghe, and Robert A Bender. Ammonia assimilation and glutamate formation in caulobacter crescentus. *Journal of Bacteriology*, 133(1):225–230, 1978.

[50] Himatkumar V Patel, Kavita A Vyas, Roshan L Mattoo, Maurice Southworth, Francine B Perler, Donald Comb, and Saul Roseman. Properties of the c-terminal domain of enzyme i of the escherichia coli phosphotransferase system. *Journal of Biological Chemistry*, 281(26):17579–17587, 2006.

[51] Laetitia Houot, Sarah Chang, Bradley S Pickering, Cedric Absalon, and Paula I Watnick. The phosphoenolpyruvate phosphotransferase system regulates vibrio cholerae biofilm formation through multiple independent pathways. *Journal of bacteriology*, 192(12):3055–3067, 2010.

[52] Yue Zhen Li, Dan Wang, Xue Ying Feng, Jian Jiao, Wen Xin Chen, and Chang Fu Tian. Genetic analysis reveals the essential role of nitrogen phosphotransferase system components in sinorhizobium fredii ccbau 45436 symbioses with soybean and pigeonpea plants. *Applied and Environmental Microbiology*, 82(4):1305–1315, 2016.

[53] J Wang, Ernst Dieter Gilles, Joseph W Lengeler, and Knut Jahreis. Modeling of inducer exclusion and catabolite repression based on a pts-dependent sucrose and non-pts-dependent glycerol transport systems in escherichia coli k-12 and its experimental verification. *Journal of Biotechnology*, 92(2):133–158, 2001.

[54] Pieter W Postma, Joseph W Lengeler, and GR372926 Jacobson. Phosphoenolpyruvate: carbohydrate phosphotransferase systems of bacteria. *Microbiological Reviews*, 57(3):543–594, 1993.

[55] Roshan L Mattoo and E Bruce Waygood. Determination of the levels of hpr and enzyme i of the phosphoenolpyruvate–sugar phosphotransferase system in escherichia coli and salmonella typhimurium. *Canadian Journal of Biochemistry and Cell Biology*, 61(1):29–37, 1983.

[56] BJ Scholte, AR Schuitema, and PW Postma. Isolation of iiiglc of the phosphoenolpyruvate-dependent glucose phosphotransferase system of salmonella typhimurium. *Journal of Bacteriology*, 148(1):257–264, 1981.

[57] Sören Abel, Tabitha Bucher, Micaël Nicollier, Isabelle Hug, Volkhard Kaever, Pia Abel zur Wiesch, and Urs Jenal. Bi-modal distribution of the second messenger c-di-gmp controls cell fate and asymmetry during the caulobacter cell cycle. *PLoS Genetics*, 9(9):e1003744, 2013.

[58] Camille Benoist, Cyprien Guérin, Philippe Noirot, and Etienne Dervyn. Constitutive stringent response restores viability of bacillus subtilis lacking structural maintenance of chromosome protein. *PloS One*, 10(11):e0142308, 2015.

[59] Cara C Boutte, Jonathan T Henry, and Sean Crosson. ppgpp and polyphosphate modulate cell cycle progression in caulobacter crescentus. *Journal of Bacteriology*, 194(1):28–35, 2012.

[60] Tatyana L Povolotsky and Regine Hengge. 'life-style'control networks in escherichia coli: signaling by the second messenger c-di-gmp. *Journal of Biotechnology*, 160(1-2):10–16, 2012.

[61] Sören Abel, Peter Chien, Paul Wassmann, Tilman Schirmer, Volkhard Kaever, Michael T Laub, Tania A Baker, and Urs Jenal. Regulatory cohesion of cell cycle and cell differentiation through interlinked phosphorylation and second messenger networks. *Molecular Cell*, 43(4):550–560, 2011.

[62] Reed A Goodwin and Daniel J Gage. Biochemical characterization of a nitrogen-type phosphotransferase system reveals that enzyme eintr integrates carbon and nitrogen signaling in sinorhizobium meliloti. *Journal of Bacteriology*, 196(10):1901–1907, 2014.

[63] Roshni R Kharadi, Luisa F Castiblanco, Christopher M Waters, and George W Sundin. Phosphodiesterase genes regulate amylovoran production, biofilm formation, and virulence in erwinia amylovora. *Applied and Environmental Microbiology*, 85(1):e02233–18, 2019.

[64] Erin B Purcell and Rita Tamayo. Cyclic diguanylate signaling in gram-positive bacteria. *FEMS Microbiology Reviews*, 40(5):753–773, 2016.

[65] S Abel. *Analysis of the c-di-GMP mediated cell fate determination in Caulobacter crescentus*. PhD thesis, Universität Basel, Department of Biozentrum, 2009.

[66] Kamal Kishore Joshi, Christine M Battle, and Peter Chien. Polar localization hub protein popz restrains adaptor-dependent clpxp proteolysis in caulobacter crescentus. *Journal of Bacteriology*, 200(20):e00221–18, 2018.

[67] Fabian M Commichau, Karl Forchhammer, and Jörg Stülke. Regulatory links between carbon and nitrogen metabolism. *Current Opinion in Microbiology*, 9(2):167–172, 2006.

[68] Josef Deutscher, Francine Moussan Désirée Aké, Meriem Derkaoui, Arthur Constant Zébré, Thanh Nguyen Cao, Houda Bouraoui, Takfarinas Kentache, Abdelhamid Mokhtari, Eliane Milohanic, and Philippe Joyet. The bacterial phosphoenolpyruvate: carbohydrate phosphotransferase system: regulation by protein phosphorylation and phosphorylation-dependent protein-protein interactions. *Microbiology and Molecular Biology Reviews*, 78(2):231–256, 2014.

[69] Werner Kundig and Saul Roseman. Sugar transport: I. isolation of a phosphotransferase system from escherichia coli. *Journal of Biological Chemistry*, 246(5):1393–1406, 1971.

[70] Chang-Ro Lee, Young-Ha Park, Miri Kim, Yeon-Ran Kim, Soyoung Park, Alan Peterkofsky, and Yeong-Jae Seok. Reciprocal regulation of the autophosphorylation of enzyme intr by glutamine and α-ketoglutarate in e scherichia coli. *Molecular Microbiology*, 88(3):473–485, 2013.

[71] Matthew J Brauer, Jie Yuan, Bryson D Bennett, Wenyun Lu, Elizabeth Kimball, David Botstein, and Joshua D Rabinowitz. Conservation of the metabolomic response to starvation across two divergent microbes. *Proceedings of the National Academy of Sciences*, 103(51):19302–19307, 2006.

[72] Takashi Osanai, Akira Oikawa, Tomokazu Shirai, Ayuko Kuwahara, Hiroko Iijima, Kan Tanaka, Masahiko Ikeuchi, Akihiko Kondo, Kazuki Saito, and Masami Yokota Hirai. Capillary electrophoresis–mass spectrometry reveals the distribution of carbon metabolites during nitrogen starvation in s ynechocystis sp. pcc 6803. *Environmental Microbiology*, 16(2):512–524, 2014.

[73] Jie Yuan, Christopher D Doucette, William U Fowler, Xiao-Jiang Feng, Matthew Piazza, Herschel A Rabitz, Ned S Wingreen, and Joshua D Rabinowitz. Metabolomics-driven quantitative analysis of ammonia assimilation in e. coli. *Molecular Systems Biology*, 5(1):302, 2009.

[74] Boris M Hogema, Jos C Arents, Rechien Bader, Kevin Eijkemans, Hiromi Yoshida, Hideyuki Takahashi, Hiroji Aiba, and Pieter W Postma. Inducer exclusion in escherichia coli by non-pts substrates: the role of the pep to pyruvate ratio in determin-

ing the phosphorylation state of enzyme iiaglc. *Molecular Microbiology*, 30(3):487–498, 1998.

[75] Boris Gorbatyuk and Gregory T Marczynski. Regulated degradation of chromosome replication proteins dnaa and ctra in caulobacter crescentus. *Molecular Microbiology*, 55(4):1233–1245, 2005.

[76] K Flärdh, Torsten Axberg, Nan H Albertson, and Staffan Kjelleberg. Stringent control during carbon starvation of marine vibrio sp. strain s14: molecular cloning, nucleotide sequence, and deletion of the rela gene. *Journal of Bacteriology*, 176(19):5949–5957, 1994.

[77] Bryson D Bennett, Elizabeth H Kimball, Melissa Gao, Robin Osterhout, Stephen J Van Dien, and Joshua D Rabinowitz. Absolute metabolite concentrations and implied enzyme active site occupancy in escherichia coli. *Nature Chemical Biology*, 5(8):593–599, 2009.

[78] Meir Fischer, Thomas P Zimmerman, and Steven A Short. A rapid method for the determination of guanosine 5-diphosphate-3-diphosphate and guanosine 5-triphosphate-3-diphosphate by high-performance liquid chromatography. *Analytical Biochemistry*, 121(1):135–139, 1982.

[79] Diego Gonzalez, Jennifer B Kozdon, Harley H McAdams, Lucy Shapiro, and Justine Collier. The functions of dna methylation by ccrm in caulobacter crescentus: a global approach. *Nucleic Acids Research*, 42(6):3720–3735, 2014.

[80] Caitlin Janine Light. *cis-2-Decenoic Acid Signaling and Dispersion in Pseudomonas aeruginosa: The Role of Dispersed Cells in Virulence and Pathogenesis*. PhD thesis, State University of New York at Binghamton, 2017.

[81] Meng How Tan, Jennifer B Kozdon, Xiling Shen, Lucy Shapiro, and Harley H McAdams. An essential transcription factor, scip, enhances robustness of caulobacter cell cycle regulation. *Proceedings of the National Academy of Sciences*, 107(44):18985–18990, 2010.

[82] Alexander T Schredl, Yannet G Perez Mora, Anabel Herrera, Math P Cuajungco, and Sean R Murray. The caulobacter crescentus ctra p1 promoter is essential for the coordination of cell cycle events that prevent the overinitiation of dna replication. *Microbiology*, 158(Pt 10):2492, 2012.

[83] Justine Collier, Harley H McAdams, and Lucy Shapiro. A dna methylation ratchet governs progression through a bacterial cell cycle. *Proceedings of the National Academy of Sciences*, 104(43):17111–17116, 2007.

[84] Kenneth C Keiler and Lucy Shapiro. tmrna is required for correct timing of dna replication in caulobacter crescentus. *Journal of Bacteriology*, 185(2):573–580, 2003.

[85] Justine Collier, Sean Richard Murray, and Lucy Shapiro. Dnaa couples dna replication and the expression of two cell cycle master regulators. *The EMBO Journal*, 25(2):346–356, 2006.

[86] Xiaofeng Zhou, Jiarui Wang, Jonathan Herrmann, WE Moerner, and Lucy Shapiro. Asymmetric division yields progeny cells with distinct modes of regulating cell cycle-dependent chromosome methylation. *Proceedings of the National Academy of Sciences*, 116(31):15661–15670, 2019.

[87] Bo Zhou, Jared M Schrader, Virginia S Kalogeraki, Eduardo Abeliuk, Cong B Dinh, James Q Pham, Zhongying Z Cui, David L Dill, Harley H McAdams, and Lucy Shapiro. The global regulatory architecture of transcription during the caulobacter cell cycle. *PLoS Genet*, 11(1):e1004831, 2015.

[88] Jared M Schrader, Gene-Wei Li, W Seth Childers, Adam M Perez, Jonathan S Weissman, Lucy Shapiro, and Harley H McAdams. Dynamic translation regulation in caulobacter cell cycle control. *Proceedings of the National Academy of Sciences*, 113(44):E6859–E6867, 2016.

[89] Shenghua Li, Paul Brazhnik, Bruno Sobral, and John J Tyson. Temporal controls of the asymmetric cell division cycle in caulobacter crescentus. *PLoS Computational Biology*, 5(8):e1000463, 2009.

[90] A.Antonio Iniesta and Lucy Shapiro. A bacterial control circuit integrates polar localization and proteolysis of key regulatory proteins with a phospho-signaling cascade. *PNAS*, 105(43):16602–16607, 2008.

[91] Fei Li, Kartik Subramanian, Minghan Chen, John J Tyson, and Yang Cao. A stochastic spatiotemporal model of a response-regulator network in the caulobacter crescentus cell cycle. *Physical Biology*, 13(3):035007, 2016.

[92] Minghan Chen, Fei Li, Kartik Subramanian, John Tyson, and Yang Cao. Two-dimensional model of bipolar popz polymerization in caulobacter crescentus. In *Proceedings of the 6th ACM Conference on Bioinformatics, Computational Biology and Health Informatics*, pages 37–46, 2015.

[93] Chunrui Xu and Yang Cao. A spatiotemporal model of polarity and spatial gradient establishment in caulobacter crescentus. In *Proceedings of the 12th ACM Conference on Bioinformatics, Computational Biology, and Health Informatics*, pages 1–10, 2021.

[94] Andreas Kaczmarczyk, Antje M Hempel, Christoph von Arx, Raphael Böhm, Badri N Dubey, Jutta Nesper, Tilman Schirmer, Sebastian Hiller, and Urs Jenal. Precise timing of transcription by c-di-gmp coordinates cell cycle and morphogenesis in caulobacter. *Nature Communications*, 11(1):1–16, 2020.

[95] Kamal Kishore Joshi, Madeleine Sutherland, and Peter Chien. Cargo engagement protects protease adaptors from degradation in a substrate-specific manner. *Journal of Biological Chemistry*, 292(26):10973–10982, 2017.

[96] Mark Wortinger, Marcella J Sackett, and Yves V Brun. Ctra mediates a dna replication checkpoint that prevents cell division in caulobacter crescentus. *The EMBO Journal*, 19(17):4503–4512, 2000.

[97] Ann Reisenauer and Lucy Shapiro. Dna methylation affects the cell cycle transcription of the ctra global regulator in caulobacter. *The EMBO Journal*, 21(18):4969–4977, 2002.

[98] Ellen M Judd, Kathleen R Ryan, WE Moerner, Lucy Shapiro, and Harley H McAdams. Fluorescence bleaching reveals asymmetric compartment formation prior to cell division in caulobacter. *Proceedings of the National Academy of Sciences*, 100(14):8235–8240, 2003.

[99] Keren Lasker, Thomas H Mann, and Lucy Shapiro. An intracellular compass spatially coordinates cell cycle modules in caulobacter crescentus. *Current Opinion in Microbiology*, 33:131–139, 2016.

[100] Antonio A. Iniesta, Patrick T. McGrath, Ann Reisenauer, Harley H. McAdams, and Lucy Shapiro. A phospho-signaling pathway controls the localization and activity of a protease complex critical for bacterial cell cycle progression. *Proceedings of the National Academy of Sciences*, 103(29):10935–10940, 2006.

[101] Paul Wassmann, Carmen Chan, Ralf Paul, Andreas Beck, Heiko Heerklotz, Urs Jenal, and Tilman Schirmer. Structure of bef3–modified response regulator pled: implications for diguanylate cyclase activation, catalysis, and feedback inhibition. *Structure*, 15(8):915–927, 2007.

[102] Anna Duerig, Sören Abel, Marc Folcher, Micael Nicollier, Torsten Schwede, Nicolas Amiot, Bernd Giese, and Urs Jenal. Second messenger-mediated spatiotemporal control of protein degradation regulates bacterial cell cycle progression. *Genes & Development*, 23(1):93–104, 2009.

[103] Ralf Paul, Stefan Weiser, Nicholas C Amiot, Carmen Chan, Tilman Schirmer, Bernd Giese, and Urs Jenal. Cell cycle-dependent dynamic localization of a bacterial response regulator with a novel di-guanylate cyclase output domain. *Genes & Development*, 18(6):715–727, 2004.

[104] Jérôme Coppine, Andreas Kaczmarczyk, Kenny Petit, Thomas Brochier, Urs Jenal, and Régis Hallez. Regulation of bacterial cell cycle progression by redundant phosphatases. *Journal of Bacteriology*, 202(17):e00345–20, 2020.

[105] Patrick H Viollier, Nitzan Sternheim, and Lucy Shapiro. A dynamically localized histidine kinase controls the asymmetric distribution of polar pili proteins. *The EMBO Journal*, 21(17):4420–4428, 2002.

[106] Andrew Dingwall and Lucille Shapiro. Rate, origin, and bidirectionality of *Caulobacter* chromosome replication as determined by pulsed-field gel electrophoresis. *Proceedings of the National Academy of Sciences*, 86(1):119–123, 1989.

[107] Kalyanmoy Deb, Amrit Pratap, Sameer Agarwal, and TAMT Meyarivan. A fast and elitist multiobjective genetic algorithm: Nsga-ii. *IEEE Transactions on Evolutionary Computation*, 6(2):182–197, 2002.

[108] Tyler H. Chang, Layne T. Watson, Jeffery Larson, Nicole Neveu, William Thacker, Shubhangi Deshpande, and Thomas C. H. Lux. Algorithm xxxx: Vtmop: Solver for blackbox multiobjective optimization problems. 2021, In press.

[109] Jian He, Layne T Watson, and Masha Sosonkina. Algorithm 897: Vtdirect95: serial and parallel codes for the global optimization algorithm direct. *ACM Transactions on Mathematical Software (TOMS)*, 36(3):1–24, 2009.

[110] Brandon D Amos, David R Easterling, Layne T Watson, William I Thacker, Brent S Castle, and Michael W Trosset. Algorithm xxx: Qnstop—quasi-newton algorithm for stochastic optimization. Technical report, Department of Computer Science, Virginia Polytechnic Institute & State ..., 2014.

[111] Minghan Chen, Brandon D Amos, Layne T Watson, John J Tyson, Young Cao, Clifford A Shaffer, Michael W Trosset, Cihan Oguz, and Gisella Kakoti. Quasi-newton stochastic optimization algorithm for parameter estimation of a stochastic model of the budding yeast cell cycle. *IEEE/ACM Transactions on Computational Biology and Bioinformatics*, 16(1):301–311, 2017.

[112] Patrick T. McGrath, Antonio A. Iniesta, Kathleen R. Ryan, Lucy Shapiro, and Harley H. McAdams. A dynamically localized protease complex and a polar specificity factor control a cell cycle master regulator. *Cell*, 124(3):535–547, 2006.

[113] Phillip Aldridge, Ralf Paul, Patrick Goymer, Paul Rainey, and Urs Jenal. Role of the ggdef regulator pled in polar development of caulobacter crescentus. *Molecular Microbiology*, 47(6):1695–1708, 2003.

[114] Julia Holtzendorff, Dean Hung, Peter Brende, Ann Reisenauer, Patrick H Viollier, Harley H McAdams, and Lucy Shapiro. Oscillating global regulators control the genetic circuit driving a bacterial cell cycle. *Science*, 304(5673):983–987, 2004.

[115] Ann Reisenauer, Kim Quon, and Lucy Shapiro. The ctra response regulator mediates temporal control of gene expression during the caulobacter cell cycle. *Journal of Bacteriology*, 181(8):2430–2439, 1999.

[116] Ibrahim J Domian, Kim C Quon, and Lucy Shapiro. Cell type-specific phosphorylation and proteolysis of a transcriptional regulator controls the g1-to-s transition in a bacterial cell cycle. *Cell*, 90(3):415–424, 1997.

[117] Susan Schlimpert. *About rings and crossbands-Characterization of proteins involved in cell division and compartmentalization in Caulobacter crescentus*. PhD thesis, Philipps University, Marburg, 2011.

[118] Chunrui Xu, Bronson R Weston, John J Tyson, and Yang Cao. Cell cycle control and environmental response by second messengers in caulobacter crescentus. *BMC Bioinformatics*, 21(14):1–19, 2020.

[119] Diane L Haakonsen, Andy H Yuan, and Michael T Laub. The bacterial cell cycle regulator gcra is a σ70 cofactor that drives gene expression from a subset of methylated promoters. *Genes & Development*, 29(21):2272–2286, 2015.

[120] Kamal Kishore Joshi and Peter Chien. Regulated proteolysis in bacteria: Caulobacter. *Annu Rev Genet*, 50:423–445, 2016.

[121] David J Leslie, Christian Heinen, Frederic D Schramm, Marietta Thüring, Christopher D Aakre, Sean M Murray, Michael T Laub, and Kristina Jonas. Nutritional control of dna replication initiation through the proteolysis and regulated translation of dnaa. *PLoS Genetics*, 11(7):e1005342, 2015.

[122] Rachel Wright, Craig Stephens, Gary Zweiger, Lucy Shapiro, and MR Alley. Caulobacter lon protease has a critical role in cell-cycle control of dna methylation. *Genes & Development*, 10(12):1532–1542, 1996.

[123] Guanglai Li, Christopher S Smith, Yves V Brun, and Jay X Tang. The elastic properties of the caulobacter crescentus adhesive holdfast are dependent on oligomers of n-acetylglucosamine. *Journal of Bacteriology*, 187(1):257–265, 2005.

[124] Kartik Subramanian, Mark R Paul, and John J Tyson. Potential role of a bistable histidine kinase switch in the asymmetric division cycle of caulobacter crescentus. *PLoS Computational Biology*, 9(9):e1003221, 2013.

[125] Kartik Subramanian, Mark R Paul, and John J Tyson. Dynamical localization of divl and plec in the asymmetric division cycle of caulobacter crescentus: a theoretical investigation of alternative models. *PLoS Computational Biology*, 11(7):e1004348, 2015.

[126] Joseph A Lesley and Lucy Shapiro. Spot regulates dnaa stability and initiation of dna replication in carbon-starved caulobacter crescentus. *Journal of Bacteriology*, 190(20):6867–6880, 2008.

[127] Leticia Britos, Eduardo Abeliuk, Thomas Taverner, Mary Lipton, Harley McAdams, and Lucy Shapiro. Regulatory response to carbon starvation in caulobacter crescentus. *PloS One*, 6(4):e18179, 2011.

[128] Bradford S Powell, Donald L Court, Toshifumi Inada, Yoshikazu Nakamura, Valerie Michotey, Xuewen Cui, Aiala Reizer, Milton H Saier Jr, and Jonathan Reizer. Novel proteins of the phosphotransferase system encoded within the rpon operon of escherichia coli: Enzyme iiantr affects growth on organic nitrogen and the conditional lethality of an erats mutant. *Journal of Biological Chemistry*, 270(9):4822–4839, 1995.

[129] Max Chavarría, Tobias Fuhrer, Uwe Sauer, Katharina Pflüger-Grau, and Víctor de Lorenzo. Cra regulates the cross-talk between the two branches of the phosphoenolpyruvate: phosphotransferase system of pseudomonas putida. *Environmental Microbiology*, 15(1):121–132, 2013.

[130] Patrick D Curtis and Yves V Brun. Getting in the loop: regulation of development in caulobacter crescentus. *Microbiology and Molecular Biology Reviews*, 74(1):13–41, 2010.

[131] Diego Gonzalez and Justine Collier. Effects of (p) ppgpp on the progression of the cell cycle of caulobacter crescentus. *Journal of Bacteriology*, 196(14):2514–2525, 2014.

[132] Christos G Tsokos, Barrett S Perchuk, and Michael T Laub. A dynamic complex of signaling proteins uses polar localization to regulate cell-fate asymmetry in caulobacter crescentus. *Developmental Cell*, 20(3):329–341, 2011.

[133] Emanuele G Biondi, Jeffrey M Skerker, Muhammad Arif, Melanie S Prasol, Barrett S Perchuk, and Michael T Laub. A phosphorelay system controls stalk biogenesis during cell cycle progression in caulobacter crescentus. *Molecular Microbiology*, 59(2):386–401, 2006.

[134] Alycia N Bittner, Allison Kriel, and Jue D Wang. Lowering gtp level increases survival of amino acid starvation but slows growth rate for bacillus subtilis cells lacking (p) ppgpp. *Journal of Bacteriology*, 196(11):2067–2076, 2014.

[135] Stefano Sanselicio, Matthieu Bergé, Laurence Théraulaz, Sunish Kumar Radhakrishnan, and Patrick H Viollier. Topological control of the caulobacter cell cycle circuitry by a polarized single-domain pas protein. *Nature Communications*, 6(1):1–14, 2015.

[136] Badri N Dubey, Elia Agustoni, Raphael Böhm, Andreas Kaczmarczyk, Francesca Mangia, Christoph von Arx, Urs Jenal, Sebastian Hiller, Iván Plaza-Menacho, and Tilman Schirmer. Hybrid histidine kinase activation by cyclic di-gmp–mediated domain liberation. *Proceedings of the National Academy of Sciences*, 117(2):1000–1008, 2020.

[137] Yan Zhu, Ling Qin, Takeshi Yoshida, and Masayori Inouye. Phosphatase activity of histidine kinase envz without kinase catalytic domain. *Proceedings of the National Academy of Sciences*, 97(14):7808–7813, 2000.

[138] Shuo Li. *Kinetics Study of WalK Phosphatase activity in Streptococcus pneumoniae*. PhD thesis, Indiana University, 2011.

[139] TuAnh Ngoc Huynh and Valley Stewart. Negative control in two-component signal transduction by transmitter phosphatase activity. *Molecular Microbiology*, 82(2):275–286, 2011.

[140] Yixiang Liu, Joshua Rose, Shaojia Huang, Yangbo Hu, Qiong Wu, Dan Wang, Conggang Li, Maili Liu, Pei Zhou, and Ling Jiang. A ph-gated conformational switch regulates the phosphatase activity of bifunctional hiska-family histidine kinases. *Nature Communications*, 8(1):1–10, 2017.

[141] Keren Lasker, Jared M Schrader, Yifei Men, Tyler Marshik, David L Dill, Harley H McAdams, and Lucy Shapiro. Caulobrowser: A systems biology resource for caulobacter crescentus. *Nucleic Acids Research*, 44(D1):D640–D645, 2016.

[142] Patrick T McGrath, Antonio A Iniesta, Kathleen R Ryan, Lucy Shapiro, and Harley H McAdams. A dynamically localized protease complex and a polar specificity factor control a cell cycle master regulator. *Cell*, 124(3):535–547, 2006.

[143] Antonio A Iniesta, Patrick T McGrath, Ann Reisenauer, Harley H McAdams, and Lucy Shapiro. A phospho-signaling pathway controls the localization and activity of a protease complex critical for bacterial cell cycle progression. *Proceedings of the National Academy of Sciences*, 103(29):10935–10940, 2006.

[144] Leticia Cristina Britos Cavagnaro. *Regulatory Response to Environmental Challenge in Caulobacter crescentus*. Stanford University, 2011.

[145] Christine Jacobs, Nora Ausmees, Stuart J Cordwell, Lucy Shapiro, and Michael T Laub. Functions of the ccka histidine kinase in caulobacter cell cycle control. *Molecular Microbiology*, 47(5):1279–1290, 2003.

[146] Xiaofeng Zhou and Lucy Shapiro. Cell cycle-controlled clearance of the ccrm dna methyltransferase by lon is dependent on dna-facilitated proteolysis and substrate polar sequestration. *bioRxiv*, page 293738, 2018.

[147] Björn Grünenfelder, Gabriele Rummel, Jiri Vohradsky, Daniel Röder, Hanno Langen, and Urs Jenal. Proteomic analysis of the bacterial cell cycle. *Proceedings of the National Academy of Sciences*, 98(8):4681–4686, 2001.

[148] Lin Cheng and Kenneth C Keiler. Correct timing of dnaa transcription and initiation of dna replication requires trans translation. *Journal of Bacteriology*, 191(13):4268–4275, 2009.

[149] Carolina Tropini and Kerwyn Casey Huang. Interplay between the localization and kinetics of phosphorylation in flagellar pole development of the bacterium caulobacter crescentus. 2012.

[150] Hubert Lam, Jean-Yves Matroule, and Christine Jacobs-Wagner. The asymmetric spatial distribution of bacterial signal transduction proteins coordinates cell cycle events. *Developmental Cell*, 5(1):149–159, 2003.

[151] Y Erin Chen, Carolina Tropini, Kristina Jonas, Christos G Tsokos, Kerwyn C Huang, and Michael T Laub. Spatial gradient of protein phosphorylation underlies replicative asymmetry in a bacterium. *Proceedings of the National Academy of Sciences*, 108(3):1052–1057, 2011.

[152] Kathleen R Ryan and Lucy Shapiro. Temporal and spatial regulation in prokaryotic cell cycle progression and development. *Annual Review of Biochemistry*, 72(1):367–394, 2003.

[153] Ibrahim J Domian, Kim C Quon, and Lucy Shapiro. The control of temporal and spatial organization during the caulobacter cell cycle. *Current Opinion in Genetics & Development*, 6(5):538–544, 1996.

[154] Ralf Paul, Tina Jaeger, Sören Abel, Irene Wiederkehr, Marc Folcher, Emanuele G Biondi, Michael T Laub, and Urs Jenal. Allosteric regulation of histidine kinases by their cognate response regulator determines cell fate. *Cell*, 133(3):452–461, 2008.

[155] Peter S Angelastro, Oleksii Sliusarenko, and Christine Jacobs-Wagner. Polar localization of the ccka histidine kinase and cell cycle periodicity of the essential master regulator ctra in caulobacter crescentus. *Journal of Bacteriology*, 192(2):539–552, 2010.

[156] Christine Jacobs, Ibrahim J Domian, Janine R Maddock, and Lucy Shapiro. Cell cycle–dependent polar localization of an essential bacterial histidine kinase that controls dna replication and cell division. *Cell*, 97(1):111–120, 1999.

[157] Samuel W Duvall and W Seth Childers. Design of a histidine kinase fret sensor to detect complex signal integration within living bacteria. *ACS Sensors*, 5(6):1589–1596, 2020.

[158] Thomas H Mann and Lucy Shapiro. Integration of cell cycle signals by multi-pas domain kinases. *Proceedings of the National Academy of Sciences*, 115(30):E7166–E7173, 2018.

[159] Joshua A Holmes, Shelby E Follett, Haibi Wang, Christopher P Meadows, Krisztina Varga, and Grant R Bowman. Caulobacter popz forms an intrinsically disordered hub in organizing bacterial cell poles. *Proceedings of the National Academy of Sciences*, 113(44):12490–12495, 2016.

[160] Jean-Yves Matroule, Hubert Lam, Dylan T Burnette, and Christine Jacobs-Wagner. Cytokinesis monitoring during development: rapid pole-to-pole shuttling of a signaling protein by localized kinase and phosphatase in caulobacter. *Cell*, 118(5):579–590, 2004.

[161] Kimberly Ann Kowallis. *Regulatory Mechanisms of a Bacterial Multi-Kinase Network*. PhD thesis, University of Pittsburgh, 2020.

[162] Grant R Bowman, Luis R Comolli, Guido M Gaietta, Michael Fero, Sun-Hae Hong, Ying Jones, Julie H Lee, Kenneth H Downing, Mark H Ellisman, Harley H McAdams, et al. Caulobacter popz forms a polar subdomain dictating sequential changes in pole composition and function. *Molecular Microbiology*, 76(1):173–189, 2010.

[163] Géraldine Laloux and Christine Jacobs-Wagner. How do bacteria localize proteins to the cell pole? *Journal of cell science*, 127(1):11–19, 2014.

[164] Kerwyn Casey Huang and Kumaran S Ramamurthi. Macromolecules that prefer their membranes curvy. *Molecular Microbiology*, 76(4):822–832, 2010.

[165] Eleonora García Véscovi, Mariela I Sciara, and María E Castelli. Two component systems in the spatial program of bacteria. *Current Opinion in Microbiology*, 13(2):210–218, 2010.

[166] Lars D Renner and Douglas B Weibel. Mind and mine interact with anionic phospholipids and regulate division plane formation in escherichia coli. *Journal of Biological Chemistry*, 287(46):38835–38844, 2012.

[167] Melanie L Lawler, David E Larson, Aaron J Hinz, David Klein, and Yves V Brun. Dissection of functional domains of the polar localization factor podj in caulobacter crescentus. *Molecular Microbiology*, 59(1):301–316, 2006.

[168] Kartik Subramanian, Mark R Paul, and John J Tyson. De novo production of turing activator generates polarity in pattern formation. *Advances in Systems and Synthetic Biology*, 2014.

[169] Michelle Aaron, Godefroid Charbon, Hubert Lam, Heinz Schwarz, Waldemar Vollmer, and Christine Jacobs-Wagner. The tubulin homologue ftsz contributes to cell elongation by guiding cell wall precursor synthesis in caulobacter crescentus. *Molecular Microbiology*, 64(4):938–952, 2007.

[170] Benedetto Terrana and Austin Newton. Pattern of unequal cell division and development in caulobacter crescentus. *Developmental Biology*, 44(2):380–385, 1975.

[171] Manuel Campos, Ivan V Surovtsev, Setsu Kato, Ahmad Paintdakhi, Bruno Beltran, Sarah E Ebmeier, and Christine Jacobs-Wagner. A constant size extension drives bacterial cell size homeostasis. *Cell*, 159(6):1433–1446, 2014.

[172] AM Turing. The chemical basis of morphogenesis. *Bulletin of Mathematical Biology*, 52(1/2):153–197, 1952.

[173] Hans Meinhardt and Alfred Gierer. Pattern formation by local self-activation and lateral inhibition. *Bioessays*, 22(8):753–760, 2000.

[174] Adam M Perez, Thomas H Mann, Keren Lasker, Daniel G Ahrens, Michael R Eckart, and Lucy Shapiro. A localized complex of two protein oligomers controls the orientation of cell polarity. *MBio*, 8(1):e02238–16, 2017.

[175] Grant R Bowman, Luis R Comolli, Jian Zhu, Michael Eckart, Marcelle Koenig, Kenneth H Downing, WE Moerner, Thomas Earnest, and Lucy Shapiro. A polymeric protein anchors the chromosomal origin/parb complex at a bacterial cell pole. *Cell*, 134(6):945–955, 2008.

[176] Grant R Bowman, Adam M Perez, Jerod L Ptacin, Eseosa Ighodaro, Ewa Folta-Stogniew, Luis R Comolli, and Lucy Shapiro. Oligomerization and higher-order assembly contribute to sub-cellular localization of a bacterial scaffold. *Molecular Microbiology*, 90(4):776–795, 2013.

[177] Mohit Kumar, Mario S Mommer, and Victor Sourjik. Mobility of cytoplasmic, membrane, and dna-binding proteins in escherichia coli. *Biophysical journal*, 98(4):552–559, 2010.

[178] Aurelio A Teleman, Peter L Graumann, Daniel Chi-Hong Lin, Alan D Grossman, and Richard Losick. Chromosome arrangement within a bacterium. *Current Biology*, 8(20):1102–1109, 1998.

[179] William C Nierman, Tamara V Feldblyum, Michael T Laub, Ian T Paulsen, Karen E Nelson, Jonathan Eisen, John F Heidelberg, MRK Alley, Noriko Ohta, Janine R Maddock, et al. Complete genome sequence of caulobacter crescentus. *Proceedings of the National Academy of Sciences*, 98(7):4136–4141, 2001.

[180] Paula Montero Llopis, Audrey F Jackson, Oleksii Sliusarenko, Ivan Surovtsev, Jennifer Heinritz, Thierry Emonet, and Christine Jacobs-Wagner. Spatial organization of the flow of genetic information in bacteria. *Nature*, 466(7302):77–81, 2010.

[181] Joseph C Chen, Alison K Hottes, Harley H McAdams, Patrick T McGrath, Patrick H Viollier, and Lucy Shapiro. Cytokinesis signals truncation of the podj polarity factor by a cell cycle-regulated protease. *The EMBO Journal*, 25(2):377–386, 2006.

[182] W Seth Childers, Qingping Xu, Thomas H Mann, Irimpan I Mathews, Jimmy A Blair, Ashley M Deacon, and Lucy Shapiro. Cell fate regulation governed by a repurposed bacterial histidine kinase. *PLoS Biology*, 12(10):e1001979, 2014.

[183] Sarah J Reisinger, Sarah Huntwork, Patrick H Viollier, and Kathleen R Ryan. Divl performs critical cell cycle functions in caulobacter crescentus independent of kinase activity. *Journal of Bacteriology*, 189(22):8308–8320, 2007.

[184] Sarah Jane Reisinger. *The role of DivL in Caulobacter crescentus cell cycle progression*. University of California, Berkeley, 2007.

[185] Stephen A Sciochetti, Noriko Ohta, and Austin Newton. The role of polar localization in the function of an essential caulobacter crescentus tyrosine kinase. *Molecular Microbiology*, 56(6):1467–1480, 2005.

[186] Matthieu Bergé and Patrick H Viollier. End-in-sight: cell polarization by the polygamic organizer popz. *Trends in Microbiology*, 26(4):363–375, 2018.

[187] Christine Jacobs, Dean Hung, and Lucy Shapiro. Dynamic localization of a cytoplasmic signal transduction response regulator controls morphogenesis during the caulobacter cell cycle. *Proceedings of the National Academy of Sciences*, 98(7):4095–4100, 2001.

[188] Patrick D Curtis, Ellen M Quardokus, Melanie L Lawler, Xiaoyun Guo, David Klein, Joseph C Chen, Randy J Arnold, and Yves V Brun. The scaffolding and signalling functions of a localization factor impact polar development. *Molecular Microbiology*, 84(4):712–735, 2012.

[189] François Jacob, Sydney Brenner, and François Cuzin. On the regulation of dna replication in bacteria. In *Cold Spring Harbor Symposia on Quantitative Biology*, volume 28, pages 329–348. Cold Spring Harbor Laboratory Press, 1963.

[190] WD Donachie and KJ Begg. Growth of the bacterial cell. *Nature*, 227(5264):1220–1224, 1970.

[191] Richard A Daniel and Jeff Errington. Control of cell morphogenesis in bacteria: two distinct ways to make a rod-shaped cell. *Cell*, 113(6):767–776, 2003.

[192] MA De Pedro, Jose Carlos Quintela, JV Höltje, and Heinz Schwarz. Murein segregation in escherichia coli. *Journal of Bacteriology*, 179(9):2823–2834, 1997.

[193] Badri N Dubey, Christian Lori, Shogo Ozaki, Geoffrey Fucile, Ivan Plaza-Menacho, Urs Jenal, and Tilman Schirmer. Cyclic di-gmp mediates a histidine kinase/phosphatase switch by noncovalent domain cross-linking. *Science Advances*, 2(9):e1600823, 2016.

[194] Josef Deutscher, Christof Francke, and Pieter W Postma. How phosphotransferase system-related protein phosphorylation regulates carbohydrate metabolism in bacteria. *Microbiology and Molecular Biology Reviews*, 70(4):939–1031, 2006.

[195] Anne Galinier and Josef Deutscher. Sophisticated regulation of transcriptional factors by the bacterial phosphoenolpyruvate: sugar phosphotransferase system. *Journal of Molecular Biology*, 429(6):773–789, 2017.

[196] Andreas Kremling, Katharina Pflüger-Grau, Max Chavarría, Jacek Puchalka, Vitor-Martins dos Santos, and Víctorde Lorenzo. Modeling and analysis of flux distributions in the two branches of the phosphotransferase system in pseudomonas putida. *BMC Systems Biology*, 6(1):1–13, 2012.

[197] Evelyn M Witkin. Ultraviolet-induced mutation and dna repair. *Annual Review of Genetics*, 3(1):525–552, 1969.

[198] Joshua W Modell, Tracy K Kambara, Barrett S Perchuk, and Michael T Laub. A dna damage-induced, sos-independent checkpoint regulates cell division in caulobacter crescentus. *PLoS Biology*, 12(10):e1001977, 2014.

[199] Raquel Paes Da Rocha, Apua César de Miranda Paquola, Marilis do Valle Marques, Carlos Frederico Martins Menck, and Rodrigo S Galhardo. Characterization of the sos regulon of caulobacter crescentus. *Journal of Bacteriology*, 190(4):1209–1218, 2008.

[200] Yogita Sardessai and Saroj Bhosle. Tolerance of bacteria to organic solvents. *Research in Microbiology*, 153(5):263–268, 2002.

[201] Kristina Heinrich, Patrick Sobetzko, and Kristina Jonas. A kinase-phosphatase switch transduces environmental information into a bacterial cell cycle circuit. *PLoS Genetics*, 12(12):e1006522, 2016.

[202] Ganhui Lan, Charles W Wolgemuth, and Sean X Sun. Z-ring force and cell shape during division in rod-like bacteria. *Proceedings of the National Academy of Sciences*, 104(41):16110–16115, 2007.

[203] Justine Collier. Cell division control in caulobacter crescentus. *Biochimica et Biophysica Acta (BBA)-Gene Regulatory Mechanisms*, 1862(7):685–690, 2019.

[204] Géraldine Laloux and Christine Jacobs-Wagner. Spatiotemporal control of popz localization through cell cycle–coupled multimerization. *Journal of Cell Biology*, 201(6):827–841, 2013.

[205] Piotr Szwedziak, Qing Wang, Tanmay AM Bharat, Matthew Tsim, and Jan Löwe. Architecture of the ring formed by the tubulin homologue ftsz in bacterial cell division. *eLife*, 3:e04601, 2014.

[206] Ganhui Lan, Brian R Daniels, Terrence M Dobrowsky, Denis Wirtz, and Sean X Sun. Condensation of ftsz filaments can drive bacterial cell division. *Proceedings of the National Academy of Sciences*, 106(1):121–126, 2009.

[207] François Beaufay, Jérôme Coppine, Aurélie Mayard, Géraldine Laloux, Xavier De Bolle, and Régis Hallez. A nad-dependent glutamate dehydrogenase coordinates metabolism with cell division in caulobacter crescentus. *The EMBO Journal*, 34(13):1786–1800, 2015.

[208] Martin Thanbichler and Lucy Shapiro. Mipz, a spatial regulator coordinating chromosome segregation with cell division in caulobacter. *Cell*, 126(1):147–162, 2006.

[209] Wei Zhao, Samuel W Duvall, Kimberly A Kowallis, Chao Zhang, Dylan T Tomares, Haley N Petitjean, and W Seth Childers. Scaffold-scaffold interactions regulate cell polarity in a bacterium. *bioRxiv*, 2020.

[210] Narendra S Goel and Nira Richter-Dyn. *Stochastic models in biology*. Elsevier, 2016.

[211] Minghan Chen and Yang Cao. Analysis and remedy of negativity problem in hybrid stochastic simulation algorithm and its application. *BMC Bioinformatics*, 20(12):1–16, 2019.

[212] Kousik Sundararajan and Erin D Goley. Cytoskeletal proteins in caulobacter crescentus: spatial orchestrators of cell cycle progression, development, and cell shape. *Prokaryotic Cytoskeletons*, pages 103–137, 2017.

[213] Uniprot: the universal protein knowledgebase in 2021. *Nucleic Acids Research*, 49(D1):D480–D489, 2021.

[214] Christos G Tsokos and Michael T Laub. Polarity and cell fate asymmetry in caulobacter crescentus. *Current Opinion in Microbiology*, 15(6):744–750, 2012.